GENERATION AND ANALYSIS OF SPECTRUM-COMPATIBLE EARTHQUAKE TIME-HISTORIES USING WAVELETS

by

LUIS ALBERTO MONTEJO VALENCIA

A thesis submitted in partial fulfillment of
the requirements for the degree of

MASTER OF SCIENCE
in
CIVIL ENGINEERING

UNIVERSITY OF PUERTO RICO
MAYAGÜEZ CAMPUS
2004

Approved by:

Miguel A. Pando, Ph.D. — Date
Member, Graduate Committee

José A. Martínez Cruzado, Ph.D. — Date
Member, Graduate Committee

Luis E. Suárez, Ph.D. — Date
President, Graduate Committee

José Arroyo Caraballo, Ph.D. — Date
Representative of the Graduate School

Ismael Pagán Trinidad, M Sc. — Date
Chairperson of the Department

ABSTRACT

A wavelet-based procedure is presented to generate artificial accelerograms compatible with a prescribed seismic design spectrum. The acceleration time-history of an actual earthquake is decomposed into a number of time histories using the continuous wavelet transform. Each component time history is then suitably scaled so that the response spectrum of the revised accelerogram matches the target spectrum. A new wavelet, based on the impulse response function of an underdamped oscillator, has been proposed for this purpose. A procedure to perform a baseline correction of the compatible accelerograms is also presented. The artificial accelerograms were analyzed in time and frequency using the wavelet transform and the Fourier transform, to examine how the spectral content of the signal evolves with time. An alternative way to match the design spectrum termed the "two-band matching procedure" is proposed with the objective of preserving the non-stationary characteristics of the original record in the modified accelerogram.

RESUMEN

Se presenta un procedimiento para generar registros artificiales compatibles con un espectro de diseño. Para este propósito se desarrolla una nueva “wavelet” basada en la función de respuesta a impulso unitario para un oscilador sub-amortiguado. El procedimiento consiste en descomponer el registro original en un número adecuado de funciones llamadas “detalles” y entonces reconstruir la señal escalando los detalles de tal manera que el espectro de respuesta de la señal reconstruida concuerde con un espectro de diseño previamente especificado. Una metodología para la corrección de línea de base de registros compatibles es presentada también. Los registros artificiales son analizados en el dominio del tiempo y la frecuencia haciendo uso de la transformada “wavelet” junto con la transformada de Fourier y de esta manera analizar el cambio en el contenido de frecuencias del acelerograma con el tiempo. Un procedimiento alternativo para ajustar un espectro de diseño llamado “ajuste en dos bandas” es propuesto con el objetivo de mantener las características no estacionarias del registro original en el modificado.

A mis padres: Alcira y Luis Alberto.

A mi hermano: Brian Daniel.

A quien llena mi vida de dulzura: Aidcer Linalynn.

ACKNOWLEDGMENTS

I would like to thank Dr. Luis Suarez for making me feel extremely comfortable during the last two years and for his great support throughout this research. I would also like to acknowledge Dr. Carlos Prato for his guidance and advice.

Special thanks to the Puerto Rico Strong Motion Network for providing the financial support to make this research possible.

I also want to thank the members of my committee Dr. José A. Martínez Cruzado and Dr. Miguel A. Pando.

I am grateful to the University of Puerto Rico, and to the Civil Engineering and Surveying Department for the opportunity to pursue my graduate studies at this institution.

I would like to recognize support given by my friends and classmates, specially Mohammad Saffar, Hector Lopez (Chepe), Monica Ospinal (la Paloma), Fabian Consuegra, Orlando Cundumi (el Negro), Delio Andres Ramirez, Jairo Diaz, Jorge Botero (el Paisa), Cecilia Hernandez, Amelia Hernandez, Jorge Muract (el Pibe), Eduardo Sosa, Leonardo Cocco, Joanna Cataño, Juan Roman (Juancho), Edualdo Torres, Miguel Ruiz, Peter Gonzales, Wilmel Varela, Yessenia Lugo, Omaira Santos and Gustavo Pacheco.

Finally, I would like to thank my parents, brother and Aidcer for giving me their love and continuous support.

CONTENTS

LIST OF FIGURES

LIST OF TABLES

CHAPTER I

INTRODUCTION

1.1 Problem Description

The response of structures under earthquake ground motions can be calculated either using a (pseudo-acceleration) response spectrum or an acceleration time history. For design purposes, seismic codes provide a design spectrum, i.e., a smooth response spectrum that (hopefully) takes into account every possible earthquake likely to occur in a given zone with a certain probability of occurrence. Because special care is taken to define a reliable design spectrum, and since the response spectrum method is a simple and well-established procedure, it is the most common approach to perform linear analysis of buildings and other conventional structures. However, for seismic analysis of many critical structures (such as power plants, dams, tall buildings, cable-stayed bridges, etc) a step-by-step time analysis is usually done. Moreover, the application of the response spectrum method to nonlinear analysis is not straightforward and it is still the object of studies. Thus, in many cases a nonlinear time history analysis is done, which requires accelerograms representative of earthquakes expected at the site. Except for very few regions of the world where a set of recorded accelerograms is available, artificial earthquakes are often used for the dynamic analysis. These artificial earthquakes are defined by accelerograms that are "consistent" with a design spectrum, i.e., they are such that if their response spectra are calculated, they will be approximately equal to a prescribed or target spectrum. The artificial accelerograms can be generated from the superposition of sine waves with random phases and the resulting amplitude modulated by a smooth function to account for the transient character of the seismic motions, such as in the method proposed by Gasparini and Vanmarcke (1976) and coded in their program SIMQKE. These methods are perhaps the most attractive for design code applications since the required input, a response spectrum, is almost always available and therefore the criteria for the generation of records are very easily specified. However, there are many pitfalls in the use of artificial records, which tend to have unrealistically high duration and numbers of cycles of motion, especially for inelastic analysis (Naeim and Lew, 1995). Moreover, as it will shown later in this study, the widely used SIMQKE methodology may produce accelerograms with deficient characteristics. These facts increase the need to have better procedures available for the generation of spectrum compatibles time-histories.

This thesis intends to address this concern by developing a wavelet based procedure to modify a recorded accelerogram so that the response spectrum of the revised record matches a specified design spectrum. In addition, the wavelet transform along with the Fourier transform can be very effective to examine the characteristics of the artificial and original records.

1.2 Previous Works

For the purposes of this work, three different types of accelerograms can be defined:

- Real accelerograms recorded in past earthquakes;

- Synthetic accelerograms generated from models of the seismic fault rupture;
- Artificial accelerograms generated to match target response spectra.

This thesis deals with the generation of the last type of accelerograms.

Different methods aimed at generating artificial accelerograms that are compatible with a specified design spectrum have been proposed since the 70's. Scanlan and Sachs (1974) presented a method to synthesize an earthquake record as a time-modulated sum of harmonic functions with random phases uniformly distributed in the interval $[0, 2\pi]$. The duration D_0 of the accelerogram was preselected, and the acceleration at a time t was computed from the following equation:

$$a_g(t) = m(t)\sum_{i=1}^{N} A_i \cos\left(\frac{2\pi it}{D_0} + \phi_i\right) \tag{1.1}$$

The variable ϕ_i is a random phase angle with a uniform distribution in the interval $\left[0, 2\pi\right]$. The symbol $m(t)$ represents a deterministic modulating envelope function of the form:

$$m(t) = \begin{cases} \left(\dfrac{t}{t_1}\right)^2 & ; \quad 0 \le t \le t_1 \\ 1 & ; \quad t_1 < t < t_2 \\ e^{-\alpha(t_2 - t_1)} & ; \quad t_2 \le t \le D_0 \end{cases} \tag{1.2}$$

where t_1, t_2 and α are preselected parameters. The form of the modulating envelope given by equation 1.2 reflects the three phases of the strength of strong ground shaking. The strength of the ground motion increases rapidly from zero to a time t_1, it remains constant between t_1 and t_2, and decreases exponentially after t_2. Figure 1.1 shows the envelope function $m(t)$ for $D_0 = 12s$, $t_1 = 3s$, $t_2 = 5s$ and $\alpha = 1$.

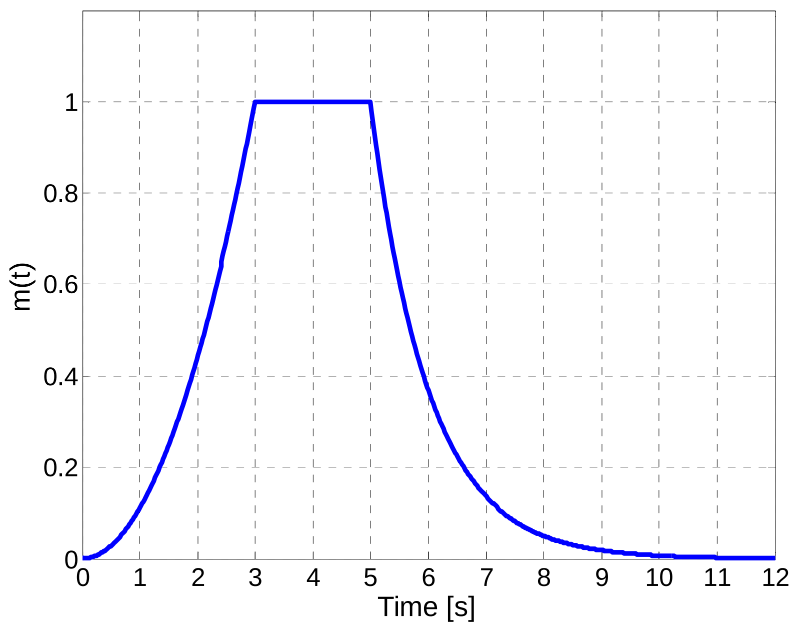

Figure 1.1. Deterministic modulating envelope function m(t).

Similar methods to the one presented by Scanlan and Sachs were proposed by Vanmarcke and Gasparini (1976), Iyengar and Rao (1979) and Preumont (1980, 1984). These methods are based on the iterative evaluation of the Fourier amplitudes so they match the response spectrum of the artificial time history with the target spectrum within a specified tolerance. These approaches did not account for the temporal variation of the frequency characteristics of the ground motion, and simply relied on a white noise signal with a time-dependent modulating function to simulate the nonstationarity in the ground motion. However, assuming a time-invariant frequency content of the ground motion may not be acceptable due to their sensitivity to the characteristics of individual pulses and their sequence within a ground acceleration time history (O'Connor and Ellingwood 1987).

Levy and Wilkinson (1976) represented the artificial record as the product of a modulating envelope function and a sum of harmonic functions. They used the following equation:

$$a_g(t) = m(t)\sum_{i=1}^{N} A_i \sin(\omega_i t) \tag{1.3}$$

The frequencies ω_i of the harmonic functions were selected so that they had overlapping points for the damping ratio of the target spectrum. The modulating envelope *m(t)* was selected by using the time variation of the strength of actual earthquakes such as the 1940 El Centro earthquake. The amplitudes A_i are scaled by the ratio of the target spectrum and the spectrum of $a_g(t)$ for each ω_i.

Others methods similar to that due to Levy and Wilkinson were proposed by Trifunac (1971), Wong and Trifunac (1979), Lee and Trifunac (1985, 1987, 1989), Lee (1990) and Trifunac (1990).These methods obtained more realistic time-histories by using the group velocity curves of various waves to compute the instant of first arrival and the relative phases of these waves. Watabe, Masao and Tohdo (1987), Gupta and Joshi (1993) and Shrinkhande and Gupta (1996) used the phase characteristics of recorded accelerograms.

There are other methods for generation of artificial accelerograms compatible with a design spectrum that are based on the modification of a recorded earthquake. Methods based on this feature were proposed by Tsai (1972); Rizzo, Shaw and Jarecki (1975); Lilhanad and Tsen (1988) and Mukherjee and Gupta (2002). Tsai (1972) proposed a procedure to modify an existing earthquake record that either suppresses or amplifies a local portion of its response spectrum without significantly affecting the remaining parts. To suppress undesirable frequencies the record was modified by passing it through a two-degree-of-freedom mechanical filter. To locally raise the input response spectrum, harmonic components of appropriate amplitude, central frequency, and phase were superimposed to the original record.

Rizzo, Shaw and Jarecki (1975) used the Fourier transform to modify existing records. The basic idea behind this approach is that the amplitude of the Fourier transform and the velocity response spectrum are in close agreement when the damping ratio is zero. Thus, they proposed to select an existing earthquake record and compute its amplitude Fourier spectrum and the response spectrum. Next, the response spectrum is compared against the target spectrum; the difference is used to modify the amplitude Fourier spectrum. The modification involves either scaling by a function of frequency or adding a function of frequency.

Lilhanand and Tsen (1988) adjusted actual earthquakes time histories to match the design spectra while minimizing the perturbations of their original characteristics. This method is a time-domain procedure based on the observation that the time at which the spectral response of a time history occurs, say t_i, is not perturbed by a small adjustment made on the time history. The accelerogram only is modified at a time t_i and it requires to solve a set of linear equations in an iterative way.

Most recently, Mukherjee and Gupta (2002) proposed a wavelet-based procedure to decompose a recorded accelerogram into a desired number of time-histories with nonoverlapping frequency contents. Each of the time-histories was suitably scaled to match its response spectrum with a specified design spectrum.

Some investigations (Naeim and Lew 1995, Bommer and Rugeri 2002) have revealed significant potential problems associated with the indiscriminate use of artificial spectrum compatible time histories in seismic design. Naeim and Lew (1995) demonstrated that such scaling of accelerograms is inconsistent with the definition and the purpose of design spectra and it may lead to unrealistic and physically incorrect ground motion accelerograms with serious practical implications. They generated a set of artificial accelerograms by means of two iterative procedures that involve scaling the Fourier amplitudes of the processed signal to match the corresponding amplitudes of the target response spectrum. An analysis performed to these artificial earthquakes showed that their displacement time histories obtained via direct double integration produced very unrealistic and physically impossible results and its input energy spectra exhibit high level of input energy spread over a very wide band of periods.

Bommer and Rugeri (2002) obtained artificial acceleration time-histories compatible with the design spectrum for an S1 soil site from the French seismic design code. The records, generated using the program SIMQKE, were found to be rather severe, specially for such a region of low to moderate seismicity.

1.3 Scope of the Thesis

The main goal of the thesis is to develop a wavelet based procedure to modify a recorded accelerogram so that its response spectrum matches a specified design spectrum. A second objective of the research is to develop a procedure to perform a baseline correction of the artificial earthquakes obtained. This is necessary since many available methods to perform baseline correction modify the frequency content of the record, and thus the application of these procedures to an artificial record could yield a non-compatible accelerogram. Here non-compatible means that the response spectrum of the corrected accelerogram does not match the target spectrum.

Another task to be undertaken as part of this work is an analysis in time and frequency (using the Continuous Wavelet Transform and the Fourier Transform). The analysis will include the recorded time-histories, the wavelet modified time-histories, and a set of spectrum-compatible time-histories generated by numerical simulation using the program WinSIMQKE. This program, which is a Windows version of the original SIMQKE code, was developed at the Civil Engineering & Surveying department of UPR-M. The objective behind this analysis is to examine the temporal variation of the frequency characteristics of the artificial ground motions generated by the two methodologies. In the case of the wavelet based approach, the frequency content of the modified records will be compared with the characteristics of the recorded accelerograms.

1.4 General Organization of the Thesis

Chapter I contains a general introduction to the thesis. The motivation and problem description are briefly discussed. The chapter continues with a review of the most relevant previous works on the subject of generation of artificial accelerograms that are compatible with a specified design spectrum. The scope and organization of the thesis are also included in the first chapter.

Chapter II contains an introduction to the wavelet theory used to develop the proposed spectrum-matching procedure and a complete description of a new proposed impulse response wavelet. There is also a complete explanation of the proposed methodology to modify appropriately historic earthquake records so that their spectra match the design spectrum. The methodology proposed is coded in *Matlab*® to make easier its implementation. At the end of the chapter several examples are presented to show the implementation and to verify the accuracy of the results of the proposed methodology.

Chapter III begins presenting some basic concepts that are necessary to understand and implement the procedure to perform the baseline correction of the spectrum compatible time histories. The procedure used for the baseline correction is explained in detail. This procedure was also coded in *Matlab*®. The chapter concludes with some examples to illustrate the application of the procedure and to corroborate that the baseline correction corrects the end velocities and displacements. Finally, it is verified that the method does not affect the compatibility of the records with the target spectrum.

Chapter IV is devoted to the analysis of the artificial earthquake records. The concepts of Arias Intensity, frequency analysis using the Fourier Transform and time-frequency analysis using the Wavelet Transform are explained. Also included in this chapter is the generation of a set of spectrum-compatible time-histories using the program SIMQKE. The use of this popular program is briefly described. A time-frequency analysis of the recorded time-histories, the wavelet modified time-histories, and the SIMQKE artificial time-histories is performed. The temporal variation of the frequency characteristics of the artificial and real ground motions is examined. In the case of the wavelet approach the frequency content characteristics are compared with those of the recorded accelerograms. It is shown that the simulated accelerograms obtained with SIMQKE lead to velocity and displacement time histories, as well as frequency contents that are very unrealistic. It is shown that in some cases the wavelet approach produces records that have very different characteristics than the real records which were used as starting point for their generation. This implies that the process may modify the original record such that this accelerogram no longer has the geologic, tectonic and source characteristics associated with the original records.

Due to the results obtained in Chapter IV, an alternative methodology to modify the records is proposed in Chapter V. This method is referred to as the “two-band matching procedure”. The previously mentioned problems occurred first and foremost because the smoothed response spectra used in design do not commonly correspond to the expected motion from a single realistic scenario. It is rather some envelope of many ground motions representative of different seismic sources. Therefore, it is proposed to divide the design spectrum (in this case the spectrum prescribed in the UBC-97) in two parts: one governed by local events and other that represents the effect of distant events. Two records associated with these different earthquakes are selected and modified to match each zone of the proposed spectra. It is shown that with the new matching procedure the temporal variations in the frequency content of the modified accelerogram are better retained.

The thesis ends with the conclusions and recommendations presented in Chapter VI. A summary of the main findings and achievements are included. A list of areas and specific topics where it is deemed that more work would be beneficial is also provided.

CHAPTER II

GENERATION OF ARTIFICIAL EARTHQUAKES

2.1 Introduction

This chapter is the core of the thesis and deals with the problem of generating spectrum-compatible artificial accelerograms. The continuous wavelet transform is used to decompose a recorded accelerogram into a desired number of component time histories. Next, each of the time histories is appropriately scaled so that its response spectrum matches a specified design spectrum at selected periods. The modified components are used to reconstruct an updated accelerogram and the process is repeated until convergence is obtained. To achieve this goal, a new wavelet, based on the impulse response function of an underdamped oscillator is proposed. The procedure is illustrated by modifying five recorded accelerograms with different characteristics so that their spectra match a ground design spectrum. The spectrum prescribed in the UBC-97 (ICBO 1997) code for a seismic zone 3 and soil type S_B (rock) is used as target in the numerical examples.

2.2 The Continuous Wavelet Transform

Conceptually the wavelet transform can be better explained by comparing it with the Fourier transform. The Fourier transform expresses any arbitrary transient function of time with duration T as the sum of a set of sinusoids (an infinite number in the case of the Continuous Fourier Transform).

Mathematically, the continuous Fourier transform is defined as:

$$F(\omega) = \int_{-\infty}^{\infty} f(t) e^{-i\omega t} dt \tag{2.1}$$

The result of the transform is the Fourier coefficients $F(\omega)$, which when multiplied by a sinusoid of corresponding frequency ω, yields the constituent sinusoidal components of the original signal. This is illustrated schematically in Figure 2.1.

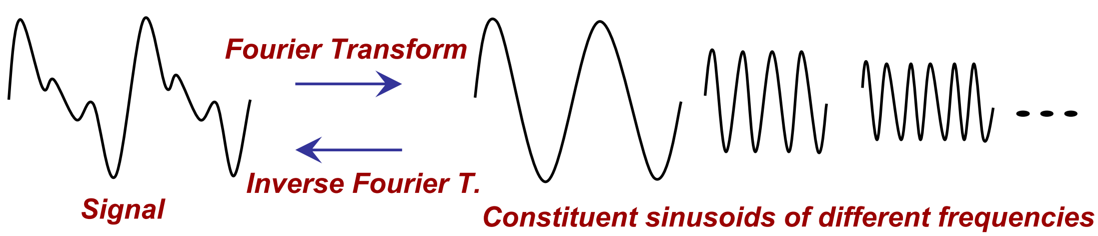

Figure 2.1. The Fourier and Inverse Fourier Transform.

Instead of breaking the signal down into a series of sinusoids which have constant amplitude, wavelet analysis modifies this mathematical technique by separating the signal into a series of wavelets, which are functions that have a very narrow frequency content and are also limited in length. The signal can be decomposed into a set of signals with different dominant frequencies occurring at different times. This decomposition is carried out by convoluting the signal with the wavelet of interest.

The continuous wavelet transform (*CWT*) is defined as the sum over all time of the signal multiplied by scaled and shifted versions of the wavelet function ψ:

$$C(scale, position) = \int_{-\infty}^{\infty} f(t)\psi(scale, position, t)dt \qquad (2.2)$$

The result of the *CWT* are wavelet coefficients *C* which are function of scale and position. Multiplying each coefficient by the appropriately scaled and shifted wavelet yields the constituent wavelets of the original signal This is illustrated schematically in Figure 2.2.

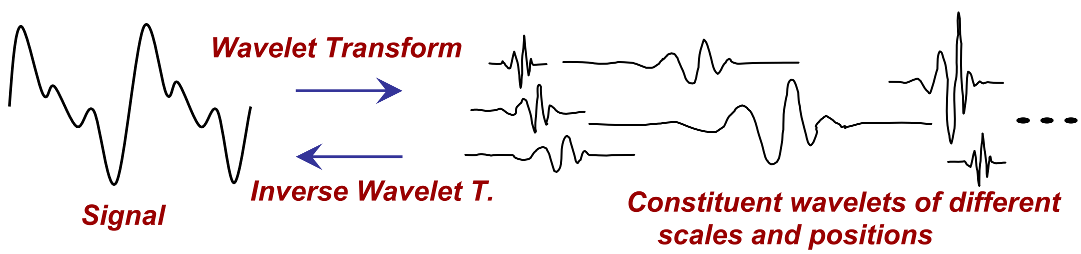

Figure 2.2. The Wavelet and Inverse Wavelet Transform.

Wavelet analysis starts by selecting from the existing wavelet families a basic wavelet function that can be a function of space *x* or time *t*. In the application of this thesis, the wavelets will be functions of time. The basic wavelet function, known as the "mother wavelet" $\psi(t)$, is then dilated (stretched or compressed) by a quantity *s* and translated in space by *p* to generate a set of basis functions $\psi_{s,p}(t)$ as follows:

$$\psi_{s,p}(t) = \frac{1}{\sqrt{s}}\psi\left(\frac{t-p}{s}\right) \qquad (2.3)$$

The function $\psi_{s,p}(t)$ is centered at *p* and it has a spread proportional to *s*. The wavelet transform (in its continuous or discrete version) correlates the function *f(t)* with $\psi_{s,p}(t)$. As mentioned before, the continuous wavelet transform is the sum over all times of the signal multiplied by the scaled and shifted version of the mother wavelet defined in equation 2.3:

$$C(s,p) = \frac{1}{\sqrt{s}} \int_{-\infty}^{\infty} f(t)\ \psi\left(\frac{t-p}{s}\right) dt = \int_{-\infty}^{\infty} f(t)\ \psi_{sp}(t)\, dt \tag{2.4}$$

The scale *s* and the position *p* are real numbers and $s > 0$. The result of the transform, i.e. the wavelet coefficients, shows how well a wavelet function $\psi_{s,p}(t)$ correlates with the signal analyzed.

The CWT has an inverse: the inverse CWT permits to recover the signal from its coefficients *C(s,p)* and is defined as

$$f(t) = \frac{1}{K_\psi} \int_{s=0}^{\infty} \int_{p=-\infty}^{\infty} C(s,p)\psi_{s,p}(t)\, dp \frac{ds}{s^2} \tag{2.5}$$

where the reconstruction constant K_ψ depends on the wavelet type, and is defined as:

$$K_\psi = \int_0^\infty \frac{|\psi(\omega)|^2}{\omega} d\omega < \infty \tag{2.6}$$

where $\psi(\omega)$ is the Fourier transform of the mother wavelet $\psi(t)$.

Another important concept for the applications of the wavelet theory presented in this thesis is the “detail function”. The detail functions are defined by fixing the scale *s* and sum on the position *p* in equation 2.5:

$$D(s,t) = \int_{-\infty}^{\infty} C(s,p)\psi_{s,p}(t)\frac{1}{s^2} dp = \frac{1}{s^{5/2}} \int_{-\infty}^{\infty} C(s,p)\psi\left(\frac{t-p}{s}\right) dp \tag{2.7}$$

Replacing equation 2.7 in equation 2.5, the signal can be recovered as:

$$f(t) = \frac{1}{K_\psi} \int_0^\infty D(s,t)\, ds \tag{2.8}$$

In practice, the detail functions will be calculated at discrete values s_j of the scale s and the integral will be replaced by a summation:

$$f(t) \simeq \frac{1}{K_\psi} \sum_{j=1}^{N-1} D_j(t) \cdot \Delta s_j \tag{2.9}$$

where $\Delta s_j = s_{j+1} - s_j$.

2.3 The New Impulse Response Wavelet

The selection of the proper wavelet for a given application is crucial for the successful implementation of the wavelet transform. For the generation of artificial earthquakes several candidates were tried during the course of the investigation. With the exception of the wavelet used by Basu and Gupta (1998), which is a modified form of the wavelet known as "Littlewood–Paley (L-P) basis function", all the other wavelets were unable to achieve the objective. The wavelet used by Basu and Gupta (1998) is defined as follows.

$$\psi(t) = \frac{1}{\pi\sqrt{(\sigma-1)}} \frac{\sin(\sigma\pi t) - \sin(\pi t)}{t} \tag{2.10}$$

Where σ is a parameter that controls how rapidly the wavelet decays. Figure 2.3 shows the Littlewood-Paley wavelet for $\sigma = 2^{1/4}$.

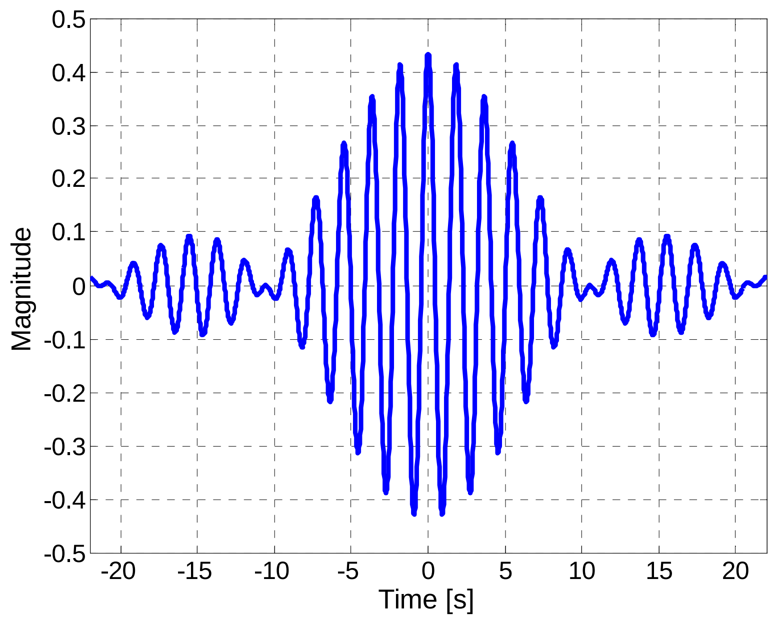

Figure 2.3. The Littlewood-Paley wavelet used by Basu and Gupta for $\sigma = 2^{1/4}$.

It is not clear why the other wavelets employed were not useful for the generation of artificial spectrum compatible records with the procedure (to be described later). One possible reason could be that they have fast temporal decays, which is not the case of the signal from an earthquake record. A new wavelet is proposed for the applications that are the objective of this thesis, based on the impulse response function of an underdamped oscillator. The mother wavelet has the following form:

$$\psi(t) = e^{-\zeta \Omega |t|} \sin \Omega t \tag{2.11}$$

where ζ and Ω are two parameters that govern the decrement and the time variation of the wavelet. They can be identified with the damping ratio ζ and natural frequency Ω of a single degree of freedom oscillator. The wavelet must be defined for $t < 0$ and it should go to zero as $t \to \infty$ and as $t \to -\infty$. Therefore, the absolute value of t is used in the exponential. This, in turn, leads to an antisymmetric wavelet as it is shown in Figure 2.4.

The Fourier transform $\psi(\omega)$ of the wavelet function $\psi(t)$ proposed in equation 2.11 is defined by:

$$\psi(\omega) = F[\psi(t)] = \int_{-\infty}^{\infty} \psi(t) e^{-i\omega t} dt = \int_{-\infty}^{\infty} e^{-\zeta\Omega|t|} \sin\left(\Omega t\right) e^{-i\omega t} dt \tag{2.12}$$

$$\psi(\omega) = \frac{4i\zeta\omega\Omega^2}{\omega^4 + 2(\zeta^2 - 1)\omega^2\Omega^2 + (\zeta^2 + 1)\Omega^4} \tag{2.13}$$

The graph of the absolute value of the expression in equation 2.13 is shown in Figure 2.5.

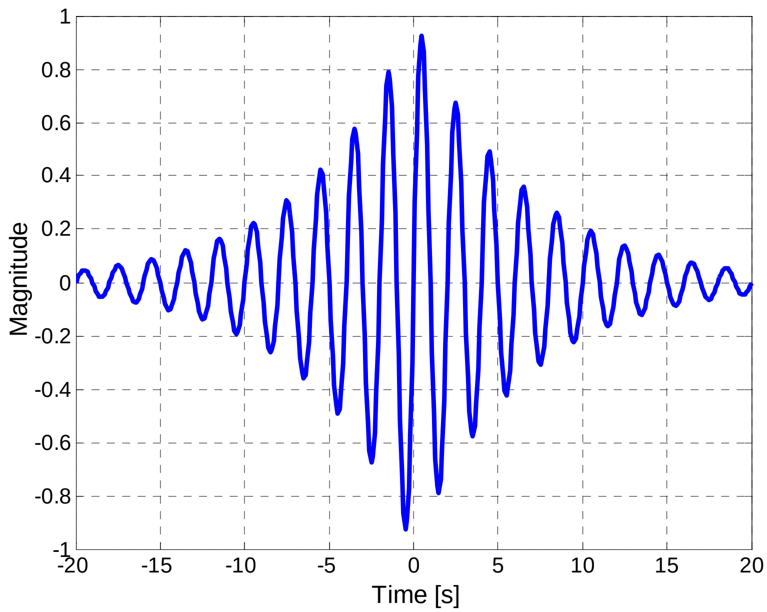

Figure 2.4. The proposed Impulse Response Wavelet for $\zeta = 0.05$ *and* $\Omega = \pi$ *rad/s.*

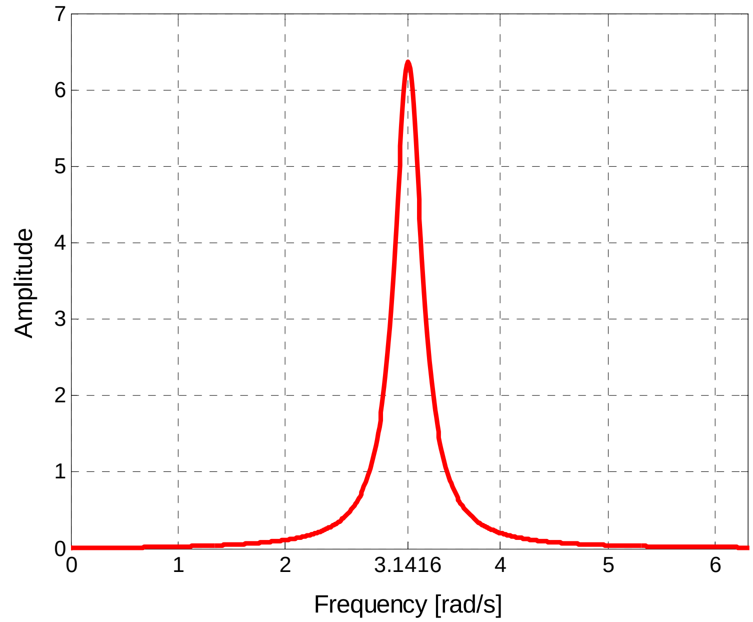

Figure 2.5. The Fourier transform of the Impulse Response Wavelet for $\zeta = 0.05$ *and* $\Omega = \pi$ *rad/s.*

It can be seen from Figure 2.4 that the wavelet function is limited in extent in the time domain, and from the Fourier transform of the wavelet in Figure 2.5, it is also bounded in the frequency domain. Increasing the value for ζ gives a greater compactness in the time domain, but less so in the frequency domain. A larger ζ reduces the amplitude of the peak in the Fourier transform. The value of Ω controls the dominant frequency of the wavelet. The values of the parameters $\zeta = 0.05$ and $\Omega = \pi$, used to generate Figures 2.3 and 2.4, are the same values which were found to be convenient for the modification of the recorded accelerograms.

For the impulse response wavelet, the reconstruction constant K_ψ required in equation 2.5 can be obtained from equation 2.6 using the Fourier transform given in equation 2.13:

$$K_{\psi} = \frac{-4\zeta\left(\zeta^2-1\right)+\pi\left(\zeta^2+1\right)^2+2\left(\zeta^2+1\right)^2\tan^{-1}\left(\frac{1}{2\zeta}-\frac{\zeta}{2}\right)}{4\zeta\left(\zeta^2+1\right)^2\Omega^2} \tag{2.14}$$

For $\zeta = 0.05$ and $\Omega = \pi$, the value of K_{ψ} is 3.18.

For the discrete implementation for the wavelet transform another function, is required besides the mother wavelet. Although this work does not deal with the discrete transform, to complete the characterization of the new impulse response wavelet we will discuss this function.

Suppose that the wavelet transform *C*(*s,p*) is only available for small scales, for instance $s < s_0$ and one needs to recover the function *f*(*t*). In this case we need the complement somehow the information corresponding to *C(s,p)* for $s > s_0$. To obtain this information another function $\phi(t)$, referred to as the *scaling function*, is introduced. According to Mallat (1999), the modulus of the Fourier transform of the scaling function is defined by:

$$\left|\Theta(\omega)\right|^2 = \int_1^{\infty} \frac{\left|\psi(s\omega)\right|^2}{s} ds \tag{2.15}$$

Applying equation 2.15 in the case of the impulse response wavelet leads to:

$$\left|\Theta(\omega)\right| = \frac{1}{2}\sqrt{\frac{\pi\omega^4+2\left(\pi\left(\zeta^2-1\right)-2\zeta\right)\Omega^2\omega^2+\left(-4\zeta^3+4\zeta+\pi\left(\zeta^2+1\right)^2\right)\Omega^4-2\left(\omega^4+2\left(\zeta^2-1\right)\Omega^2\omega^2+\left(\zeta^2+1\right)^2\Omega^4\right)\cot^{-1}\left(\frac{2\zeta}{\zeta^2+\frac{\omega^2}{\Omega^2}-1}\right)}{\zeta\Omega^2\left(\omega^4+2\left(\zeta^2-1\right)\Omega^2\omega^2+\left(\zeta^2+1\right)^2\Omega^4\right)}} \tag{2.16}$$

Figures 2.5 and 2.6 show, respectively, the modulus of the Fourier transform of the scaling function and the scaling function associated with the impulse response wavelet.

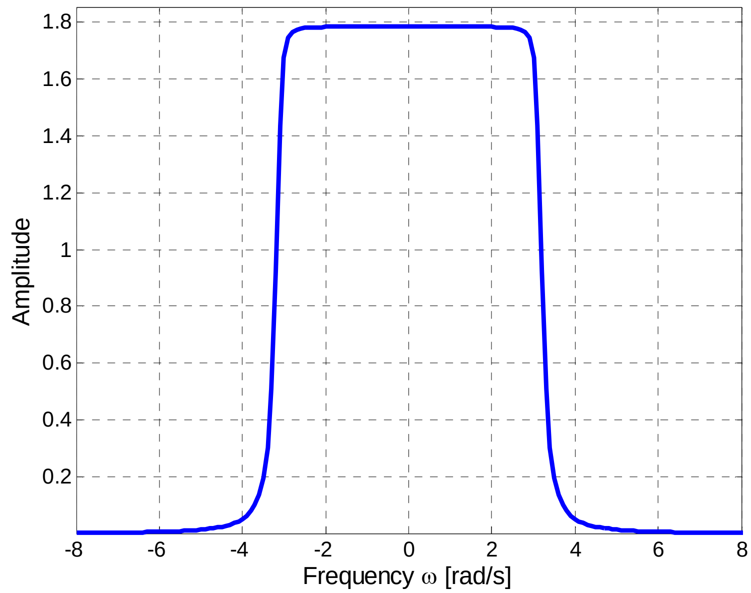

Figure 2.6. The Fourier transform of the scaling function associated to the Impulse Response Wavelet for $\zeta = 0.05$ *and* $\Omega = \pi$ *rad/s.*

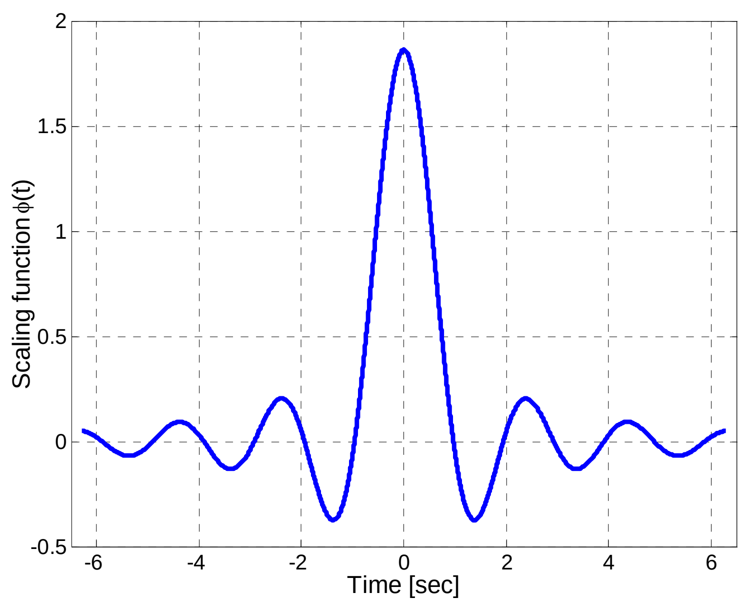

Figure 2.7. The scaling function associated to the Impulse Response Wavelet for $\zeta = 0.05$ *and* $\Omega = \pi$ *rad/s.*

2.4 The Proposed Spectrum-Matching Procedure

The proposed spectrum-matching procedure is based on the possibility of decomposing a recorded accelerogram into a finite number of time histories with a dominant frequency and then scaling those iteratively such that the resultant time-history is compatible with the specified design spectrum. The procedure is described in a step-by-step way next:

1. Read the earthquake data file $\ddot{X}_g(t)$ sampled at *Nt* points and define the type of spectrum that $\ddot{X}_g(t)$ is required to match (in our case, a PSA spectrum). Even though the procedure could be applied to any recorded accelerogram, it is desirable to choose one that has been recorded under similar conditions of earthquake source mechanisms and site geology.

2. Define the parameters *s* and *p* as follows:

$$s_j = 2^{j/\exp} \quad ; \quad j = -(N_0 - 1), -(N_0 - 2), \ldots, -(N_0 - N) \tag{2.17}$$

$$p_n = n \cdot \Delta p \quad ; \quad n = 0, 1, \ldots, Nt = \frac{t_f}{\Delta t} \tag{2.18}$$

   The value of *exp* will control the separation between the frequencies (or periods) that will be used for the modification of the record. The higher the value of *exp*, the lesser the separation between frequencies. After several tests, it was found convenient for the present application to use a value of *8* for *exp*. The values of N_0 and *N*, together with the value of *exp*, will define the bandwidth between the discrete frequencies. These parameters were taken equal to N_0=*51* and *N*=*63* for the numerical implementations. The times t_f and Δt are the final time and the sampling rate of the accelerogram, respectively.

3. Calculate the continuous wavelet transform applying the discrete version of equation 2.4.:

$$C(s_j, p_n) \simeq \frac{\Delta t}{\sqrt{s_j}} \sum_{k=1}^{Nt} \ddot{X}_g(t_k)\psi\left(\frac{t_k - p_n}{s_j}\right) \tag{2.19}$$

4. Calculate the "detail functions" $D(s,t)$ using the discrete form of equation 2.7:

$$D_j(t) = \frac{\Delta t}{s_j^{5/2}} \sum_{n=1}^{Nt} C(s_j, p_n)\psi\left(\frac{t - p_n}{s_j}\right) \tag{2.20}$$

5. For the proposed impulse response wavelet, the dominant frequency for each detail function can be defined by examining equations 2.3 and 2.9 as follows:

$$\psi\left(\frac{t - p_n}{s_j}\right) = e^{-\xi\Omega\left|\frac{t-p_n}{s_j}\right|} sin\left(\frac{\Omega t - p_n}{s_j}\right) \tag{2.21}$$

$$\omega_j = \frac{\Omega}{s_j} \quad ; \quad T_j = \frac{2\pi}{\Omega} s_j; j = 1, 2, ..., N \tag{2.22}$$

Based on equations 2.17 it could be said that *j* will take values from *j = -50* to *12*, this implies that *s* will take values from *s = 0.0131* to *2.8284*. Using equations 2.22, the frequencies will take values from *ω = 0.1768Hz (T = 5.6569 s)* to *38.0546 Hz (T = 0.0263 s)*. The predominant frequency for several detail functions are shown in Table 2.1, Figures 2.13 to 2.17 show these details and its Fourier transform for the case of the wavelet decomposition of an earthquake record.

Table 2.1. Dominant frequencies of selected details.

Detail #	j	s_j	ω_j [rad/s]	T_j [s]	f (Hz)
1	-50	0.0131	239.1	0.0263	38.05
10	-41	0.0287	109.6	0.0573	8.33
20	-31	0.0682	46.1	0.1363	7.34
40	-11	0.3856	8.1	0.7711	1.30
60	9	2.1810	1.4	4.3620	0.23

6. Reconstruct the accelerogram applying equation 2.8:

$$\ddot{X}_g(t) \simeq \sum_{j=1}^{N-1} D_j(t) \cdot \Delta s_j \tag{2.23}$$

7. Calculate the ground response spectrum of the reconstructed signal $\ddot{X}_g(t)$ at the values of the periods T_j defined by the discrete values of s_j in equation 2.21 (a few of these values are shown in Table 2.1). Then compute the ratios γ_j between the values of the target and the calculated spectra:

$$\gamma_j = \frac{\left[Sa(T_j)\right]_{target}}{\left[Sa(T_j)\right]_{reconstructed}} \tag{2.24}$$

8. Multiply the detail functions $D(s_j,t)$ by these ratios and obtain a new accelerogram using equation 2.23. Calculate the response spectrum of this updated accelerogram, compute a set of new ratios γ_j and correct the previous detail functions. The process continues until the ratios become sufficiently close to 1 or a pre-established maximum number of iteration is reached.

In order to verify the convergence of the iterative process, a measure of the error is needed. It is proposed to use the Root-Mean-Square of the differences in percent at each of the N periods. The error can be calculated in each iteration using the following equation.

$$e(\%) = \sqrt{\frac{1}{N}\sum_{j=1}^{N}\left(\frac{PSA(T_j)_{target} - PSA(T_j)_{reconstructed}}{PSA(T_j)_{target}}\right)^2} *100 \qquad (2.25)$$

2.5 Numerical Examples

To illustrate the procedure proposed, the records of five earthquakes with widely different characteristics have been selected. It is desired to modify these records so they will be compatible with the ground design spectrum prescribed in the UBC-97 (ICBO 1997) code for a seismic zone 3 and soil type S_B (rock). The target spectrum is shown in Figure 2.8. The ground motion records used in the thesis and their main characteristics are shown in Table 2.2.

Table 2.2. Earthquake motions used for the numerical examples.

Earthquake date, time and magnitude	Station	Distance (km)	USGS Site Class.	Comp	PGA (g)	Total duration (s)
Coalinga, CA 1983/05/09 02:49 Ms(4.7)	1608 Oil Field Fire St	Hypocentral (12.1)	A	360	0.178	10
Loma Prieta, CA 1989/10/18 00:05 Ms(7.1)	58117 Treasure Is.	Closest to fault (82.9)	D	090	0.159	40
Coyote Lake, CA 1979/08/06 17:05 Ms(5.6)	57217 C.L Dam	Closest to fault (3.2)	A	160	0.157	28
Friuli, Italy 1976/09/15 03:15 Ms(5.7)	8014 Forgaria C.	Hypocentral (13.5)	B	000	0.26	22
Round Vallley, CA 1984/11/23 19:12 Ms(5.7)	1661 Mc Creek-S	Hypocentral (19.0)	C	270	0.088	7

These records were obtained from the PEER Strong Motion Database (http://peer.berkely.edu/smcat). It was verified that the final velocity and displacement of each of the five accelerogram were zero at the end of the record.

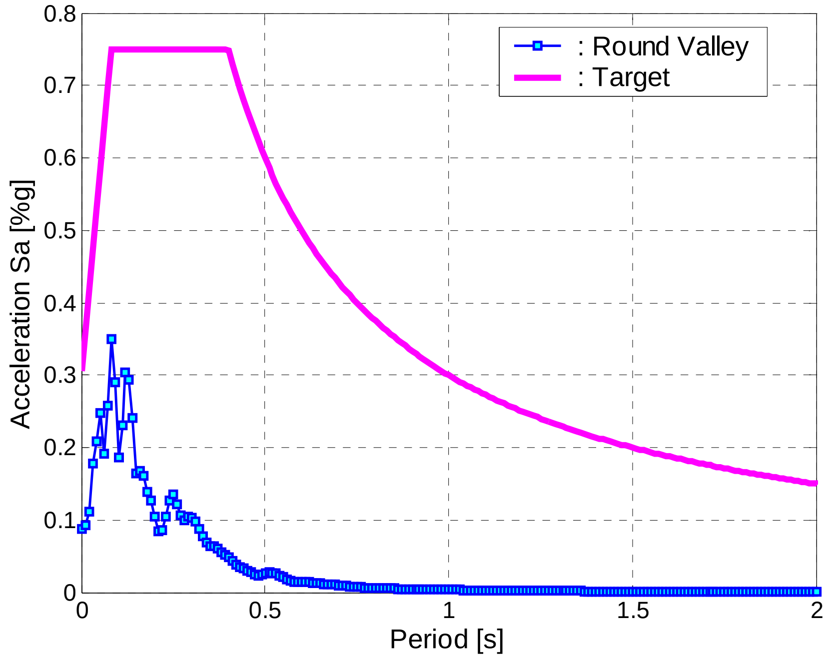

Figure 2.8. The UBC-97 zone 3-soil S_B design spectrum and the original response spectrum of the Round Valley record for 5% damping ratio.

Figures 2.8 to 2.22 show the spectrum-matching procedure applied to the Round Valley earthquake. The trace of the original Round Valley record is shown in Figure 2.9. This ground motion has a peak ground acceleration (PGA) equal to 0.088g and the total duration is approximately 7s.

The PGA of the target design spectrum is 0.3g. The acceleration in this and all other plots is shown as a fraction of the acceleration of gravity, and for brevity is indicated as %g.

The response spectrum for a 5% damping ratio of the original record is displayed in Figure 2.8. Figure 2.10 shows the coefficients *C(s,p)* that result from the application of equation 2.18 to the signal shown in Figure 2.9. Note that for the values of the scaling factor greater than about 0.5, the wavelet coefficients decrease significantly. According to equation 2.21 this corresponds to a dominant period of the signal of $T = \left(2\pi / \pi \right) 0.5 = 1s$.

Figure 2.11 is similar to Figure 2.10, but now the wavelet coefficients *C(s,p)* are shown in two dimensions and their absolute values are plotted. This is the usual form to graph the coefficients and it is called a Wavelet Map. The lighter colors indicate higher values of the wavelet coefficients. Observing this graph one can conclude that the original accelerogram has dominant component signals around 2 to 4 seconds, and their frequencies are associated with values of the scaling factor from less than 0.3. Figure 2.12 is a zoom of Figure 2.11. This figure allows us to identify 0.06 as the scaling factor associated with the lightest color. This value corresponds to a frequency of $\omega = \pi / 0.06 = 52.36\, rad/s$ and a period of 0.12 seconds. It is interesting to observe that the higher accelerations in the record of Figure 2.9 occur from 2 to 4 seconds. Also the response spectrum has the highest peak in the vicinity of a period equal to 0.12 s (see Figure 2.8).

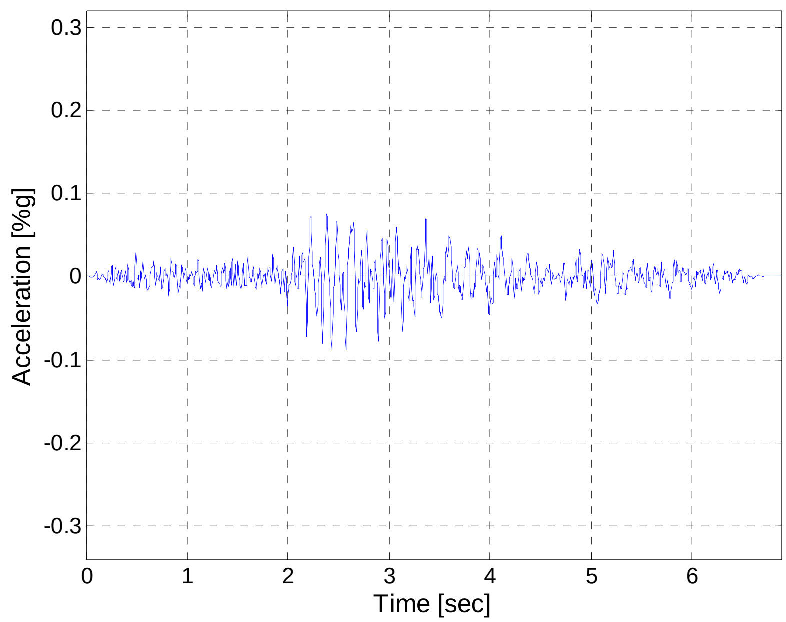

Figure 2.9. Original acceleration time history of the Round Valley earthquake.

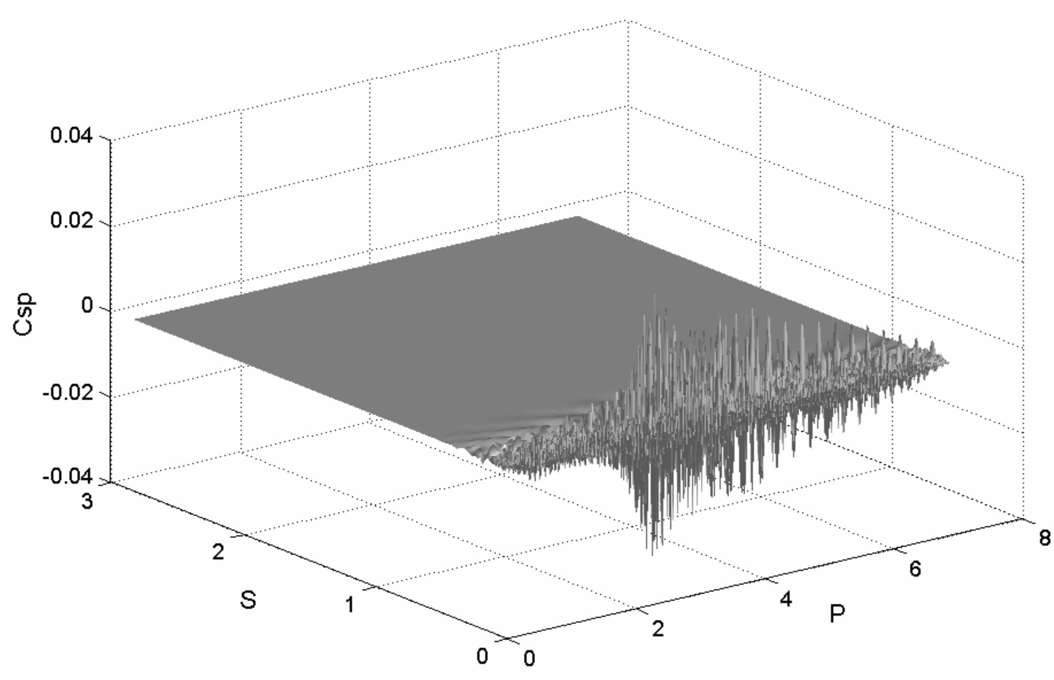

Figure 2.10. Coefficients C(s,p) from the Continuous Wavelet Transform.

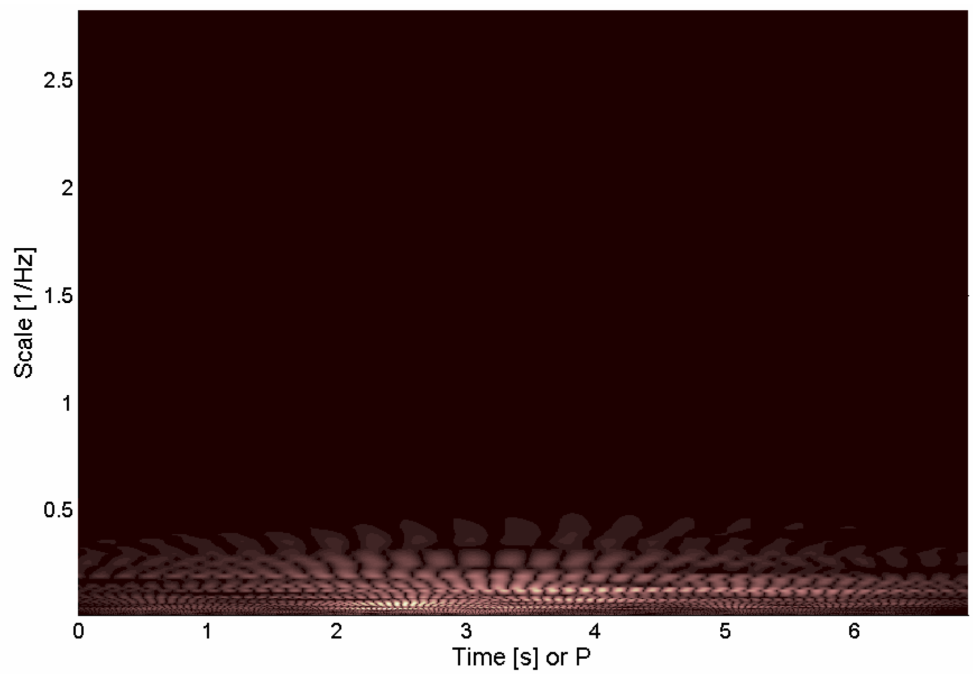

Figure 2.11. Top view of the absolute values of the coefficients C(s,p) for the signal of the Round Valley earthquake.

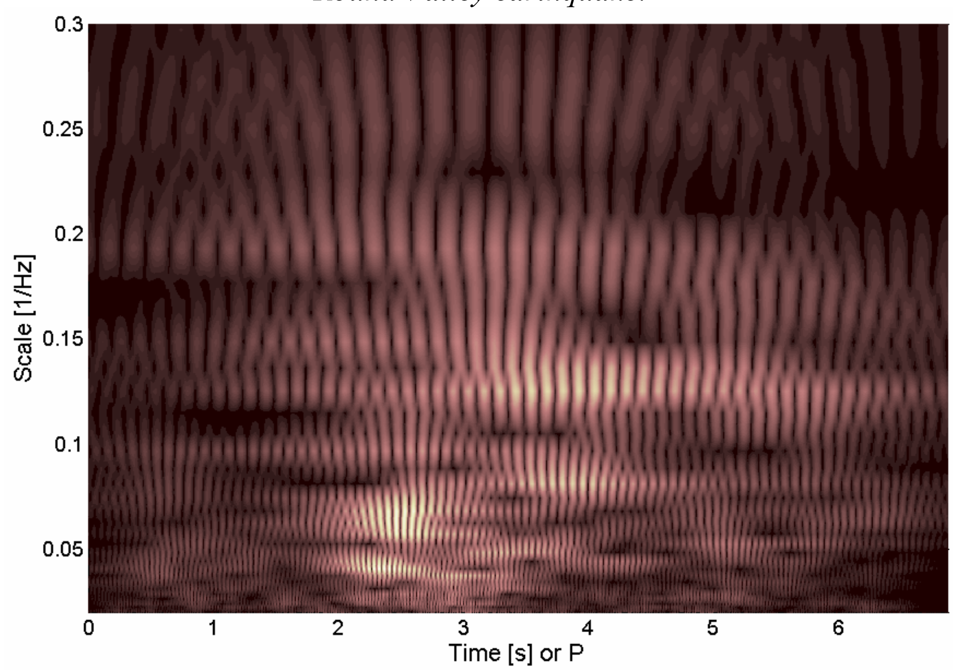

Figure 2.12. Zoom of Figure 10.

The following five figures show the detail functions defined in equation 2.19. Also shown in the same figures is the modulus of the Fourier transform of $D_j(t)$. The original spectrum is shown alongside with the “smoothed” spectrum. The latter spectrum is obtained by performing a running average of the original spectrum, i.e. calculating each new value as the average of the values at the neighboring points. The smooth spectrum allows one to more clearly appreciate the dominant frequencies. The details functions shown in Figures 2.13 through 2.17 correspond to the scale parameters listed in Table 2.1. It can be seen that each detail function has a dominant frequency that coincides with that listed in Table 2.1.

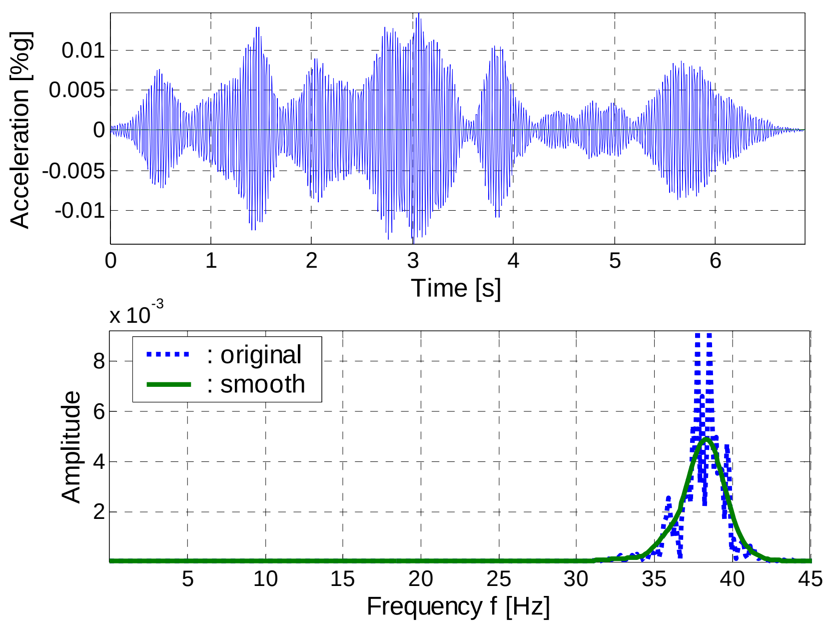

Figure 2.13. Detail function # 1(j=-50) and the magnitude of its Fourier transform with a dominant frequency at 38 Hz.

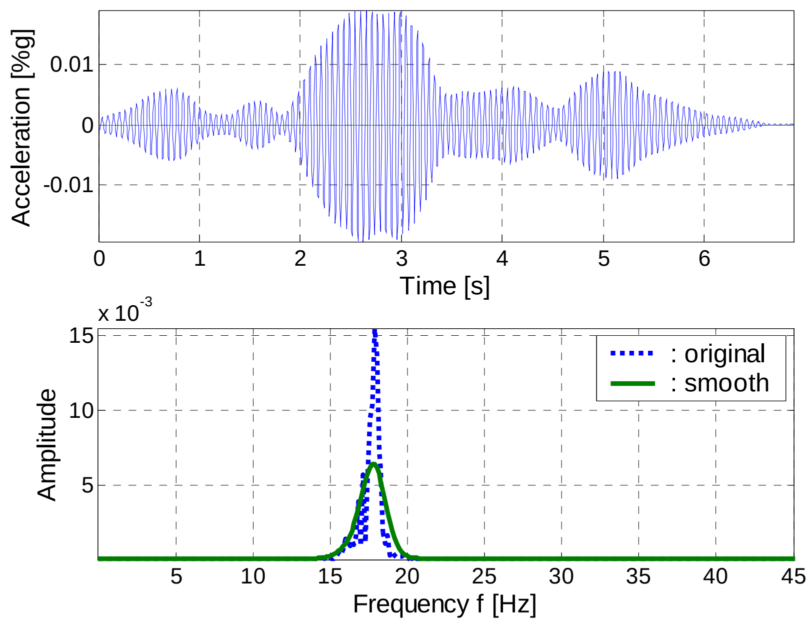

Figure 2.14. Detail function # 10 (j=-41) and the magnitude of its Fourier transform with a dominant frequency at 17.5 Hz.

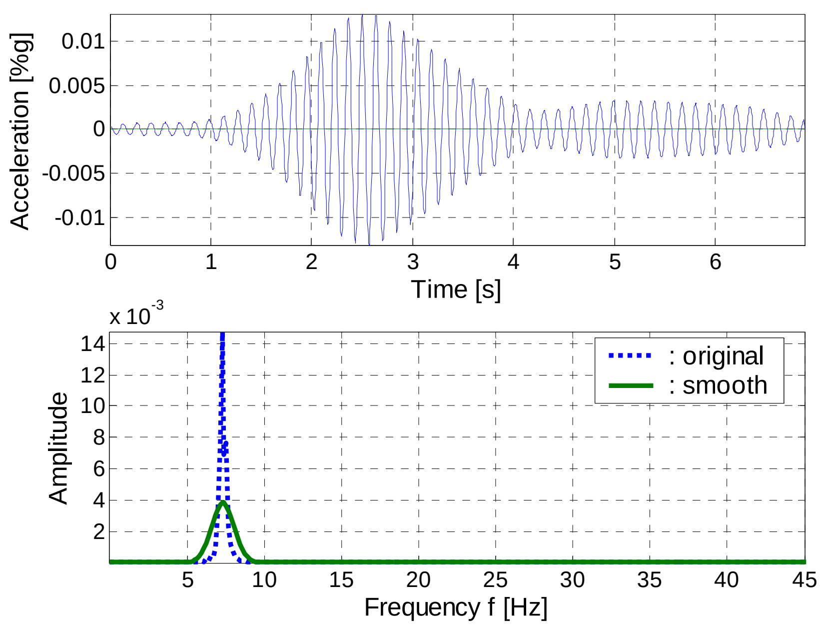

Figure 2.16. Detail function # 20 (j=-31) and the magnitude of its Fourier transform with a dominant frequency at 7.3 Hz.

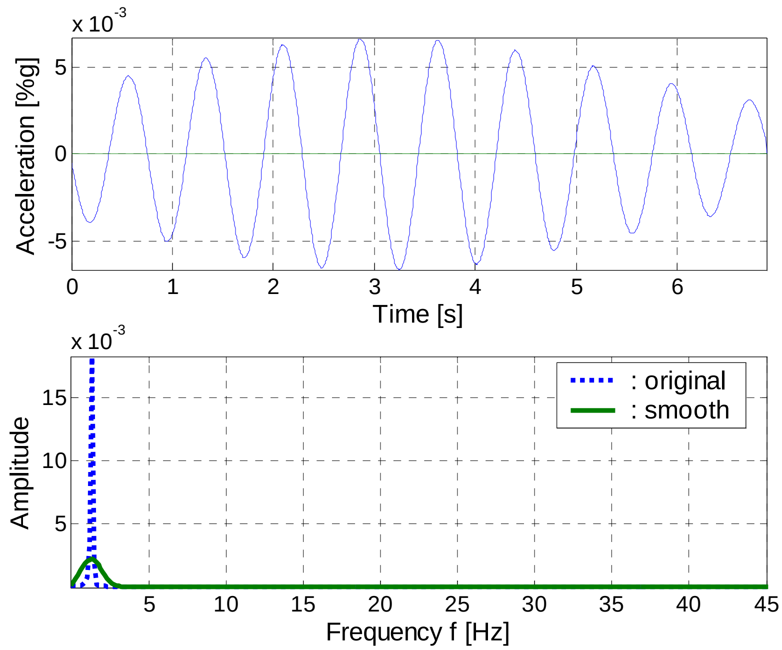

Figure 2.17. Detail function # 40 (j=-11) and the magnitude of its Fourier transform with a dominant frequency at 1.3 Hz.

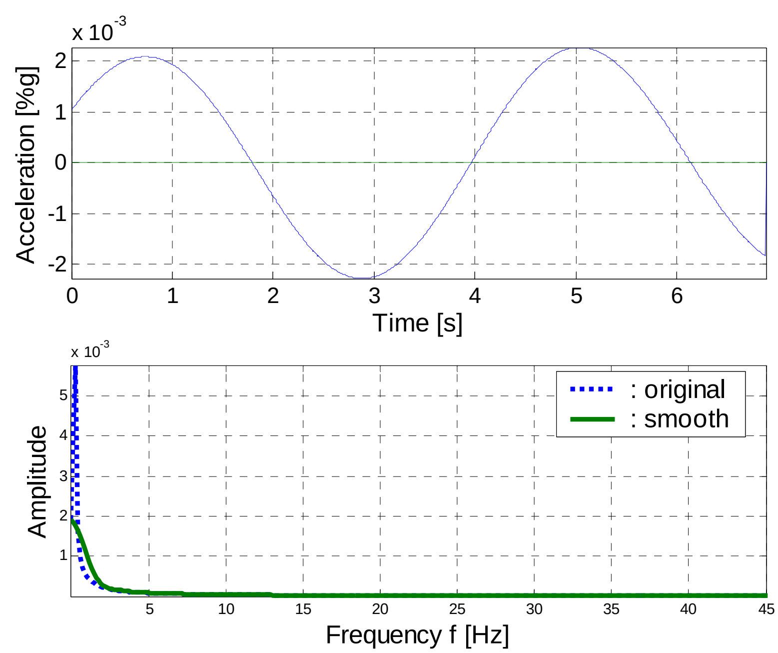

Figure 2.17. Detail function # 60 (j=9) and the amplitude of its Fourier transform with a dominant frequency at 0.23 Hz.

Figure 2.18 shows the results of the matching procedure at each iteration step, i.e. the response spectra of the acceleration time histories obtained by adding the detail functions corrected with the factor γ_j defined in equation 2.24.

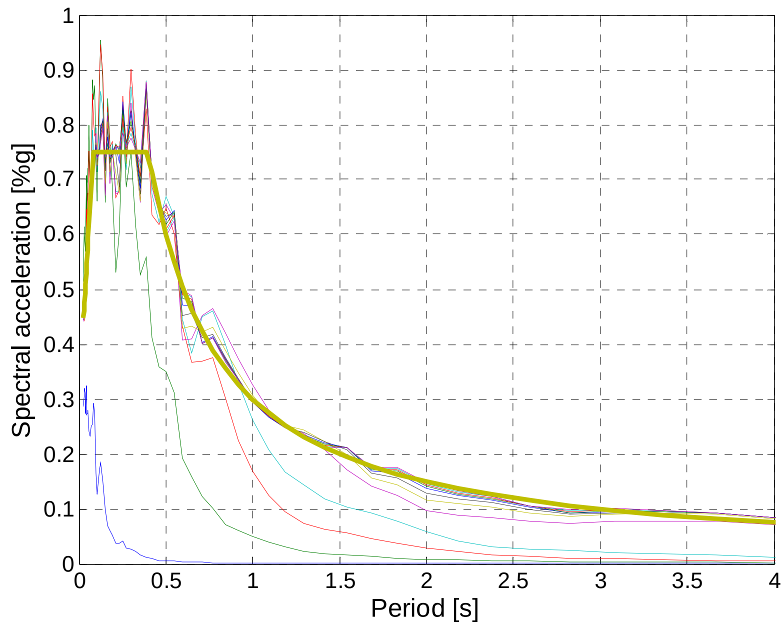

Figure 2.18. The target spectrum and the spectra of the modified record of the Round Valley earthquake after each iteration step.

For a better visualization the results at each of the last iteration step are shown separately in Figure 2.19. The spectrum is evaluated at each of the dominant periods of the 63 detail functions ranging from 0.026 to 5.657 seconds (Figure 2.19 only shows the spectrum in the range 0 – 4 seconds). The response spectrum of the modified record evaluated at periods equally spaced at intervals of 0.05 seconds is shown in Figure 2.20.

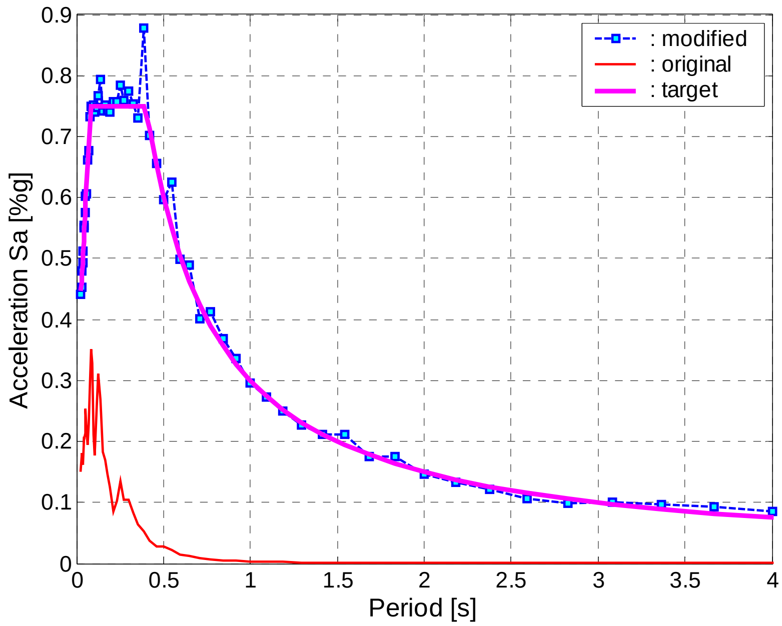

Figure 2.19. The target spectrum and the spectra of the original and modified Round Valley record (evaluated at the details dominant periods).

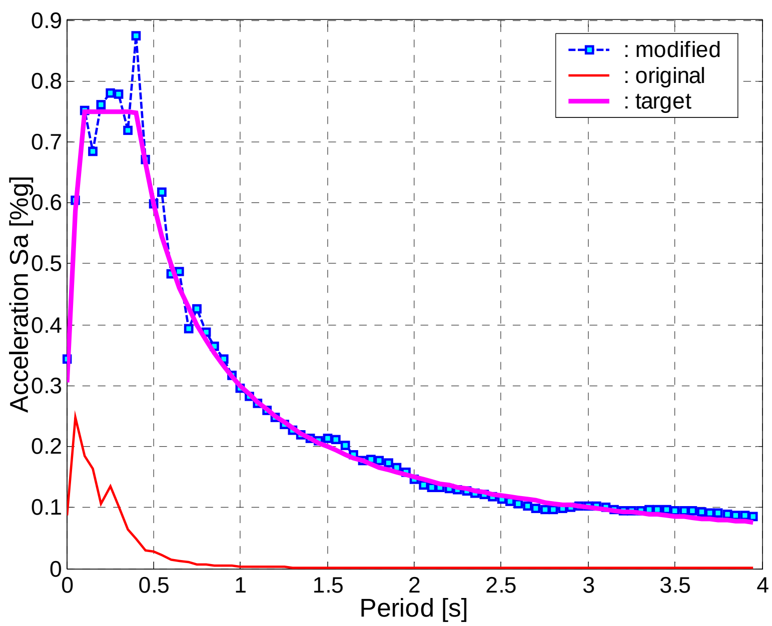

Figure 2.20. The target spectrum and the spectra of the original and modified Round Valley record (evaluated at equally spaced periods spaced 0.05 seconds apart).

The final accelerogram, compatible with the UBC spectrum, is displayed in Figure 2.21. This accelerogram should be compared with the original one, shown in Figure 2.9. Note that the total duration of the earthquake record remains the same (7 seconds). Note also that some of the high frequency components have been eliminated (or its relative contribution highly diminished). The record is not yet ready to be used, as explained in the following chapter. The final figure with results for the Round Valley earthquake shows the RMS error defined in equation 2.24 as a function of the iteration steps. Figure 2.22 shows that the error begins at about 60% and rapidly decreases as the iteration process progress. After the seventh cycle the error tends to diminish less quickly. The process was stopped at the eleventh cycle when the RMS error was less than 6 percent.

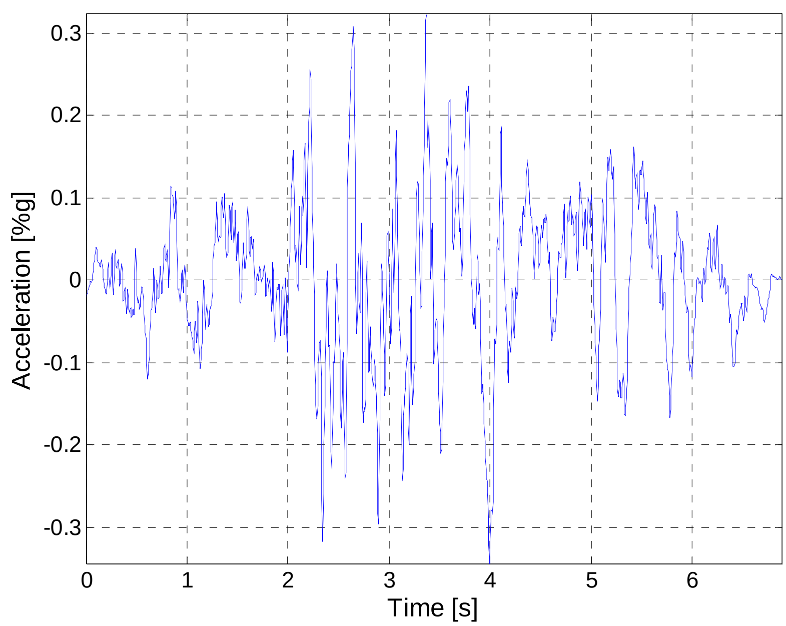

Figure 2.21. The modified spectrum-compatible accelerogram of the Round Valley earthquake.

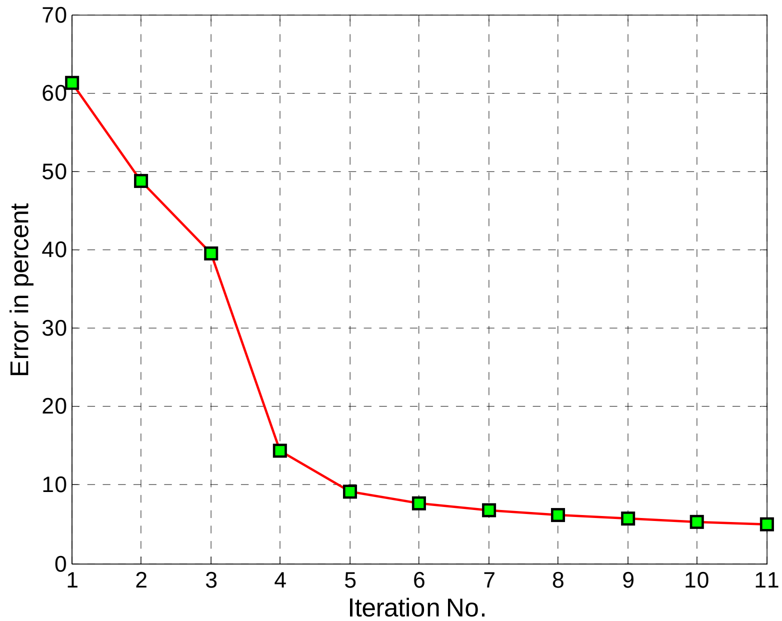

Figure 2.22. Variation of RMS error with the iteration step for the Round Valley earthquake.

Figures 2.23 to 2.30 show the results of same procedure just demonstrated for the Round Valley earthquake but this time for an accelerogram registered during the 1976 Friuli earthquake.

Figure 2.23 displays the original record, which has a total duration of 22 seconds and a maximum acceleration of 0.26g. The coefficients *C(s,p)* obtained from the continuous wavelet transform (using the proposed wavelet) are shown in Figure 2.24. The same coefficients are shown in a two dimensional plot in Figure 2.25. It is recalled that the lighter colors correspond to higher absolute values of the coefficients *C(s,p)*. It can be seen that at the lower values of the scale *s* the coefficients have higher values around 3 to 6 seconds. It must be kept in mind that the scale *s* is inversely proportional to the frequency (see equation 2.21), i.e. the lower scales correspond to higher frequencies.

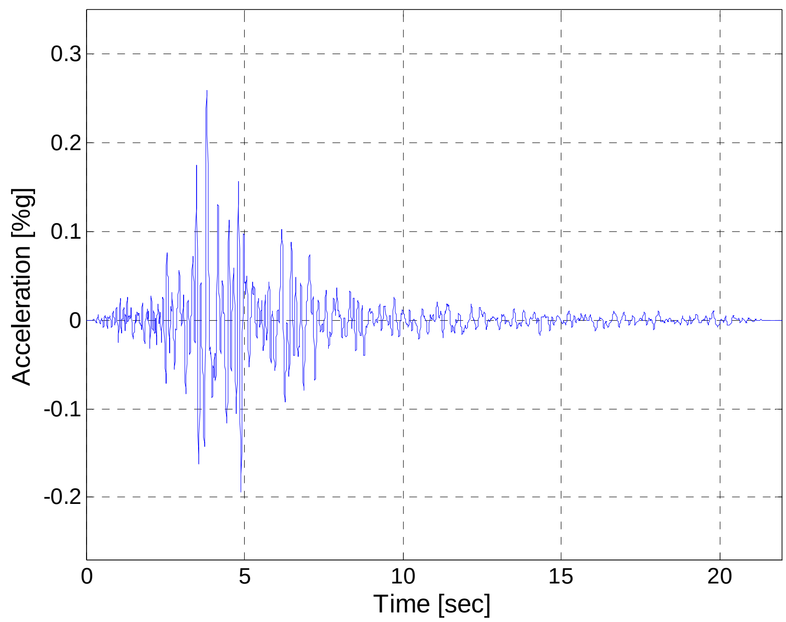

Figure 2.23. Original acceleration time history of the Friuli earthquake.

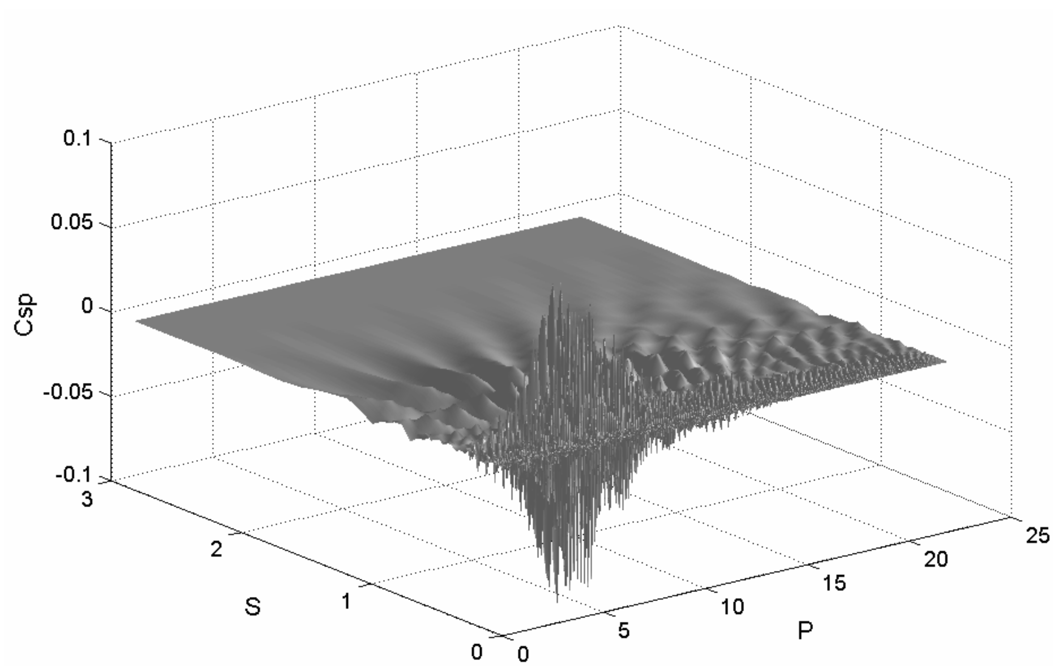

Figure 2.24. Coefficients C(s,p) from the Continuous Wavelet Transform for the Friuli earthquake.

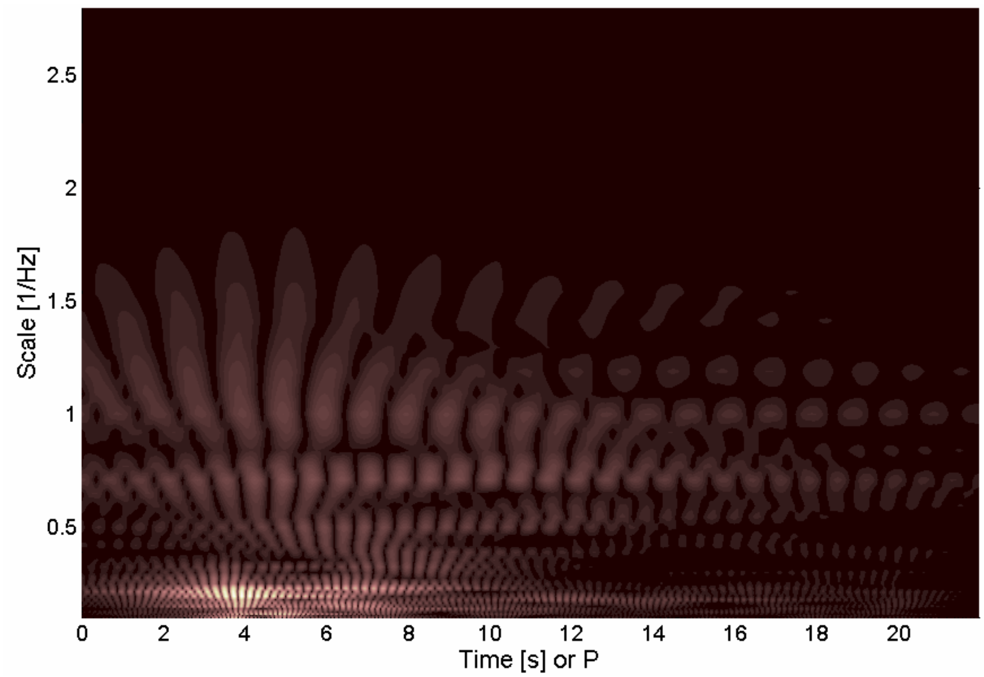

Figure 2.25. Wavelet map of the Friuli record.

Figure 2.26 presents the ground response spectra of the original and modified accelerograms at the different iteration steps. To illustrate the convergence, the target (i.e. UBC-97) design spectrum is also shown in the figure.

The final spectrum after 11 iterations is shown in Figure 2.27 along with the target spectrum. The response spectrum of the modified Friuli record was evaluated at the 63 dominant periods of the detail functions that make up the accelerogram. Also included in the figure is the original response spectrum.

The response spectrum of the modified record evaluated at periods equally spaced at intervals of 0.05 seconds is shown in Figure 2.28.

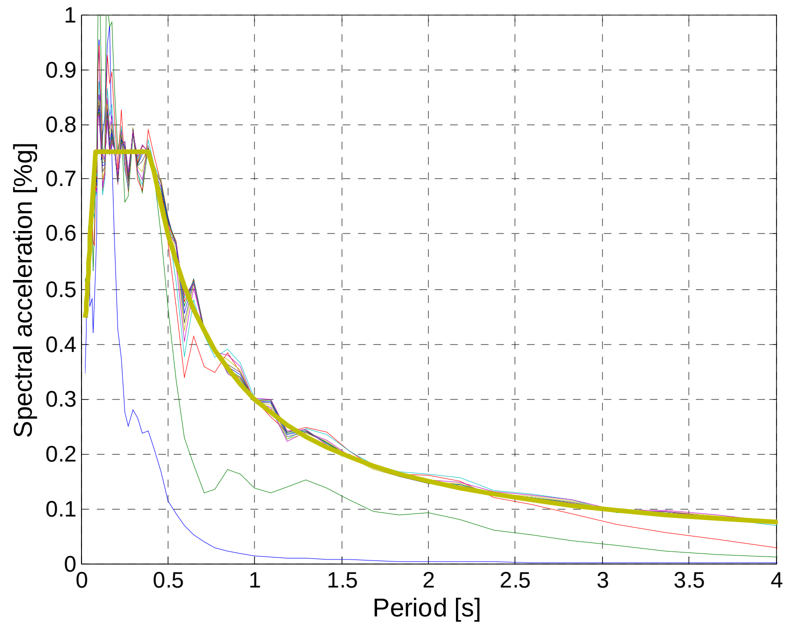

Figure 2.26. The target spectrum and the spectra of the modified records of the Friuli earthquake after each iteration step.

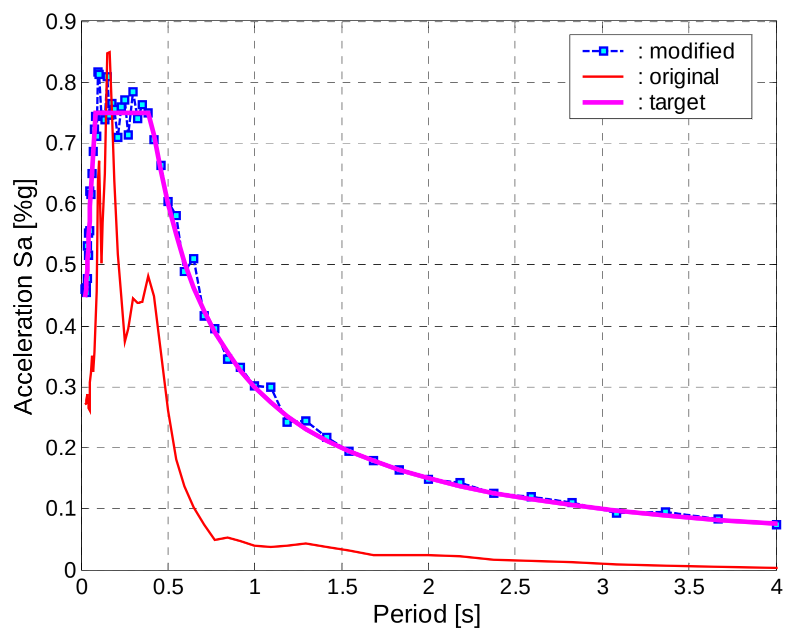

Figure 2.27. The target spectrum and the spectra of the original and modified record of the Friuli earthquake (evaluated at the details dominant periods).

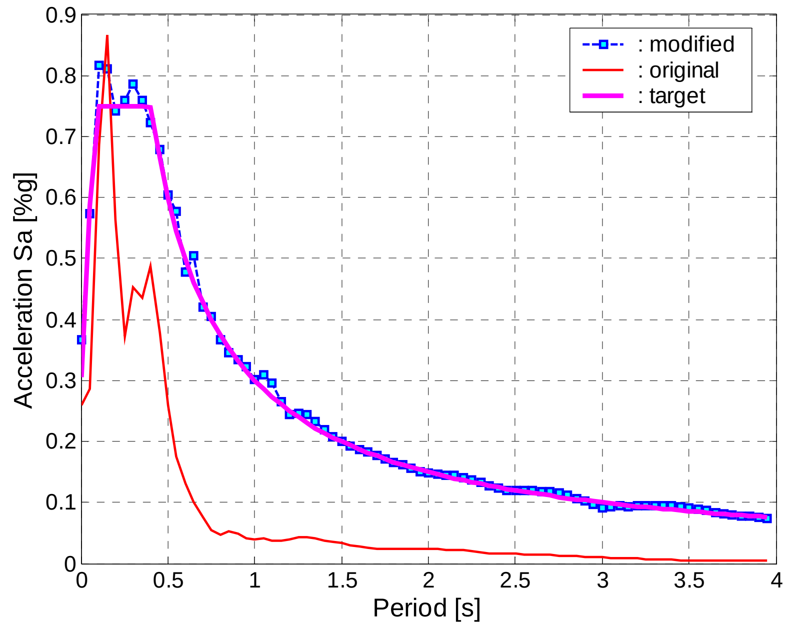

Figure 2.28. The target spectrum and the spectra of the original and modified record of the Friuli earthquake (evaluated at equally spaced periods spaced 0.05 seconds apart).

The acceleration time history corresponding to the spectrum-compatible record for the Friuli earthquake is displayed in Figure 2.29. The PGA of the modified record is 0.36g and the total duration remained unchanged. Besides scaling up the peaks (which is a trivial task), the wavelet matching procedure changed the relative importance of the detail functions that form the accelerogram. Since each detail function has a dominant frequency, in effect the process modifies the frequency content of the original record.

Figure 2.30 presents the RMS error in percent as the iteration process takes place. The trend here is similar to that observed for the Round Valley earthquake. The initial error is quite high and it diminishes quickly. The iterations were stopped when the error was about 4 percent.

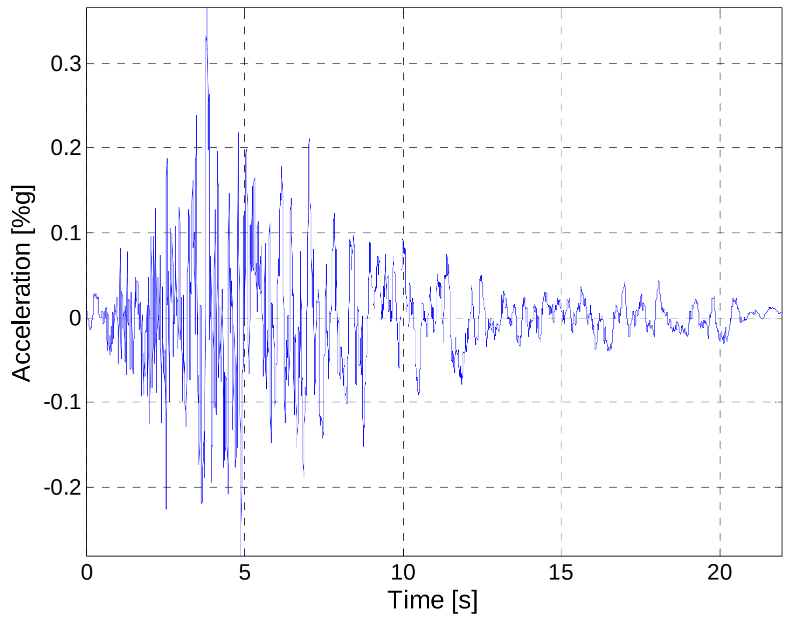

Figure 2.29. The modified spectrum-compatible accelerogram of the Friuli earthquake.

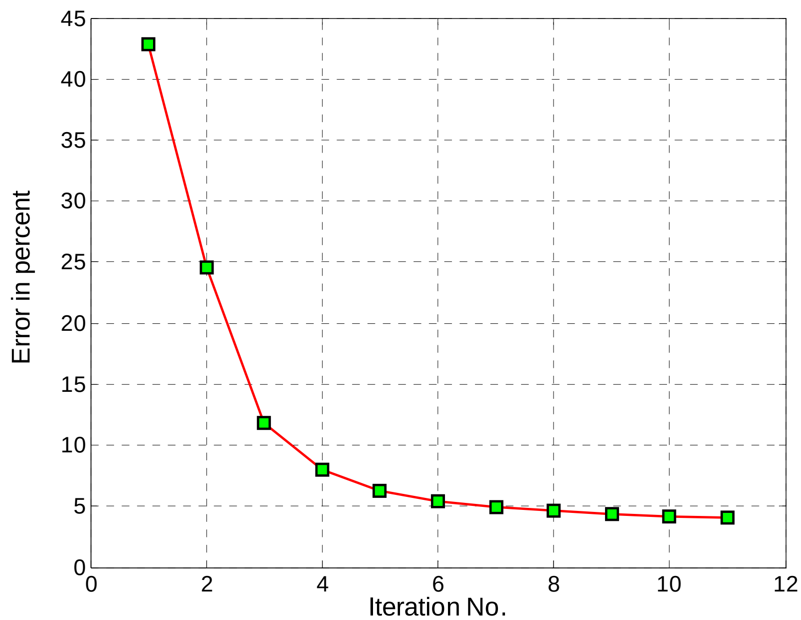

Figure 2.30. Variation of the RMS error with the iteration step for the Friuli earthquake.

The results for the remaining three records, namely the Coalinga, Coyote Lake and Loma Prieta earthquakes are shown in the next five figures, For the sake of brevity, only the original and modified records along with its final (compatible) response spectra are shown here. Figure 2.31 presents the raw accelerograms and Figure 2.32 the records after the matching procedure converged (within a tolerance margin).

Comparing Figures 2.31 and 2.32, it can be noticed that in the case of the Coyote Lake and Loma Prieta earthquakes, the wavelet-based procedures magnified the relative importance of the component signals with higher frequencies. Interestingly, in the case of the Round Valley earthquake, the opposite was true, i.e. the components with lower frequencies were the ones that were augmented. For the other two records, Friuli and Coalinga, it is difficult to tell which is the situation from a visual comparison of the original and modified accelerograms.

Figures 2.33 to 2.35 show, respectively, the original modified and target spectra for the Coalinga, Coyote Lake and Loma Prieta records. The response spectra of the modified records are evaluated at constant intervals of 0.05 seconds.

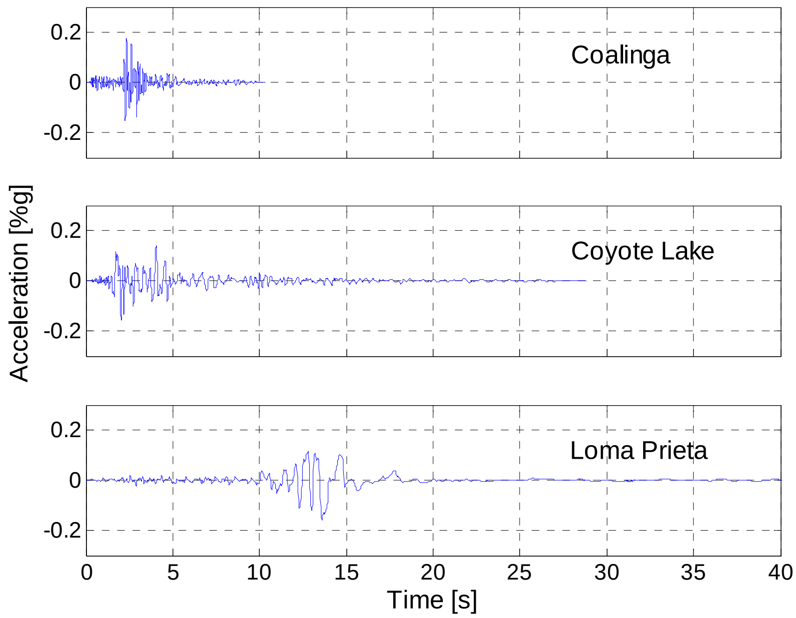

Figure 2.31. Original records of the Coalinga, Coyote Lake and Loma Prieta earthquakes.

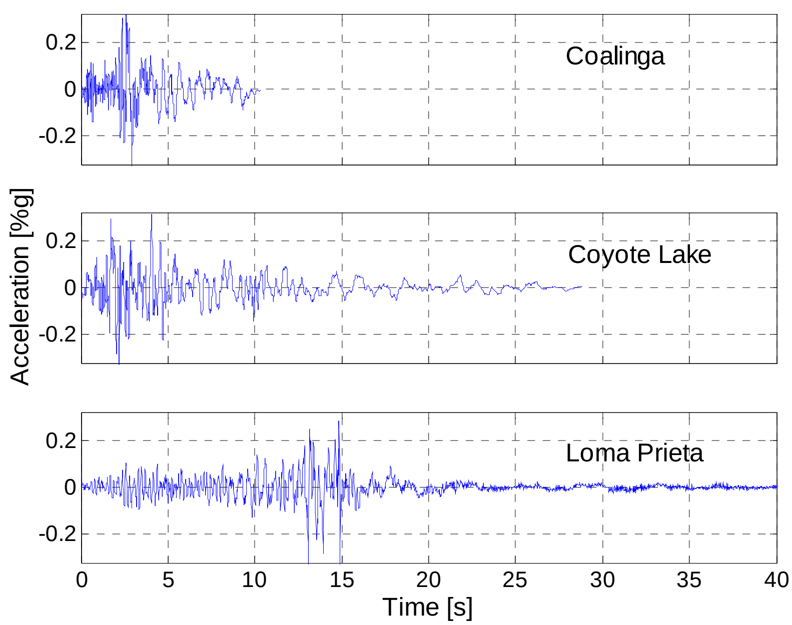

Figure 2.32. Modified records of the Coalinga, Coyote Lake and Loma Prieta earthquakes.

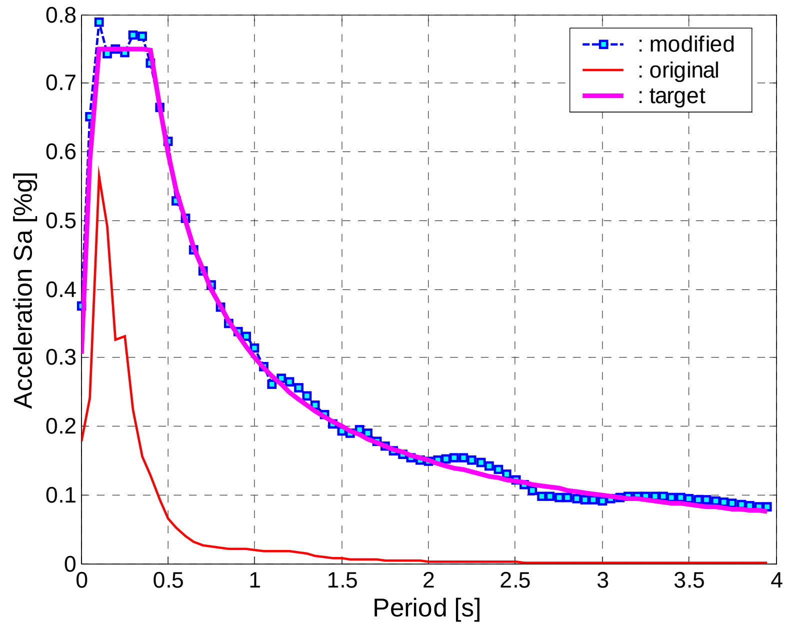

Figure 2.33. The target spectrum and the spectra of the original and modified record of the Coalinga earthquake evaluated at periods spaced at 0.05 seconds intervals.

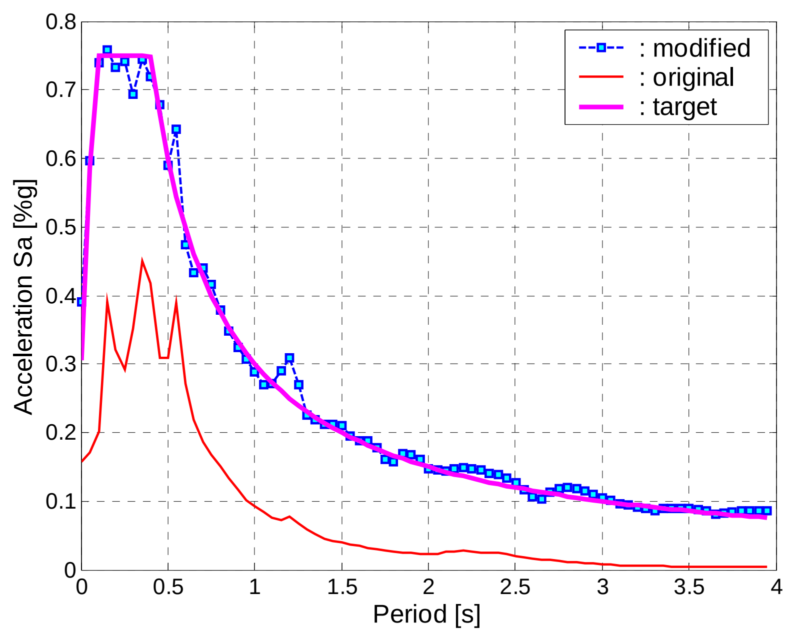

Figure 2.34. The target spectrum and the spectra of the original and modified record of the Coyote Lake evaluated at periods spaced at 0.05 seconds intervals.

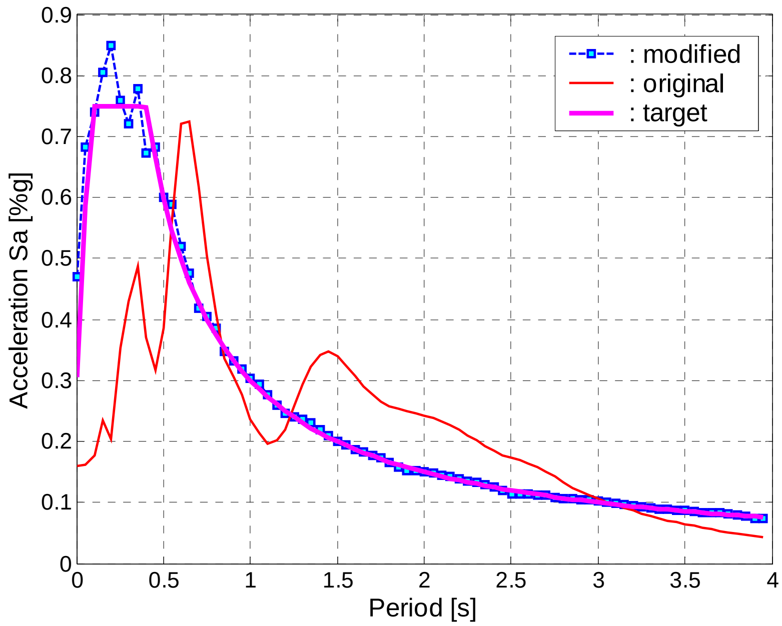

Figure 2.35. The target spectrum and the spectra of the original and modified record of the Loma Prieta earthquake evaluated at periods spaced at 0.05 seconds intervals.

2.6 Summary

This chapter presented a description of the wavelet-based procedure used to modify a recorded accelerogram, so that it becomes compatible with a prescribed design spectrum. The original signal was decomposed into detail functions using the continuous wavelet transform along with a new proposed wavelet. The new wavelet is based on the impulse response function of underdamped oscillators. Through an iterative procedure, the detail signals were scaled up or down according to the ratios between the values of the desired design spectrum and the calculated response spectrum at a series of discrete periods. Each of these periods corresponds to a dominant period of the detail functions. It was found that the procedure converges rapidly and accurately to the desired results.

CHAPTER III

BASELINE CORRECTION

3.1 Introduction

This chapter addresses the problem of obtaining reliable and physically velocities and displacements from artificial spectrum compatible accelerograms without affecting the compatibility of the records with the target spectrum.

When a non-linear analysis of a structure is performed for its seismic verification or design, it is a requirement that the spectrum compatible accelerogram satisfies the fundamental laws of physics: acceleration records must have zero velocity at the end. Also, except when there are permanent ground displacements, the displacement at the final time should be zero. Since, when needed, the structural analysis programs estimate ground velocity and displacement from the direct integration of the acceleration record, they will obtain unreasonable values if the accelerograms do not satisfy these requirements.

Figure 3.1 shows the displacement and velocity time-histories obtained via trapezoidal integration of the UBC-97 spectrum compatible accelerogram based on the record of the Friuli earthquake. It is evident that the results obtained are unrealistic and physically impossible. For example, the ground displacement trace shown in Figure 3.1 never crosses the zero line and it has a permanent displacement of 100 cm at the end.

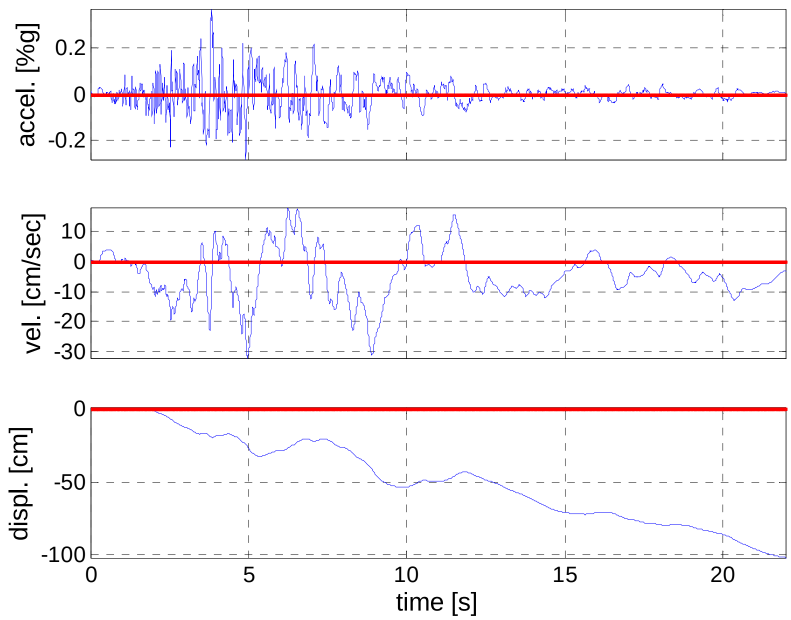

Figure 3.1. Velocity and displacement obtained by numerical integration of the modified acceleration record of the Friuli earthquake.

Seismograph records are usually corrected by a step-by-step time-domain process, generally based on methods developed at the California Institute of Technology in Pasadena, California (Trifunac and Lee, 1973) and further adapted by the U.S Geological Survey (Converse, 1984). Since these methods can modify the frequency content of the record, their use to correct a spectrum compatible accelerogram could result in a non-compatible accelerogram after the correction. This fact calls for the use of a different procedure to perform the baseline correction of compatible records.

3.2 Basic Concepts

Any earthquake acceleration time series can be approximately considered as a sum of acceleration pulses, such as the one shown in Figure 3.2.

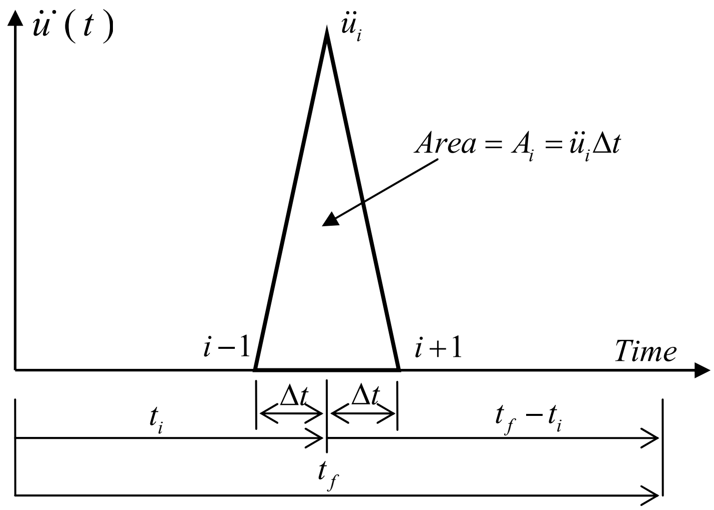

Figure 3.2. Typical Earthquake Acceleration Pulse

The velocity produced by a single acceleration pulse is given by the area A_i of the pulse. If the acceleration pulse is triangular as that shown in Figure 3.2, the area is $A_i = \ddot{u}_i \Delta t$. Therefore, one can calculate the exact velocity at the end of the record as the sum of the areas of the pulses A_i over the complete accelerogram:

$$\dot{u}_f = \sum_{i=1}^{f} \ddot{u}_i \Delta t = \Delta \dot{U} \tag{3.1}$$

where $\Delta \dot{U}$ is the non-zero value that needs to be corrected.

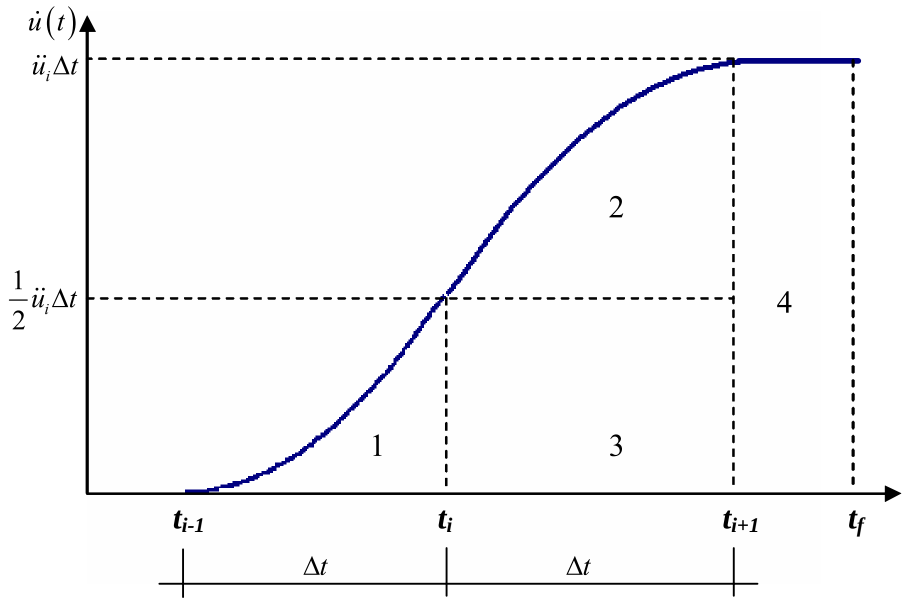

Figure 3.3. Velocity as a function of time for a triangular acceleration pulse.

Figure 3.3 shows the velocity as a function of time due to the single acceleration pulse displayed in Figure 3.2. During the first interval Δt the velocity is given by a parabolic spandrel (equation 3.2) which is obtained by integrating the linear acceleration from t_{i-1} to t.

$$\dot{u}(t) = \frac{1}{2}\frac{\ddot{u}_i}{\Delta t}\left(t - t_{i-1}\right)^2 \tag{3.2}$$

The velocity at a time $t_i \le t \le t_{i+1}$ is given by the parabolic equation 3.3:

$$\dot{u}(t) = -\frac{1}{2}\frac{\ddot{u}_i}{\Delta t}\left(t - t_{i-1}\right)^2 + \ddot{u}_i(t - t_i) + \frac{1}{2}\ddot{u}_i\Delta t \tag{3.3}$$

After the time t_{i+1} the velocity remains constant until the final time t_f. The displacement at the end of the interval t_f due to the single acceleration pulse in Figure 3.2 is the area under the curve in Figure 3.3. This can be calculated as the sum of the four areas identified as 1, 2, 3 and 4 in this figure. It is easy to show that these areas are:

$$\begin{aligned} A_1 &= \frac{1}{6}\ddot{u}_i \Delta t^2 \\ A_2 &= \frac{1}{3}\ddot{u}_i \Delta t^2 \\ A_3 &= \frac{1}{2}\ddot{u}_i \Delta t^2 \\ A_4 &= \ddot{u}_i \Delta t \left[t_f - \left(t_i + \Delta t \right) \right] \end{aligned} \tag{3.4}$$

The displacement at the end of the record (i.e. at time t_f) due to the simple pulse at time t_i is the sum of the four areas, i.e.,

$$\left(u_f \right)_i = \frac{1}{6}\ddot{u}_i \Delta t^2 + \frac{1}{3}\ddot{u}_i \Delta t^2 + \frac{1}{2}\ddot{u}_i \Delta t^2 - \ddot{u}_i \Delta t^2 + \ddot{u}_i \Delta t \left(t_f - t_i \right)$$

$$\left(u_f \right)_i = \ddot{u}_i \Delta t \left(t_f - t_i \right) \tag{3.5}$$

The displacement at time t_f due to the different pulses is the sum of the displacements in equation 3.6.

$$u_f = \sum_{i=1}^{f} \left(u_f \right)_i = \sum_{i=1}^{f} \left(t_f - t_i \right) \ddot{u}_i \Delta t = \Delta U \tag{3.6}$$

The quantity ΔU in equation 3.6 is the non-zero displacement that we are seeking to correct.

3.3 The Proposed Correction Procedure

The procedure to correct the raw accelerogram was briefly cited in an appendix of a book by E. Wilson (2002). There are no detailed explanations of the procedure in this reference, and even its is not sufficiently clear. Therefore, a through explanation of the procedure and its basis are provided in this section.

The idea is to correct a small subset of the discrete acceleration values $\ddot{u}_i$ such that the final displacement and velocity are zero. It is proposed to correct the first t_L seconds of the accelerogram to achieve zero displacement at the end of the record. Since the time $t_L = L\ \Delta t$, this implies that the first "L" data points of the record will be corrected. The expression 3.6 to calculate the corrected displacement u_f^c at the end of the record can now be divided as follows

$$u_f^c = \sum_{i=1}^{L}\left(t_f - t_i\right)g_i\ddot{u}_i\,\Delta t + \sum_{i=1}^{L}\left(t_f - t_i\right)\ddot{u}_i\,\Delta t + \sum_{i=L+1}^{f}\left(t_f - t_i\right)\ddot{u}_i\,\Delta t \tag{3.7}$$

where g_i are the weights used to correct the first L values of the accelerogram. We know that the second and third summation terms give ΔU, and thus we require that

$$\sum_{i=1}^{L}\left(t_f - t_i\right)g_i\ddot{u}_i\,\Delta t = -\Delta U \tag{3.8}$$

It is evident now that by imposing this requirement the displacement u_f^c in equation 3.7 will become zero. The simplest way to correct the acceleration points, i.e. to define the weights g_i, is to use a linear function *g(t)*. To avoid a discontinuity in the acceleration record, the linear function should decrease from a given value at time $t = 0$ to zero at time $t = t_L$. Thus the linear function is defined as

$$g(t) = \alpha_d\,\frac{t_L - t}{t_L} \quad ; \quad 0 \le t \le t_L \tag{3.9}$$

The function *g(t)* is shown in Figure 3.4. Since the time is sampled at constant intervals Δt, substituting t_L and t by the discrete times $\Delta t\ L$ and $\Delta t\ (i\text{-}1)$ we obtain the weights g_i in equation 3.8:

$$g_i = \alpha_d\,\frac{L-(i-1)}{L} \quad ; \quad 1 \le i \le L+1 \tag{3.10}$$

The factor α_d can be obtained by substituting equation 3.10 in 3.8, which leads to:

$$\alpha_d \sum_{i=1}^{L} \frac{L-(i-1)}{L}\left(t_f - t_i\right)\ddot{u}_i \Delta t = -\Delta U \tag{3.11}$$

Once this factor is obtained, the correction weights are applied to the first L points of the original accelerogram. Recalling equations 3.7 and 3.10, the corrected values of the acceleration are

$$\ddot{u}_i^c = \left(1+g_i\right)\ddot{u}_i = \left(1+\alpha_d \frac{L-i+1}{L}\right)\ddot{u}_i \quad ; \quad i=1,\ldots,L \tag{3.12}$$

This, in principle, should be sufficient to obtain a zero displacement at the end of the record. However, it is proposed to define two different factors α_{dp} and α_{dn} for the positive and negative values of the acceleration $\ddot{u}_i$. This is done to minimize the changes to the accelerogram: using a single factor will alter more the original values $\ddot{u}_i$. Since there are no additional equations to define two factors, it is proposed to define them as follows. Considering only the positive values of $\ddot{u}_i$, in the summation in equation 3.11, the coefficient α_{dp} is obtained from:

$$\alpha_{dp} \Delta t \sum_{i=1}^{L} \frac{L-(i-1)}{L}\left(t_f - t_i\right)\left(\ddot{u}_i\right)_+ = \frac{-\Delta U}{2} \tag{3.13}$$

where $\left(\ddot{u}_i\right)_+$ are the positive values of the sequence $\ddot{u}_i$.

The coefficient α_{dn} is obtained from a similar expression but including only the negative values of $\ddot{u}_i$, identified as $\left(\ddot{u}_i\right)_-$:

$$\alpha_{dn} \Delta t \sum_{i=1}^{L} \frac{L-(i-1)}{L}\left(t_f - t_i\right)\left(\ddot{u}_i\right)_- = \frac{-\Delta U}{2} \tag{3.14}$$

The corrected acceleration values $\ddot{u}_i^c$ are still given by the equation 3.12 but now if the original $\ddot{u}_i$ is positive, α_d must be replaced by α_{dn}, and vice versa, if it is negative α_{dp} must be used.

The next task is to correct the acceleration such that the velocity at the end of the record is zero. It is proposed to modify now the last "L" values of $\ddot{u}_i$ (i.e. the last t_L seconds of the accelerogram). From equation 3.1 the corrected velocity at the end of the record is written as

$$\dot{u}_f^c = \sum_{i=1}^{f-L-1} \ddot{u}_i \Delta t + \sum_{i=f-L}^{f} \ddot{u}_i \Delta t + \sum_{i=f-L}^{f} h_i \ddot{u}_i \Delta t \tag{3.15}$$

The first two terms in equation 3.15 are equal to $\Delta \dot{U}$, i.e. to the error in the end velocity. This value will be corrected with the last term. Here again a linear function $h(t)$, shown in Figure 3.4, will be used to define the weights: the continuous time function and the weights h_i are

$$h(t) = \alpha_v \frac{t - \left(t_f - t_L\right)}{t_L} \quad ; \quad t_f - t_L \le t \le t_f \tag{3.16}$$

$$h_i = \alpha_v \frac{i - \left(f - L + 1\right)}{L} \quad ; \quad f - L + 1 \le i \le f \tag{3.17}$$

The coefficient α_v is obtained by requiring that the last summation in equation 3.15 be equal to the first two terms, that is

$$\alpha_v \sum_{i=f-L+1}^{f} \frac{i - \left(f - L + 1\right)}{L - 1} \ddot{u}_i \Delta t = -\Delta \dot{U} \tag{3.18}$$

The acceleration record corrected for zero end velocity is given by

$$\ddot{u}_i^c = (1+h_i)\ddot{u}_i = \left(1+\alpha_v \frac{i-(f-L+1)}{L}\right)\ddot{u}_i \qquad ; \qquad i = f-L+1,\ldots,f \tag{3.19}$$

As it was done to obtain zero end displacement, it is proposed to use two coefficients α_v: the first coefficient α_{vp} will correct the positive values of $\ddot{u}_i$ and another one α_{vn} will be applied to correct the negative values.

The coefficient α_{vp} is computed by using only the positive values of $\ddot{u}_i$, identified as $(\ddot{u}_i)_+$, in the following summation:

$$\alpha_{vp}\Delta t \sum_{i=f-L+1}^{f} \frac{i-(f-L+1)}{L-1}(\ddot{u}_i)_+ = \frac{-\Delta\dot{U}}{2} \tag{3.20}$$

whereas the coefficient α_{vn} is obtained by including only the negative values of $\ddot{u}_i$ identified as $(\ddot{u}_i)_-$:

$$\alpha_{vn}\Delta t \sum_{i=f-L+1}^{f} \frac{i-(f-L+1)}{L-1}(\ddot{u}_i)_- = \frac{-\Delta\dot{U}}{2} \tag{3.21}$$

The coefficient α_{vp} replaces α_v in equation 3.19 if $\ddot{u}_i$ is positive and, on the contrary, if the original acceleration is negative, α_{vn} must be used to calculate $\ddot{u}_i^c$.

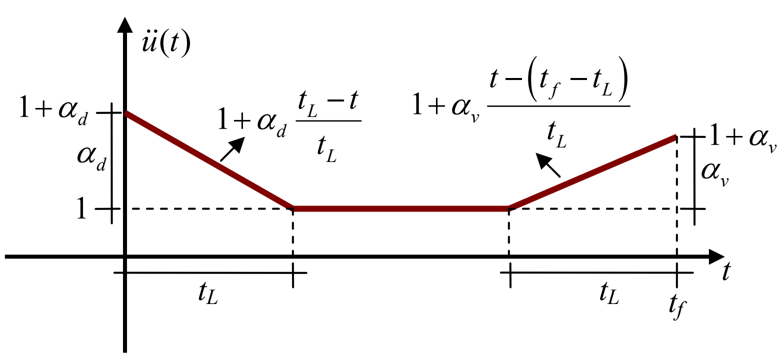

Figure 3.4. Correction functions to set displacement and velocity zero at the end of the accelerogram.

Note that four formulas were developed to correct the original accelerogram: two are used to obtain zero end displacement, equations 3.13 and 3.14, and another two equations 3.20 and 3.21, are applied to achieve zero velocity at the end of the record. Using two formulas first, say equations 3.13 and 3.14, will correct the end displacement but when the second formulas are applied, the previously corrected displacement will no longer be zero. Therefore, an iterative procedure must be implemented to achieve both zero end displacement and velocity, using a pair of formulas at a time. Table 3.1 presents a summary of the algorithm previously described to correct the displacement and velocity at the end of an earthquake record. This procedure was implemented in a *MATLAB* program.

3.4 Numerical Examples

To illustrate the procedure previously described, the modified records of the Friuli and Round Valley earthquakes synthesized in Chapter II are corrected. Figures 3.1 and 3.5 show, respectively, the displacement and velocity time-histories of the modified records of Friuli and Round Valley before the baseline correction. Figures 3.6 and 3.7 show the displacement and velocity time-histories of the modified records of Friuli and Round Valley after the baseline correction has been performed. It can be seen from this figures that the displacement and velocity at the end of the corrected accelerogram are zero as they should be.

To gain further insight into the effects of the correction procedure on the spectrum compatible records, Figures 3.8 and 3.9 show the modified accelerograms of Friuli and Round Valley before and after the baseline correction has been performed. It can be verified from these figures that since the correction is only performed to a few points at the beginning and at the end of the record, the shape of the accelerograms remain the same after the baseline correction.

One crucial required property of any displacement and velocity correction procedure intended to be applied to spectrum compatibles accelerograms is that the corrected records must still compatible with the target spectrum. In order to verify this requirement for the proposed procedure, Figures 3.10 and 3.11 show the response spectra of the accelerograms of Friuli and Round Valley before and after the baseline correction was performed. It is evident from these graphs that the response spectra remain compatible after the correction.

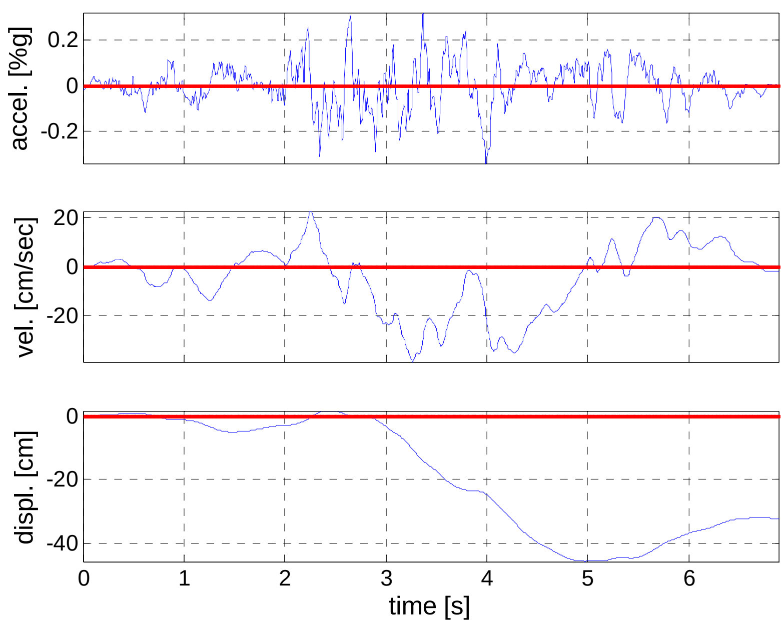

Figure 3.5. Velocity and displacement obtained by numerical integration of the modified acceleration record of the Round Valley earthquake.

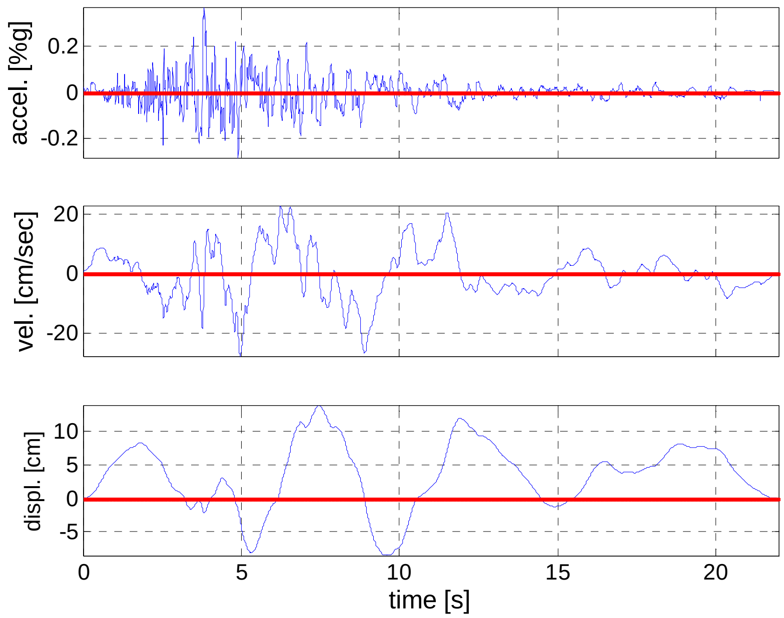

Figure 3.6. Velocity and displacement of the modified acceleration record of the Friuli earthquake after the baseline correction.

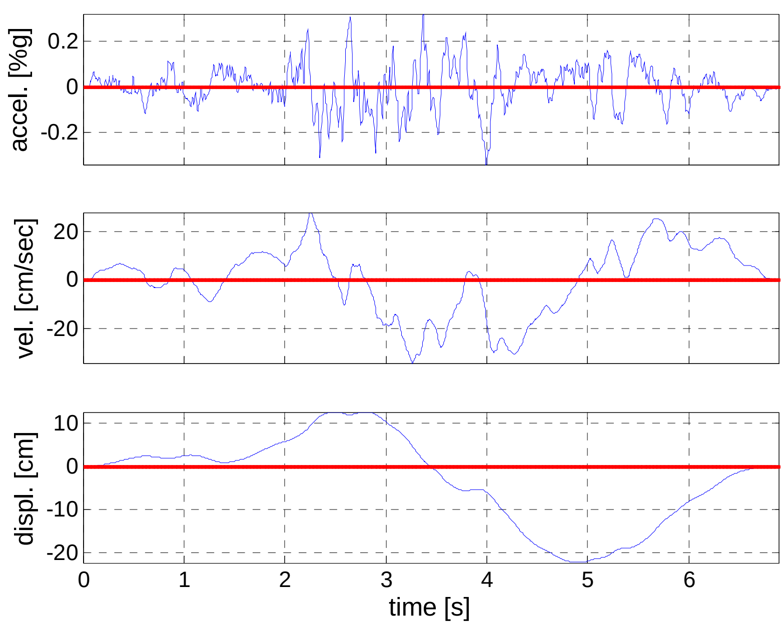

Figure 3.7. Velocity and displacement of the modified acceleration record of the Round Valley earthquake after the baseline correction.

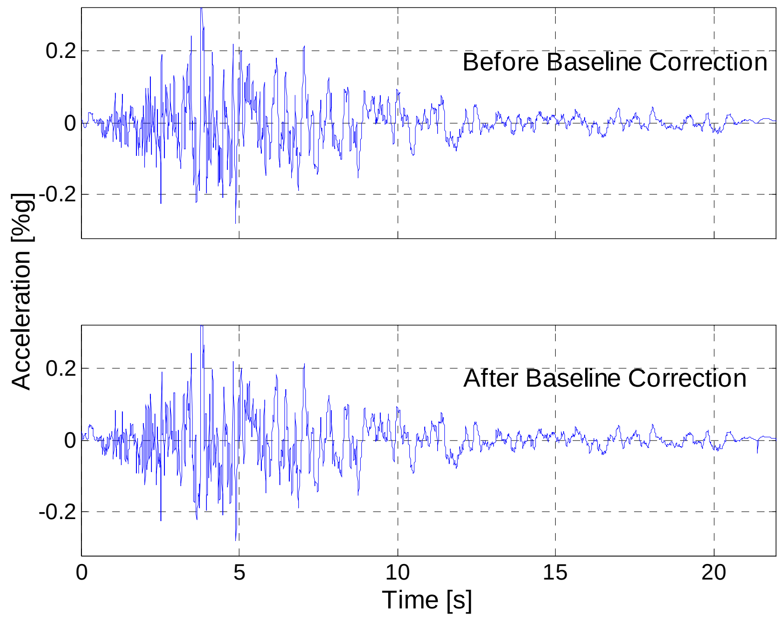

Figure 3.8. The spectrum-compatible records of Friuli, before and after performing the baseline correction.

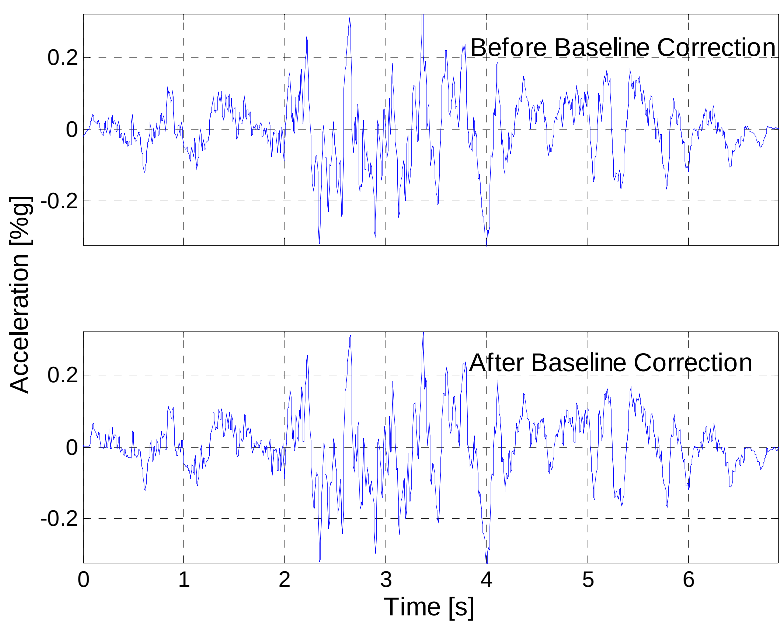

Figure 3.9. The spectrum compatible records of Round Valley, before and after performing the baseline correction.

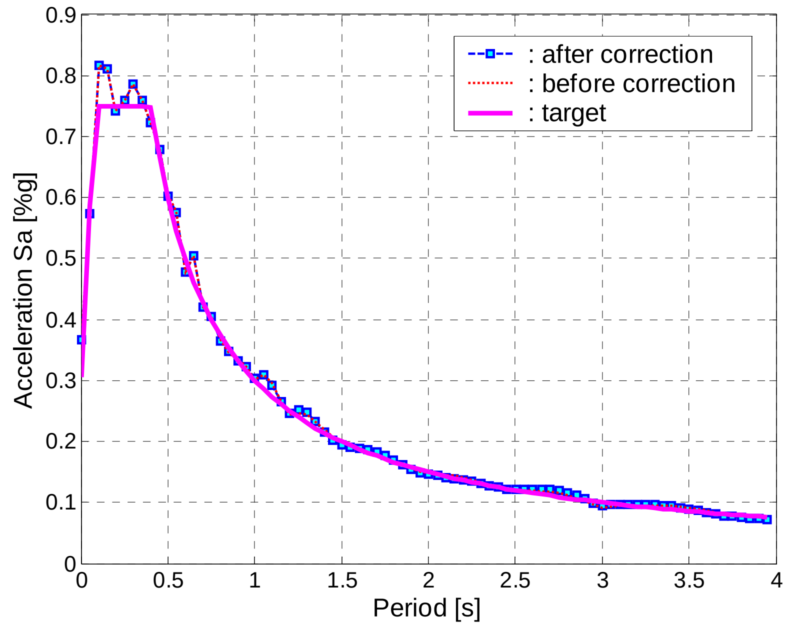

Figure 3.10. The target spectrum and the spectra of the modified record of Friuli before and after the baseline correction has been performed.

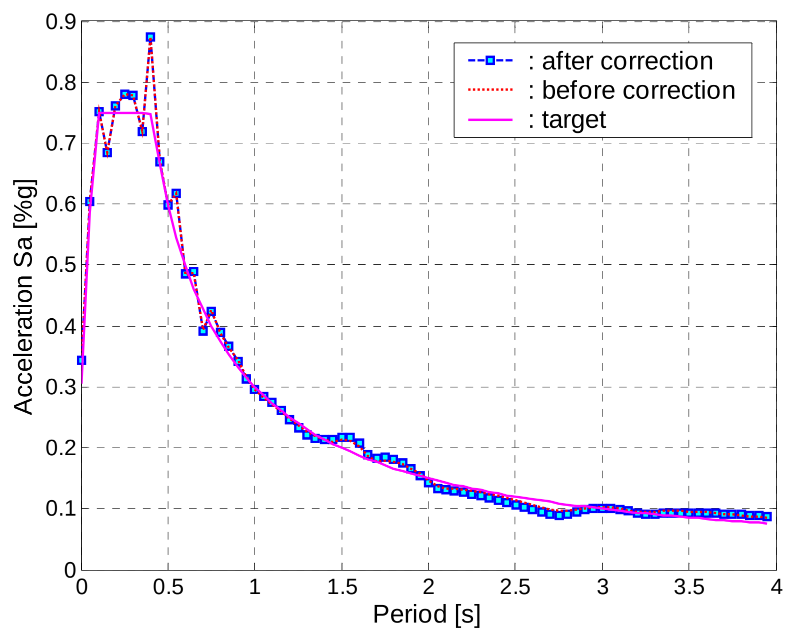

Figure 3.11. The target spectrum and the spectra of the modified record of Round Valley before and after the baseline correction has been performed.

Table 3.1 Algorithm to set displacement and velocity at end of records to zero

1. Given an uncorrected acceleration record: $\ddot{u}_1, \ddot{u}_2, ...\ddot{u}_f$, a specific number of points L to perform the correction and an admissible tolerance (*tol*) in terms of the ratio $\varepsilon_v = \frac{|v_f|}{\max|v_i|} * 100$ for the velocity and $\varepsilon_d = \frac{|u_f|}{\max|u_i|} * 100$ for the displacement,

Repeat steps 2 to 5 until tolerances are satisfied

Displacement Correction

2. Compute the displacement correction function as follows:

$$\Delta U = \sum_{i=1}^{f} \left(t_f - t_i\right) \ddot{u}_i \Delta t$$

$$\sum_{i=1}^{L} \frac{L-i}{L} \left(t_f - t_i\right) \left(\ddot{u}_i\right)_+ \Delta t = U_{pos}$$

$$\sum_{i=1}^{L} \frac{L-i}{L} \left(t_f - t_i\right) \left(\ddot{u}_i\right)_- \Delta t = U_{neg}$$

$$\alpha_{dp} = -\frac{\Delta U}{2U_{pos}} \quad \text{and} \quad \alpha_{dn} = -\frac{\Delta U}{2U_{neg}}$$

3. Correct the acceleration record:

$$\text{if } \ddot{u}_i > 0 \text{ then } \ddot{u}_i = \left(1 + \alpha_{dp} \frac{L - (i-1)}{L}\right) \ddot{u}_i; \quad i = 1, ..., L$$

$$\text{if } \ddot{u}_i < 0 \text{ then } \ddot{u}_i = \left(1 + \alpha_{dn} \frac{L - (i-1)}{L}\right) \ddot{u}_i; \quad i = 1, ..., L$$

Velocity Correction

4. Compute the velocity correction function:

$$\Delta \dot{U} = \sum_{i=1}^{f} \ddot{u}_i \Delta t$$

$$\sum_{i=f-L+1}^{f} \frac{i - (f - L + 1)}{L - 1} \left(\ddot{u}_i\right)_+ \Delta t = \dot{U}_{pos}$$

$$\sum_{i=f-L+1}^{f} \frac{i - (f - L + 1)}{L - 1} \left(\ddot{u}_i\right)_- \Delta t = \dot{U}_{neg}$$

$$\alpha_{vp} = -\frac{\Delta \dot{U}}{2\dot{U}_{pos}} \quad \text{and} \quad \alpha_{vn} = -\frac{\Delta \dot{U}}{2\dot{U}_{neg}}$$

5. Correct the acceleration record:

$$\text{if } \ddot{u}_i > 0 \text{ then } \ddot{u}_i = \left(1 + \alpha_{vp} \frac{i - (f - L)}{L}\right) \ddot{u}_i; \quad i = f - L + 1, ..., f$$

$$\text{if } \ddot{u}_i < 0 \text{ then } \ddot{u}_i = \left(1 + \alpha_{vn} \frac{i - (f - L)}{L}\right) \ddot{u}_i; \quad i = f - L + 1, ..., f$$

3.5 Summary

This chapter presented a simple and efficient methodology to perform the baseline corrections of earthquake records, that is to correct the accelerogram such that the velocity and displacement at the final time become zero. The procedure presented is due to Edward L. Wilson and is briefly described in Appendix J of a book intended for users of *SAP 2000* (Wilson, 2000). However, there is not explanation of the theory behind the technique. Herein a comprehensive explanation of the method was included.

Since the procedure modifies only a few points at the beginning and at the end of the record, the corrected accelerogram is almost the same as the original accelerogram. Typically, for the cases considered during this study, the time interval used to correct records was 0.60 seconds. The procedure is iterative but it quickly converges after a few iterations.

Although in the application presented in this chapter the procedure is used to achieve zero displacement at the end of the record, it can also be applied to obtain a prescribed non-zero displacement (ΔU). This feature can be useful for the case where it is known that there is a permanent ground displacement as a result of the earthquake.

It has been shown that the procedure does not affect the compatibility with the target spectrum. In other words, the corrected records still have a response spectrum compatible with the original design spectrum, a very important feature for the generation of artificial earthquakes. However, it is important to point out that the methodology explained in this chapter is only adequate for the correction of artificial accelerograms. Seismograph earthquake records must be corrected using some of the existent baseline-correction process that have been specially developed for this purpose.

CHAPTER IV

ANALYSIS OF EARTHQUAKE RECORDS

4.1 Introduction

It would be desirable that when a record of a historic ground motion is modified to generate a spectrum compatible accelerogram, the temporal variations in the frequency content of the original accelerogram were retained. This, in general, is not possible with any method that matches the response spectrum to a target spectrum. However, it is important to examine in detail how do the modified records change, in terms of their frequency content and strong motion duration. Therefore an analysis of the spectrum compatible accelerograms obtained in CHAPTER II is performed in this chapter. The analyses performed on these records include:

- An analysis in the frequency domain (by means of the Fourier Transform)
- An analysis in the Time-Frequency domain (using the Continuous Wavelet Transform)

- A study of the duration of the strong motion phase (using the Arias Intensity and the Husid plot)
- An examination of the energy content (performed with help of the Input Energy Spectrum)

With the purpose of comparing the characteristics of the artificial accelerograms obtained via the wavelet transform with those of artificial records obtained using a popular method, namely the program *SIMQKE*, a set of artificial accelerograms is generated using this tool. An analysis is then performed to the recorded accelerograms, to the wavelet based modified accelerograms and to the artificial accelerograms generated using *SIMQKE*. The same analyses performed to the accelerograms processed with the wavelet method are applied to the records obtained with *SIMQKE*.

4.2 Analysis in frequency domain – The Fourier Transform

The frequency content of a given ground motion can be examined by transforming the motion from a time domain to a frequency domain through the Fourier Transform. Fourier analysis is an extremely useful tool for data analysis as it breaks down a signal into constituent sinusoids of different frequencies. Most engineers are familiar with this concept and thus it facilitates its acceptance. For sampled vector data (such as an accelerogram), Fourier analysis is performed using the discrete Fourier transform (*DFT*). The DFT is usually computed using the well known Fast Fourier Transform (*FFT*). The FFT is just an efficient algorithm for computing the *DFT* of a sequence; it is not a separate transform. The DFT is particularly useful in areas such as signal and image processing, where its uses ranges from filtering, convolution, and frequency analysis to power spectrum estimation.

The continuous Fourier transform $F(\omega)$ of an accelerogram $a(t)$ is defined as

$$F(\omega) = \int_{o}^{T} a(t) e^{-i\omega t} dt \tag{4.1}$$

where T is the duration of the accelerogram. The Fourier amplitude spectrum $FS(\omega)$ is defined as the square root of the sum of the squares of real and imaginary parts of $F(\omega)$, i.e. it is the modulus of the complex function $F(\omega)$:

$$FS(\omega) = \left| F(\omega) \right| = \sqrt{\left[\int_{0}^{T} a(t) \sin \omega t dt \right]^2 + \left[\int_{0}^{T} a(t) \cos \omega t dt \right]^2} \tag{4.2}$$

Since *a(t)* has units of acceleration, $FS(\omega)$ has units of velocity. Figures 4.1 and 4.2 show the acceleration trace of the 2001 Anza (California) earthquake and its Fourier amplitude spectrum. Figure 4.2 indicates that the largest amplitude is at a frequency of approximately 12 Hz, and most of the energy in the accelerogram is in the range of 2 to 17 Hz.

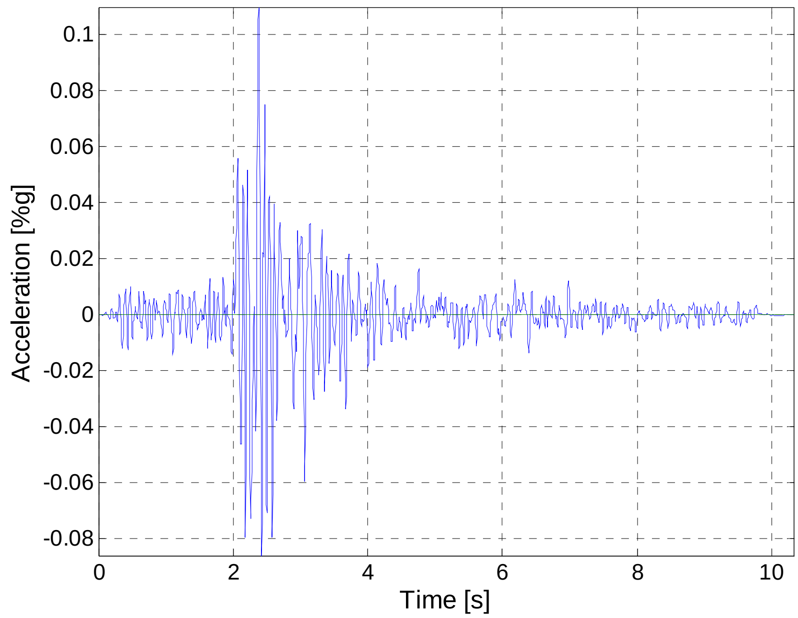

Figure 4.1. Acceleration time history of the Anza (California) earthquake

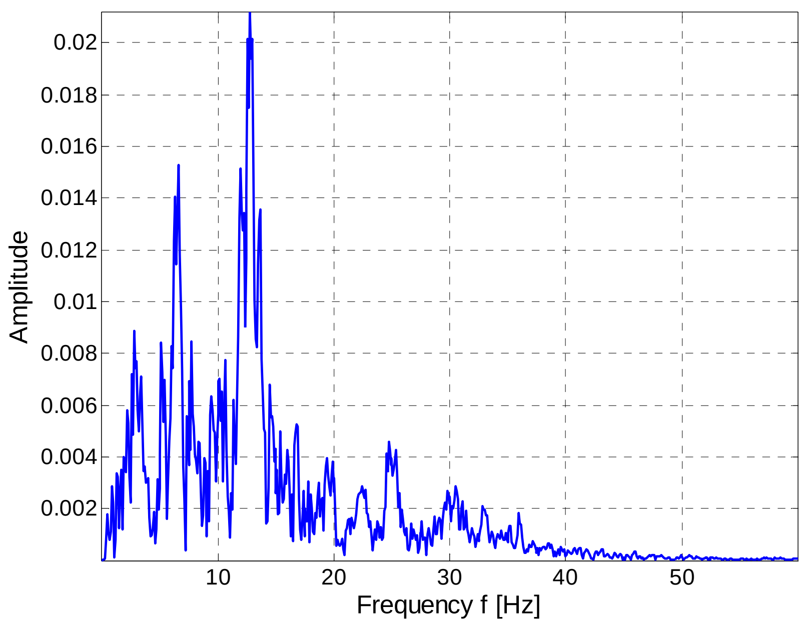

Figure 4.2. Fourier amplitude spectrum of the acceleration time history of the Anza (California) earthquake

4.3 Analysis in Time-Frequency domain – Continuous Wavelet Transform.

Fourier analysis has a weakness for certain applications. In transforming to the frequency domain, time information is lost: when looking at a Fourier transform of a signal, it is impossible to tell when a particular event took place. If the signal properties do not change much over time (a stationary signal) this drawback is not very important. However, earthquake records contain numerous nonstationary and transient characteristics. These characteristics are often the most important part of the signal, and Fourier analysis is not suited to detect them; therefore there is a need for a combined time-frequency representation. A time-frequency distribution of a signal can provide information about how the spectral content of the signal evolves with time, thus providing a tool to dissect and interpret strongly non-stationary signals. This is performed by mapping a one dimensional signal in the time domain into a two dimensional time-frequency representation. One of the methods for time-frequency analysis of earthquake records is the wavelet transform. In this chapter the new impulse response wavelet is used for this purpose. The results obtained show that this method, complemented with the Fourier Transform, is an efficient tool that can provide information on the variability with time and frequency of many characteristics of the earthquake records. To provide an example of the usefulness of this tool, the two signals shown in Figures 4.3 and 4.4 were generated. Both of them are sinusoids, the first one starts with a frequency of 1Hz, then changes to 2Hz at 4 seconds and to 4Hz at 8 seconds. The second one starts with a frequency of 4Hz, then change to 2Hz at 4 seconds and to 1Hz at 8 seconds. These harmonic time functions in which the frequency changes with time are sometimes referred to as “nonlinear signals” in the technical literature. Figure 4.5 shows the Fourier spectra of both signals: the frequency content of both signals are identical. The spectrum shows three equal dominant peaks at frequencies of 1, 2 and 4 Hz. The remaining smaller peaks are due to the fact that the signal is transient. Evidently, the Fourier spectrum captured the correct frequencies of the signals, but the fact that the three component sinusoids appear in different order is missed. However, an analysis in time-frequency domain, shown in Figures 4.6 and 4.7, allow us to identify the time where each event took place. Figure 4.6 shows the absolute values of the Continuous Wavelet Transform of the signal 1. By observing the light colors in the graph, one can detect that there is component with frequency 1 Hz that later disappears. At about that time, the light color at 2 Hz indicates that a new component appeared. Later on, bright colors appear at 4 Hz in the vertical axis indicating that the frequency content of the accelerogram changed again.

Figure 4.7 shows similar results but for signal 2. Note that now the maximum values appear in reverse order compared to the previous case.

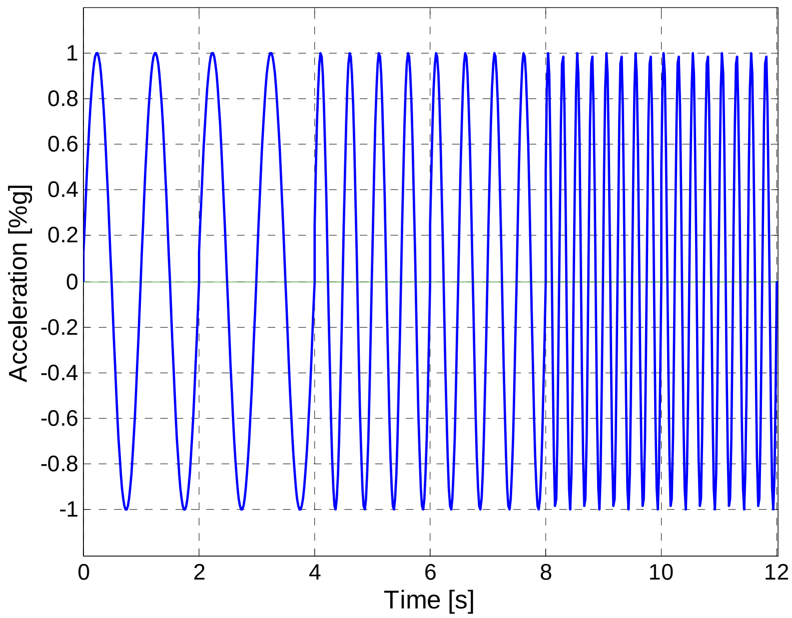

Figure 4.3. Signal 1 with frequencies 1,2, and 4 Hz

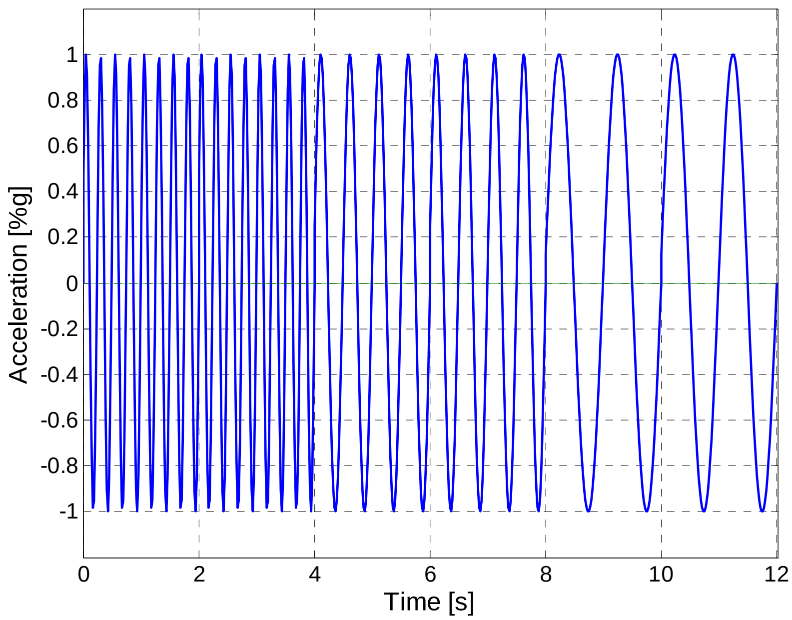

Figure 4.4. Signal 2 with frequencies 4,2, and 1 Hz

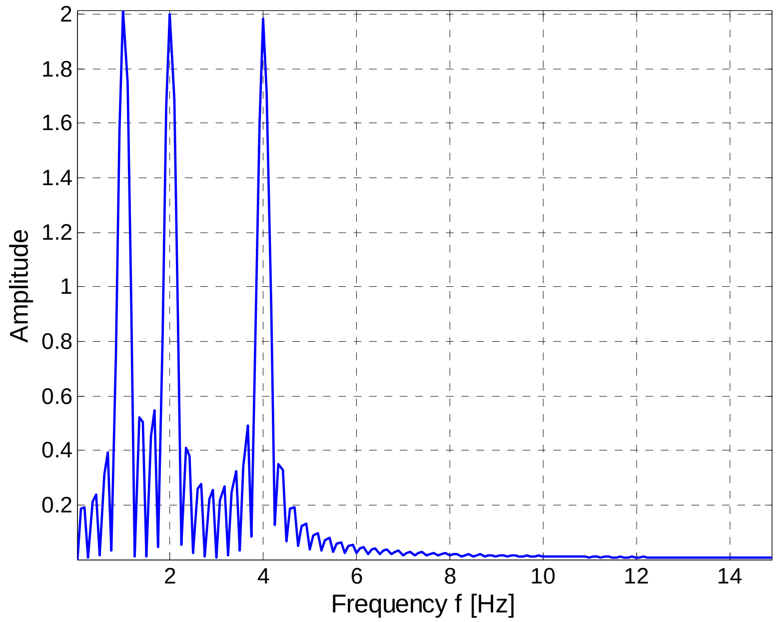

Figure 4.5. Fourier amplitude spectrum of the Signal 1 and Signal 2.

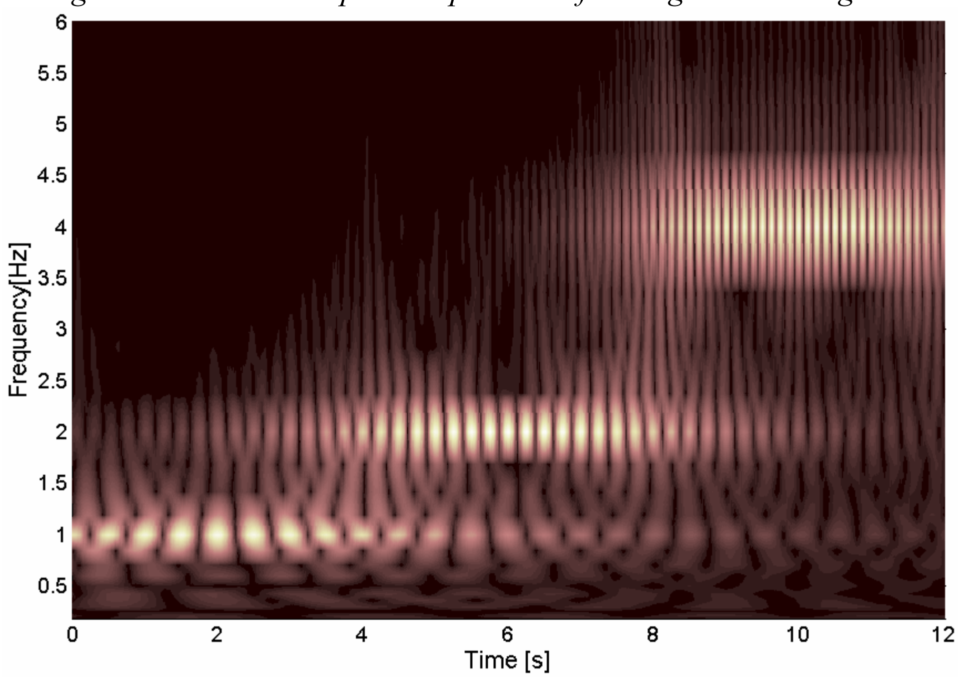

Figure 4.6. Wavelet map of Signal 1.

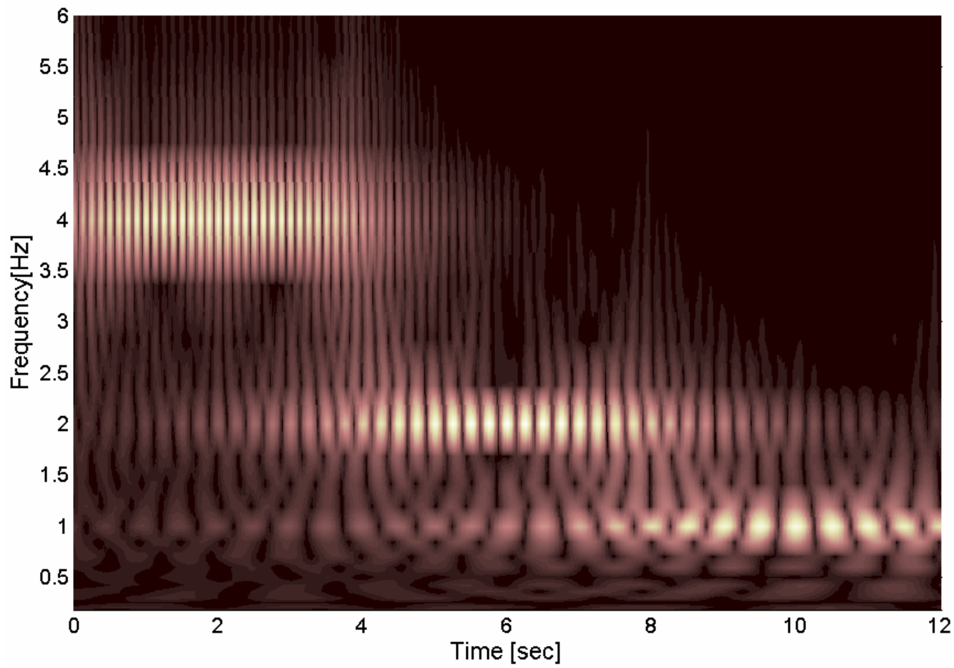

Figure 4.7. Wavelet map of Signal 2.

4.4 Comparison of the original and the wavelet based modified records

Figures 4.8 to 4.12 show the original acceleration records and the wavelet-based modified accelerograms for the five earthquakes selected for this study (Friuli, Coalinga, Loma Prieta, Round Valley and Coyote Lake). The first and obvious difference is the peak acceleration. The original records were scaled up to have a PGA equal to 0.3g. However, it can also be noticed that the maximum acceleration occurs almost at the same time in both pairs of accelerograms.

It is also evident from the accelerograms in Figures 4.8 to 4.12 that some original records were modified by the wavelet procedure more than others. For example, the modified accelerogram of the Loma Prieta earthquake (figure 4.10) has a richer frequency content than the original one. In the Coalinga record (Figure 4.9) the procedure added a low frequency component after the strong motion part of the accelerogram faded away. At a first glance, the duration of the strong motion part was changed in all records, although the degree of change varies from accelerogram to accelerogram. There is not much more that one can say from a visual analysis of the records. To obtain more information one need to resort to other tools, such as the Fourier Spectrum, Wavelet Map and Husid plot of the records.

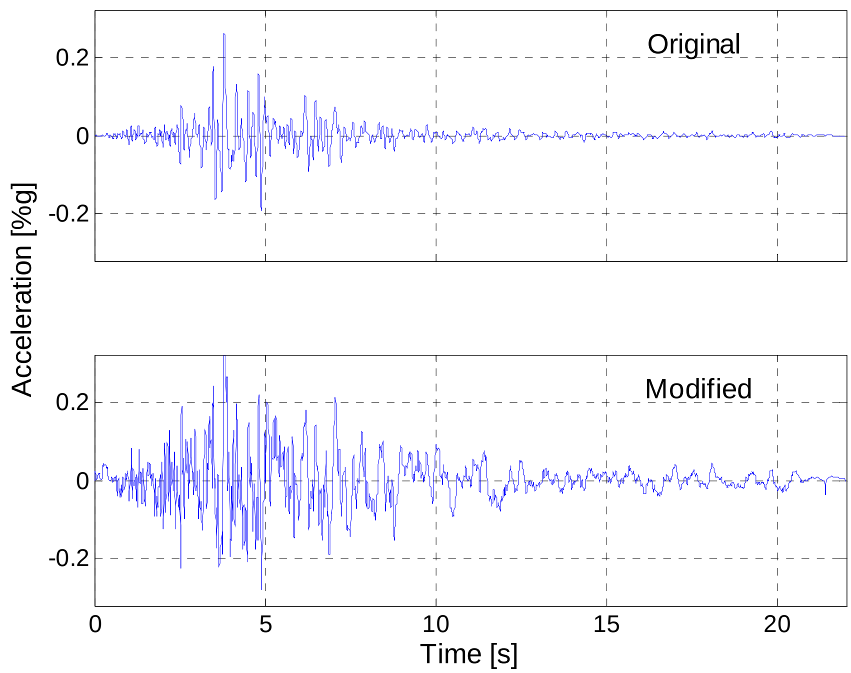

Figure 4.8. Original and modified accelerogram of the Friuli earthquake.

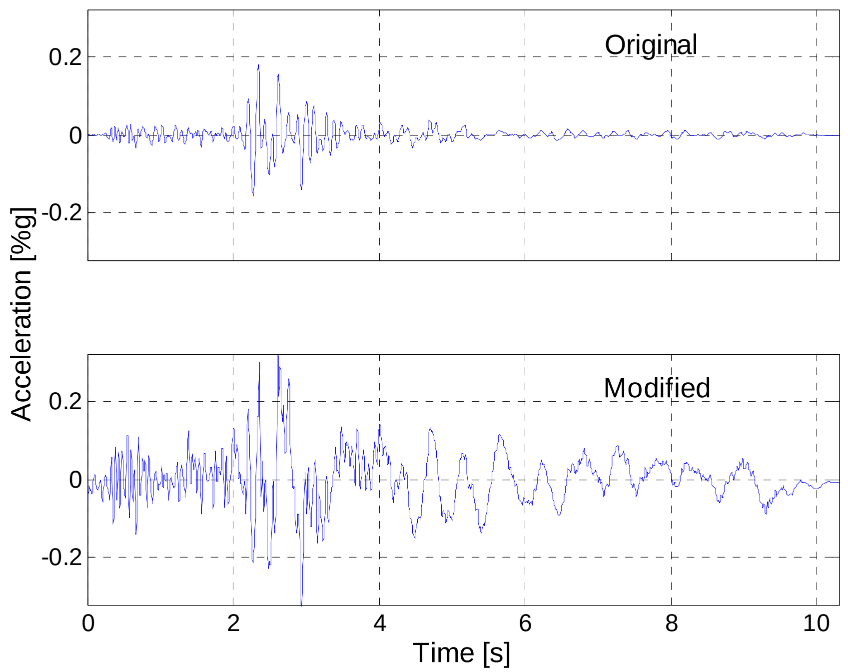

Figure 4.9. Original and modified accelerogram of the Coalinga earthquake.

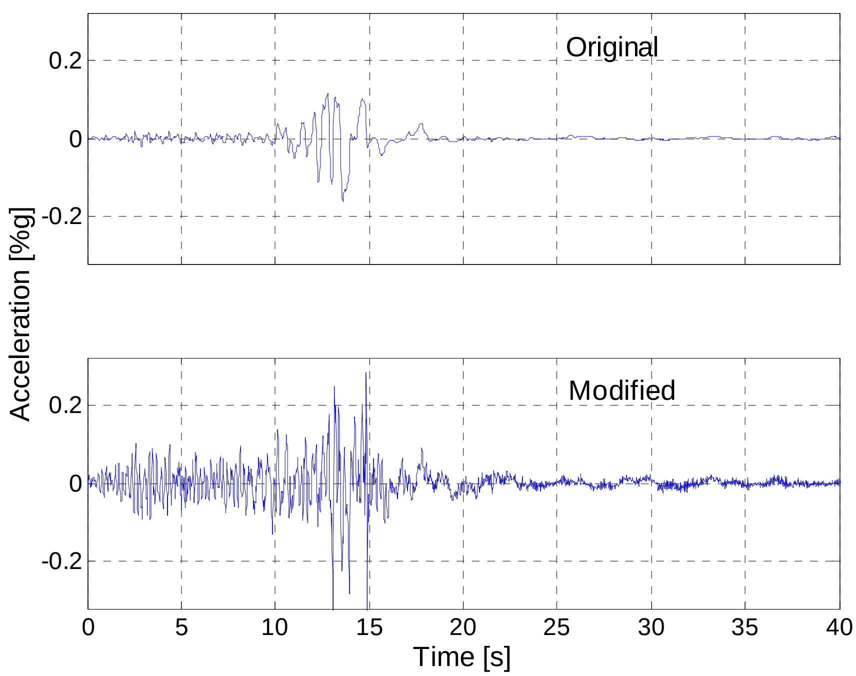

Figure 4.10. Original and modified accelerogram of the Loma Prieta earthquake.

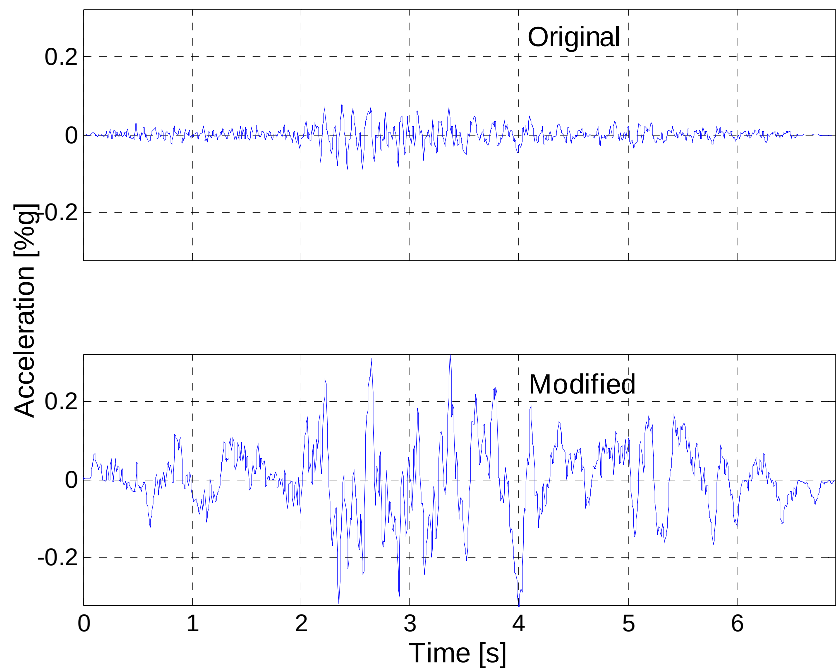

Figure 4.11. Original and modified accelerogram of the Round Valley earthquake.

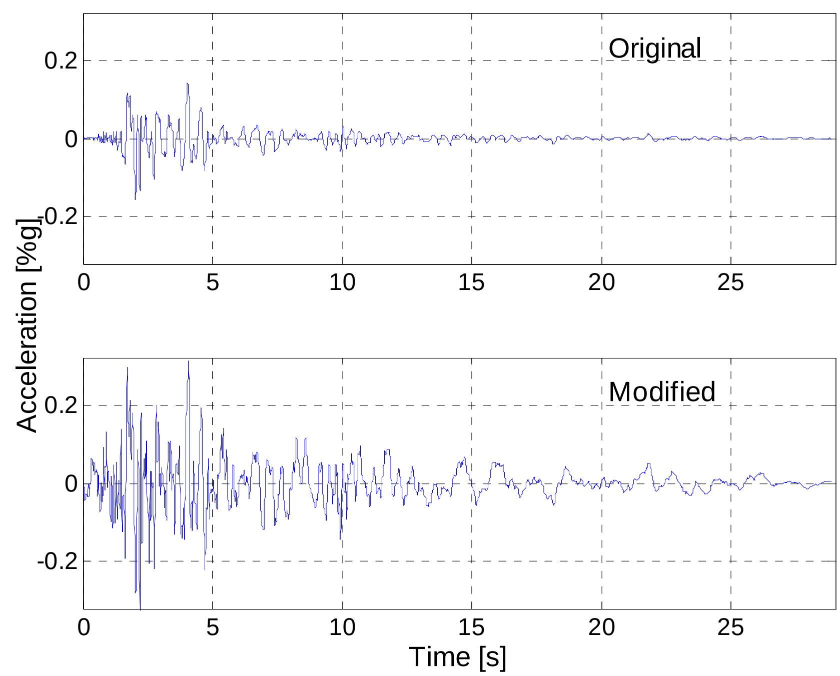

Figure 4.12. Original and modified accelerogram of the Coyote Lake earthquake.

Figures 4.13 to 4.32 show the Fourier Spectrum and the Wavelet Map of the five original and modified accelerograms. Examining the Fourier Spectra in these figures one can conclude that the frequency content and non-stationary characteristics of the modified accelerograms are very different from these of the original accelerograms used as starting point for their generation. This is a drawback of the method. Ideally, one would like to preserve the dominant frequencies and the relative importance of their components in the record. This is so because they can be considered to be associated with the geological, tectonic and source characteristics of the earthquakes that were originally selected. It can be argued that when the frequency content and strong motion duration of the original record are modified, the new record no longer represents an earthquake with the same epicentral distances, fault type, etc., that one chosen. This argument is, in principle, correct but this is a weakness common to all the techniques for generation of spectrum compatible earthquake records. The only parameter that the procedure can modify is the relative importance of the components of different frequencies that make up the accelerogram. In any event, we argue that the procedure is better than simply adding sine waves with arbitrary frequencies and random phases, which is the basis of the popular program *SIMQKE*. At least in the proposed procedure some characteristics of the original record will partially remain in the modified time history.

The change in the frequency content is more evident in those records whose original response spectrum is very far from the target spectrum. This is the case, for instance, of the acceleration record of the Round Valley earthquake (Figures 4.25 to 4.28). The original Fourier spectrum has three dominant frequencies at approximately 12.5, 7.5 and 3.5 Hz. The spectrum of the modified record shows a dominant frequency at about 2 Hz. On the other hand, the modification in the frequency content is less evident in those records whose original response spectrum is closer to the target spectrum, for example in the acceleration record of the Friuli earthquake (Figures 4.13 to 4.16). Most of the energy of both records is concentrated in the 0-10 Hz band as it can be seen in the spectra in Figures 4.13 and 4.14. The matching procedure increases the weight of the components with frequency around 15 Hz.

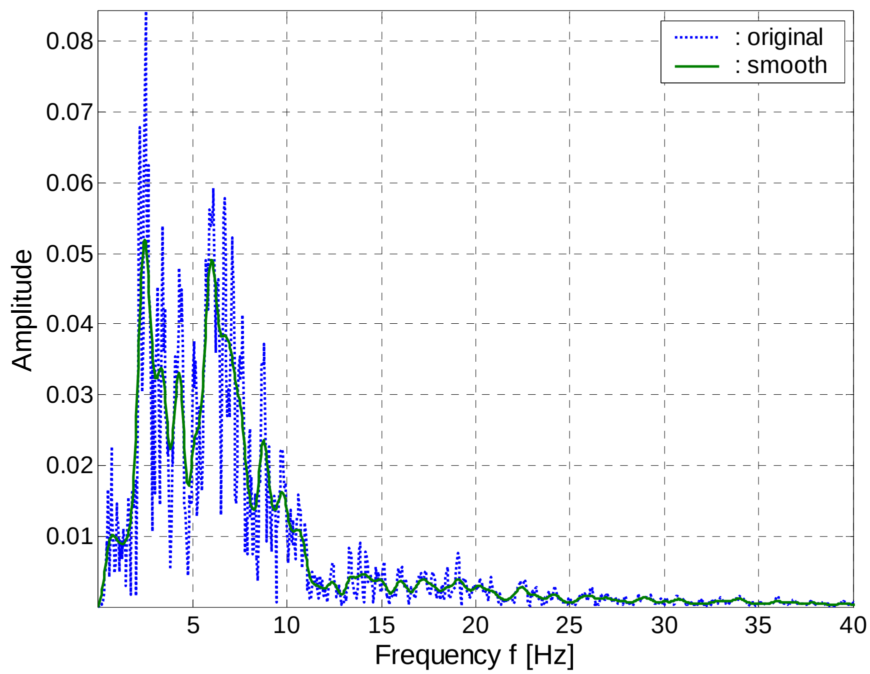

Figure 4.13. Fourier spectrum of the original record of the Friuli earthquake.

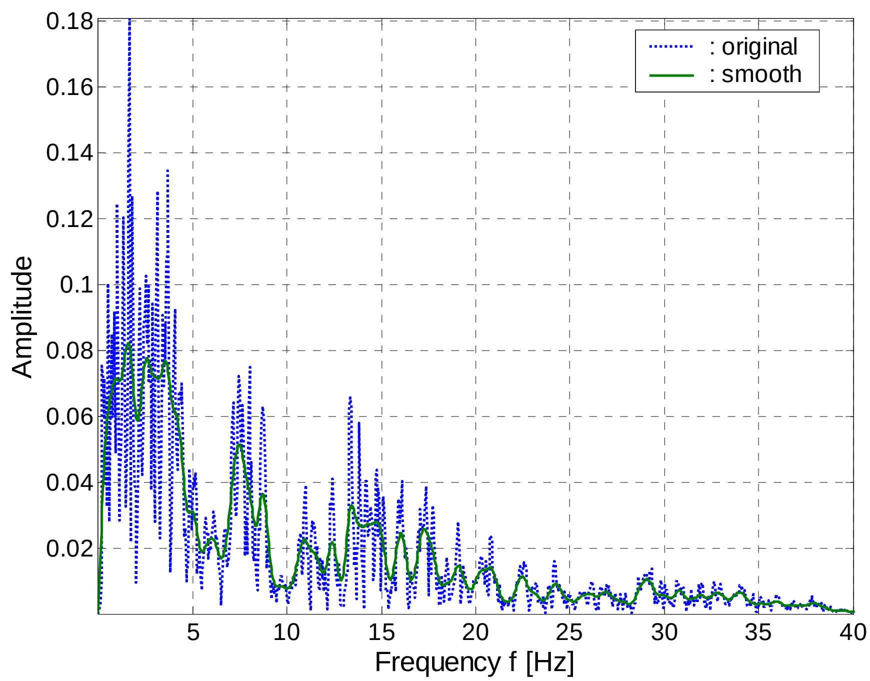

Figure 4.14. Fourier spectrum of the modified record of the Friuli earthquake.

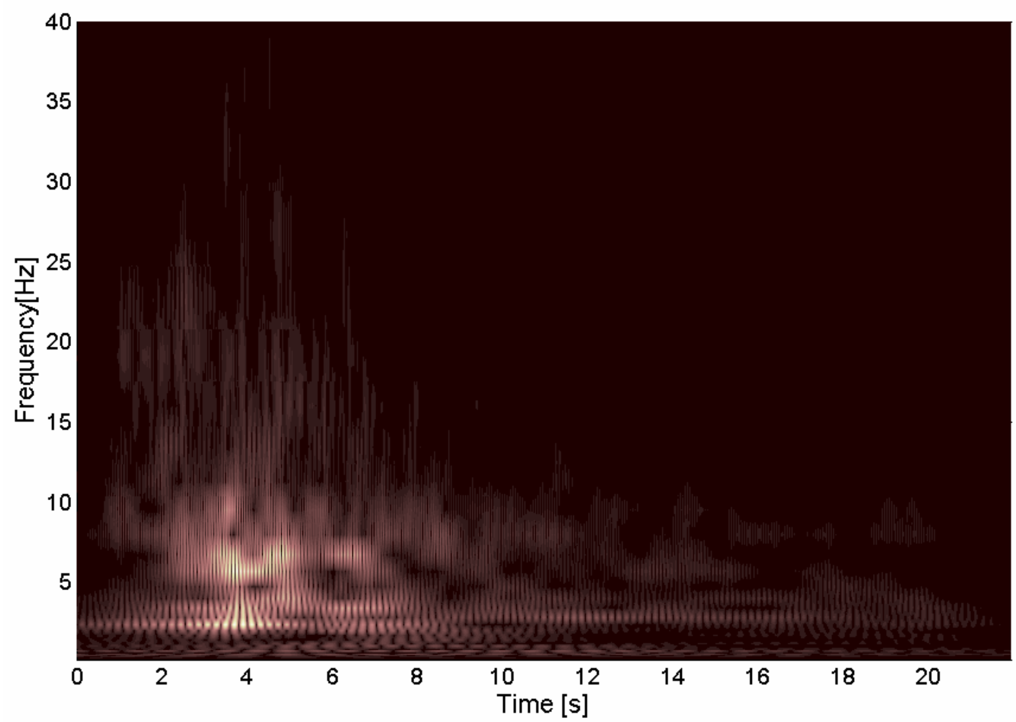

Figure 4.15. Wavelet Map of the original record of the Friuli earthquake.

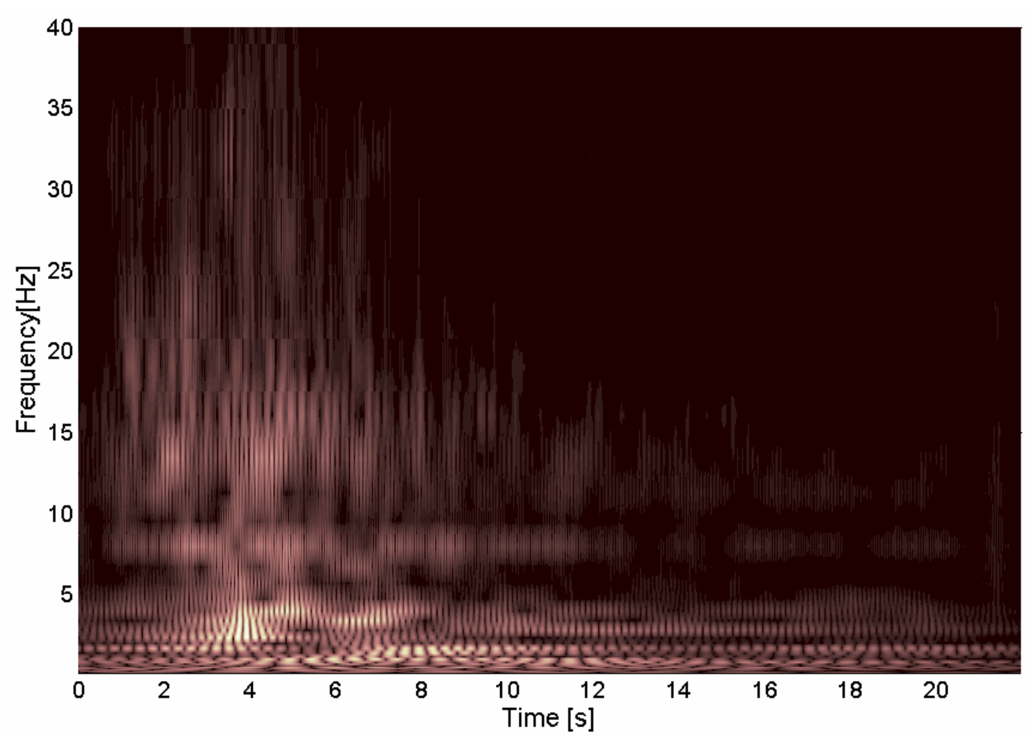

Figure 4.16. Wavelet Map of the modified record of the Friuli earthquake.

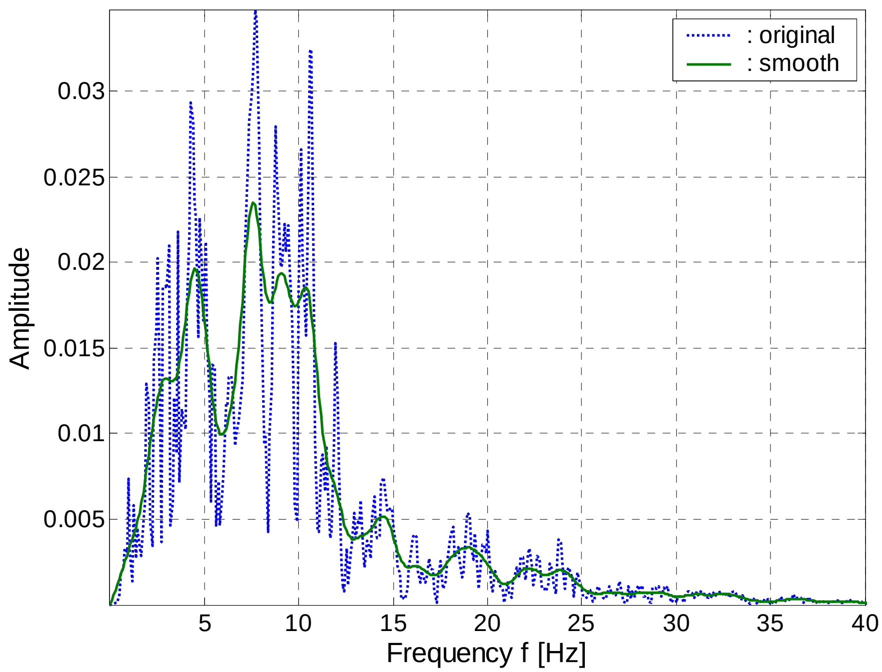

Figure 4.17. Fourier Spectrum of the original record of the Coalinga earthquake.

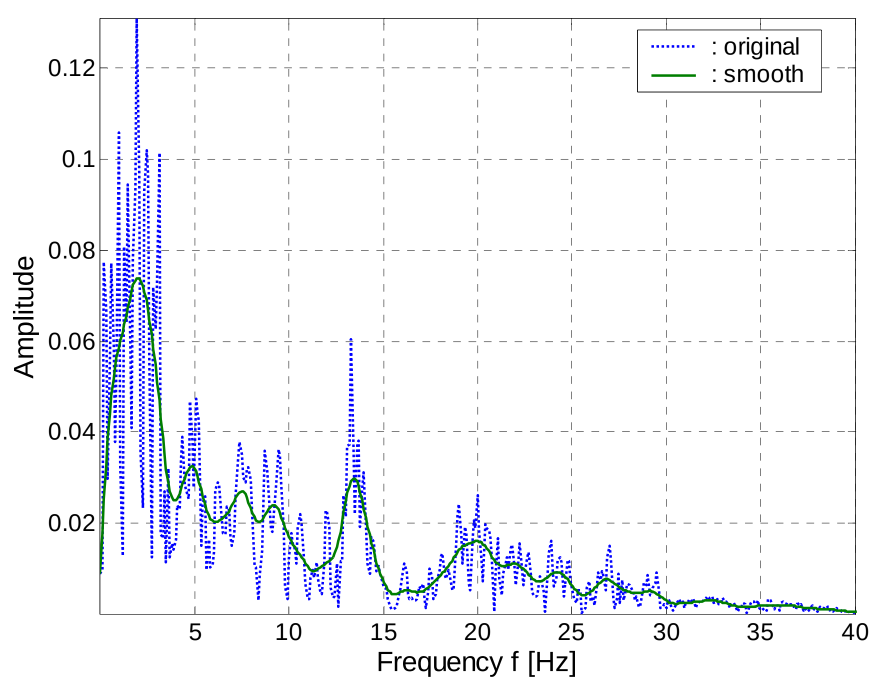

Figure 4.18. Fourier Spectrum of the modified record of the Coalinga earthquake.

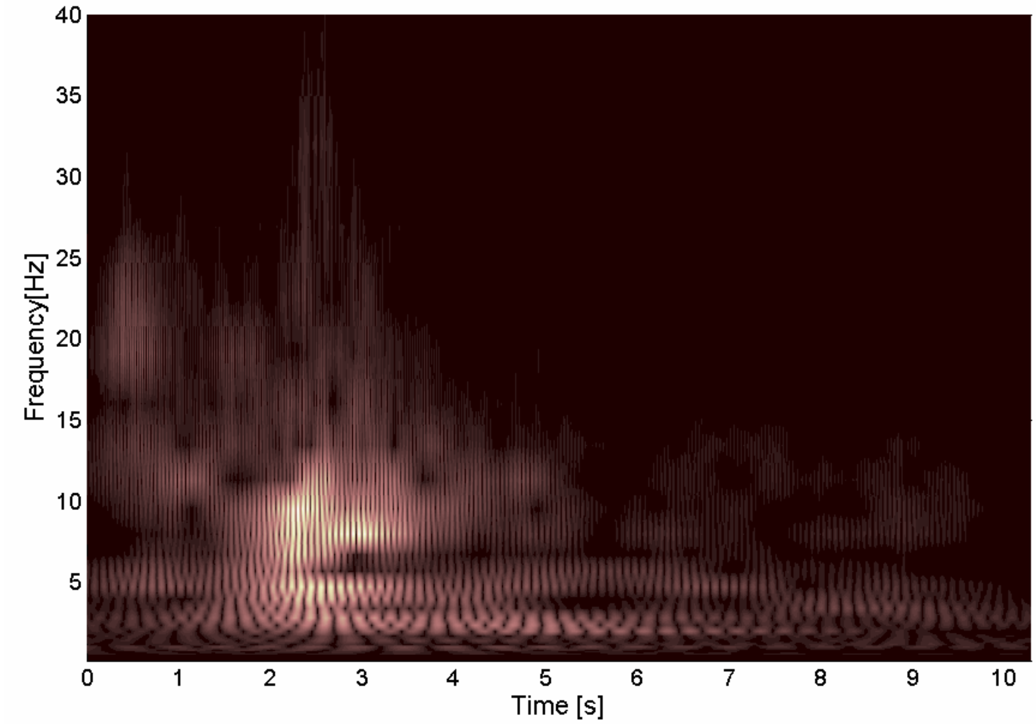

Figure 4.19. Wavelet Map of the original record of the Coalinga earthquake.

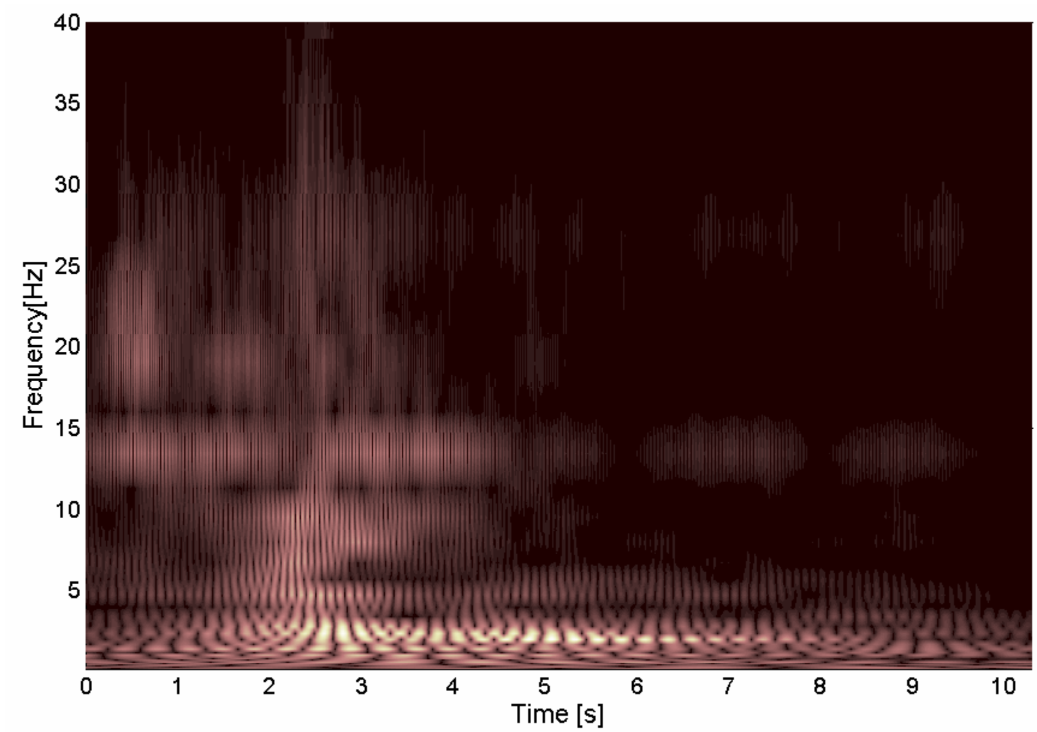

Figure 4.20. Wavelet Map of the modified record of the Coalinga earthquake.

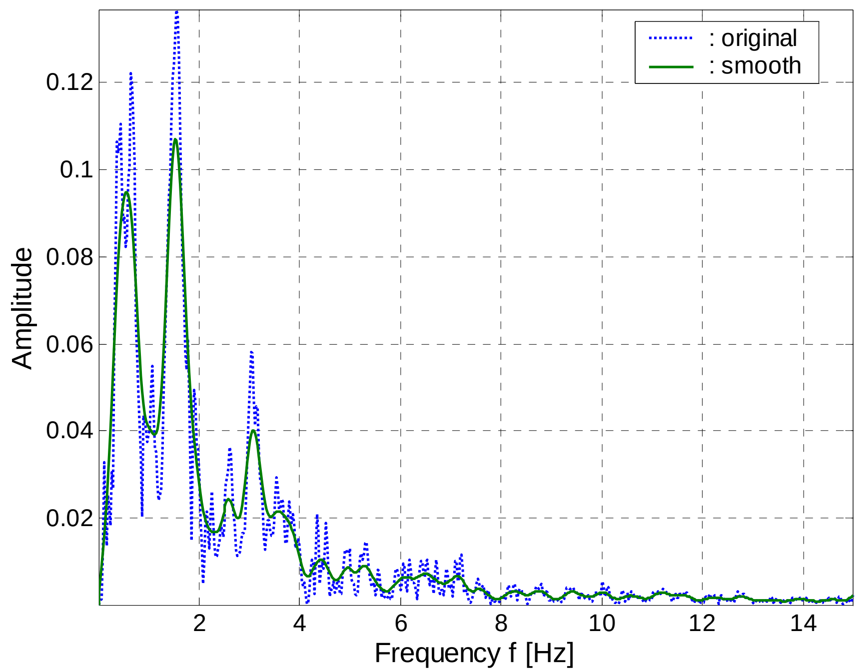

Figure 4.21. Fourier Spectrum of the original record of the Loma Prieta earthquake.

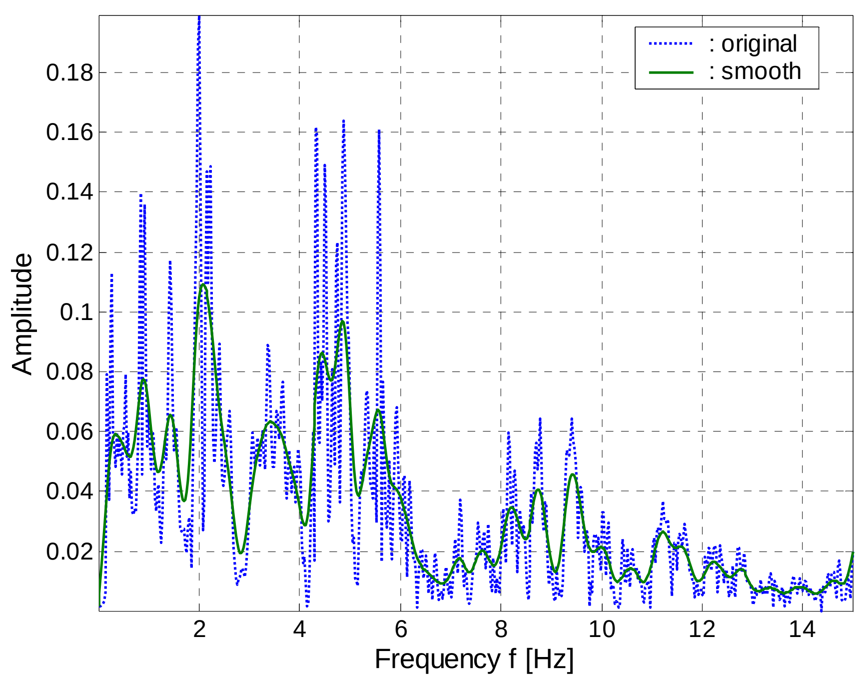

Figure 4.22. Fourier Spectrum of the modified record of the Loma Prieta earthquake.

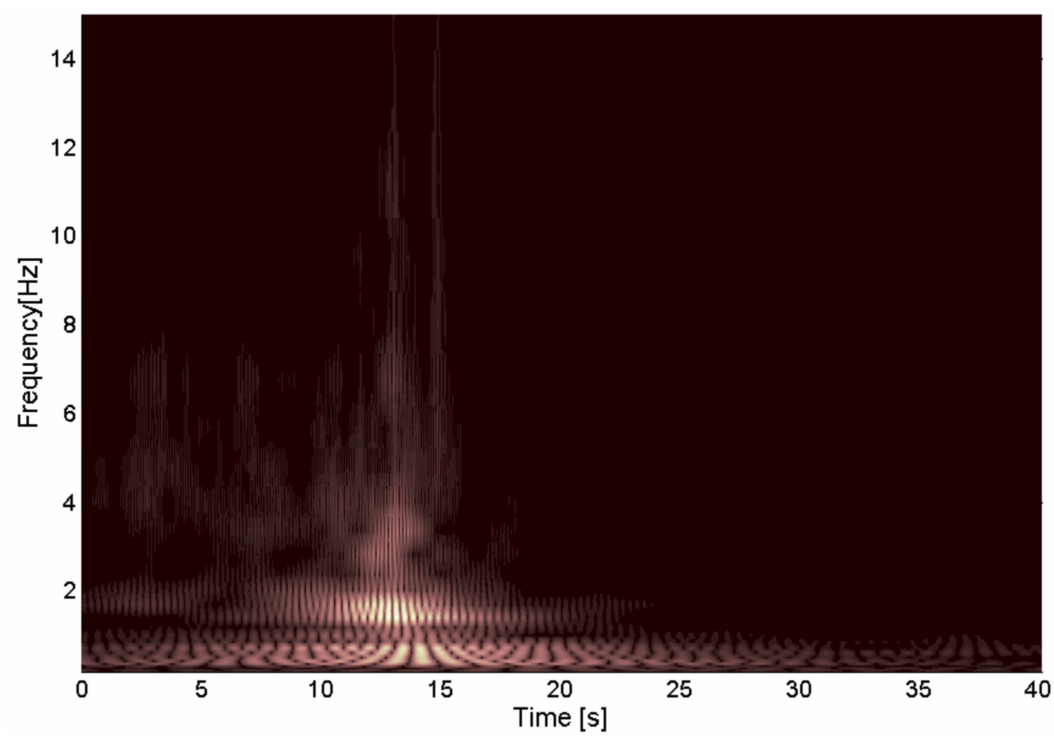

Figure 4.23. Wavelet Map of the original record of the Loma Prieta earthquake.

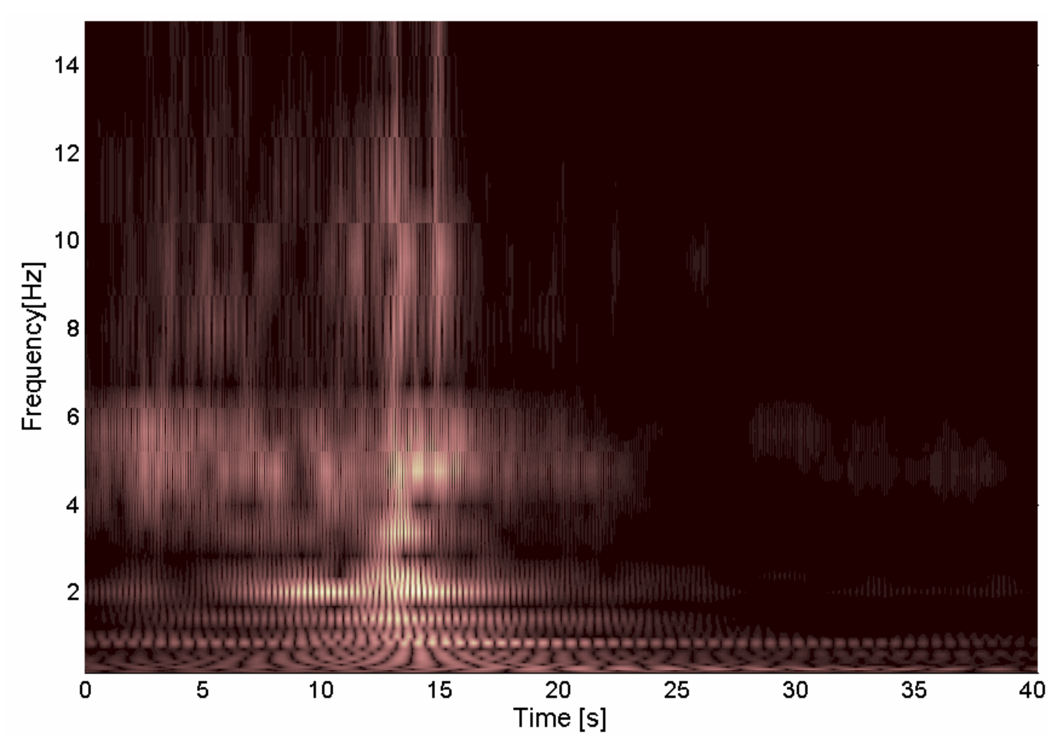

Figure 4.24. Wavelet Map of the modified record of the Loma Prieta earthquake.

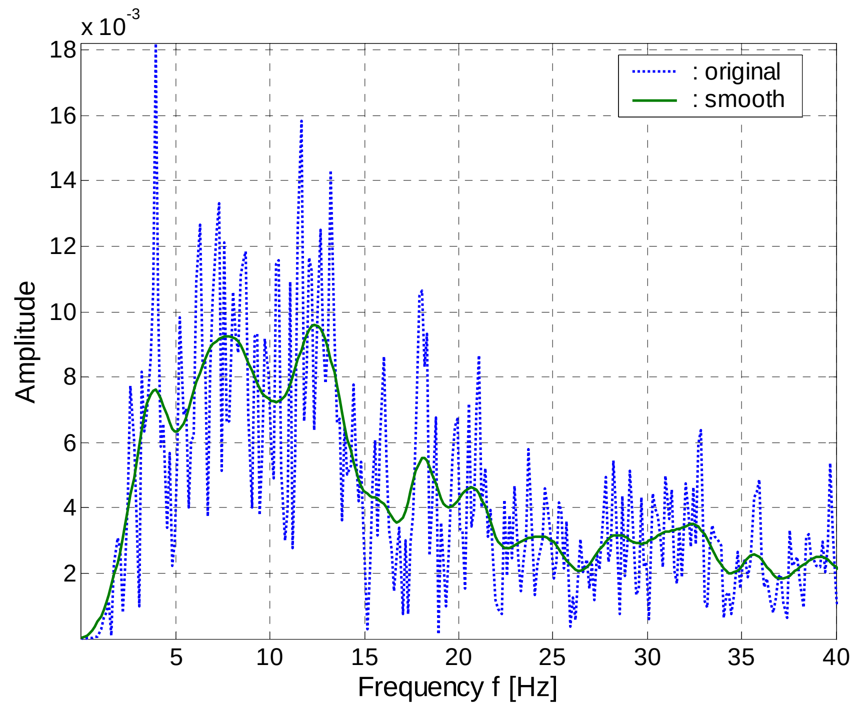

Figure 4.25. Fourier Spectrum of the original record of the Round Valley earthquake.

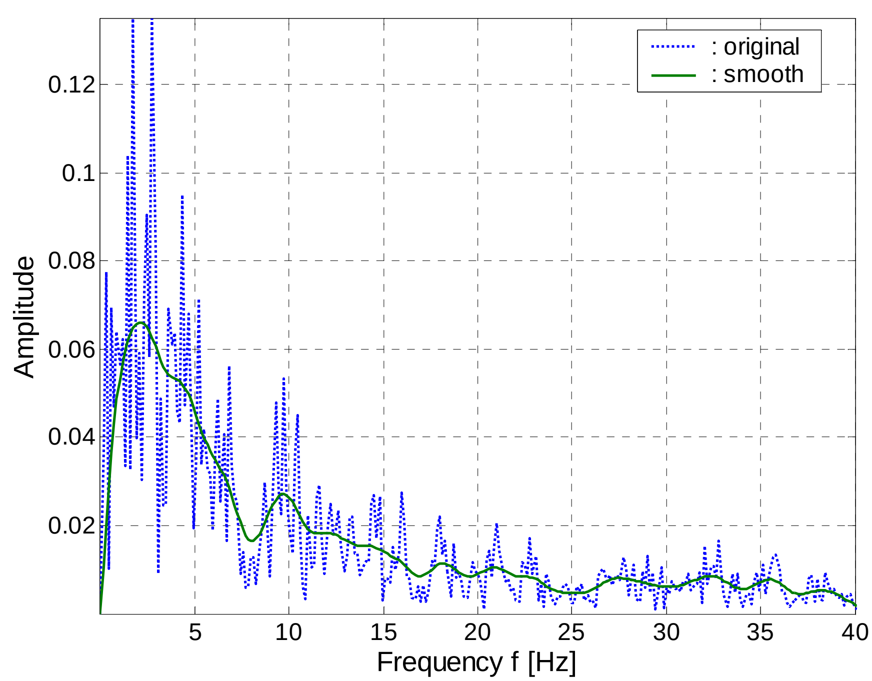

Figure 4.26. Fourier Spectrum of the modified record of the Round Valley earthquake.

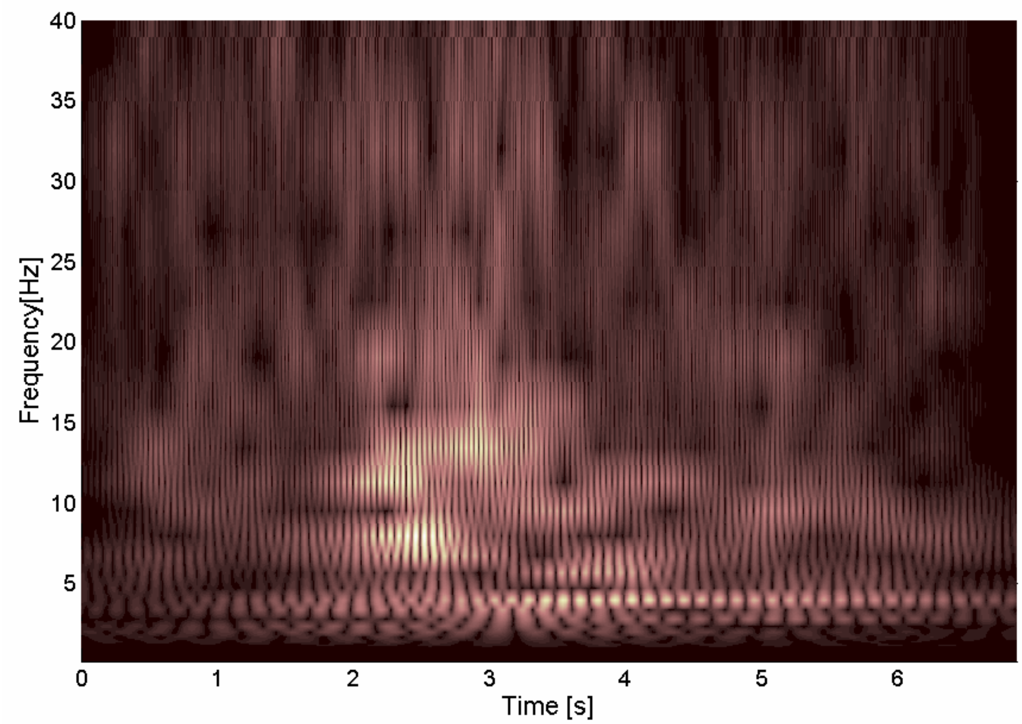

Figure 4.27. Wavelet Map of the original record of the Round Valley earthquake.

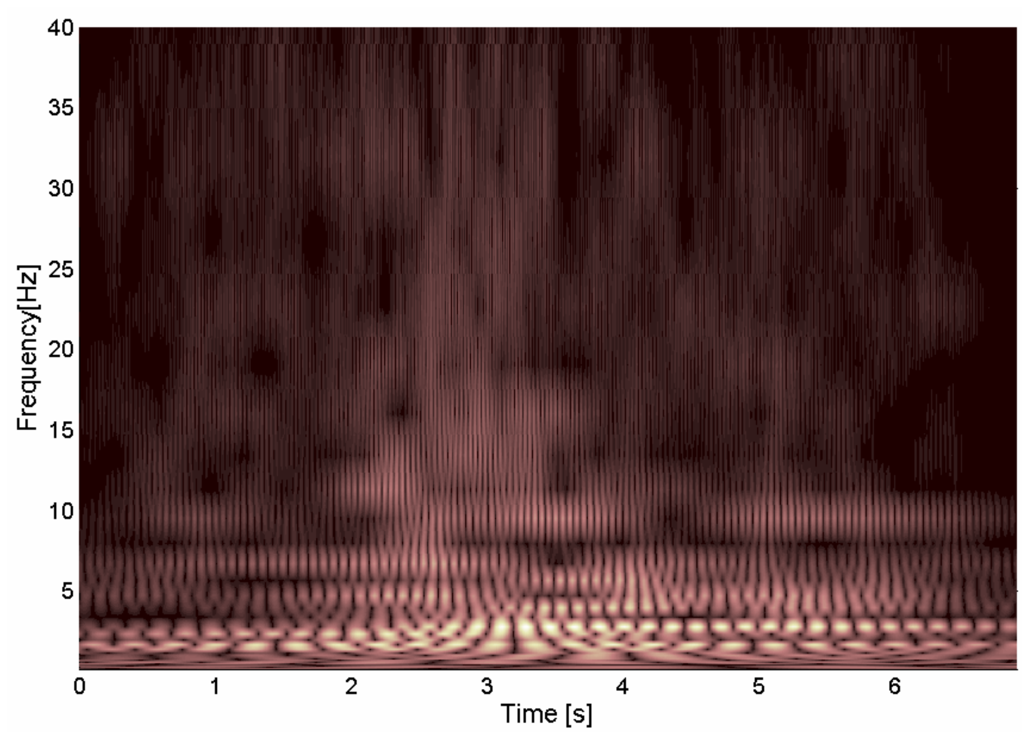

Figure 4.28. Wavelet Map of the modified record of the Round Valley earthquake.

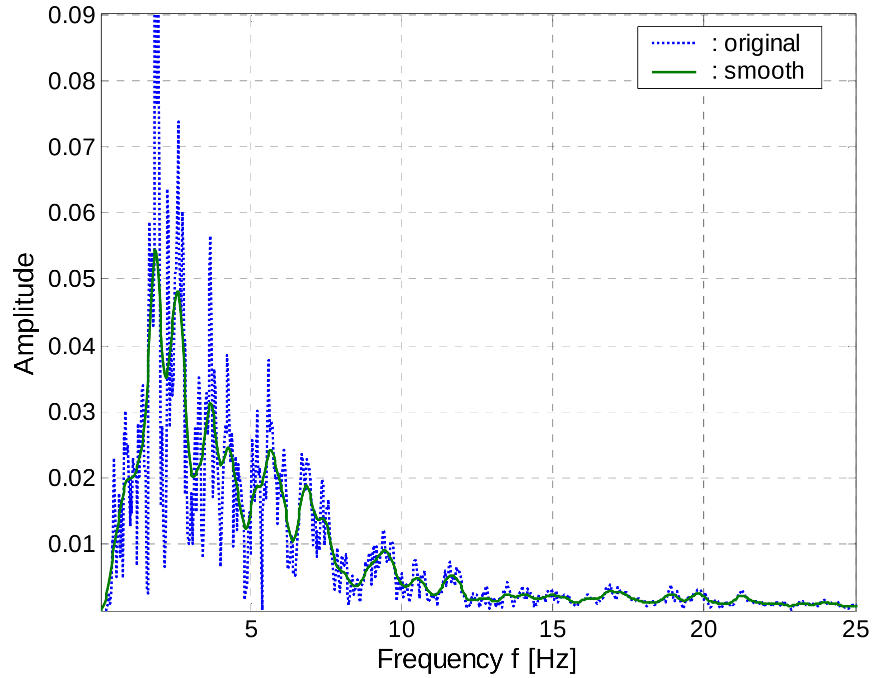

Figure 4.29. Fourier Spectrum of the original record of the Coyote Lake earthquake.

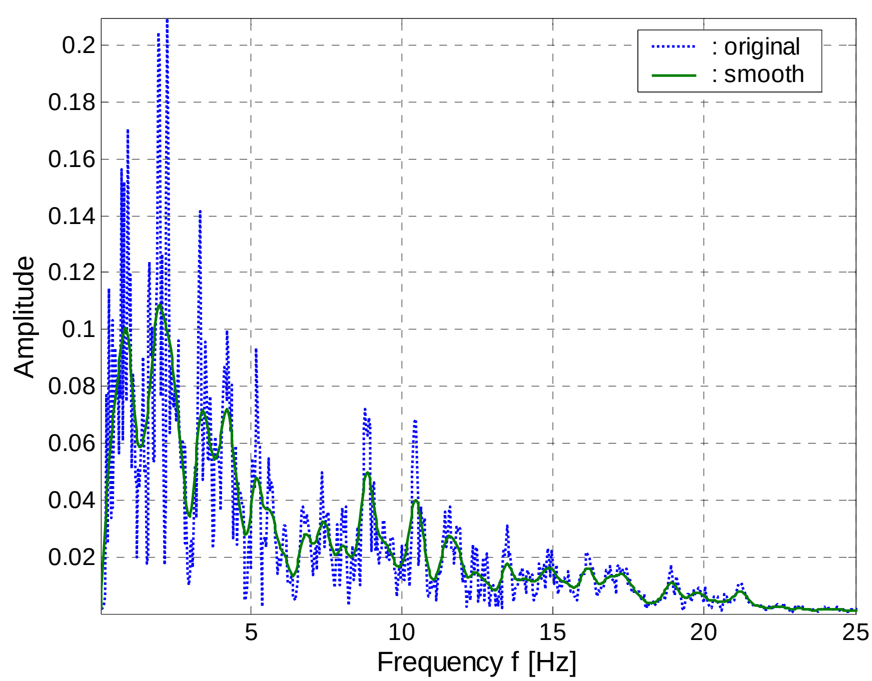

Figure 4.30. Fourier Spectrum of the modified record of the Coyote Lake earthquake.

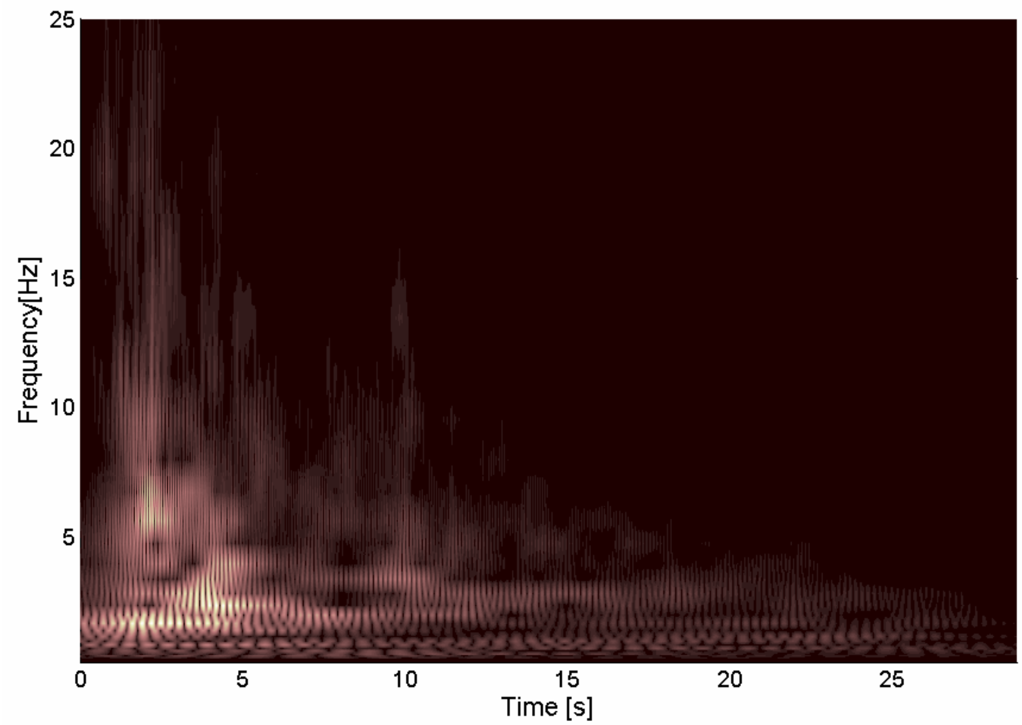

Figure 4.31. Wavelet Map of the original record of the Coyote Lake earthquake.

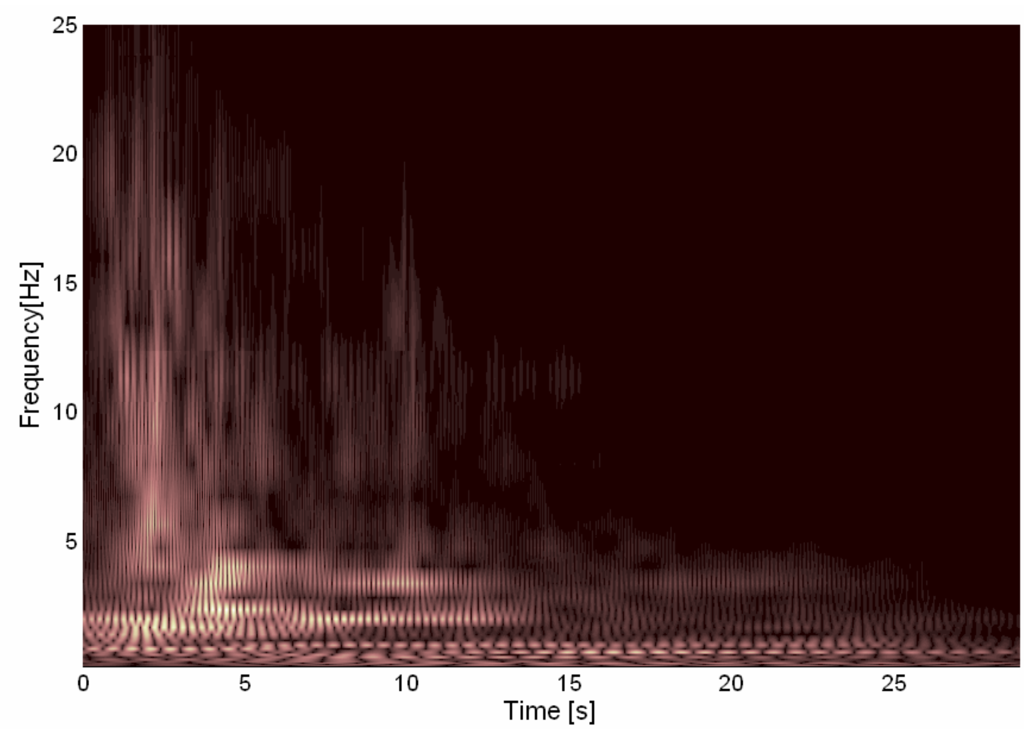

Figure 4.32. Wavelet Map of the modified record of the Coyote Lake earthquake.

4.5 Description of the computer program *SIMQKE*.

The program ***SIMQKE*** to generate synthetic accelerograms is based on the fact that the strong motion part of an earthquake record can be approximately consider as a "white noise", i.e. a random process composed of many (infinite in theory) sine waves with random phase. Therefore, an stationary accelerogram can be created using:

$$a(t) = \sum_{i=1}^{n} A_i \sin(\omega_i t + \phi_i) \tag{4.3}$$

where A_i is the amplitude and ϕ_i is the phase angle of the ith contributing sinusoid. By fixing the amplitudes A_i and then generating different arrays of phase angles, ground motions which are similar in general appearance (i.e., frequency content) but different in the "details" can be generated. The computer program uses a random number generator subroutine to produce phase angles ϕ_i with a uniform distribution in the range between 0 and 2π. The amplitudes A_i are related to the power spectral density function $G(\omega)$. The power spectral density function characterizes a stationary random process. In simple words, it expresses the relative importance (i.e., the relative contribution to the total power) of sinusoids with frequencies within some specified band. To simulate the transient character of real earthquakes, the stationary motion $a(t)$ is multiplied by a deterministic intensity function. *SIMQKE* uses trapezoidal, exponential, and compound functions. They are shown in Figure 4.33.

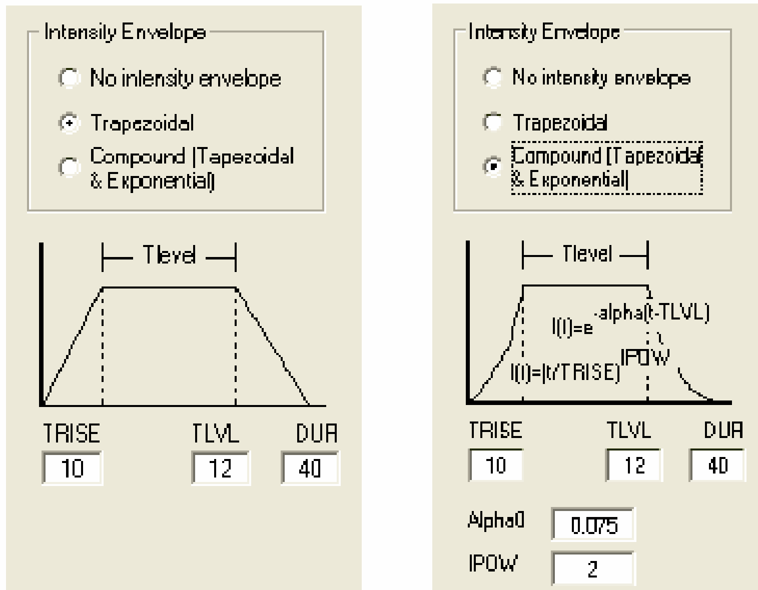

Figure 4.33. Intensity envelopes available in SIMQKE (from the *WinSIMQKE* interface).

4.6 Generation of artificial accelerograms using *SIMQKE*.

A set of 5 artificial accelerograms compatibles with the design spectrum specified in the UBC-97 (ICBO 1997) code for a seismic zone 3 and soil type S_B (rock) were generated using *WinSIMQKE* (Vázquez, 2002). This program is a Windows version of the original program SIMQKE developed by Dr. Drianfel Vázquez in the course of his doctoral studies at the Civil Engineering & Surveying Department of the University of Puerto Rico at Mayagüez.

All the accelerograms were generated using the compound intensity envelope (shown at the right side of Figure 4.33); the different parameters for the generation of the accelerograms are listed in Table 4.1.

Table 4.1 Parameters used for the generation of artificial records using SIMQKE.

Name	Duration [s]	Trise [s]	TLVL [s]	Alpha0	IPOW
Simqcase1	7	2	2	0.05	2
Simqcase2	10	3	2	0.25	1
Simqcase3	22	3	1	0.15	1
Simqcase4	30	2	3	0.15	2
Simqcase5	40	14	3	0.09	2

The accelerograms obtained and their acceleration response spectra are shown in Figures 4.34 to 4.43. The target spectrum is also superimposed in the response spectrum plots to compare the matching achieved. Note that all the acceleration histories display one or two sharp, isolated peaks. In fact, the PGA of the records is governed by these single peaks, a situation that is not common in most of the accelerograms of real earthquakes.

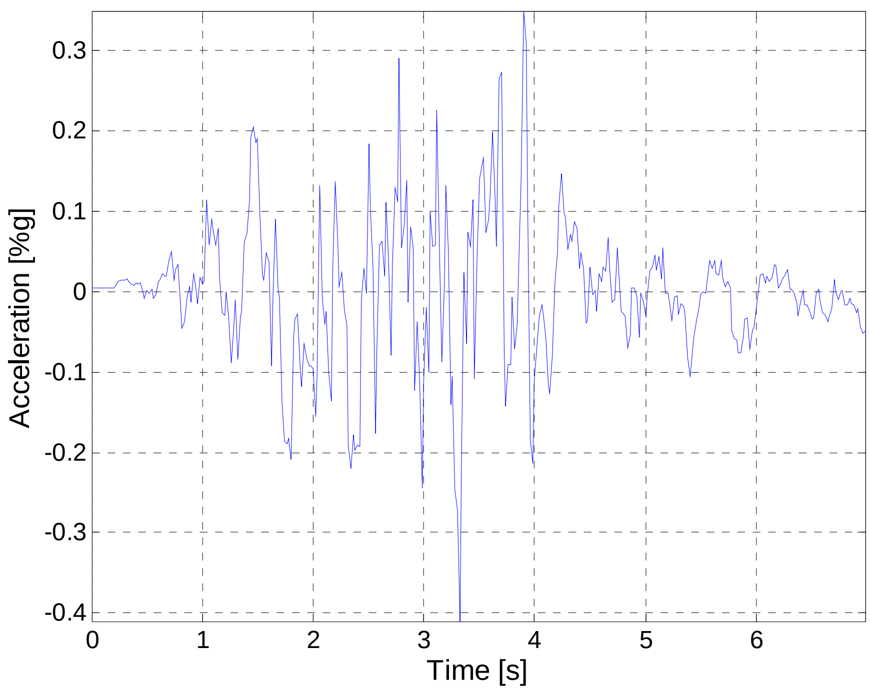

Figure 4.34. Acceleration time history of simqcase1

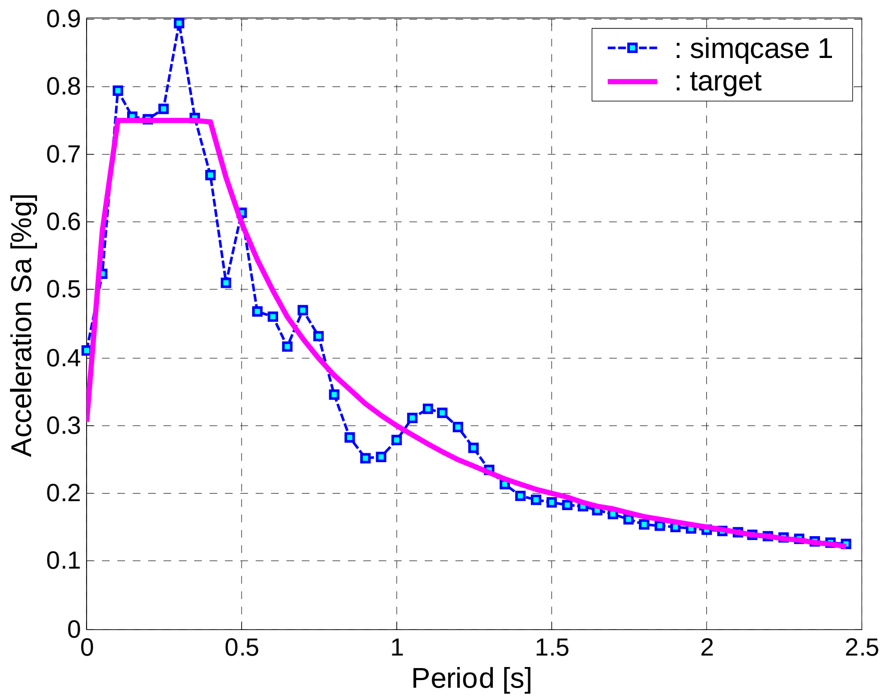

Figure 4.35. The target and the final response spectrum of simqcase1

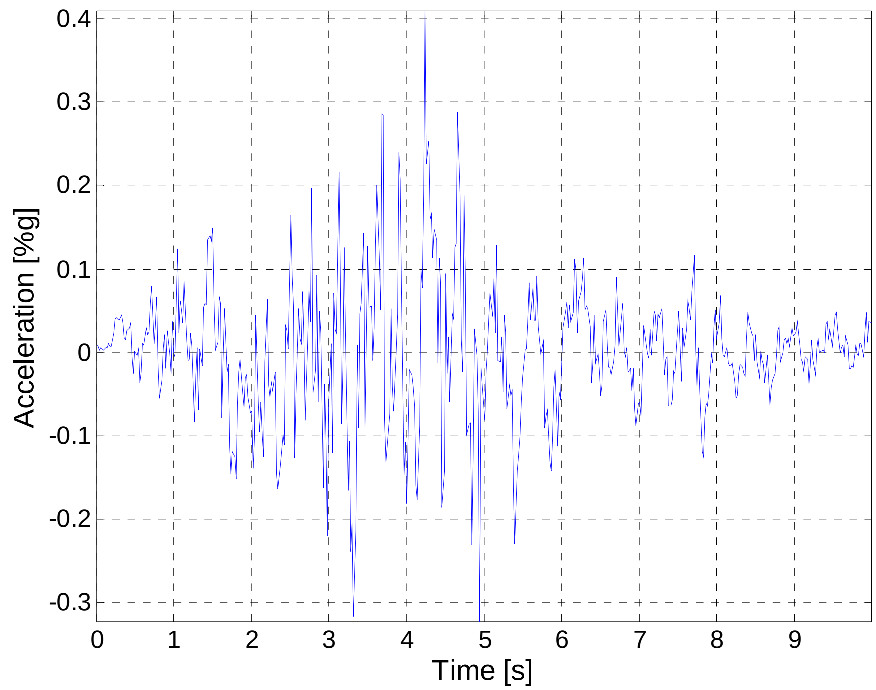

Figure 4.36. Acceleration time history of simqcase2

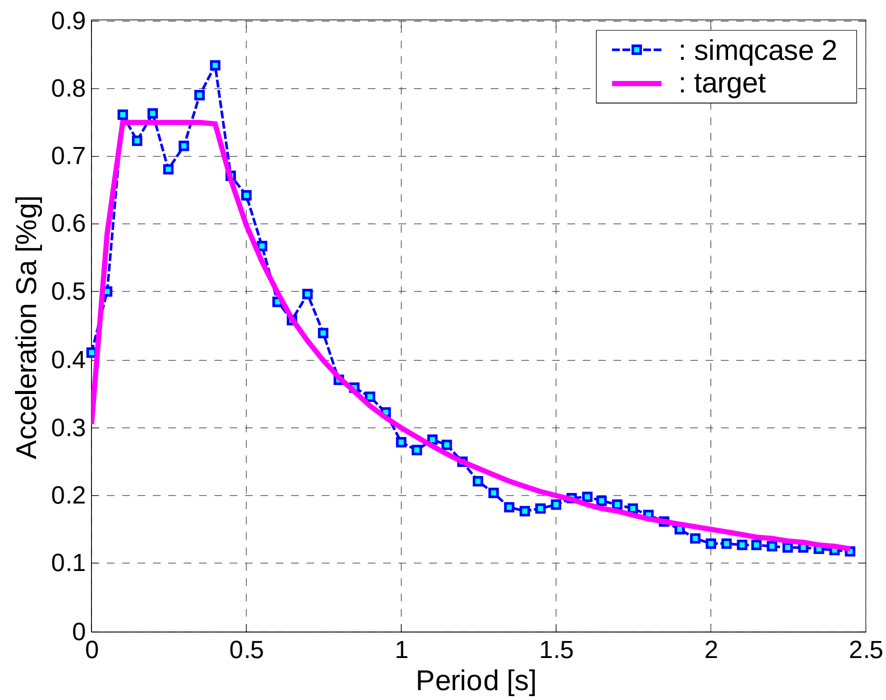

Figure 4.37. The target and the final response spectrum of simqcase2

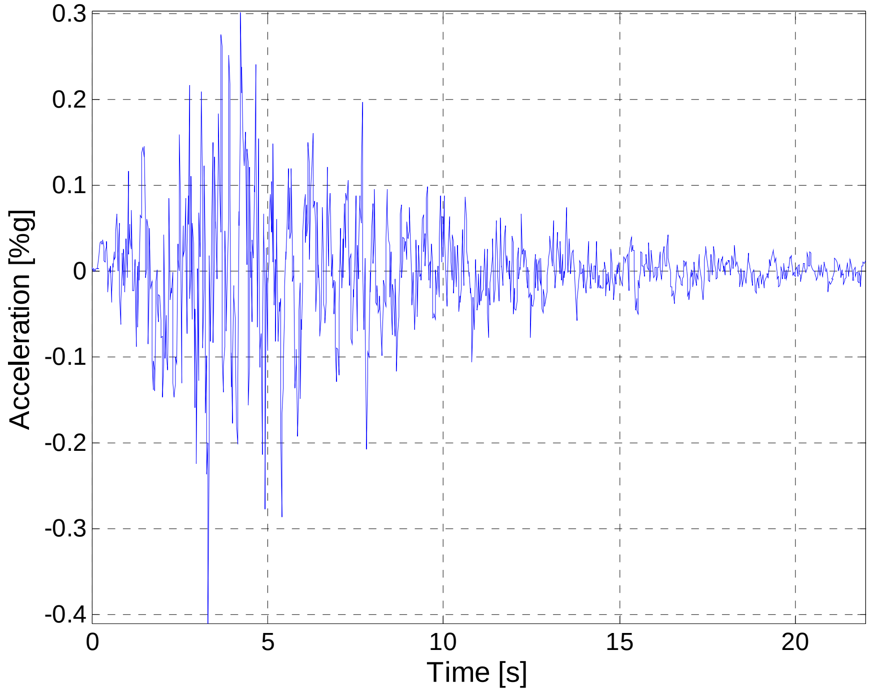

Figure 4.38. Acceleration time history of simqcase3

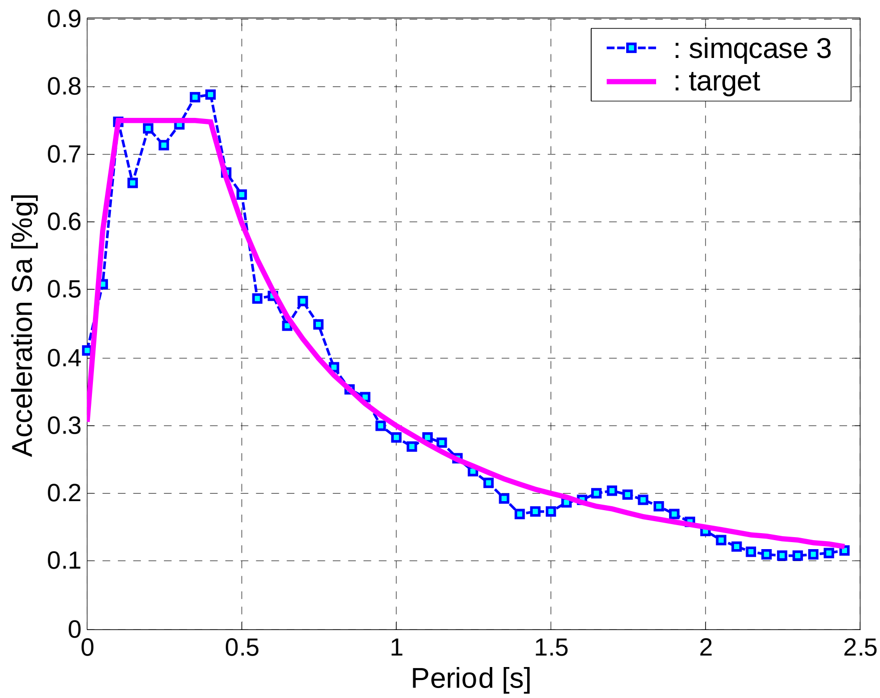

Figure 4.39. The target and the final response spectrum of simqcase3

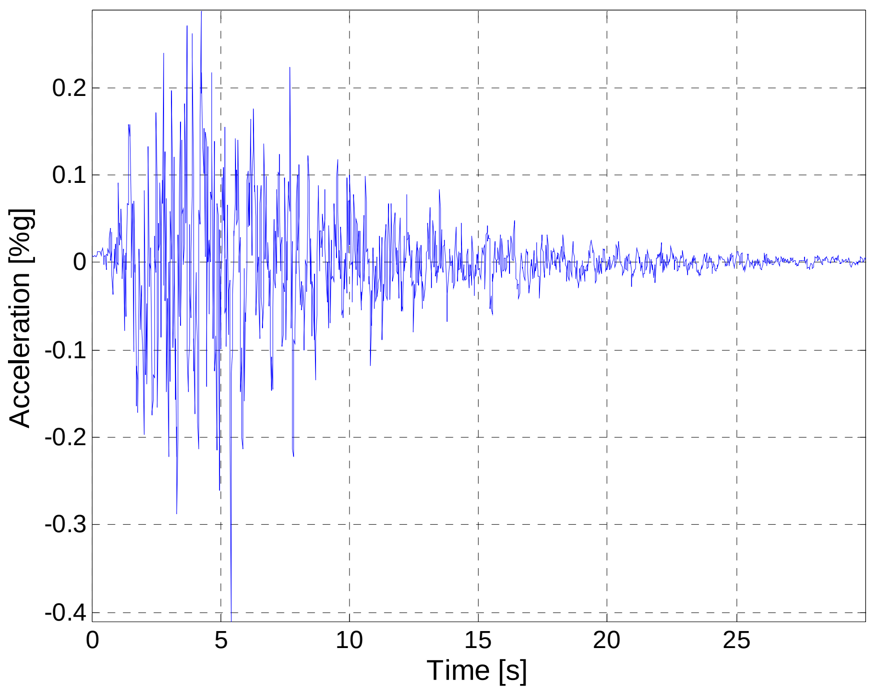

Figure 4.40. Acceleration time history of simqcase4

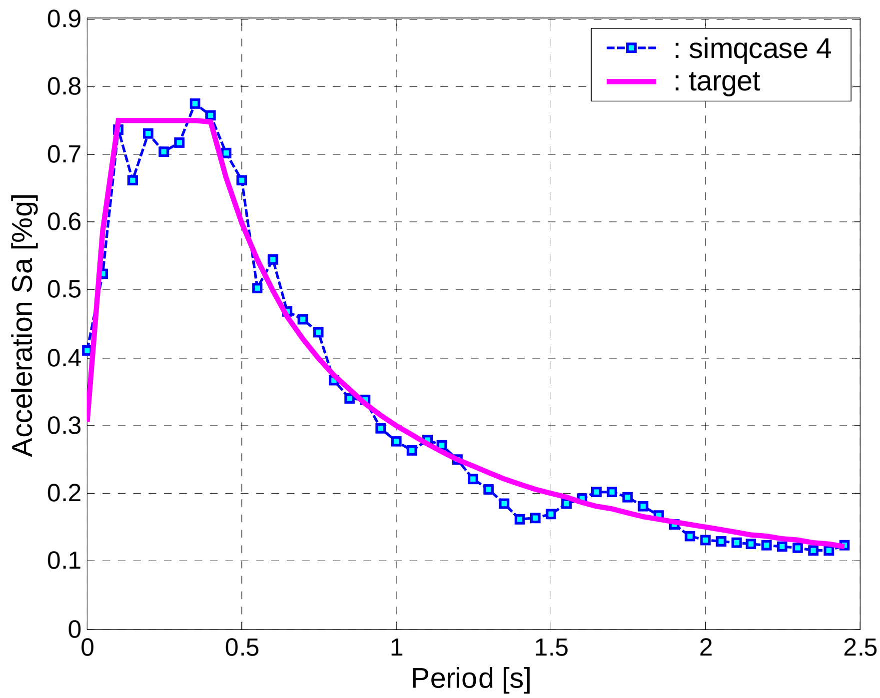

Figure 4.41. The target and the final response spectrum of simqcase4

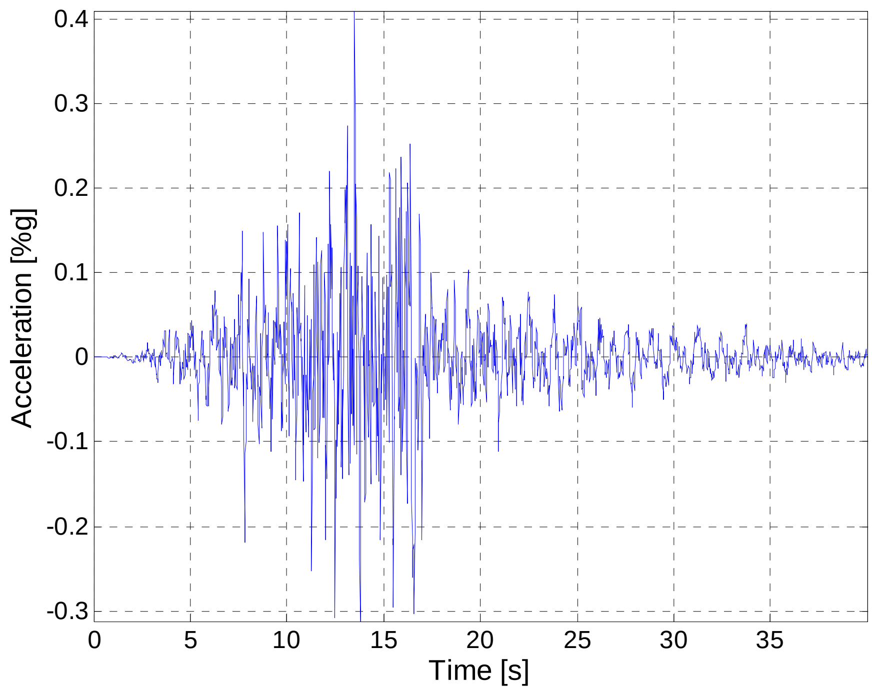

Figure 4.42. Acceleration time history of simqcase5

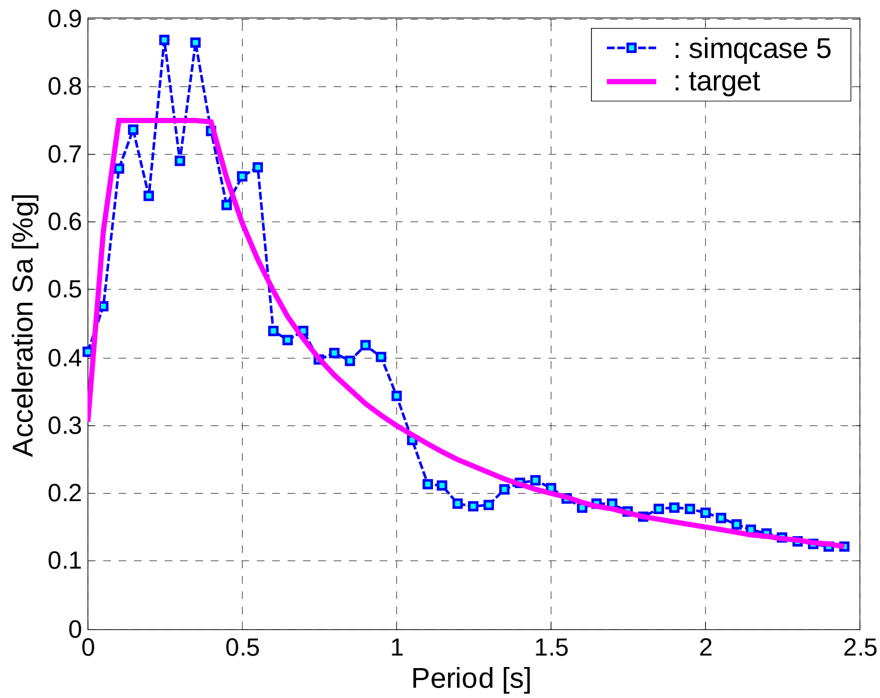

Figure 4.43. The target and the final response spectrum of simqcase5

4.7 Strong motion duration – The Husid plot

It has been shown that the duration of shaking can have a significant effect on the inelastic deformation and in the energy dissipation demands, especially for relatively weak short-period structures (Mahin, 1980). The duration of strong motions is also an important factor when acceleration time-histories are used in the analysis, such as in the calculation of soil response to bedrock motions, soil liquefaction studies and in non-linear structural dynamic analysis. Whether the accelerograms used in these cases are selected from databanks of real earthquake records or generated synthetically, it is important to ensure that the duration of shaking is consistent with the design scenario.

The approach followed in this investigation to identify and measure the strong shaking phase of accelerograms is based on the accumulation of energy in the accelerogram represented by the integral of the square of the ground acceleration. This quantity is known as the Arias intensity, AI. The Arias intensity (Arias, 1970) is defined as:

$$AI = \frac{\pi}{2g}\int_{o}^{t_r} a^2(t)dt \qquad (4.4)$$

where *a(t)* is the acceleration time history, t_r is the total duration of the accelerogram and *g* is the acceleration due to gravity. The "significant duration" is then defined as the interval over which some proportion of the total integral is accumulated. This is illustrated in Figure 4.44 for arbitrary limits AI_0 and AI_f on a plot of the build-up of the Arias intensity, known as a Husid plot (Husid, 1969).

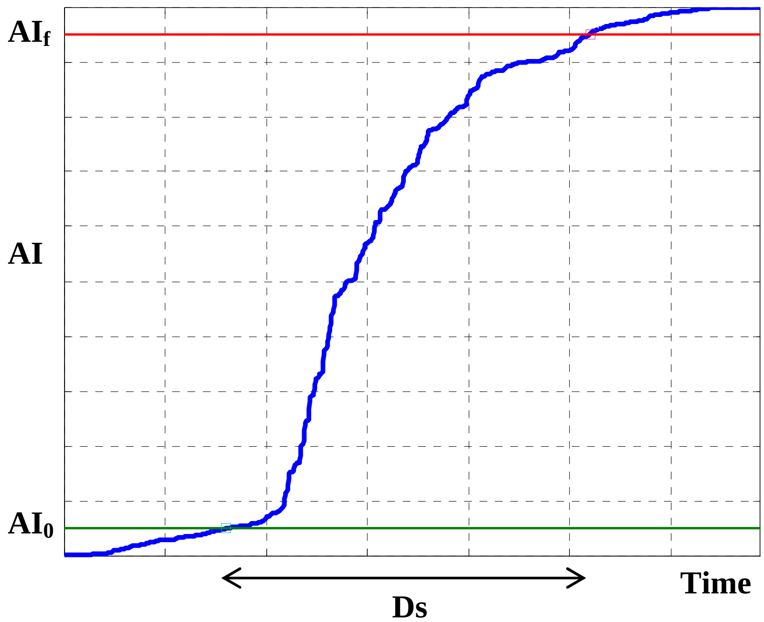

Figure 4.44. Conceptual definition of "significant duration" of an accelerogram

This concept has the advantage that it considers the characteristics of the entire accelerogram and defines a continuous time window in which the motion may be considered as strong. In this investigation the strong motion duration is defined as the interval between the times at which 5% and 95% of the total integral is attained (Trifunac and Brady, 1975).

4.8 Strong motion duration of the artificial records

The Husid's plots are used to identify the significant durations of the original and modified accelerograms. Figures 4.45 to 4.54 show these plots for the original and modified accelerograms of the five earthquakes considered. Examining these figures it is clear that the strong motion duration was increased after the original records were modified.

The lowest increase (22%) in strong motion duration occurred for the Round Valley earthquake (see Figures 4.51 and 4.52). The highest increase (223%) happened for the Loma Prieta ground motion, as it can be seen in Figures 4.49 and 4.50. The increase in the duration of the strong motion phase for the other earthquakes was 71% for Coyote Lake, 105% for Friuli, and 175% for the Coalinga earthquake.

To gain further insight into this feature of the matching procedure, we consider in detail the case of the Coalinga earthquake. As shown in Figures 4.47 and 4.48, the strong motion duration changed from 2.335 to 6.415 seconds. Observing the Husid plot of the modified record in Figure 4.48, it can be observed that there are at least three changes in slope between the 5% and the 95% intensities. Figures 4.55 displays the wavelet map above the Husid plot for the original accelerogram. Figure 4.56 shows similar plots but for the spectrum compatible record. In the original record the slope of the Husid plot between 55 and 95% is approximately constant. As it can be seen in the wavelet map in Figure 4.55, the dominant frequencies are around 8 Hz. In the Husid plot of the modified record, there is a step increase in the energy between 2.2 and 3 seconds, followed by a smaller slope (i.e., smaller rate of energy increase) between 3 and 5.7 seconds. The slope decreases further after 5.7 until 7.8 seconds. Observing the frequency decomposition in the wavelet map in Figure 4.56, one can see that the frequency content is rich in the first zone (2.2 to 3 seconds), it decreases from 3 to 5.7 seconds, then slightly diminishes from 5.7 to 7.8 seconds (the dominant wave having a frequency of about 2 Hz). Although it is more difficult to appreciate the previously mentioned features, they can also be seen in the acceleration time history in Figure 4.9.

Except for a rare record, most of the times the modified accelerogram needs to posses a richer frequency content than the original one in order to be compatible to a design spectrum. This is so because the usual design spectra have a high plateau extending from small to medium periods and it is unlikely that an original earthquake record will have components of similar intensities with these dominant periods. The matching procedure thus needs to amplify these components. As it was explained in CHAPTER II, the proposed procedure does not create nor add new components: it just amplifies (or reduces depending on the case) those waves already present in the signal. Therefore, when it increases the weight of some components, the strong motion phase of the original accelerogram will practically always be stretched.

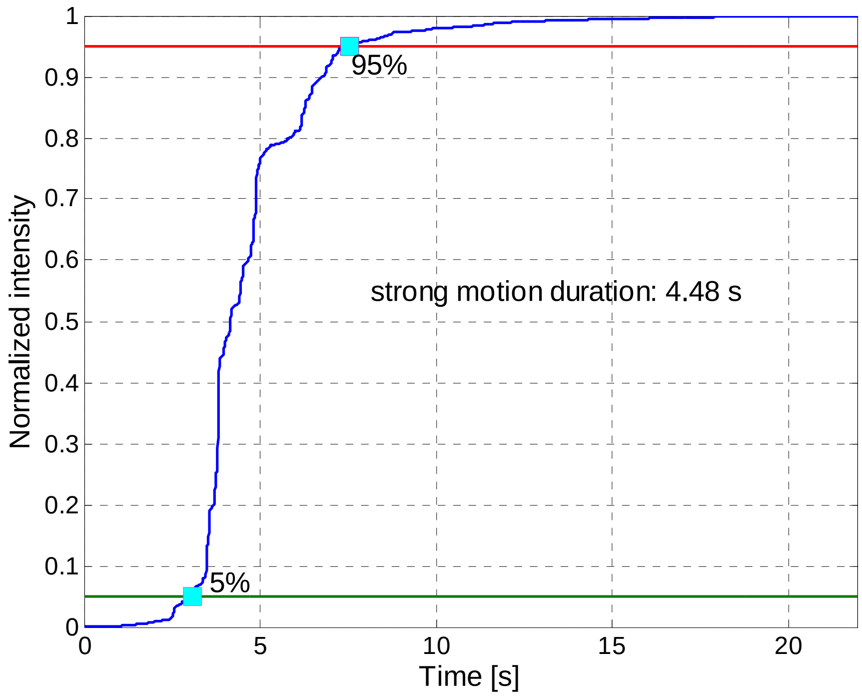

Figure 4.45. Significant duration of the original record of the Friuli earthquake

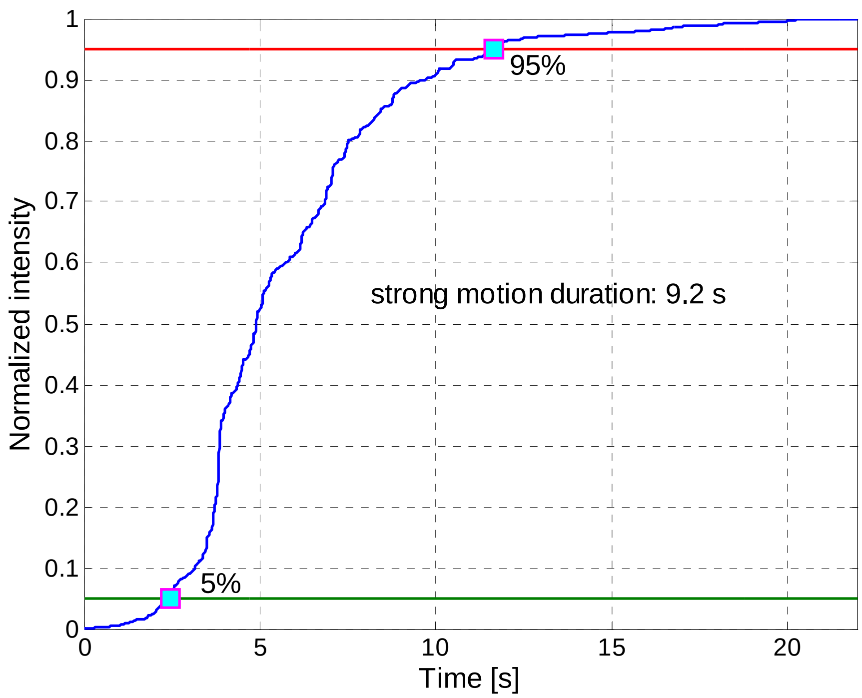

Figure 4.46. Significant duration of the modified record of the Friuli earthquake

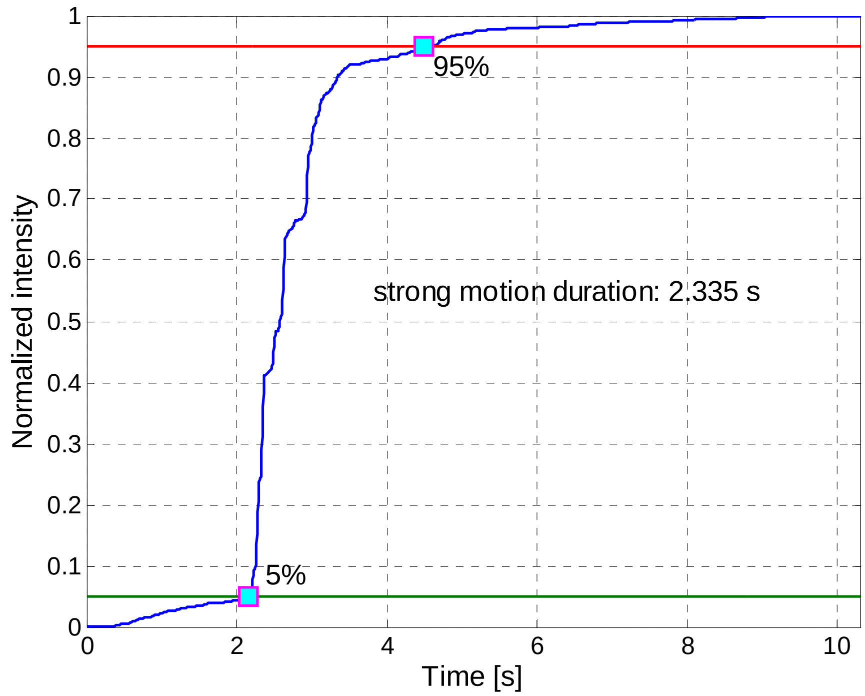

Figure 4.47. Significant duration of the original record of the Coalinga earthquake

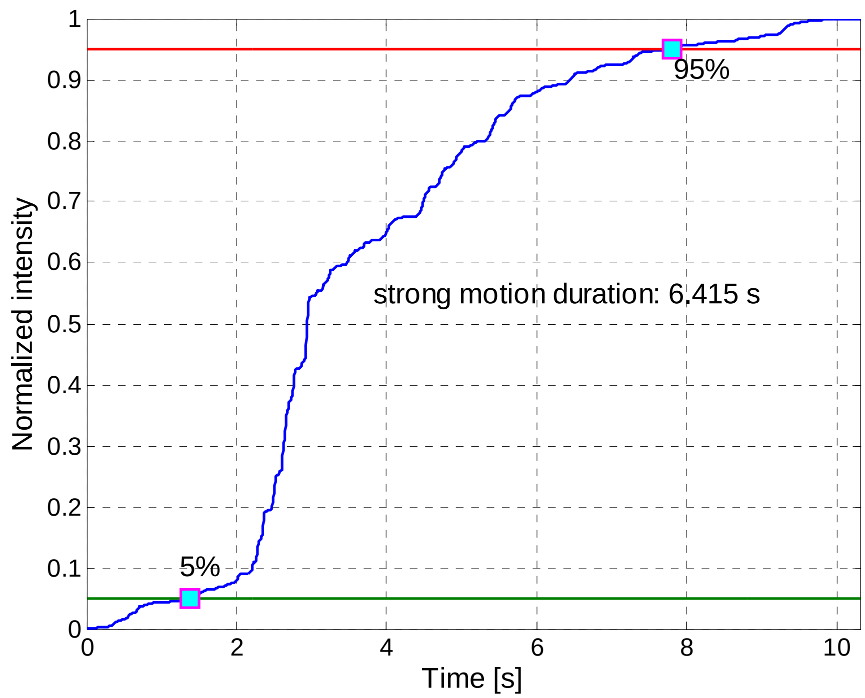

Figure 4.48. Significant duration of the modified record of the Coalinga earthquake

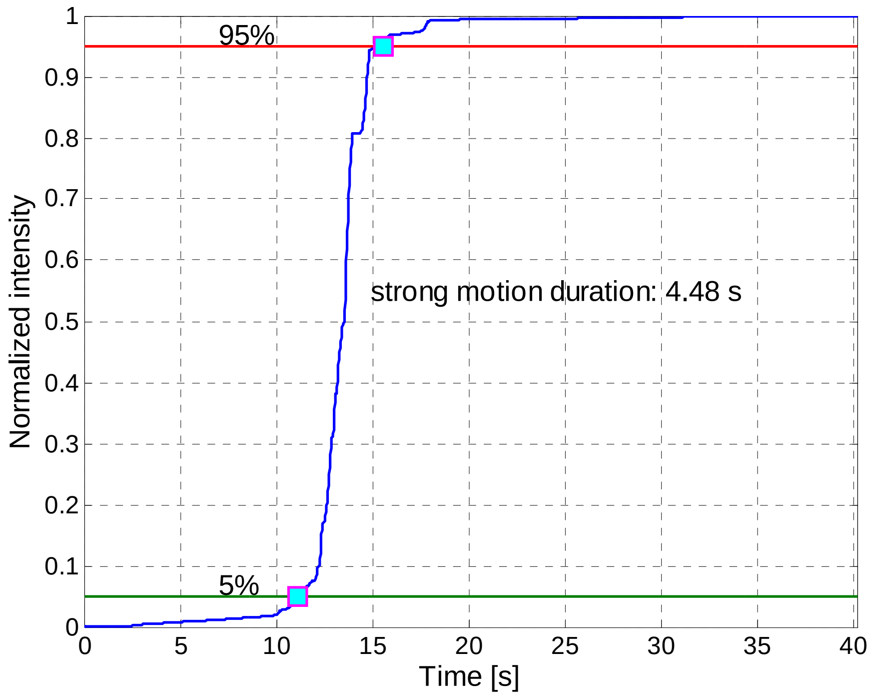

Figure 4.49. Significant duration of the original record of the Loma Prieta earthquake

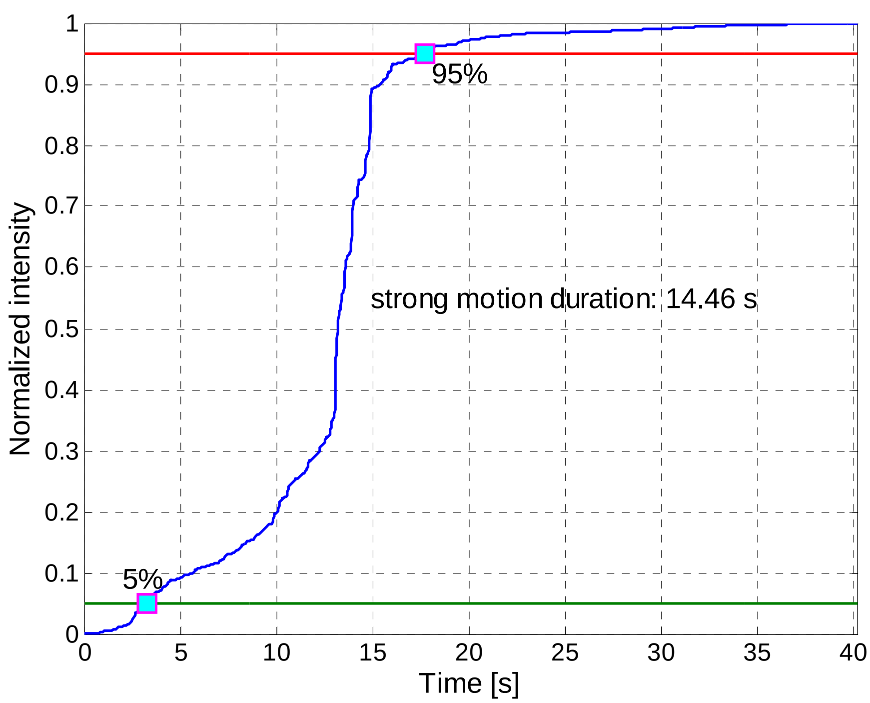

Figure 4.50. Significant duration of the modified record of the Loma Prieta earthquake

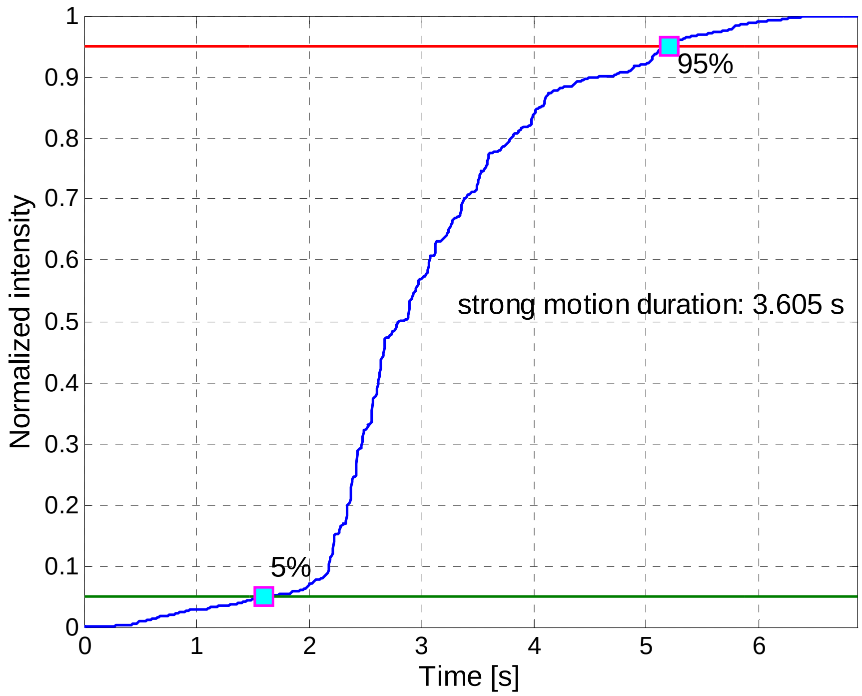

Figure 4.51. Significant duration of the original record of the Round Valley earthquake

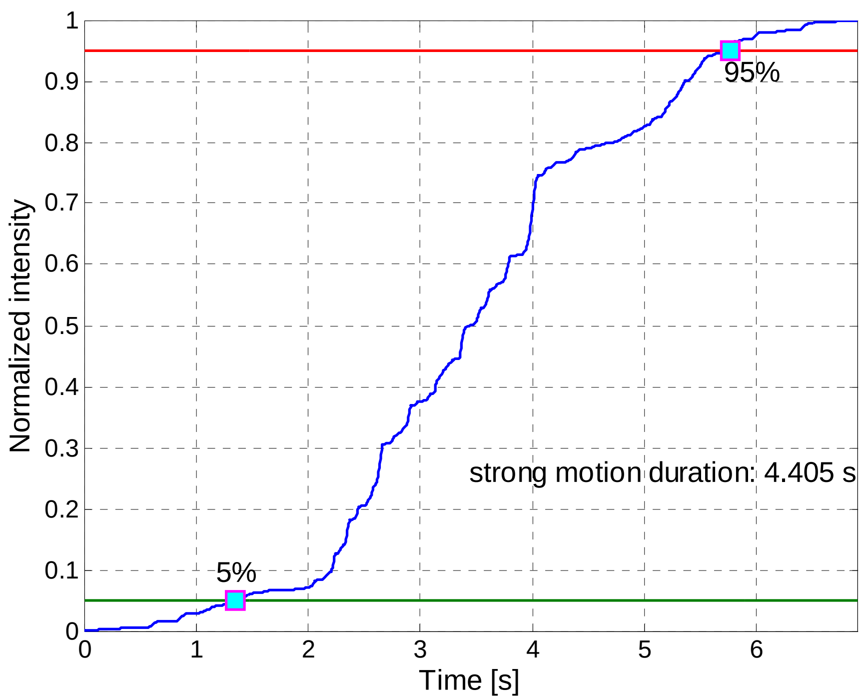

Figure 4.52. Significant duration of the modified record of the Round Valley earthquake

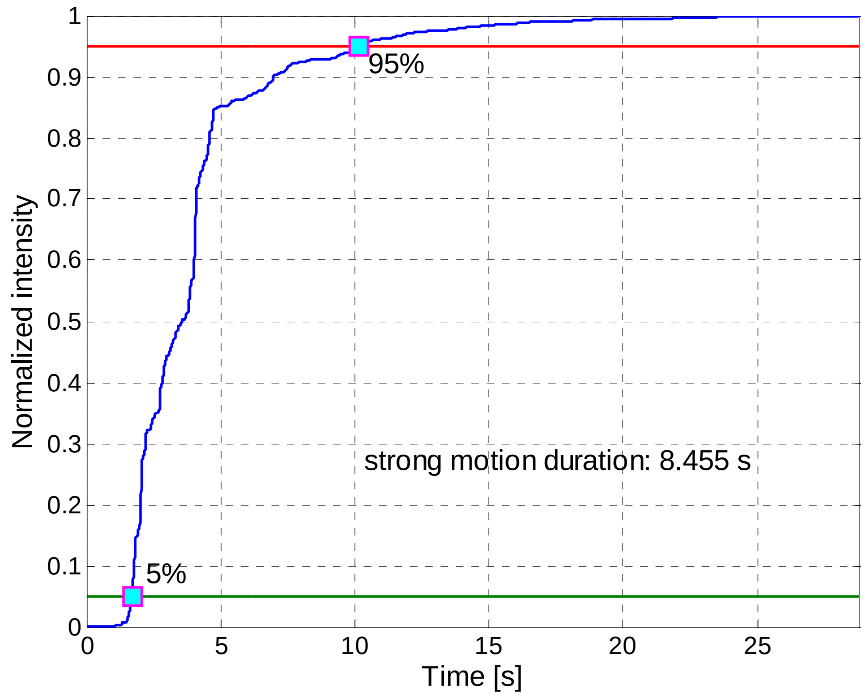

Figure 4.53. Significant duration of the original record of the Coyote Lake earthquake

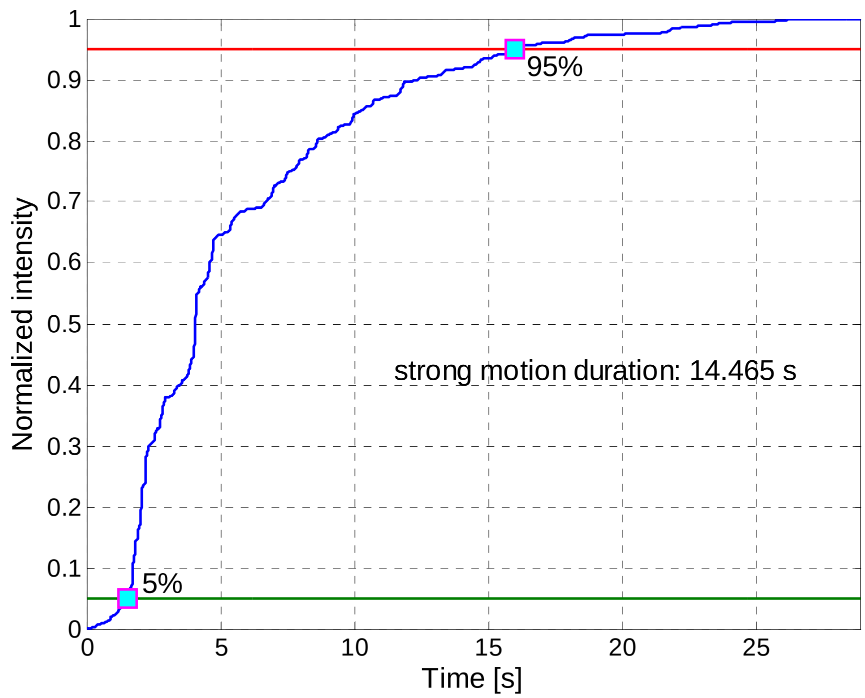

Figure 4.54. Significant duration of the modified record of the Coyote Lake earthquake

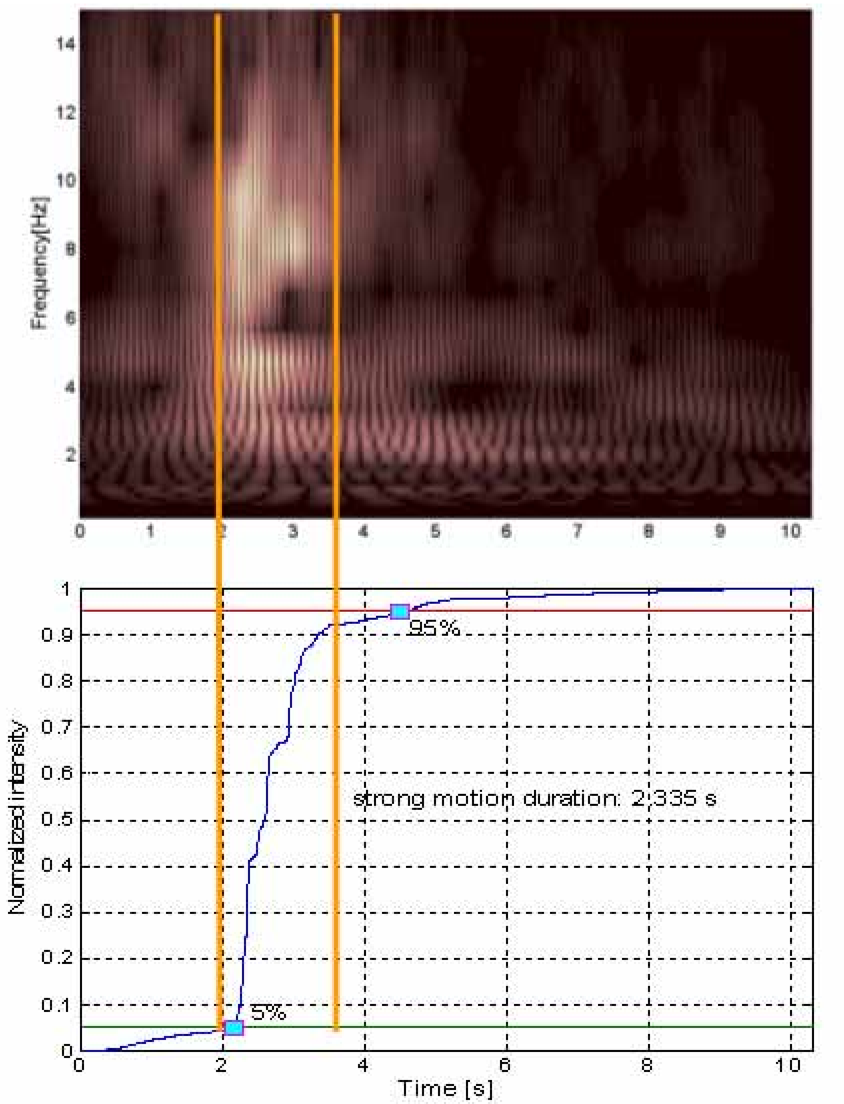

Figure 4.55. Wavelet Map and Husid Plot of the original record of the Coalinga earthquake

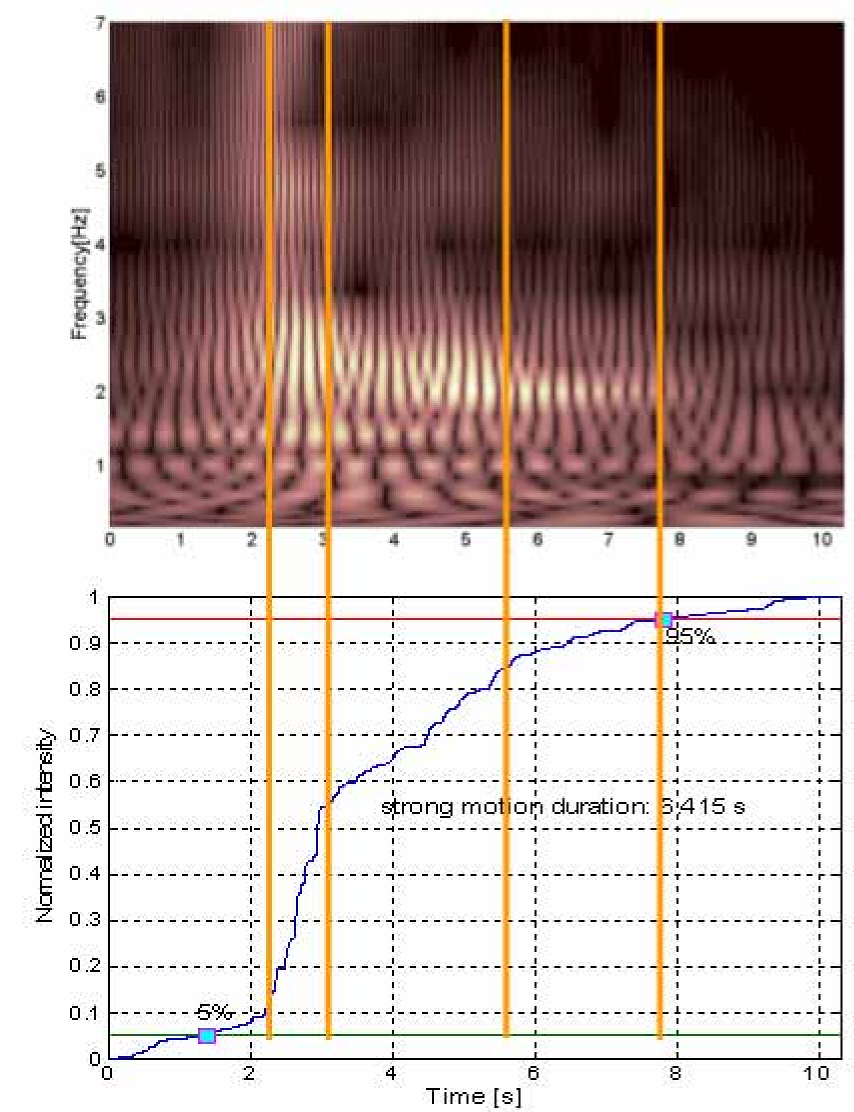

Figure 4.56. Wavelet Map and Husid Plot of the modified record of the Coalinga earthquake

4.9 Energy content – The Input Energy Spectrum

The current seismic design practice, which is based on strength considerations (implied in the use of the pseudo acceleration spectrum), does not directly account for the influence of the duration of strong motion or for the hysteretic behavior of the structure.

The hysteretic behavior is addressed indirectly by using the response modification factor R which is based primarily on the structural system selected. A design based on energy principles, on the other hand, has the potential to directly address the effects of the duration and hysteretic behavior.

In an energy-based seismic design, one needs to estimate the input energy to the structure and distribute it to its various structural components. Housner was probably the first one to recommend an energy approach for earthquake resistant design. He pointed out that when the ground motion transmits energy into the structure, some of this energy is dissipated through damping and nonlinear behavior, and the remaining is stored in the structure in the form of kinetic and elastic strain energy. Housner (1956) computed the input energy per unit mass as:

$$\frac{E_i}{m} = \frac{1}{2}(PSV)^2 \tag{4.5}$$

where m is the mass and PSV denotes the pseudo-spectral velocity.

Zahrah and Hall (1984) indicated that for linear structures under the same ground motion, the input energy spectra are generally similar in shape to the Fourier response spectra. They also pointed out that for an undamped structure equation 4.5 provides a good estimate of the amount of input energy imparted to the structure. However, Uang and Bertero (1990) argued that for linear structures the equation proposed by Housner to estimate input energy reflects the maximum elastic energy stored in the structure without consideration of the energy dissipated by damping.

In any case, the input energy spectrum of artificial accelerograms is another characteristic that can be useful to analyze these records. In the next section these spectra are calculated for the five earthquakes considered according to equation 4.5.

4.10 Input energy spectra of the artificial records

Figure 4.57 shows the input energy spectra for the original and the modified record of the Friuli earthquake computed according to equation 4.5. The spectrum of the modified record exhibits a high level of input energy spread over a very wide range of periods. On the contrary, the input energy spectrum of the original record drops rapidly for high periods. This mismatch between the energy spectra of real and artificial records was the focus of criticism for the use of artificial accelerograms (Naeim and Lew 1995). The shape of the input energy spectrum of the compatible accelerogram obtained by modifying the Friuli record is typical of all the artificial records. This is expected since the pseudo-spectral velocity (PSV) is related to the pseudo-spectral acceleration (PSA) in the following way:

$$PSV = \left(\frac{T}{2\pi}\right) PSA \tag{4.6}$$

It is obvious that any record compatible with a pseudo acceleration design spectrum *PSA(T)* will have Input Energy Spectra that is approximately given by:

$$\frac{E_i}{m} = \frac{1}{8\pi^2}\left(T * PSA\right)^2 \tag{4.7}$$

where *PSA* is the target design spectrum. This behavior can be seen in Figure 4.58 which shows the input energy spectra of the five modified records and the corresponding spectrum obtained with equation 4.7. The latter can be regarded as the input energy spectrum associated with a design spectrum, in this case the one prescribed in UBC-97. This energy spectrum has the form of a polynomial of fourth order in the period T for very short periods, then varies proportional to T^2 and finally it is constant for the longer periods. Indeed there is a discrepancy between the input energy spectra of real records and these of artificial accelerograms. However, this is caused by the shape of the pseudo acceleration design spectrum. If one accepts the design spectrum as the fundamental tool for earthquake resistant design, then one has to live with the discrepancy. The spectrum-matching procedure is not responsible for the incongruence: it is implicit in the currently used design spectra.

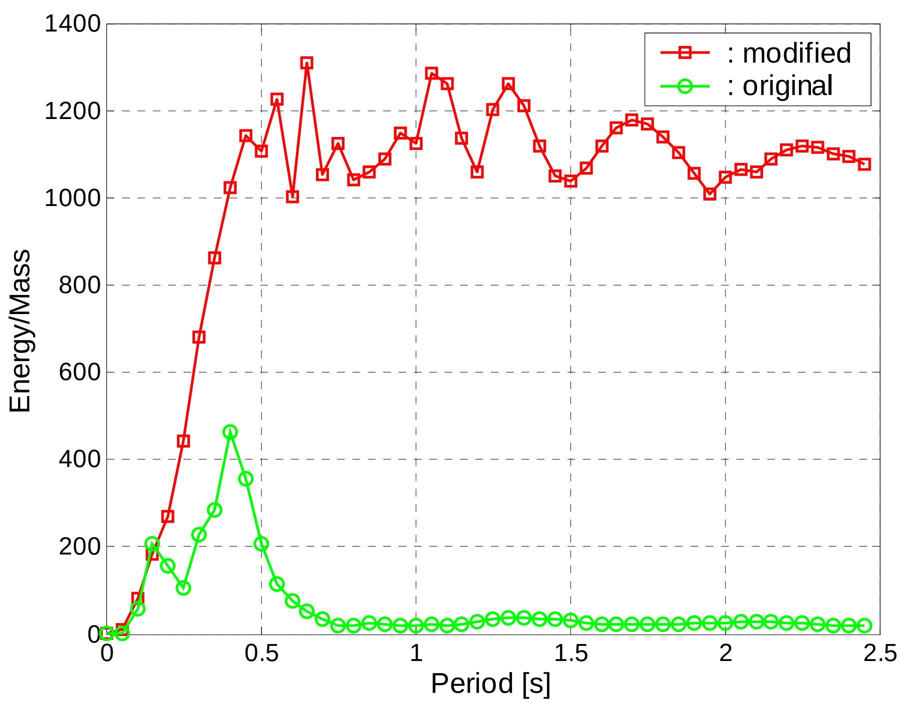

Figure 4.57. The Input Energy Spectra of the original and modified record of Friuli.

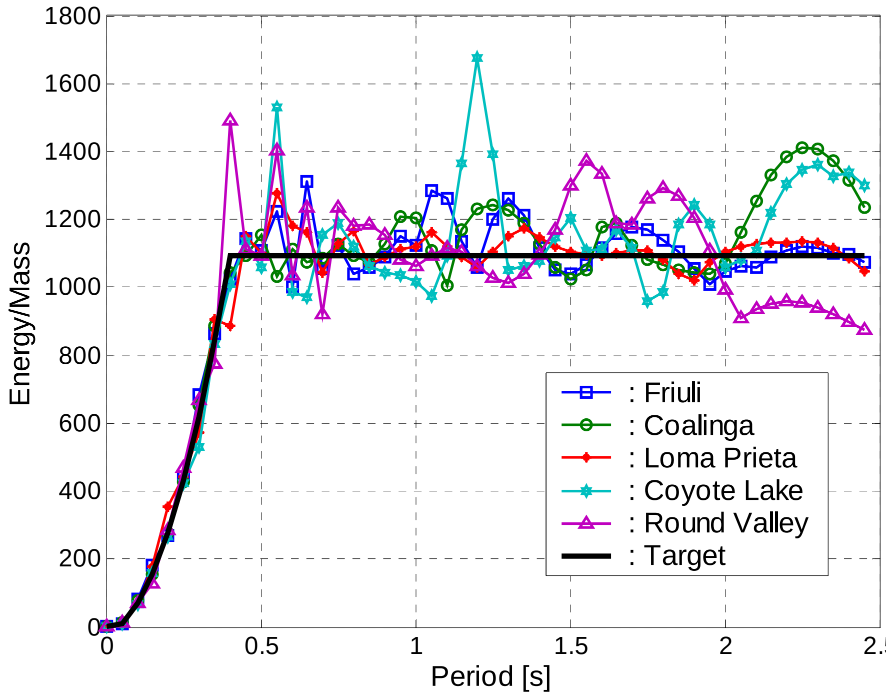

Figure 4.58. The Input Energy Spectra of the modified records and from the design spectrum.

4.11 Analysis of the artificial records generated using *SIMQKE*

An examination of the records obtained with the program *SIMQKE* is carried out in this section. As it happened with the wavelet-based matching procedure, the artificial earthquakes generated with *SIMQKE* yield accelerograms that are not corrected for zero end velocity and displacement. Indeed the displacement and velocity records obtained via direct double integration from all the five design spectrum compatible accelerograms produced unrealistic and physically impossible results. For example, Figures 4.59 and 4.60 show the displacements and velocities obtained for the records identified as simqcase3 and simqcase5, respectively. It can be seen from Figure 4.60 that the ground displacement never crosses the zero line and ends with a permanent displacement of 50 cm at the final time. This problem, however, can be easily corrected by applying the methodology for the baseline correction explained in CHAPTER III. Unfortunately, many users of *SIMQKE* are unaware of this problem. Thus, these uncorrected records are often used as input in computer programs for analysis and design of structures. Since when they need it, the structural analysis programs calculate the ground velocity and displacement from direct integration of the acceleration record, the results obtained can be very unrealistic.

Figures 4.61 to 4.75 shown the Fourier Spectrum, Wavelet Map and Husid's plot for each of the five accelerograms generated with SIMQKE. It can be seen from Figures 4.61, 4.64, 4.67 and 4.73 that the dominant frequency for all five records is around 2.4 Hz. A frequency of 2.4 Hz correspond to a period of 0.417 seconds, which is exactly the value of the right corner of the plateau of the UBC-97 design spectrum (i.e. the period beyond which the spectrum decreases inversely proportional to *T*). This is surprising since the five records are generated using quite different parameters (see Table 4.1).

Examining the Wavelet Maps, it can be noticed that even though a dominant frequency can be identified, all the records have a very wide range of frequency content for all times. This is actually expected because, as it was mentioned before, the *SIMQKE* methodology first generates ground motions that are approximate white noise process, i.e. they are rich in frequencies.

It can be noticed from the Husid plots in Figures 4.63, 4.66, 4.69, 4.72 and 4.75 and from the times identified as TLVL (T level) in Table 4.1 that the strong motion duration was increased in all cases. Of course, the TLVL is not the significant duration but it can be related to it.

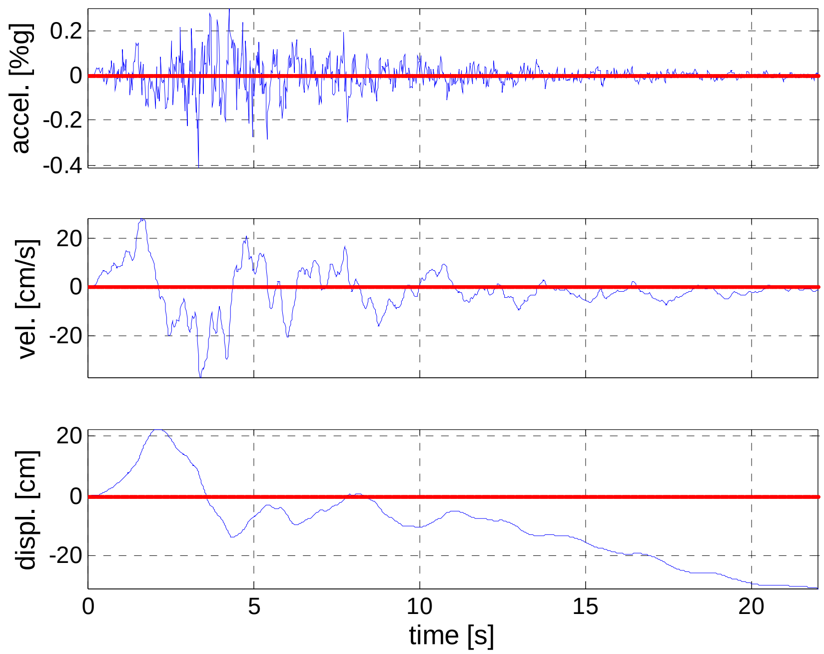

Figure 4.59. Velocity and displacement obtained by numerical integration of the artificial accelerogram simqcase3

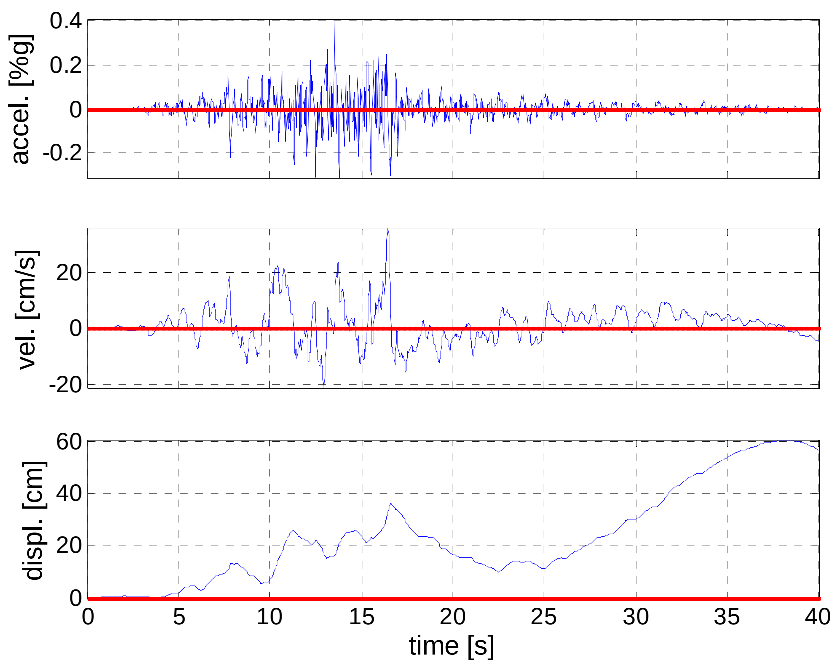

Figure 4.60. Velocity and displacement obtained by numerical integration of the artificial accelerogram simqcase5

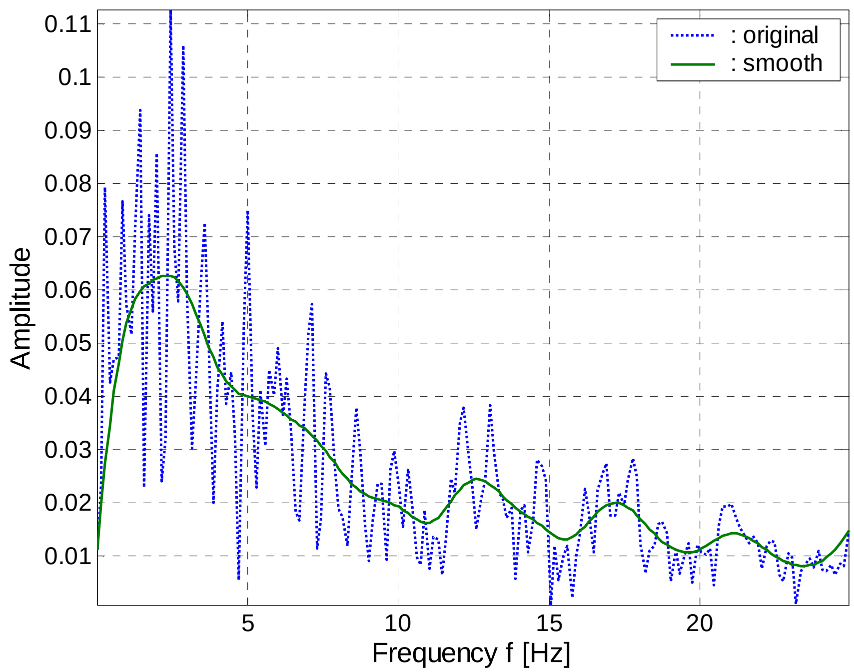

Figure 4.61. Fourier Spectrum of the artificial accelerogram simqcase1.

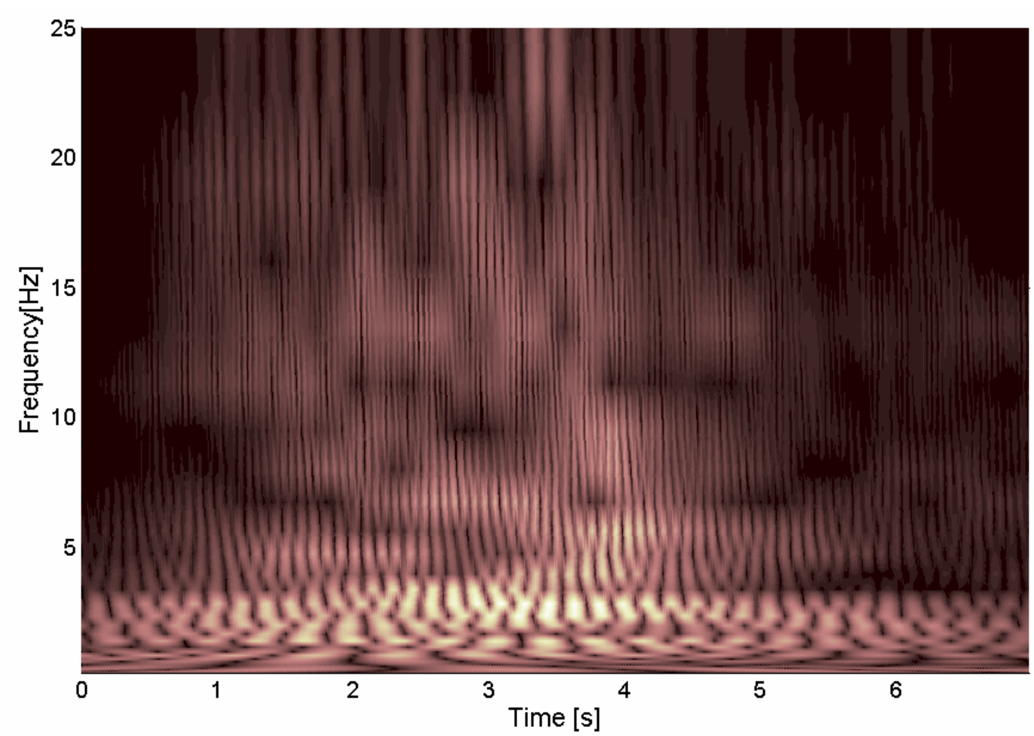

Figure 4.62. Wavelet Map of the artificial accelerogram simqcase1.

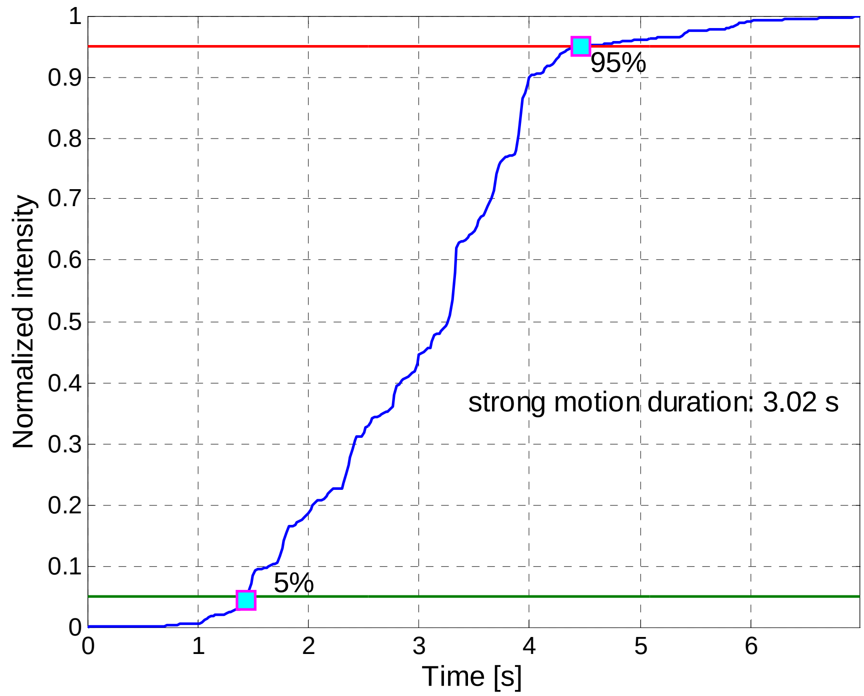

Figure 4.63. Husid's plot of the artificial accelerogram simqcase1.

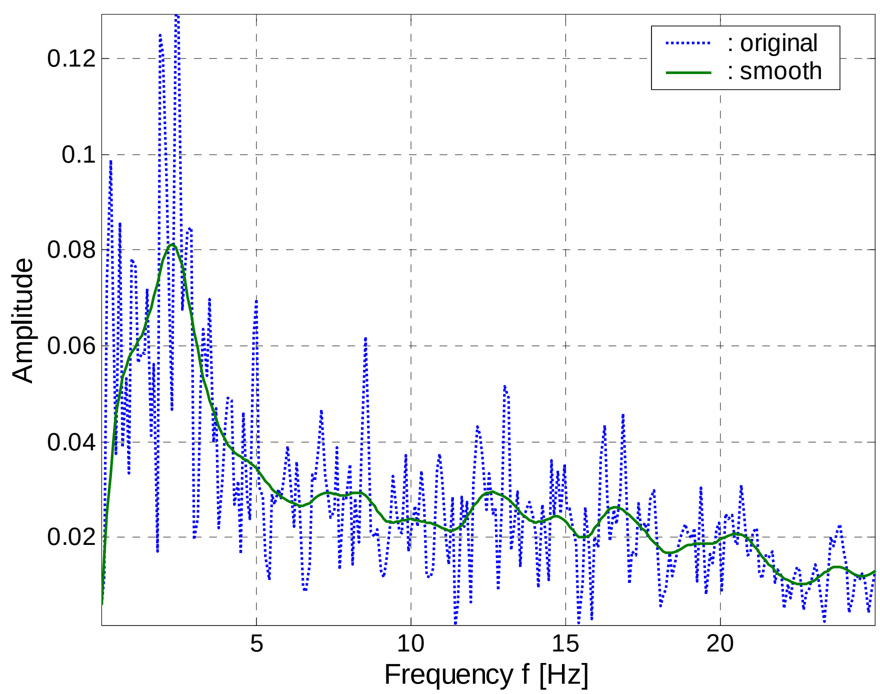

Figure 4.64. Fourier Spectrum of the artificial accelerogram simqcase2.

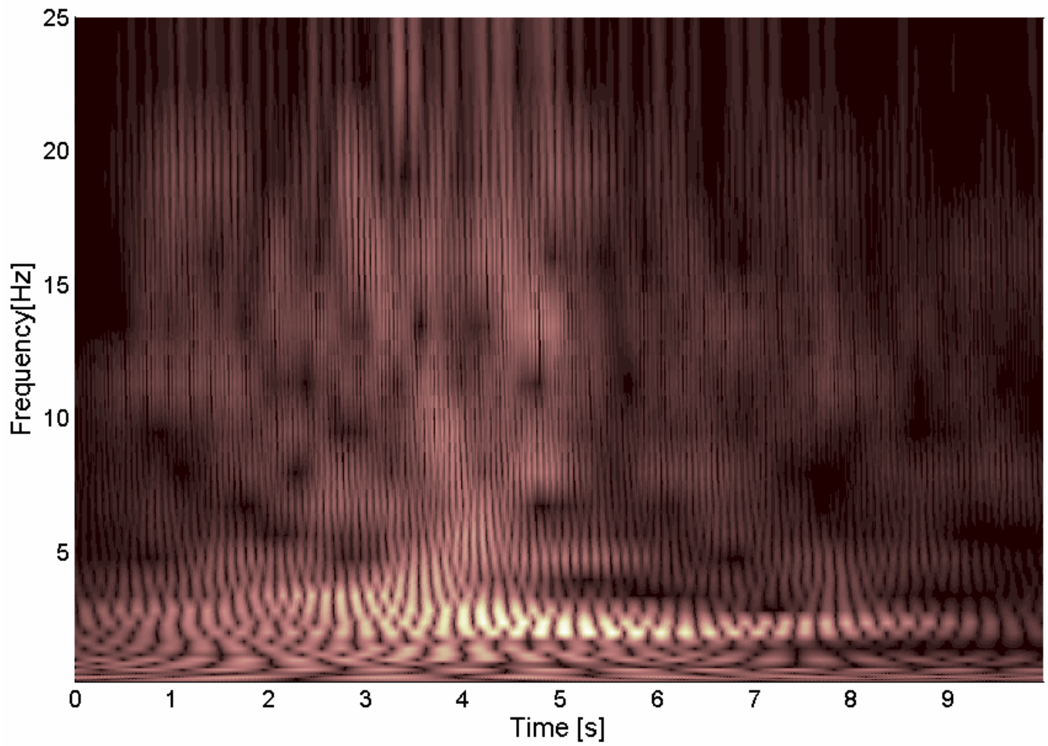

Figure 4.65. Wavelet Map of the artificial accelerogram simqcase2.

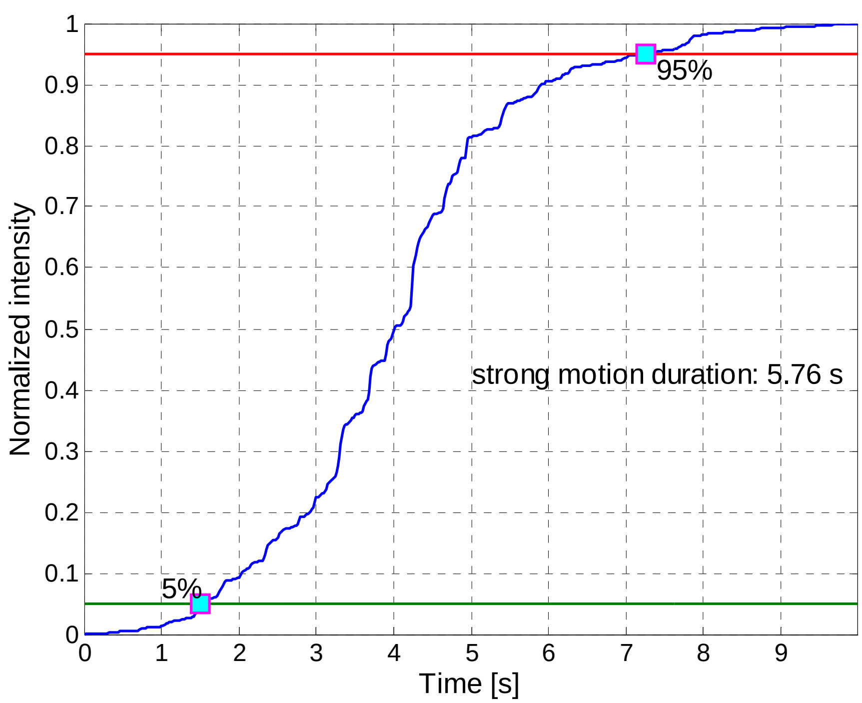

Figure 4.66. Husid's plot of the artificial accelerogram simqcase2.

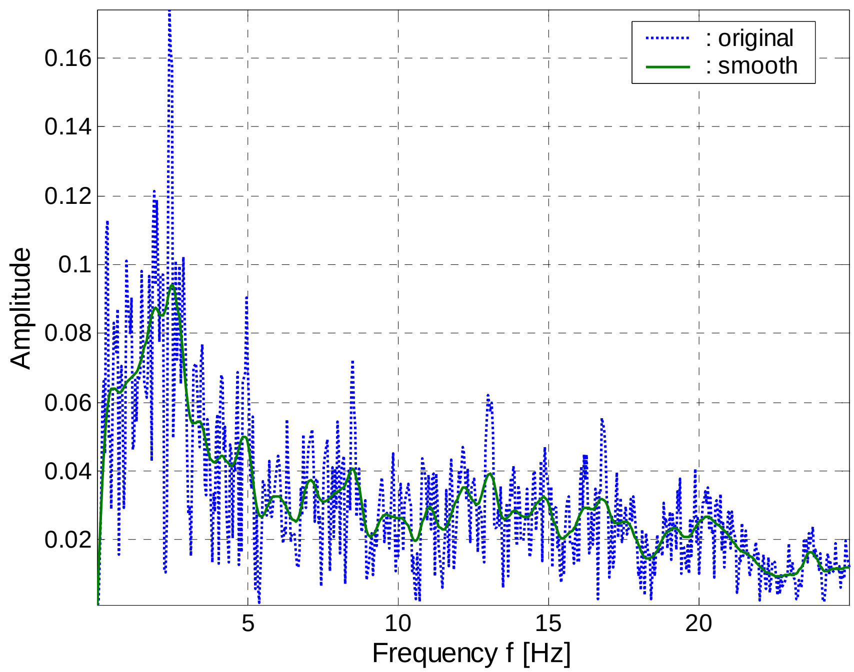

Figure 4.67. Fourier Spectrum of the artificial accelerogram simqcase3.

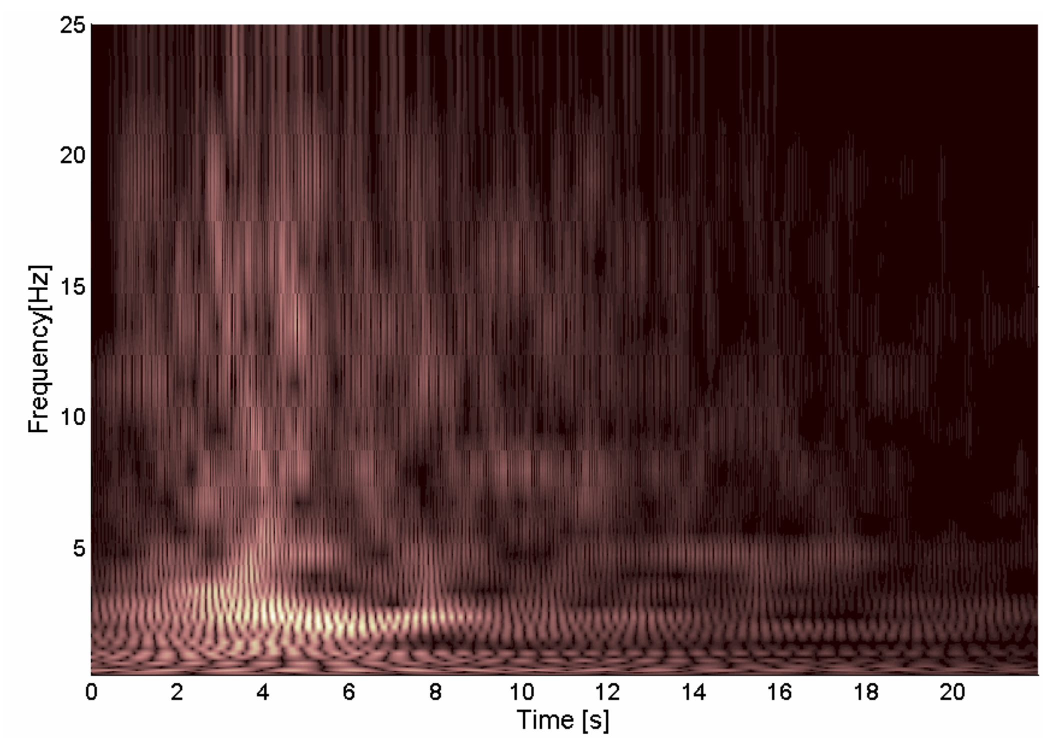

Figure 4.68. Wavelet Map of the artificial accelerogram simqcase3.

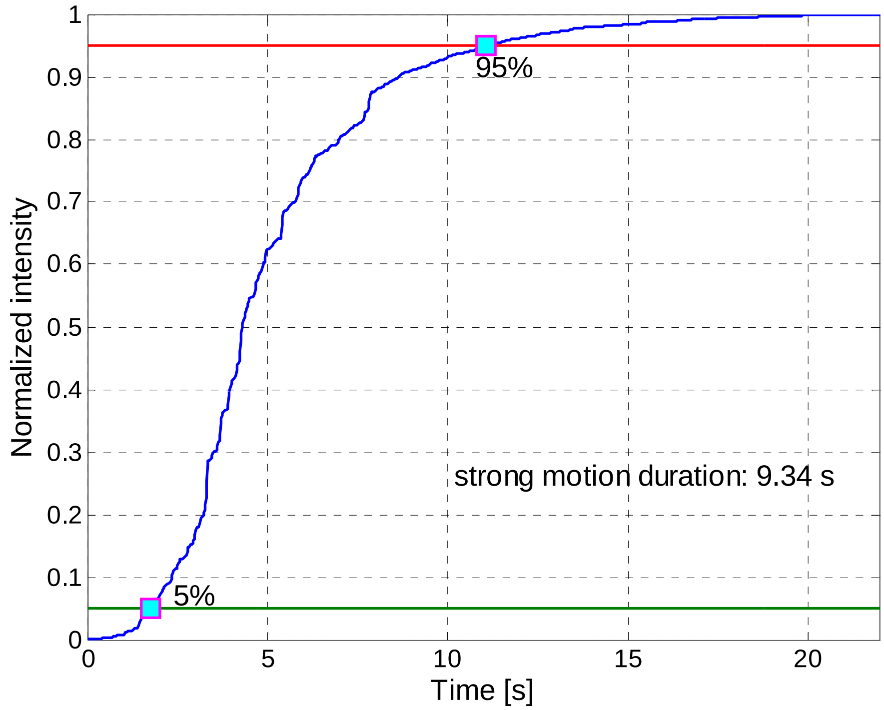

Figure 4.69. Husid's plot of the artificial accelerogram simqcase3.

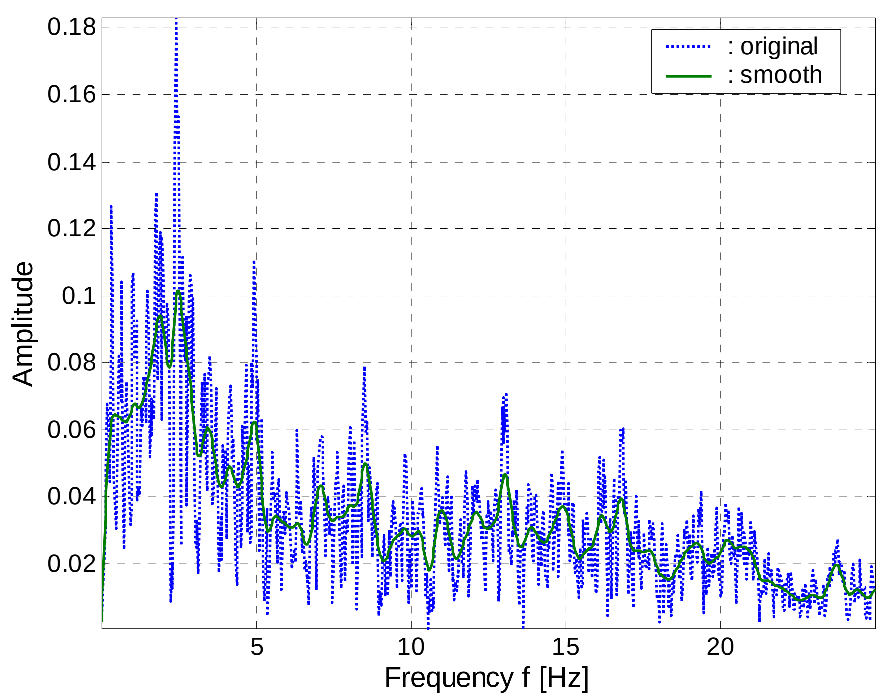

Figure 4.70. Fourier Spectrum of the artificial accelerogram simqcase4.

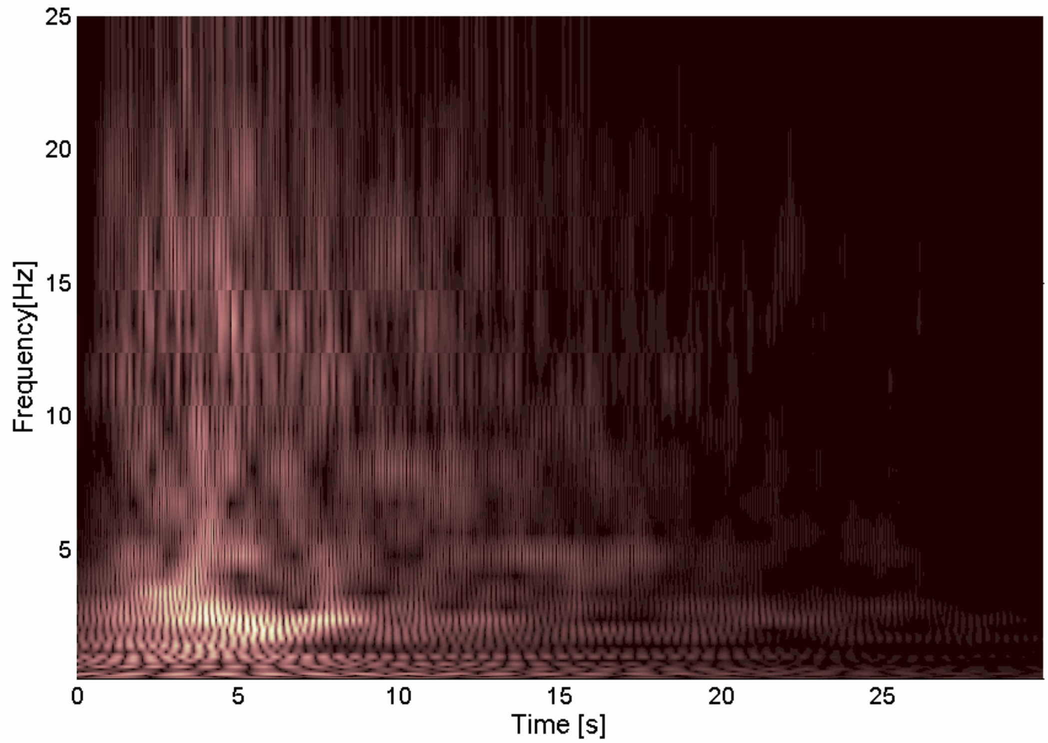

Figure 4.71. Wavelet Map of the artificial accelerogram simqcase4.

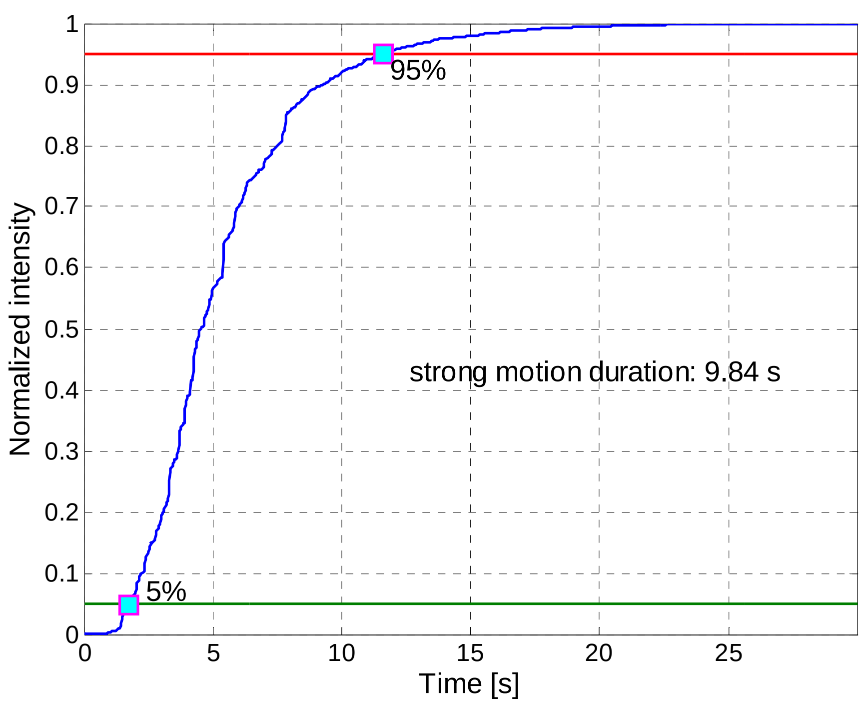

Figure 4.72. Husid's plot of the artificial accelerogram simqcase4.

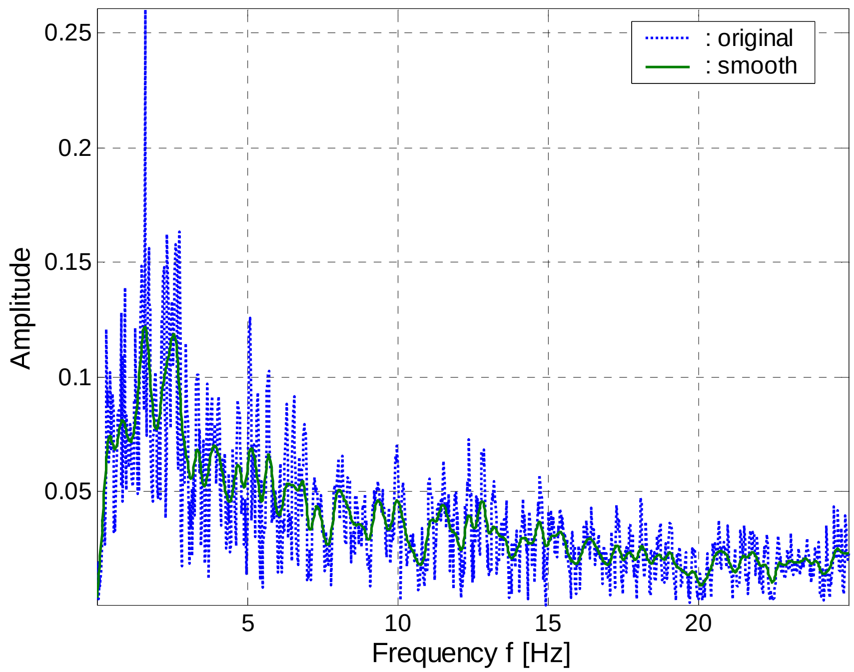

Figure 4.73. Fourier Spectrum of the artificial accelerogram simqcase5.

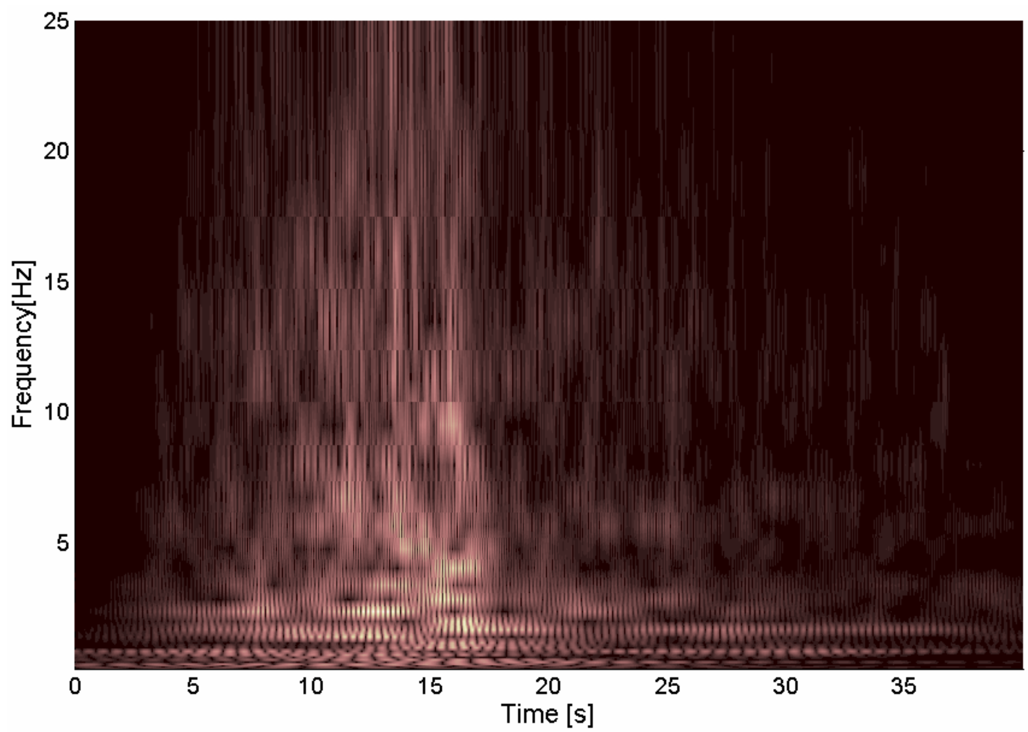

Figure 4.74. Wavelet Map of the artificial accelerogram simqcase5.

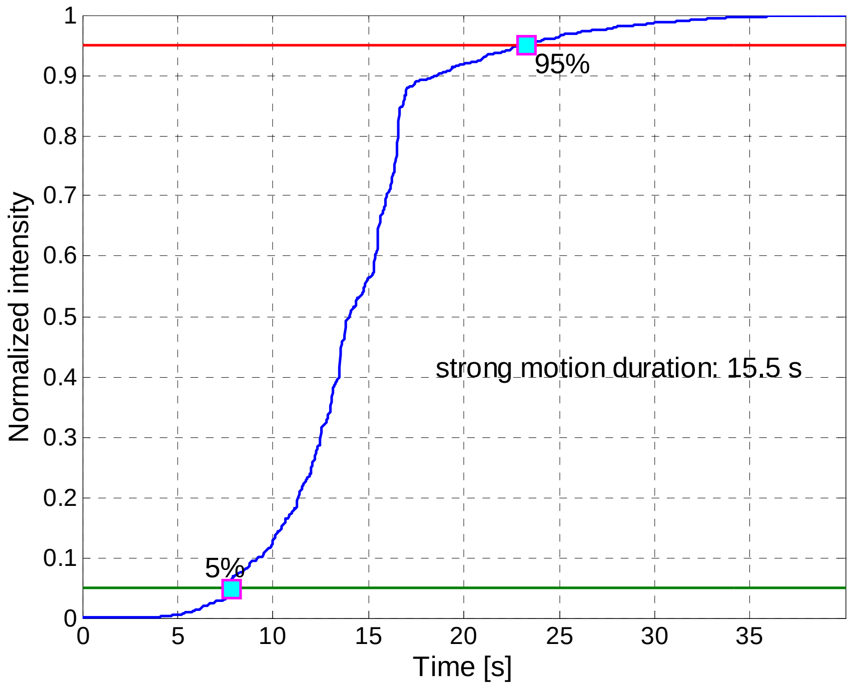

Figure 4.75. Husid's plot of the artificial accelerogram simqcase5.

4.12 Summary

This chapter presented a comprehensive analysis of the artificial accelerograms generated with the proposed procedure as well as those of the original records. The analyses showed that some of the artificial records obtained using the procedure presented in CHAPTER II have very different frequency contents and non-stationary characteristics than the real records which were used as seed for their generation. This implies that the temporal variations of frequency of the original record were not retained in the compatible record. The changes depend on how similar is the response spectrum of the original record to the target spectrum.

It was shown that combining the wavelet analysis, in particular the wavelets maps, with other tools such as the Husid plot of the earthquake intensity, can provide more insight into the characteristic of real or artificial accelerograms.

This chapter also demonstrated that the artificial accelerograms generated using SIMQKE need an appropriate baseline correction, otherwise they lead to very unrealistic velocity and displacement time histories. It was found that all the accelerograms generated with *SIMQKE* tend to have the same frequency content, in particular the same dominant frequency, irregardless of the parameters selected for their generation. This can be disadvantage for design purposes. Indeed, when a time history dynamic analysis is performed the seismic codes recommend to use a minimum number of accelerograms to account for the random nature of the earthquake phenomenon (from 3 to 5 records). However, if artificial accelerograms are used (as it is often the case), and if they are generated using *SIMQKE*, all of then will have the same predominant frequency and thus the purpose of carrying out several analyses with different inputs will be defeated (the responses will be very similar).

CHAPTER V

AN ALTERNATIVE WAY TO MATCH A DESIGN SPECTRUM

5.1 Introduction

It was verified in the previous chapter that using the proposed matching procedure the temporal variations of the frequency content of the original record were not completely retained in the compatible record. Therefore an alternative way to match a target spectrum is investigated in this chapter.

The spectrum matching procedure used for the new application is the same iterative procedure proposed in Chapter II. However, this time the original records will be modified to match only a specific part of the target spectrum based on the characteristics of the record. As a consequence, to match the design spectrum along all the periods it will be necessary to modify more than one record, each one matching different parts of the target spectrum. The procedure, which will be referred to as two-band matching procedure, will be exemplified with a numerical example.

5.2 The Elastic Design Spectrum

To define a design spectrum for a given region one can use a deterministic or a probabilistic approach (Kramer 1996). One way to define an earthquake design spectrum with the deterministic approach is to average a set of response spectra from records measured at sites with similar characteristics as that of the region of interest, such as soil conditions, epicentral distance, magnitude, source mechanism, etc. For some sites the design spectrum is obtained as the envelope of two different elastic design spectra: the short period portion of the spectrum is governed by a nearby earthquake, and the long-period portion of the design spectrum is controlled by a distant earthquake (Chopra 2001). This concept is graphically explained in Figure 5.1.

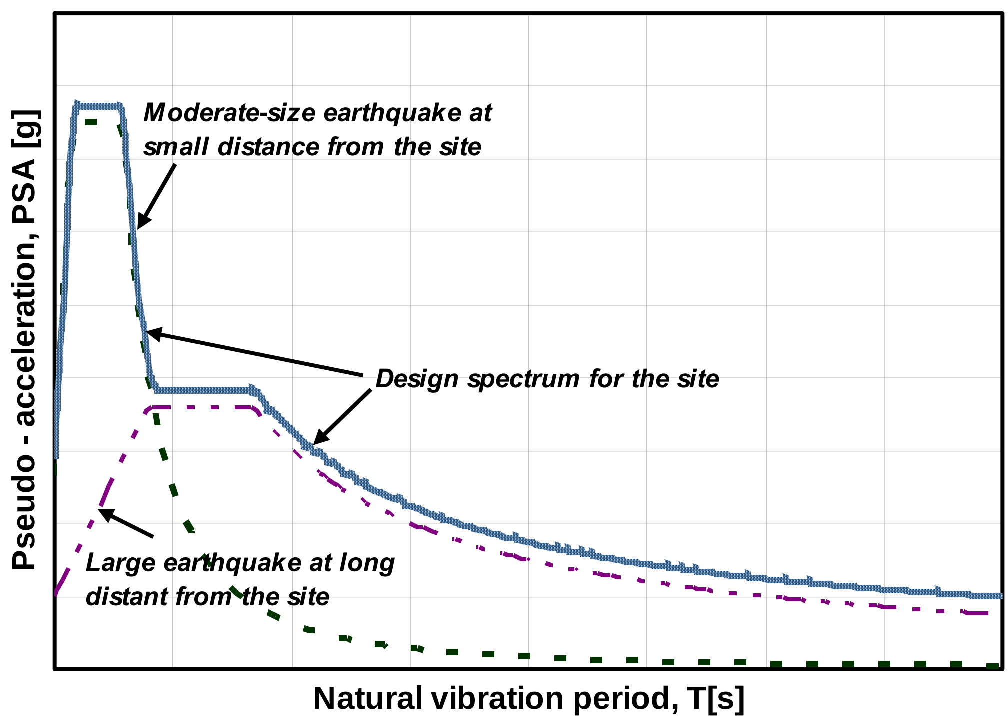

Figure 5.1 Design spectrum defined as the envelope of design spectra for earthquakes originating on two different faults.

For practical applications, design spectra are represented as smooth curves or straight lines. Since the peak ground acceleration, velocity, and displacement for various earthquakes records differ, the computed response cannot be averaged on an absolute basis. Various procedures are used to normalize response spectra before averaging is carried out (Housner 1952).

5.3 A justification for the two-band spectrum matching

Figures 5.2 and 5.3 show two different records of the same seismic event and their response spectra. The records correspond to the Loma Prieta same earthquake that occurred on October 18, 1989 but recorded in different stations. One of them was recorded in “1678 Golden Gate Bridge” with a closest distance to the rupture failure of 85.1 km and a USGS Site Classification B (Table 5.1). The other was recorded at the station “47381 Gilroy Array #3” with a closest distance to the rupture failure of 14.4 Km and a USGS Site Classification C. It can be seen from Figure 5.4 that the response spectra of these two records which represent a closer and a distant earthquake are widely different. If one compares these response spectra with a typical design spectrum, such as the prescribed in the 1997 Uniform Building Code shown in Figure 5.5, it is apparent that the spectrum of the closer record (Gilroy) resembles the short-periods part of the design spectrum ($T<Ts$) whereas the spectrum of the distant record (Golden Gate) approximately adjust to the long-periods zone of the design spectrum ($T>Ts$). Based on this observation, it is proposed to select two original records and modify them so that they match a zone of the design spectrum based on the characteristics of the response spectrum of the individual records.

Table 5.1 Site Classification

Site condition	Average shear wave velocity [m/s] to a depth of 30 m	
	USGS	NEHRP (94)
A	>750	>1500
B	360 - 750	760-1500
C	180 - 360	360-760
D	< 180	180-360
E	-	<180

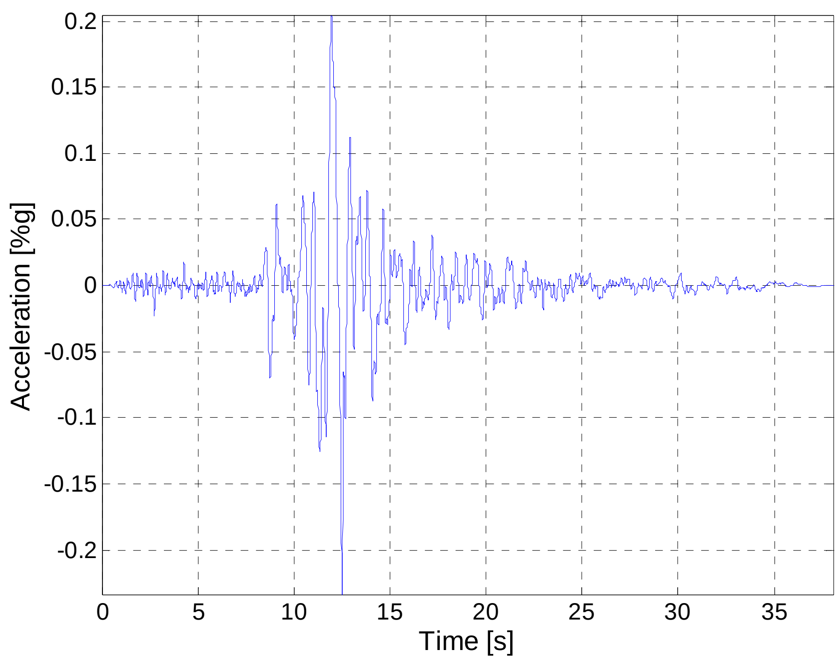

Figure 5.2 Acceleration time history of the Loma Prieta earthquake recorded at Golden Gate station.

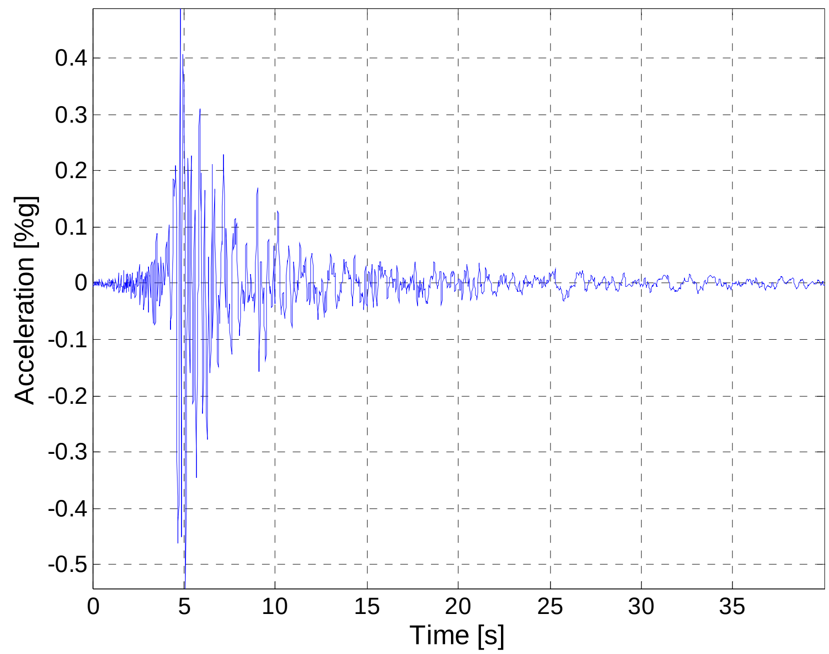

Figure 5.3 Acceleration time history of the Loma Prieta earthquake recorded at Gilroy#3 station.

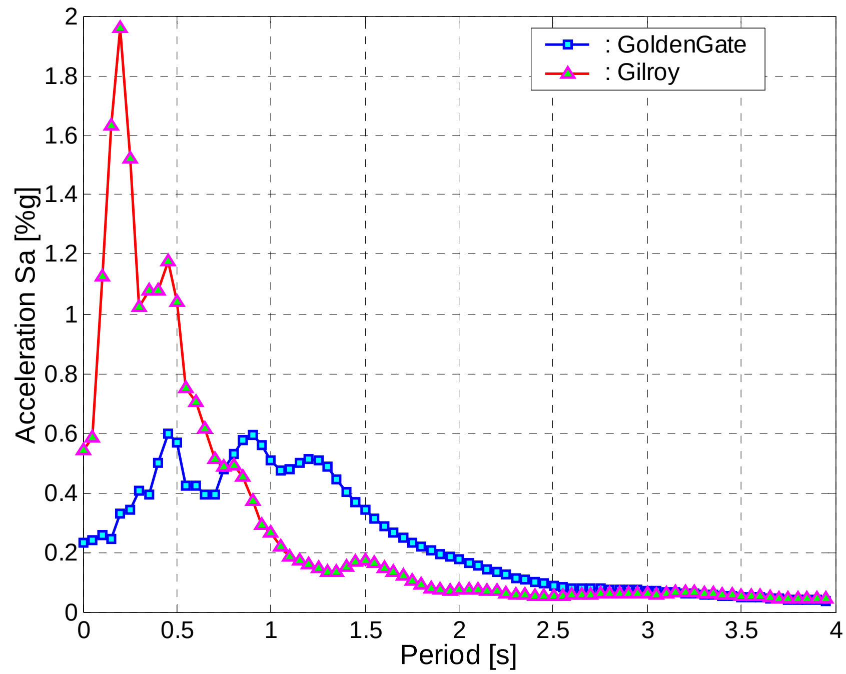

Figure 5.4 Response spectra for the records of the Loma Prieta earthquake at Gilroy#3 and Golden Gate stations.

5.4 Numerical example

As it was done in Chapter II, the design spectrum prescribed in the 1997 Uniform Building Code (ICBO 1997) will be adopted as the target spectrum. For ready reference the 1997 UBC design spectrum is again shown in Figure 5.5. The spectrum is completely defined by two seismic coefficients *Ca* and *Cv*. These coefficients are defined in the code for five seismic zones and for five different soil categories.

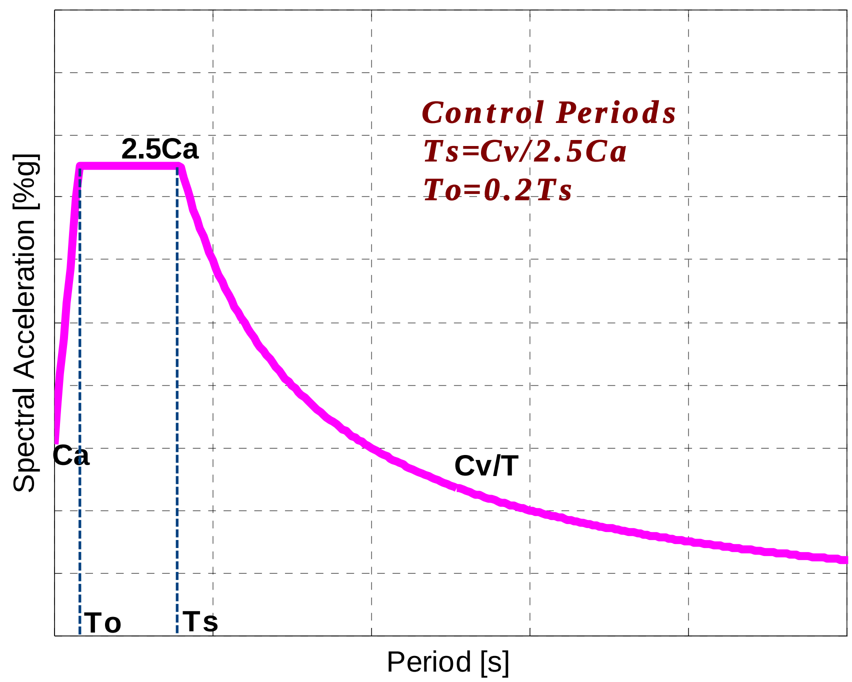

Figure 5.5 Design spectrum prescribed in the 1997 Uniform Building Code

To demonstrate the numerical implementation of the two-band matching procedure the records of the Friuli earthquake (Italy 1976) measured at Forgario Cornino station with a closest distance to the rupture failure of 13 km and a USGS Site Classification B, and the Loma Prieta earthquake (California 1989) registered at Treasure Island station with a closest distance to the rupture failure of 82.9 km and a USGS Site

Classification D have been selected. The acceleration time histories of these records are shown in Figures 5.6 and 5.7. Figure 5.8 displays the response spectra of the original accelerograms together with the design spectrum of the UBC 97 for seismic zone 3 and soil type $S_{B,}$ which will be used as target. In a real application the selection of the two records must be done with caution. In order for the procedure to provide meaningful results, each accelerogram must be representative of a near fault and distant fault seismic event.

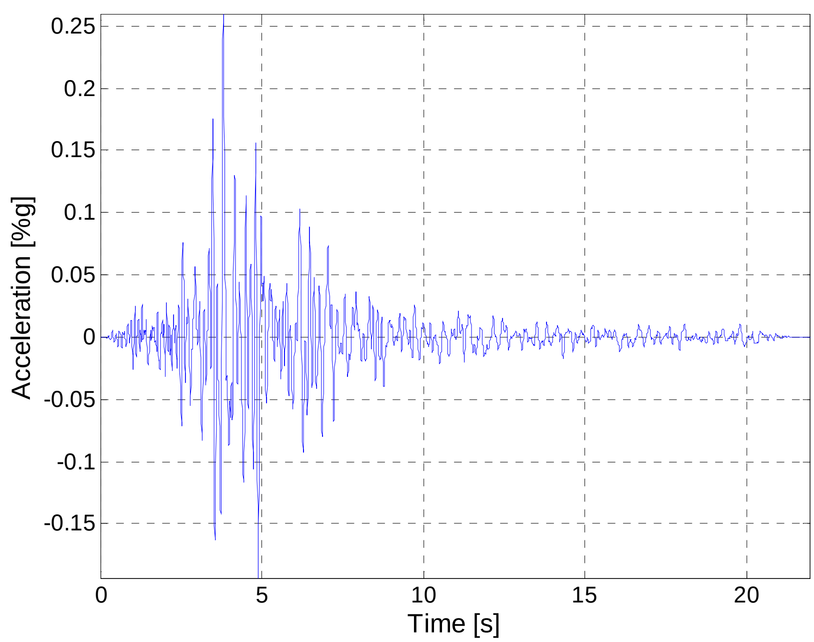

Figure 5.6 Acceleration time history of the Friuli earthquake recorded at Forgario Cornino station.

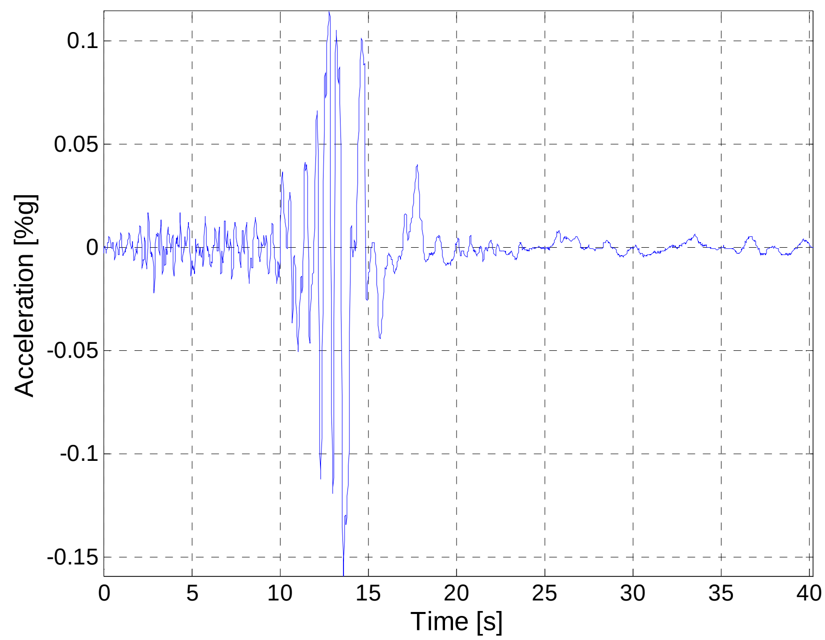

Figure 5.7 Acceleration time history of the Loma Prieta earthquake recorded at Treasure Island station.

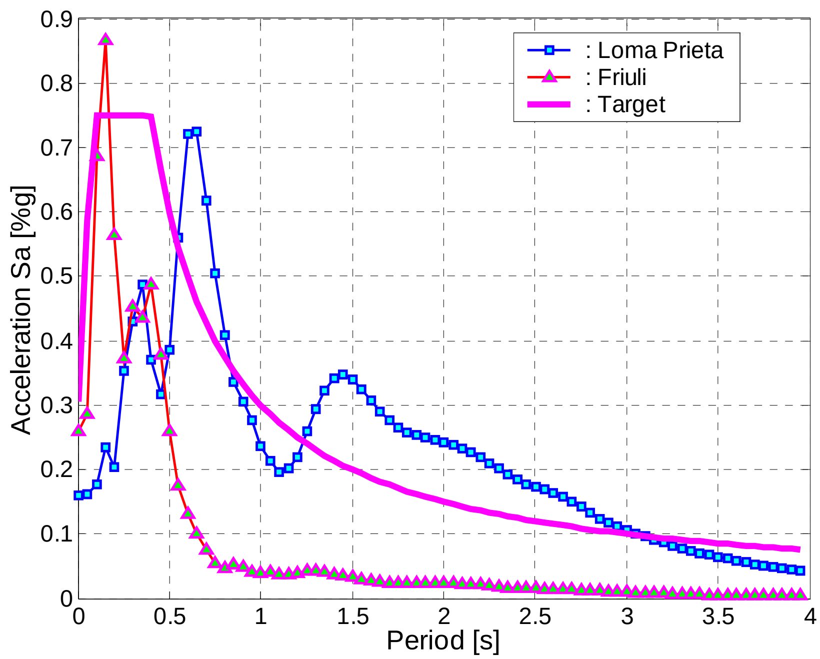

Figure 5.8 Response spectra of the Treasure Island station record of the Loma Prieta earthquake and the Forgario Cornino station record of the Friuli earthquake together with the UBC design spectrum.

Once the two earthquakes records have been selected, the next step is to scale their response spectra by an appropriate factor so that one can better visualize the periods range where each record must be modified to match the target spectrum. Figure 5.9 shows the scaled response spectra of the records: the record of Friuli was modified by a factor of 0.90 and the modification factor for the Loma Prieta record was 0.70. Based on the results of Figure 5.9 the record of Friuli will be modified to match the target spectrum in the period range 0 to 0.45s whereas the record of Loma Prieta will be modified for the same purpose in the period range 0.55 to 4s. The response spectra of the two accelerograms after they were modified with the wavelet based procedure are shown in Figure 5.10.

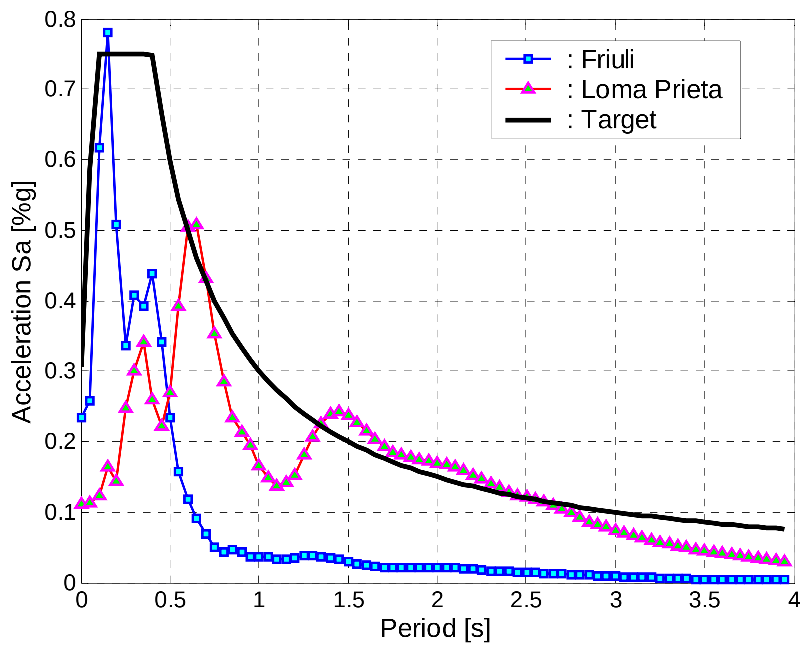

Figure 5.9 Response spectra for the scaled records of the Loma Prieta earthquake at Treasure Island Station and the Friuli earthquake at Forgario Cornino station with the UBC design spectrum.

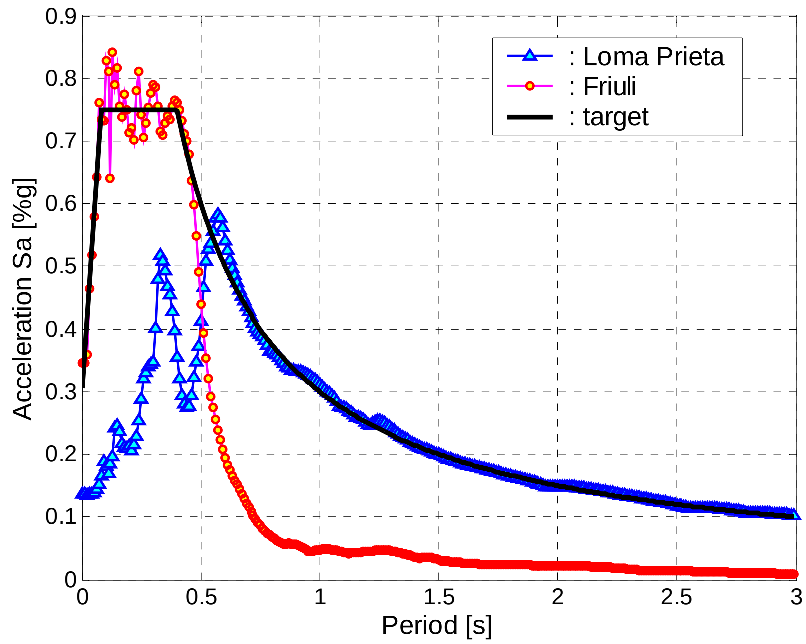

Figure 5.10 Response spectra for the modified records of the Loma Prieta earthquake at Treasure Island Station and the Friuli earthquake at Forgario Cornino station with the UBC design spectrum.

Figure 5.11 shows the accelerograms of the Friuli earthquake before and after being processed with the matching procedure. It can be seen from this figure that both accelerograms have similar general shape, for instance both have their maximum peak ground acceleration at the same time, 3.8 seconds. Figures 5.12 and 5.13 show, respectively, the Husid's plot for the original and the modified accelerograms of the Friuli earthquake. It can be seen that the strong motion duration after the modification was increased by approximately two seconds (53%). Moreover, examining Figure 5.14 one can observe that the general trend in the Husid's plot of the two records is quite similar.

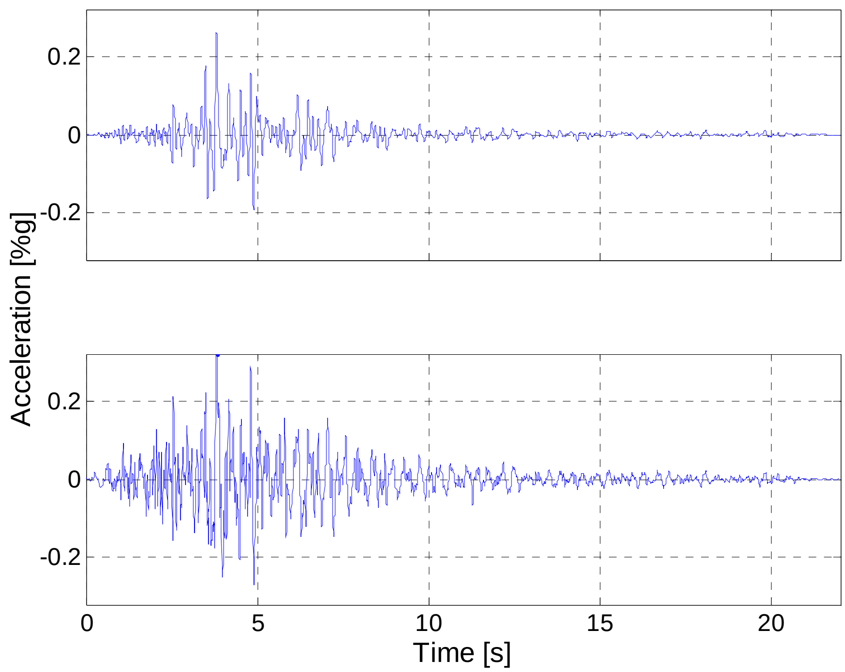

Figure 5.11 Original and modified accelerogram of the Friuli earthquake

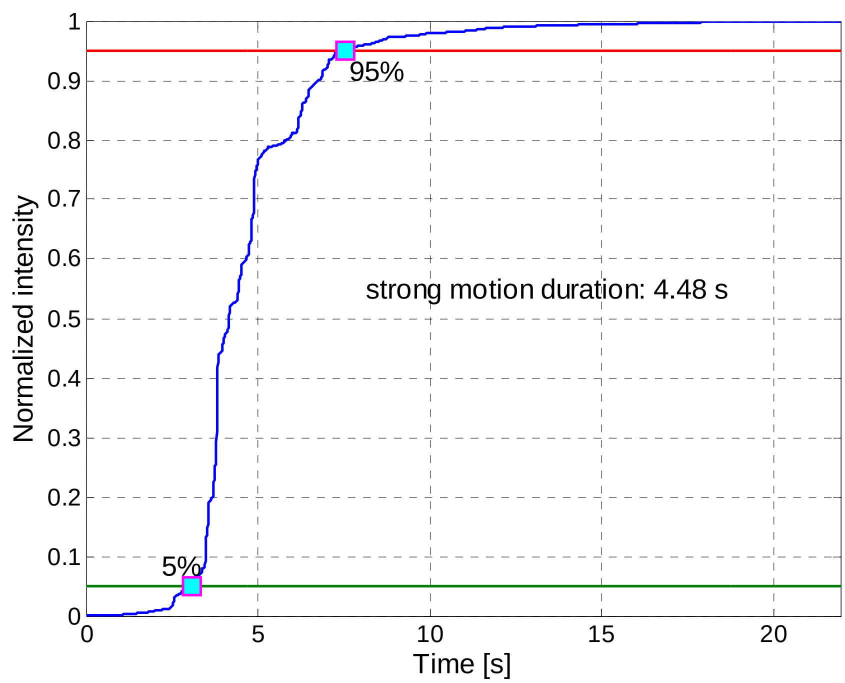

Figure 5.12 Husid's plot of the original record of the Friuli earthquake

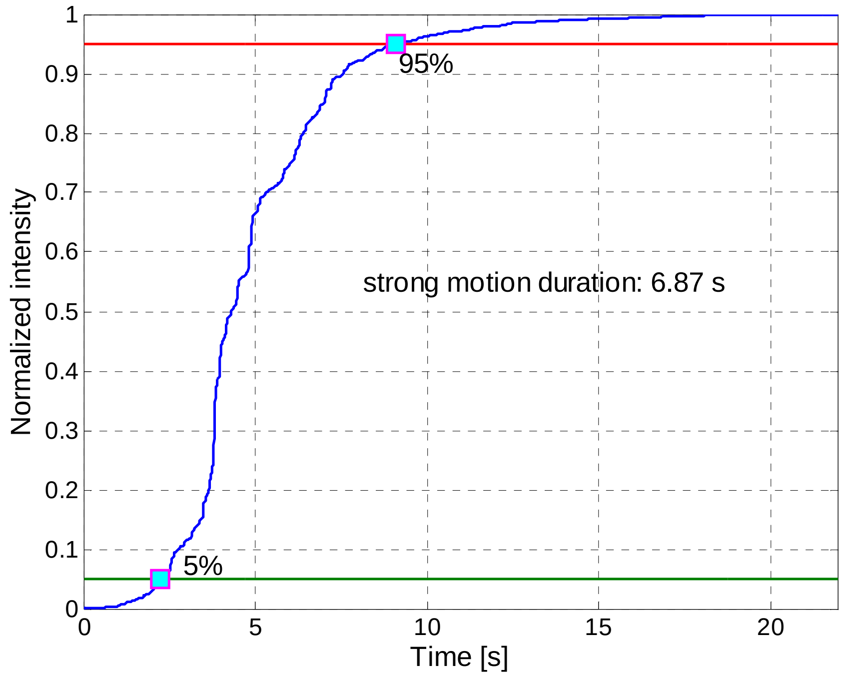

Figure 5.13 Husid's plot of the modified record of the Friuli earthquake

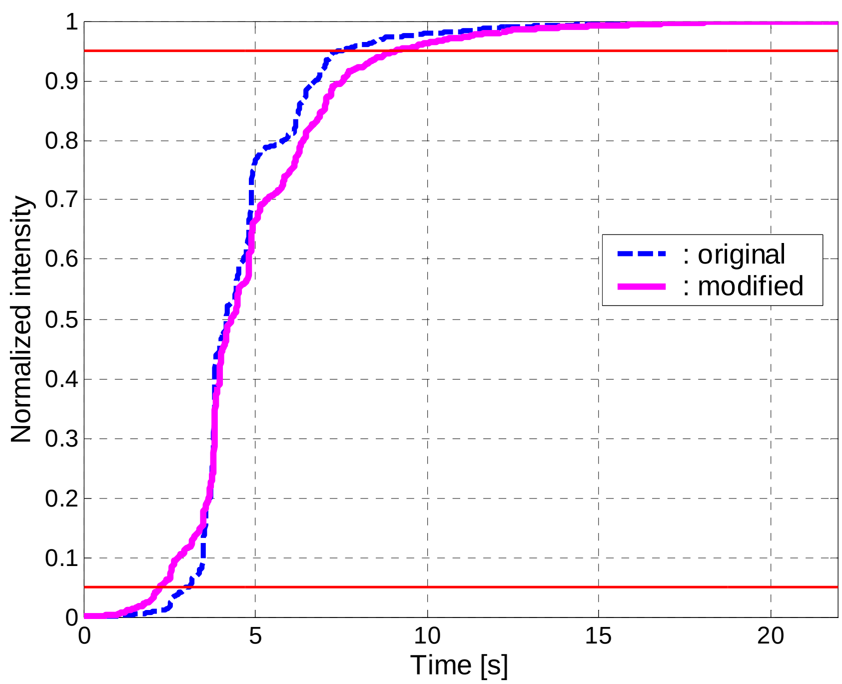

Figure 5.14 Husid's plots of the original and modified records of the Friuli earthquake

Next we take a look at the frequency content of the original and modified Friuli records. Figures 5.15 and 5.16 show, respectively, the Fourier spectrum of the original and modified accelerograms. Although the two spectra look different, some important characteristics of the original record still remain in the modified accelerogram. For instance, the dominant frequency for both accelerograms is between 2-3 Hz and almost all the frequency content of the accelerograms is between 2-10 Hz.

Figures 5.17 and 5.18 show the wavelet map of the two accelerograms of the Friuli earthquake. It is recalled that a wavelet map, i.e. a two dimensional plot of the absolute values of the wavelet transform coefficients, provides an indication of the variation in time of the frequency content of a signal. It can be observed from Figures 5.17 and 5.18 that the non-stationary characteristics of the original accelerogram are still present in the modified accelerogram.

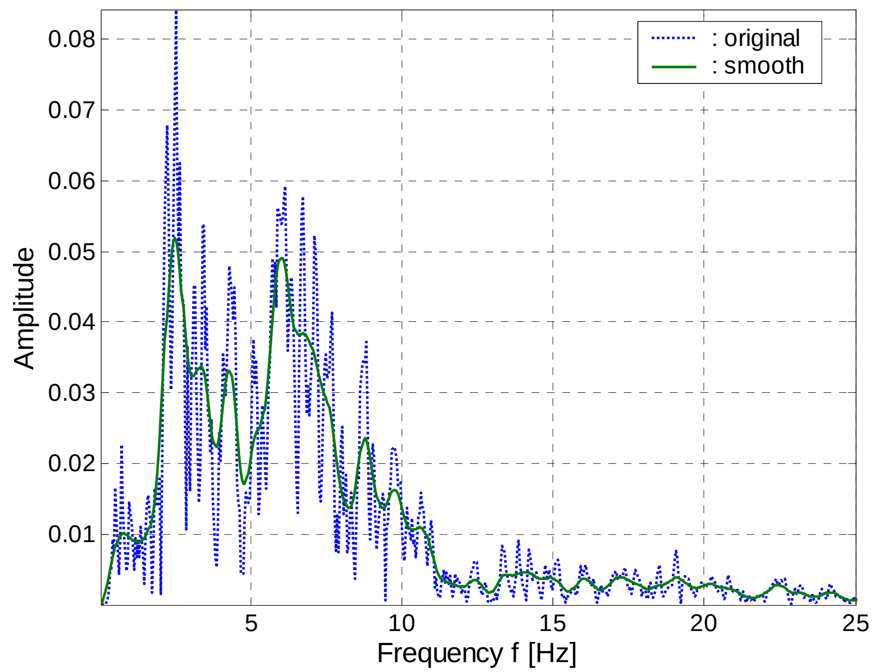

Figure 5.15 Fourier spectrum of the original record of the Friuli earthquake

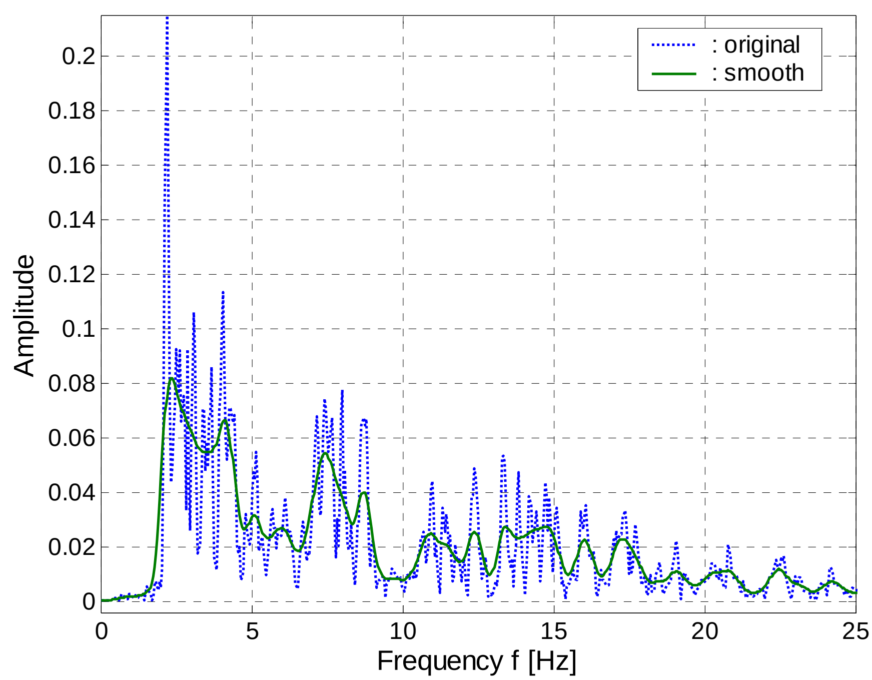

Figure 5.16 Fourier spectrum of the modified record of the Friuli earthquake

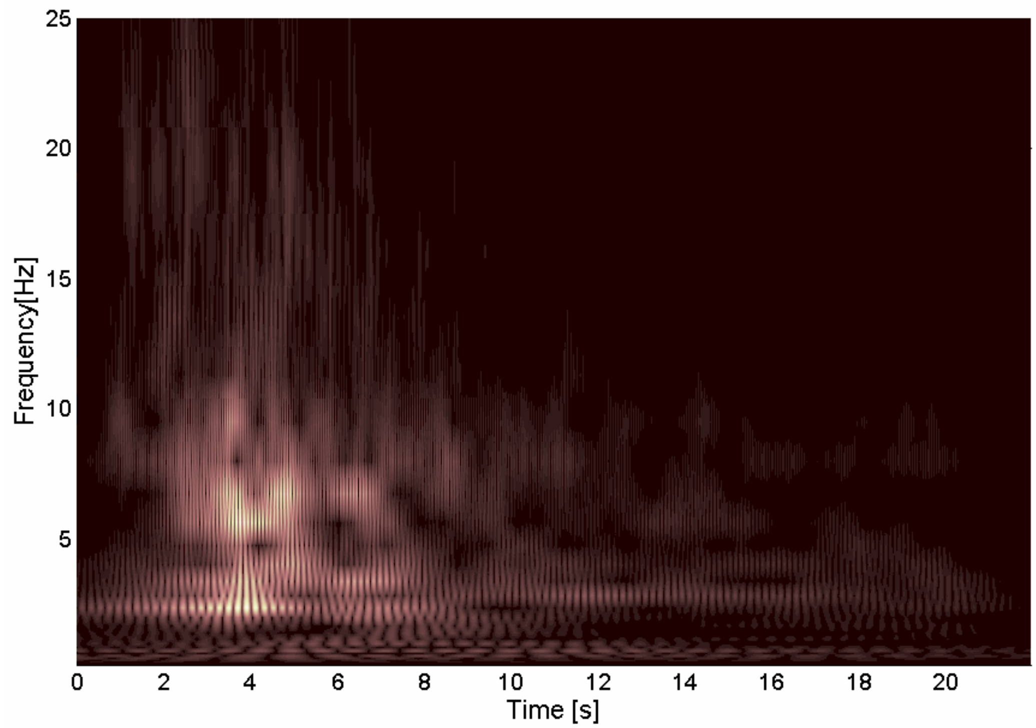

Figure 5.17 Wavelet Map of the original record of the Friuli earthquake

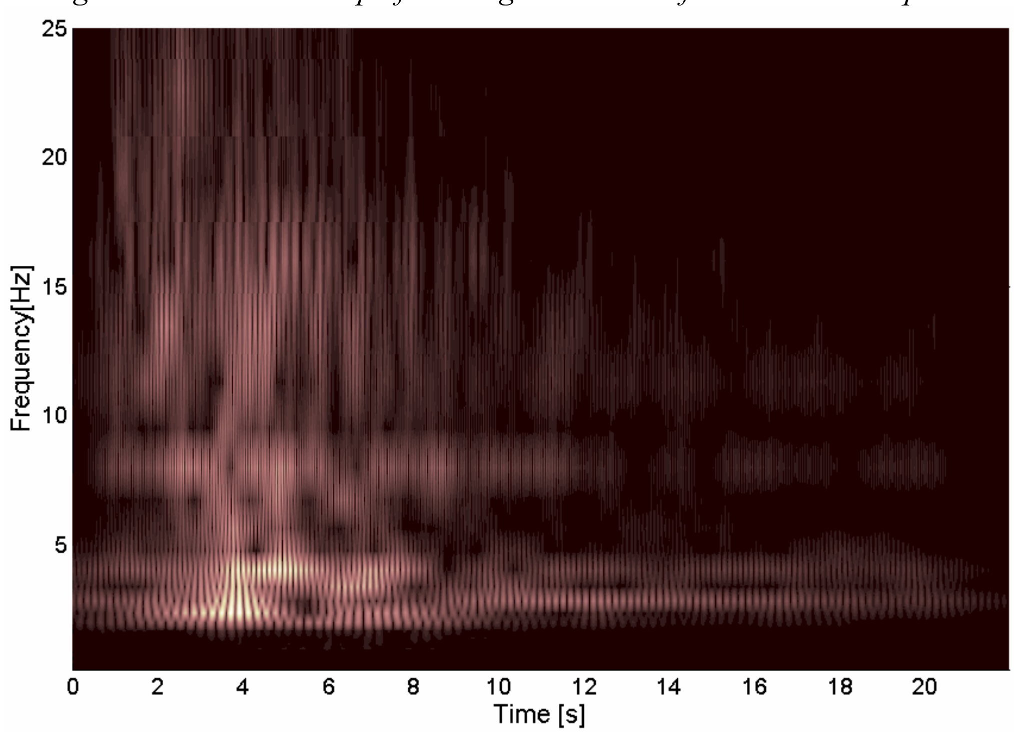

Figure 5.18 Wavelet Map of the modified record of the Friuli earthquake

The next set of figures present similar results but for the Loma Prieta record. Figure 5.19 shows the accelerogram of the Loma Prieta earthquake before and after it was modified to match the long period zone of the target spectrum. As it happened with the Friuli earthquake, it can be verified from this figure that both accelerograms have a similar general shape. The two accelerograms have maximum amplitudes between 12 and 14 seconds.

Figures 5.20 and 5.21 show, respectively, the Husid's plot for the original and the modified accelerograms of the Loma Prieta earthquake. Even though the strong motion duration in the modified record was increased by almost twelve seconds, the shape of the Husid's plot of both records between 12 and 15 seconds is very similar, as it can be verified in Figure 5.22.

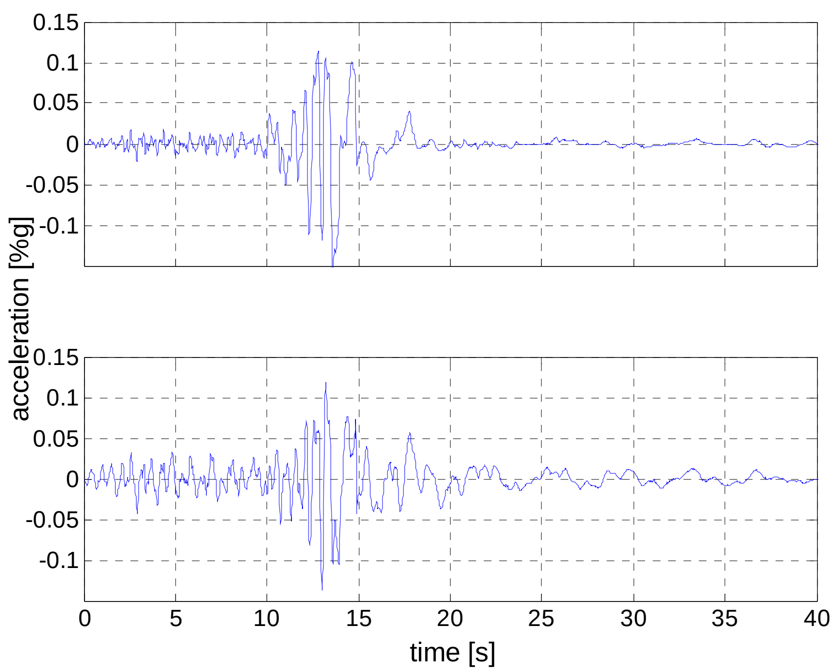

Figure 5.19 Original and modified accelerogram of the Loma Prieta earthquake

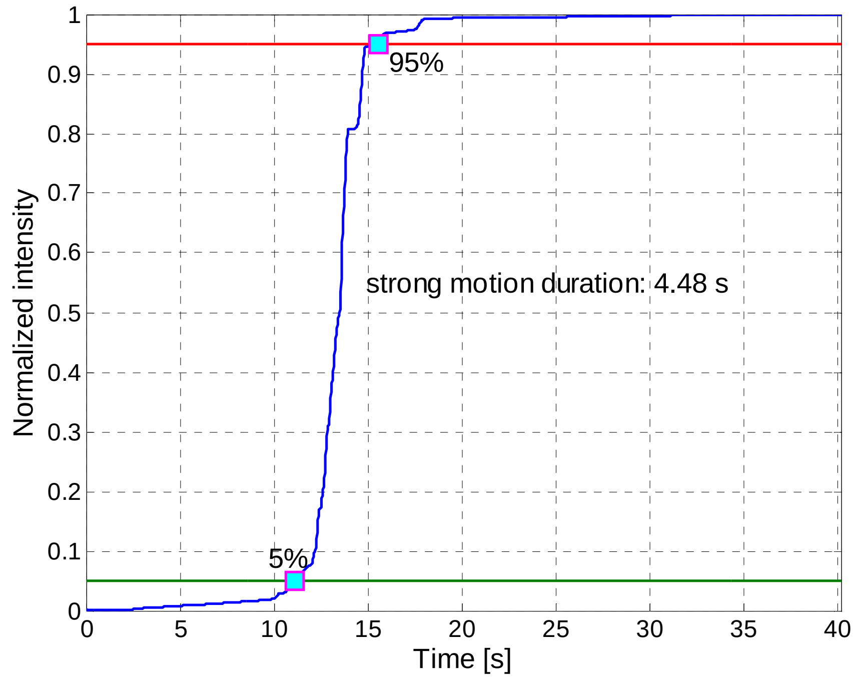

Figure 5.20 Husid's plot of the original record of the Loma Prieta earthquake

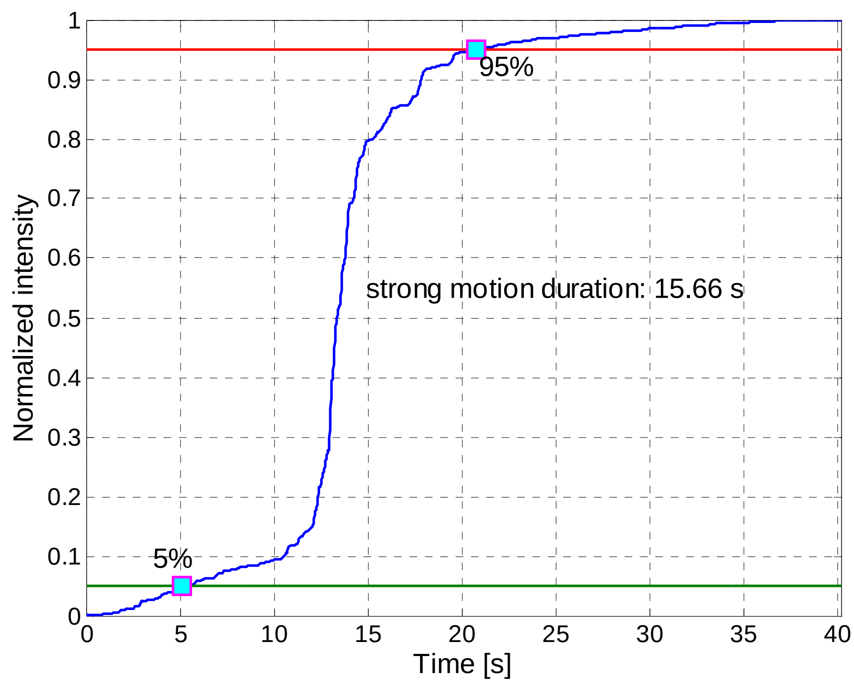

Figure 5.21 Husid's plot of the modified record of the Loma Prieta earthquake

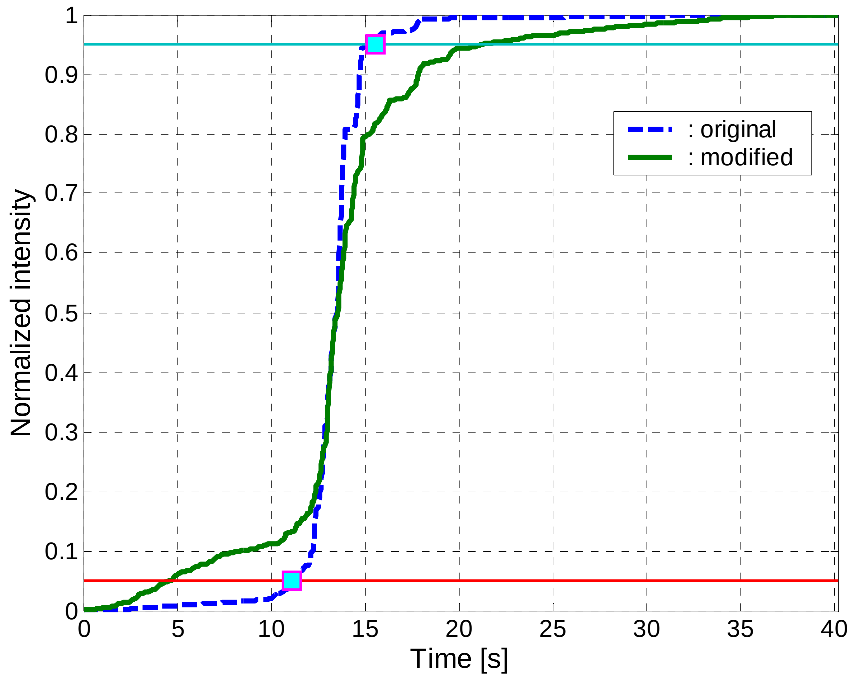

Figure 5.22 Husid's plots of the original and modified records of the Loma Prieta earthquake

Figures 5.23 and 5.24 display the Fourier spectrum of the original and modified accelerogram of the Loma Prieta earthquake. Both spectra look very similar: practically all the frequency content of the accelerograms is between 0.2 to 5 Hz and the dominant frequencies are in the range from 0.2 to 2 Hz.

Figures 5.25 and 5.26 show the wavelet map of the Loma Prieta accelerograms. Although comparing these two dimensional plots is not as straightforward as it is with the Fourier spectrum, it can be seen that both wavelet maps are quite similar.

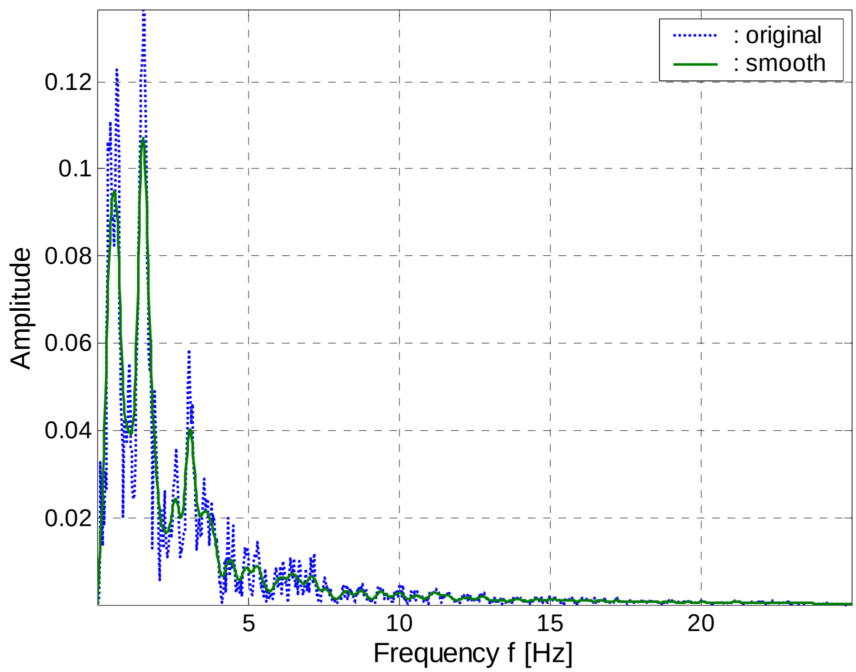

Figure 5.23 Fourier spectrum of the original record of the Loma Prieta earthquake

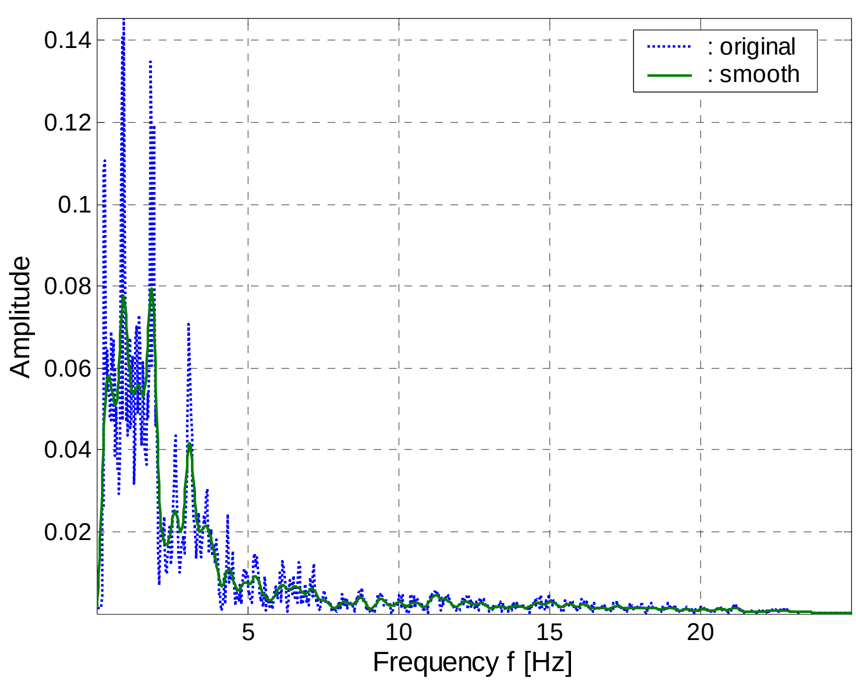

Figure 5.24 Fourier spectrum of the modified record of the Loma Prieta earthquake

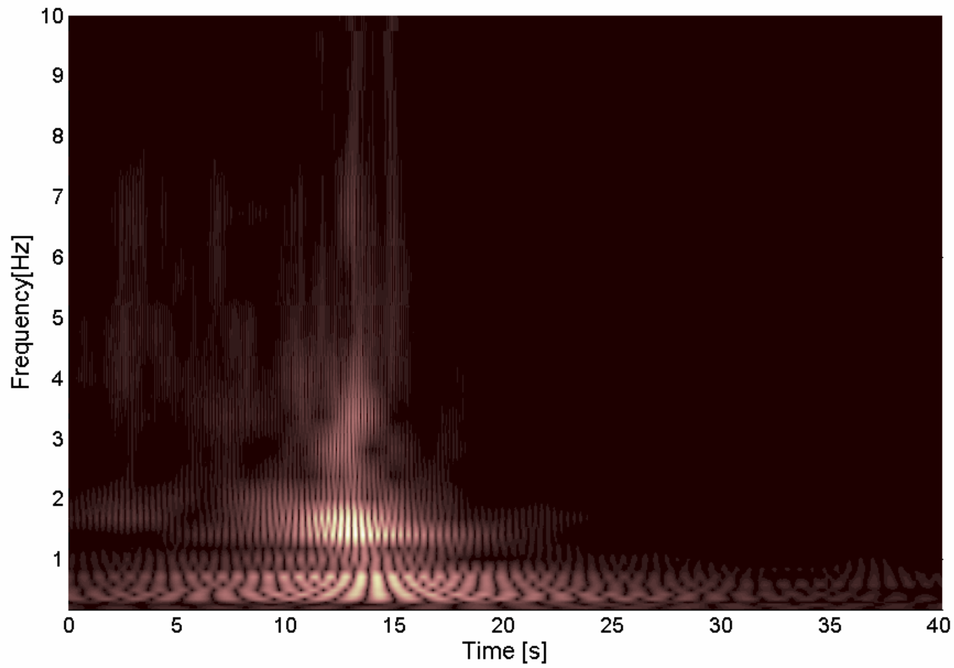

Figure 5.25 Wavelet Map of the original record of the Loma Prieta earthquake

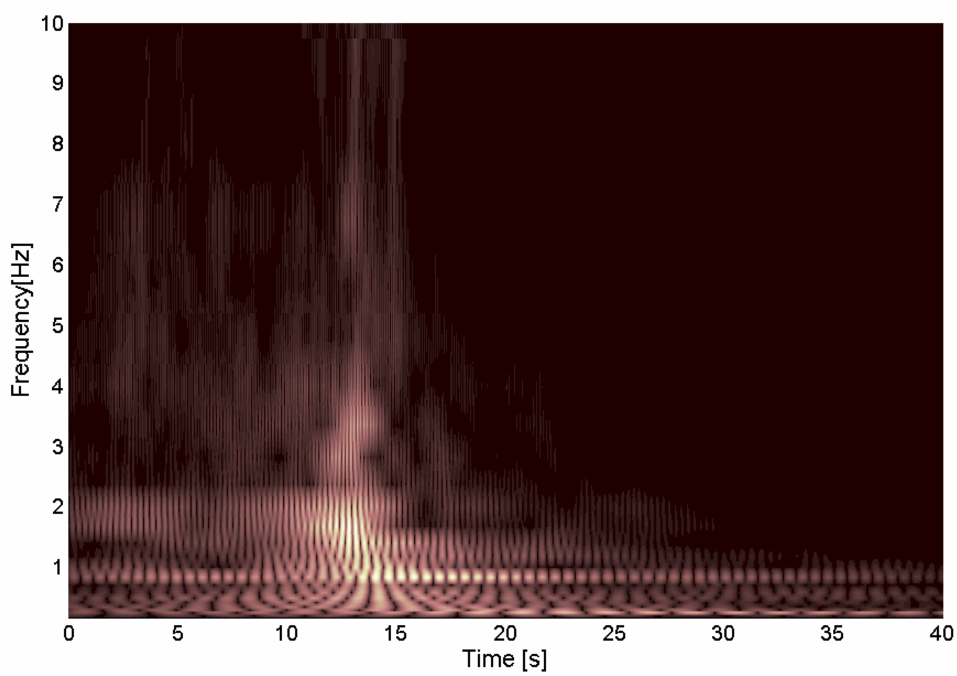

Figure 5.26 Wavelet Map of the modified record of the Loma Prieta earthquake

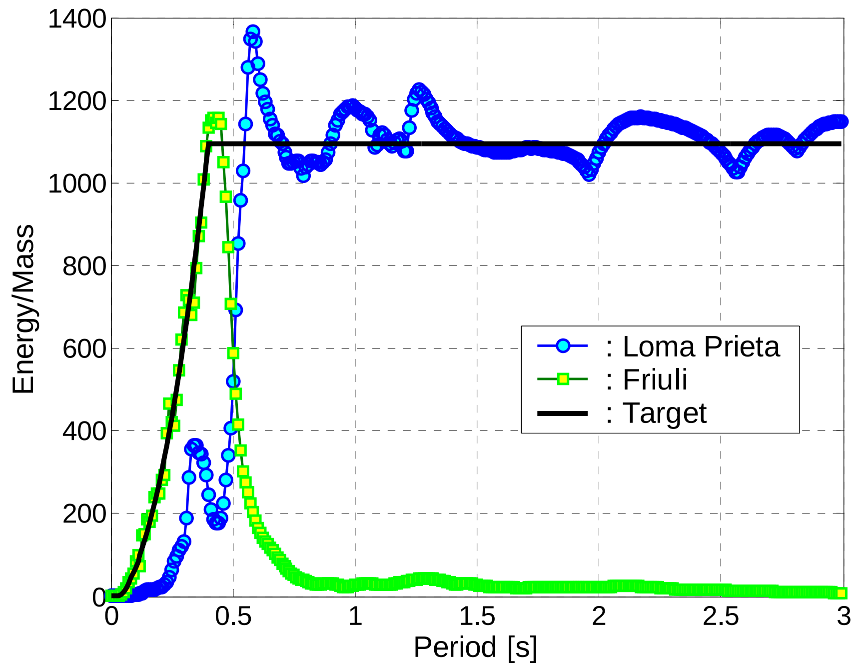

Figure 5.27. The Input Energy Spectra of the modified records and from the design spectrum.

Figure 5.27 shows the input energy spectra of the two modified records together with the input energy spectrum corresponding to the design spectrum. It can be seen from this figure that, as explained in Chapter IV, the modified records will be also compatible with the input energy spectrum obtained from the design spectrum, but this time only in the specified period ranges selected for matching. Note that the record that matches the high period region (Loma Prieta) presents an energy spectrum that is different from those of actual records (refer to Chapter IV). This can be an indication that the shape of the high period zone of design spectra is not compatible with the input energy spectra of real earthquake records. This hypothesis needs to be verified with another specific study and is beyond the scope of the thesis.

5.5 Summary

This chapter presented an alternative way to match a design spectrum using the wavelet-based procedure to modify a recorded accelerogram that was introduced in Chapter II. The procedure consists of using different earthquake records to match separately two previously defined parts of the target spectrum. The zone of the target spectrum selected for matching depends on the characteristics of the response spectrum of the individual records. One could argue that requiring more than one acceleration time history to match a response spectrum is an unnecessary nuisance for the dynamic analysis of the structures. However, if it is desired to perform an elastic or nonlinear time history analysis, the codes require the use of more than one accelerogram. For example, the UBC-97 code (see Section 131.1) requires the use of “not less than three” pairs of orthogonal horizontal components. Moreover, the code also requires that “if three time history analysis are performed, then the maximum response of the parameter of interest shall be used. If seven or more time history analyses are performed, then the average value … may be used for design”. These requirements are exactly the same as those in the SEAOC Blue Book (SEAOC 1999, Section 106.6).

Both codes also specify that for zones where there are no appropriate recorded ground motion time histories, simulated accelerograms can be used. One can use the popular program SIMQKE (Gasparini and Vanmarke 1976) to generate these accelerograms. However, as it was explained in a previous chapter, the accelerograms generated by this tool have some disadvantages: they have the same dominant frequency and have similar shapes. Thus, one of the main reasons for using several acceleration time histories (to account for the random character of the seismic motions) is defeated.

On the contrary, if existing records are modified, one can choose them so that they are associated with different seismic faults. Thus, it was proposed to select a record that represents a close earthquake with relatively short duration and another one that is representative of a distant earthquake, with longer strong motion duration.

Of course, one could choose more than two different types of earthquakes; say for instance three, where the third one can be associated with a fault at a medium epicentral distance from the site. However, for design purposes it is felt that two ground motions was an adequate compromise that appropiately accounts for the earthquakes expected at a site from different seismic sources.

A numerical example of the two-band matching procedure was presented along with a complete analysis of the original and artificial records. Based on this analysis, one can assert that the new spectrum compatible records nicely preserve the temporal variations of frequency of the original records.

CHAPTER VI

CONCLUSIONS AND RECOMMENDATIONS

6.1 Summary and conclusions

The signal analysis technique known as the wavelet transform was used in this study in novel applications. The most important application is the generation of artificial earthquakes time histories whose response spectra match a given smooth design spectrum.

Chapter II presented the wavelet-based procedure to modify a recorded accelerogram, so that it becomes compatible with a prescribed design spectrum. For completeness, a brief introduction to wavelets and the wavelets transform is presented first. The continuous wavelet transform was used to decompose a recorded accelerogram into a desired number of component time histories called detail functions. Although the detail functions are not purely harmonic, they have a predominant frequency given by the frequency of the dilated wavelet. Next, each of the time histories was appropriately scaled so that its response spectrum matches a specified design spectrum at selected periods. Each of these periods correspond to a dominant period of the detail functions.

The modified components were used to reconstruct an updated accelerogram and the process was repeated until an acceptable percent of error was obtained.

To implement the matching procedure, a new wavelet, based on the impulse response function of an underdamped oscillator was proposed. The proposed procedure was coded in *MATLAB*® and illustrated by modifying five recorded accelerograms with different characteristics. The design ground spectrum used for matching was the one prescribed in the UBC-97 (ICBO 1997) code for a seismic zone 3 and soil type S_B (rock). It was found that the procedure converges rapidly and accurately to the desired results.

Even though the response spectra of the time histories obtained in Chapter II match the target spectrum very well, these time histories were not ready to be used because they needed baseline corrections. It was shown by numerical integration of the modified acceleration time histories that the new accelerograms did not yield zero velocity or zero displacement at the end of the records. Therefore, Chapter III presented a procedure to perform a baseline correction of the spectrum compatible earthquake records without affecting their compatibility with the target spectrum. The procedure only modified a few points at the beginning and at the end of the record, and thus the corrected accelerogram obtained looks almost the same as the original one. The method is based on an original idea proposed by Wilson (2002). This procedure was coded in *MATLAB*® and illustrated by correcting two of the compatible accelerograms obtained in Chapter II. It was found that the procedure converges quickly and precisely to the desired results. The matching of the spectra of the corrected records with the target spectrum was verified.

Chapter IV was devoted to the analysis of the accelerograms obtained in Chapter II and III. With the purpose of comparing the characteristics of the accelerograms modified via the wavelet transform with those of artificial accelerograms obtained using another of the available methods, a set of artificial accelerograms was generated using the program *SIMQKE*. The analysis performed on the records include an analysis in the frequency domain (by means of the Fourier transform), an analysis in time-frequency domain (using the Continuous Wavelet transform), an inspection of the energy content (by means of the Input Energy Spectra) and a study of the ground motion duration (using the Arias Intensity and the Husid plot).

These analyses showed that some of the artificial records obtained using the procedure presented in Chapter II have very different frequency content and non-stationary characteristics than the real records which were used as seed for their generation. The similitude between the frequency content of both accelerograms will depend on how much alike the response spectrum of the original record is from the target spectrum. It was found that all the accelerograms generated with SIMQKE to match a specific response spectrum tend to have the same frequency content. This is a disadvantage if they are going to be used in time history dynamic analyses for design or verification purposes.

It was also shown in Chapter IV that the artificial accelerograms generated using SIMQKE need an appropriate baseline correction, otherwise they have very unrealistic velocity and displacement time histories.

Since the goal of retaining in the compatible record the temporal frequency variations of the original record was not completely achieved with the procedure proposed in Chapter II, an alternative method to match the target spectrum is presented in Chapter V. The procedure consists of matching only a previously defined part of the target spectrum which depends on the characteristics of the original response spectrum of the record. To match the design spectrum along all the periods of interests it will be necessary to modify a few records, each one matching different parts of the target spectrum. However, based on practical considerations, it was decided to divide the range of periods of the target spectrum in two zones. For the short period zone, a near fault earthquake record is used whereas for the intermediate and long period band, an accelerogram of an earthquake originated at a long distant is selected. The method is thus referred as the “two-band” matching procedure. A numerical example was presented and a comprehensive analysis of the original and artificial records was done. The analysis showed that the spectrum compatible records obtained preserve the temporal frequency variations of the original record.

6.2 Suggestions for further studies

At the present time, the wavelet transform has scarcely been applied to earthquake engineering. A search in the *MCEER Quakeline Database* using “wavelet” as keyword brought about 21 results, one of them in Japanese and three in Chinese. The same search using “Fourier” as keyword produced 266 results. It was shown in this investigation that the wavelet transform can be used as a powerful analytical tool to study the ground motion characteristics in both time and frequency domain. Since the capabilities of the wavelet transform were not fully utilize yet in structural engineering, further studies may lead to interesting and useful applications of this technique. Some topics that look very attractive for further applications of wavelets to the earthquake engineering field are:

- Generation of artificial records compatible with multiple-damping design spectra (Lilhanand and Tseng, 1998)
- The relationship between the accumulation patterns of energy in time with the frequency content of the accelerogram (Chapter IV) should be studied in more detail. A thorough investigation of this subject could lead to a new definition of “strong ground motion”.
- The analysis of earthquake motions using the wavelet transform from the viewpoint of input energy to the structures (Iyama and Kuwamura, 1999) is a topic worth of further investigation.
- Simulation of synthetic earthquakes controlled in both time and frequency domains (Iyama and Kuwamura, 1999).
- The extraction of the P and S waves from the complete earthquake record, in which other waves appear alongside with several types of noise. Ia another potential area of application of wavelets. This is an important step for fixing the quake’s type and location.

REFERENCES

1. Arias, A., “A Measure of Earthquakes Intensity”, Seismic Design for Nuclear Power Plants, Hansen, R., Ed., MIT Press, Cambridge, Massachusetts, 1970, pages 438-483.

2. Basu, B. and Gupta, V.K., “Seismic Response of SDOF Systems by Wavelet Modeling of Nonstationary Processes”, Journal of Engineering Mechanics, Vol. 124, No. 10, Oct. 1998, pages 1142-1150.

3. Bommer, J.J. and Martínez, A., “The Effective Duration of Earthquake Strong Motion”, Journal of Earthquake Engineering, Vol. 3, No. 2, 1999, pages 127-172.

4. Bommer, J.J. and Ruggeri, C., “The Specification of Acceleration Time- Histories in Seismic Codes”, European Earthquake Engineering, Vol. 16, No. 1, 2002, pages 3-16.

5. Bommer, J.J. and Scott, S.G., “The Feasibility of Using Real Accelerograms for Seismic Design”, *In* Implications of Recent Earthquakes on Seismic Risk, Elnashai and Antoniou, Eds., Imperial College Press, 2000, pages 115-126.

6. Bommer, J.J., Scott, S.G. and Sarma S.K., “Time-history representation of seismic hazard”, Proceedings of the Eleventh European Conference on Earthquake Engineering, September 6-11, 1998, Paris, France, A. A Balkema, Rotterdam, Holland, 1998.

7. Converse, A.M., Brady, A.G. and Joyner, W.B., “ Improvements in Strong-Motion Data Processing Procedures”, Proceedings of the 8th World Conference on Earthquake Engineering, San Francisco, California, 1984, pages 143-148.

8. Gupta, I.D. and Joshi, R.G., “On Synthesizing Response Spectrum Compatible Accelerograms”, European Earthquake Engineering, Vo. VII, No. 2, 1993, pages 25-33.

9. Haigh, S.K., Teymur, B., Madabhushi, S.P.G., Newland, D.E., “Applications of Wavelet Analysis to the Investigation of the Dynamic Behaviour of Geotechnical Structures”, Soil Dynamics and Earthquake Engineering, Vol. 22, No. 9-12, Oct.-Dec. 2002, pages 995-1005.

10. Housner, G.W., “Limit Design of Structures to Resist Earthquakes”, Procedings of the 1st World Conference on Earthquake Engineering, Los Angeles, California, 1956, pages 5.1 – 5.13.

11. Husid, L.R., “Características de Terremotos. Análisis General”, Revista del IDIEM, Vol. 8, Santiago de Chile, 1969, pages 21-42.

12. Irizarry J., "Design Earthquakes and Design Spectra for Puerto Rico's Main Cities Base don Worlwide Strong MOtion Records", Master of Science Thesis, University of Puerto Rico at Mayagüez, Mayagüez, Puerto Rico, 1999, 168 pp.

13. Iyengar, R.N and Rao, P.N., "Generation of Spectrum Compatible Accelerograms", Earthquake Engineering and Structural Dynamics, Vol. 7, 1979, pages 253-263.

14. Iyuma, J. and Kuwamura, H., "Application of Wavelets to Analysis and Simulation of Earthquake Records", Earthquake Engineering and Structural Dynamics, Vol. 28, 1999, pages 255-272.

15. Kashaee, P., Bijan, M., Sadek, F., Lew, H.S., and Gross, J.L., "Distribution of Earthquake Input Energy in Structures", Building and Fire Research Laboratory, National Institute of Standards and Technology, Gairtherburg, Maryland, 2003.

16. Kramer, S.L., "Geotechnical Earthquake Engineering", Prentice Hall, New Jersy, 1996.

17. Lee, V.W. and Trifunac, M.D., "Torsional Accelerograms", Soil Dynamics and Earthquake Engineering, Vol. 4, 1985, pages 132-139.

18. Lee, V.W. and Trifunac, M.D., "Rocking Strong Earthquake Accelerograms", Soil Dynamics and Earthquake Engineering, Vol. 6, 1987, pages 79-89.

19. Lee, V.W. and Trifunac, M.D., "A Note on Filtering Strong Motion Accelerograms to produce Response Spectra of Specified Shape and Amplitude", European Earthquake Engineering, Vol. 2, 1989, pages 38-45.

20. Lee, V.W., "Surface Strains Associated with Strong Earthquake Shaking", Structural Engineering and Earthquake Engineering, JSCE, Vol. 7, 1990, pages 187-194.

21. Levy, S. and Wilkinson, J.P.D., "Generation of Artificial Time-Histories, Rich in All Frequencies, from Given Response Spectra", Nuclear Engineering and Design, Vol. 38, 1976, pages 241-251.

22. Lilhanand, K., and Tseng, W.S., "Development and Application of Realistic Earthquake Time Histories Compatible with Multiple-Damping Design Spectra", Proceedings of the 9th World Conference of Earthquake Engineering, Tokyo-Kyoto, Japan, August 2-9, 1988.

23. Mahin, S.A., "Effects of Duration and Aftershocks on Inelastic Design Earthquakes", Proceedings of the 8th World Conference in Earthquake Engineering, San Francisco, California, 1984, pages 881-888.

24. Malhotra, P.K., "Strong Motions Records for Site-Specific Analysis", Earthquake Spectra, Vol. 19, No. 3, 2003, pages 557-578.

25. Misiti, M., Misite Y., Oppenheim, G., Poggi J.M., "Wavelet Toolbox", The Math Works Inc., Natick, Massachusetts, 2001.

26. Mukherjee, S. and Gupta, V.K., "Wavelet – Based Characterization of Design Ground Motions", Earthquake Engineering and Structural Dynamics, Vol. 31, No. 5, May 2002, pages 1173-1190.

27. Naeim, F. and Lew, M., "On the Use of Design Spectrum Compatible Time Histories", Earthquake Spectra, Vol. 11, No. 1, 1995, pages 111-127.

28. Naeim, F., "The Seismic Design Handbook", Second Edition, Kluwer Academic Publishers, Norwell, Massachusetts, 2001.

29. Newland, D.E., "Wavelet Analysis of Vibration, Part I: Theory", Journal of Vibration and Acoustics, ASME, Vol. 116, No. 4, Oct. 1994, pages 409-416.

30. O'Connor, E.I. and Ellingwood, B., "Reliability of Nonlinear Structures with Seismic Loading", Journal of Structural Engineering, ASCE, Vol. 113, 1987, pages 1011-1028.

31. Ovanesova, A. and Suárez, L. E., "Applications of Wavelet Transforms to Damage Detection in Frame Structures", Engineering Structures, Vol. 26, No. 1, January 2004, pages 39-49.

32. Premount, A., "A Method for the Generation of Artificial Earthquakes Accelerograms", Nuclear Engineering Design, Vol. 59, 1980, pages 357-368.

33. Premount, A., "The Generation of Spectrum Compatible Accelerograms for the Design of Nuclear Power Plants", Earthquake Engineering and Structural Dynamics, Vol. 12, 1984, pages 481-497.

34. Puerto Rico Seismic Network, "Significant Earthquakes in the Puerto Rico Zone", http://rmsismo.uprm.edu/English/, January 2004.

35. Rizzo, P.C., Shaw, D.E. and Jarecki, S.J., "Development of Real/Synthetic Time Histories to Match Smooth Design Spectra", Nuclear Engineering and Design, Vol. 32, 1975, pages 148-155.

36. Sato, T., Murono, Y. and Mishimura, A., "Modeling of Phase Spectrum to Simulate Design Earthquake Motion", Technical Council on Lifeline Earthquake Engineering Monograph No. 16, Optimizing Post-Earthquake Lifeline System Reliability, Proceedings of the 5th U.S. Conference on Lifeline Earthquake Engineering, ASCE, Reston, Virginia, August 1999, pages 804-813.

37. Scanlan, R.H. and Sachs, K., "Earthquake Time Histories and Response Spectra", Journal of the Engineering Mechanics Division, ASCE, Vol. 100, No. 4, 1974, pages 635-655.

38. Shrikhande, M. and Gupta, V.K., "On Generating Ensemble of Design Spectrum-Compatible Accelerograms", European Earthquake Engineering, Vol. X, No. 3, 1996, pages 49-56.

39. Spanos, P.T.D., "Digital Synthesis of Response-Design Spectrum Compatible Earthquake Records for Dynamic Analysis", The Shock and Vibration Digest, Vol. 15, No. 3, 1983, pages 21-30.

40. Trifunac, M.D and Brady, A.G., "A Study on the Duration of Strong Earthquake Ground Motion", Bulletin of the Seismic Society of America, Vol. 65, 1975, pages 581-626.

41. Trifunac, M.D. and Lee, V.W., "Routing Processing of Strong-Motion Accelerograms", California Institute of Technology, Earthquake Engineering Research Laboratory, Report No. EERL 73-03, 1979, Pasadena, California.

42. Trifunac, M.D., "A Method for Synthesizing Realistic Strong Ground Motion", Bulletin of the Seismological Society of America, Vol. 61, 1971, pages 1739-1753.

43. Trifunac, M.D., "Curvograss of Strong Ground Motions", Journal of the Engineering Mechanics, ASCE, Vol. 116, 1990, pages 1426-1432.

44. Tsai, N-C., "Spectrum-Compatible Motions for Design Purposes", Journal of Engineering Mechanics Division, ASCE, Vol. 98, 1972, pages 345-356.

45. U.S. Geological Survey, "Information about Past and Historical Earthquakes", http://earthquake.usgs.gov/activity/past.html, January 2004.

46. Uang, C.M., and Bertero, V.V., "Evaluation of Seismic Energy in Structures", Earthquake Engineering and Structural Dynamics, Vol.19, 1990, pages 77-90.

47. Vanmarcke, E.H. and Gasparini, D.A., "Simulated Earthquake Motions Compatible with Prescribed Response Spectra" Report 76-4, Dept. of Civil Engineering, Massachusetts Institute of Technology, Cambridge, Massachusetts, January 1976.

48. Vázquez, D., "Seismic Behavior and Retrofitting of Hillside and Hilly Terrain R/C Houses Raised of Gravity Columns", PhD Thesis, Departemt of Civil Engineering and Surveying, University of Puerto Rico at Mayagüez, Mayagüez, PR, 2002.

49. Walker, S.W., "A Primer on Wavelets and their Scientific Applications", Chapman & Hall/CRC, Boca Raton, Florida, 1999.

50. Watabe, M., Masao, T. and Tohdo, M., "Synthesized Earthquake Ground Motions for Earthquake Resistant Design", 5th Canadian Conference in Earthquake Engineering, Ottawa, Canada, 1987, pages 675-684.

51. Wilson, W.L., "Three-Dimensional Static and Dynamic Analysis of Structures: A Physical Approach With Emphasis on Earthquake Engineering", Third Edition, Computers and Structures Inc., Berkeley, California, 2002.

52. Wong, H.L. and Trifunac, M.D., "Generation of Artificial Strong Motion Accelerograms", Earthquake Engineering and Structural Dynamics, Vol. 7, 1979, pages 509-527.

53. Zahrah, T.F. and Hall, W.J., "Earthquake Energy Absorption in SDOF Structures", Journal of Structural Engineering, ASCE, Vol. 100, 1984, pages 1757-1772.

APPENDIX A

DEVELOPMENT OF COMPATIBLE RECORDS FOR MAYAGÜEZ, PR

A set of artificial accelerograms is generated to match the design spectrum proposed by Irizarry (1999) for Mayagüez, PR. The records used as seed for the generation of the artificial earthquakes were selected from the records applied to generate the design spectrum and from the records available for Puerto Rico. The target spectrum is shown in Figure A.1. This design spectrum coincide with the design spectrum proposed by the UBC-97 for seismic zone 4, soil profile S_B and a closest distance to seismic zone type B less than 2 km.

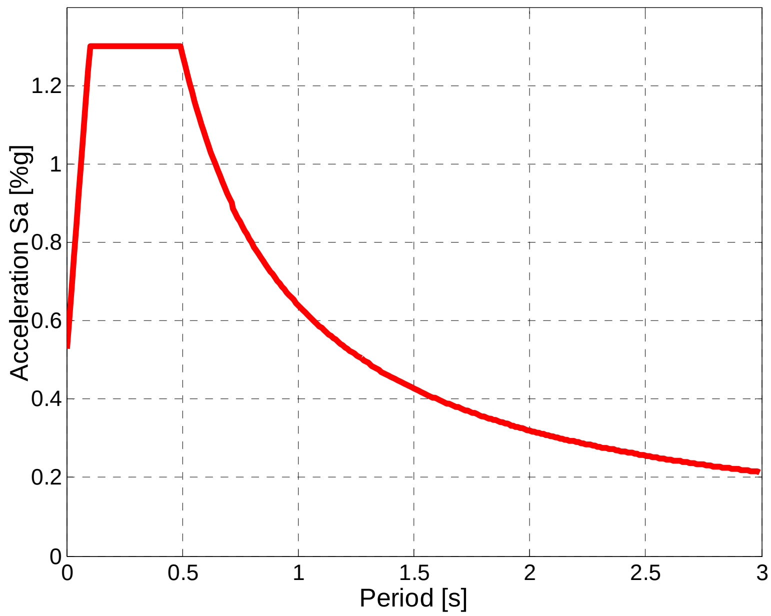

Figure A.1. Design spectrum proposed by Irizarry (1999) for Mayagüez, PR.

The ground motions used were the Loma Prieta earthquake (California, October 18/1989) at Crystal Springs station with a closest distance to the rupture failure of 46.9 km and USGS Site Classification B, Coyote Lake (California, August 6, 1979) at Gilroy station (array #6) with a closest distance to the rupture failure of 3.1 km and USGS Site Classification B, Puerto Real (Puerto Rico, July 8, 2003) at the San Germán fire station with an epicentral distance of 16.5 km and Puerto Real (Puerto Rico, July 8, 2003) at the Maricao fire station with an epicentral distance of 26.9 km. The next figures show the results obtained.

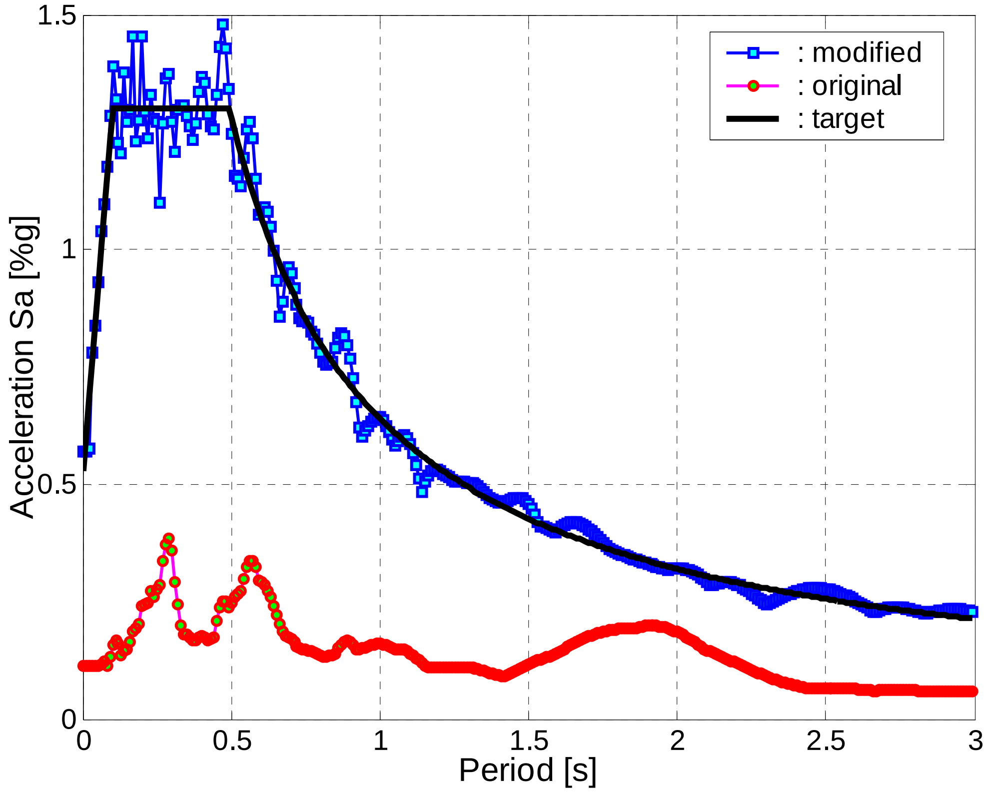

Figure A.2. The target spectrum and the spectra of the original and modified record of the Loma Prieta earthquake

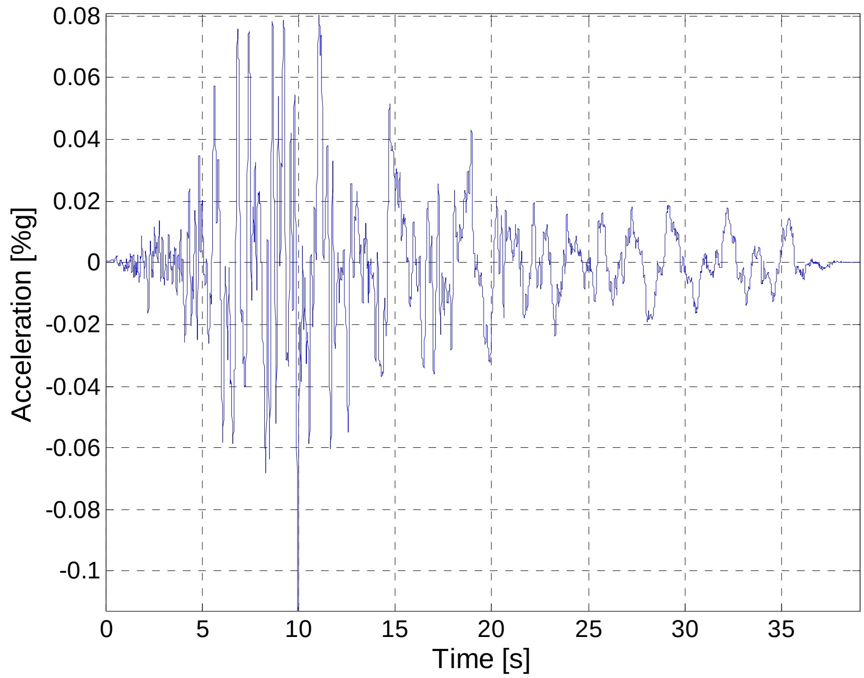

Figure A.3. Original record of the Loma Prieta earthquake.

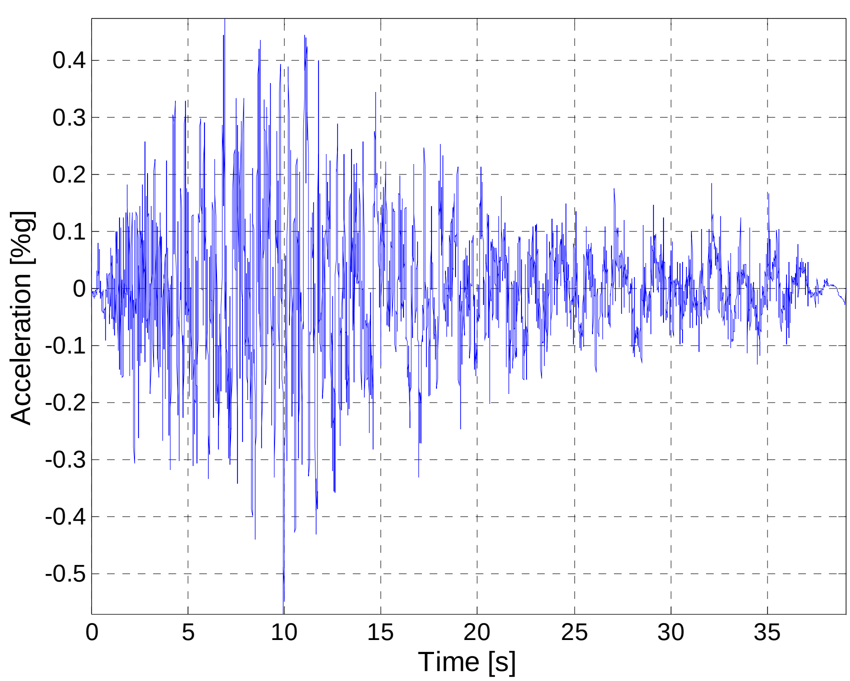

Figure A.4. Modified record of the Loma Prieta earthquake.

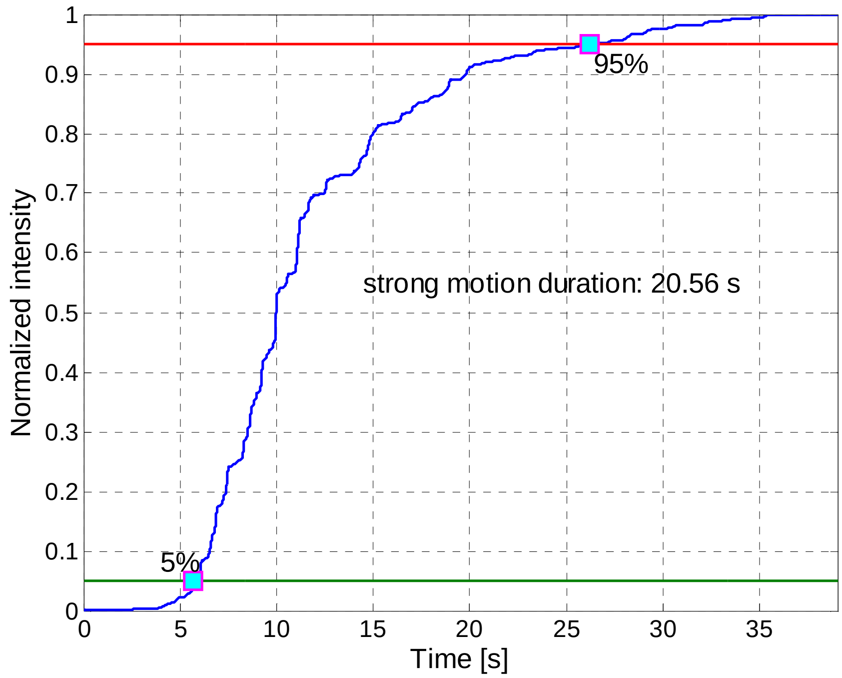

Figure A.5. Significant duration of the original record of the Loma Prieta earthquake

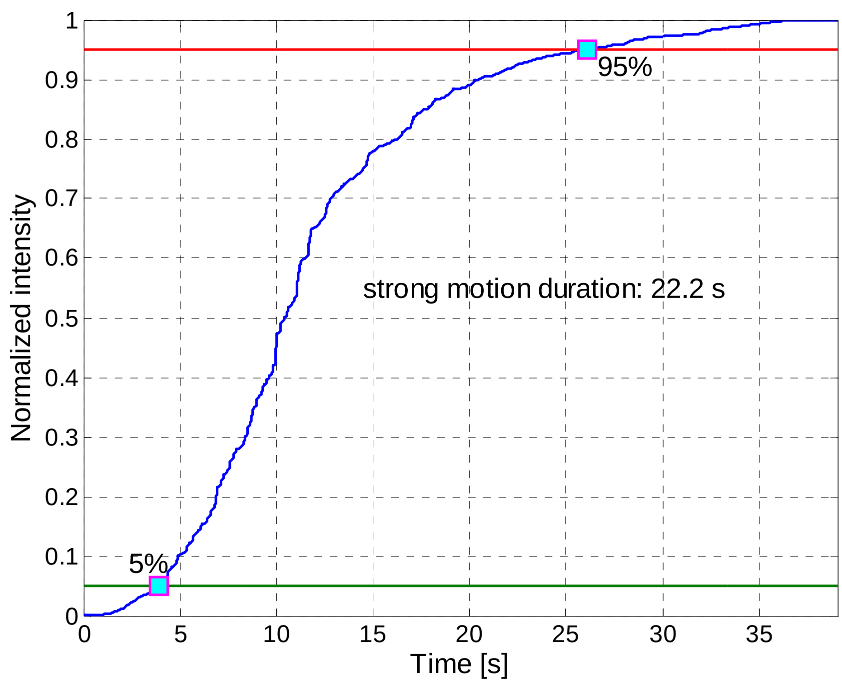

Figure A.6. Significant duration of the original record of the Loma Prieta earthquake

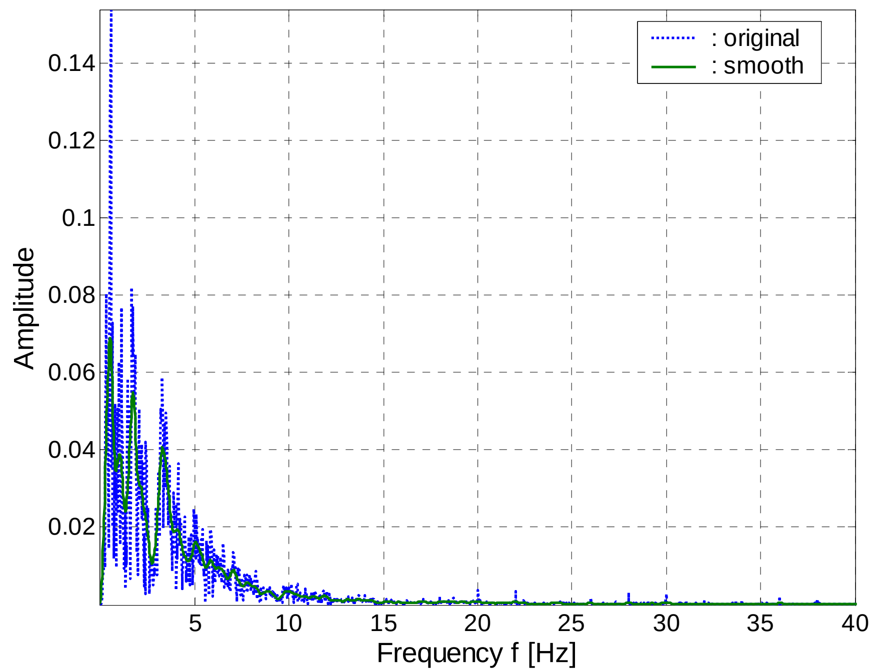

Figure A.7. Fourier spectrum of the original record of the Loma Prieta earthquake

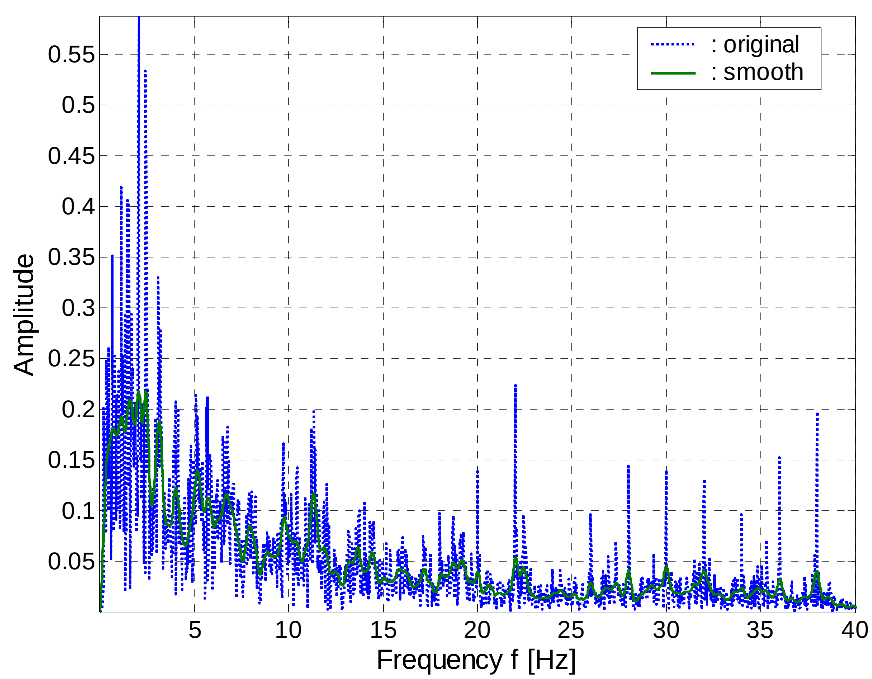

Figure A.8. Fourier spectrum of the modified record of the Loma Prieta earthquake

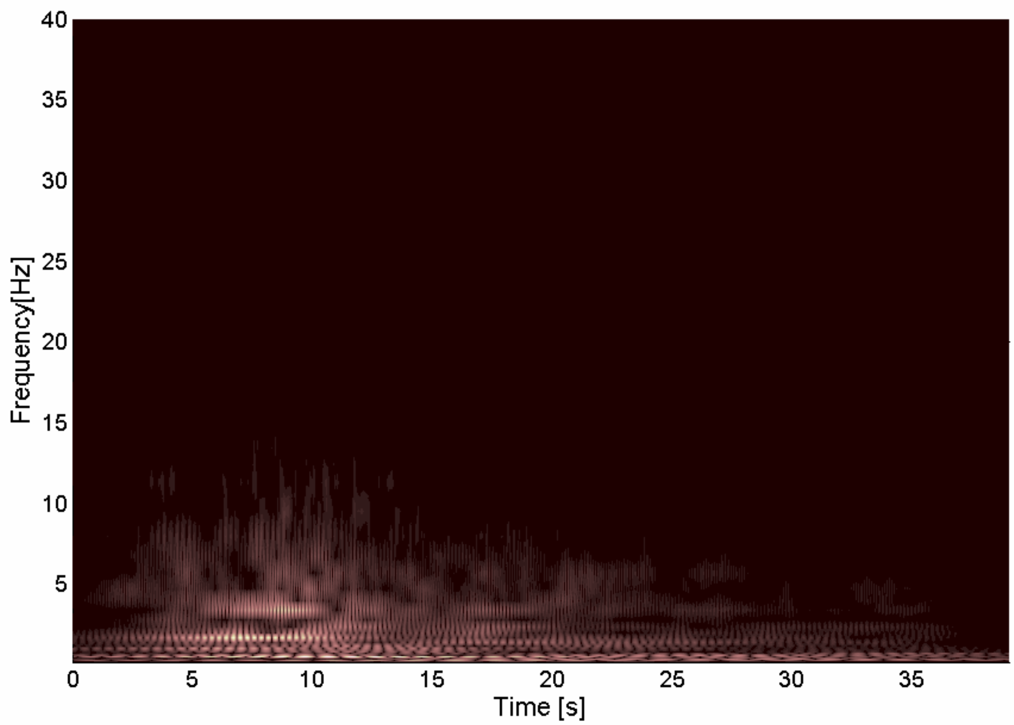

Figure A.9. Wavelet Map of the original record of the Loma Prieta earthquake

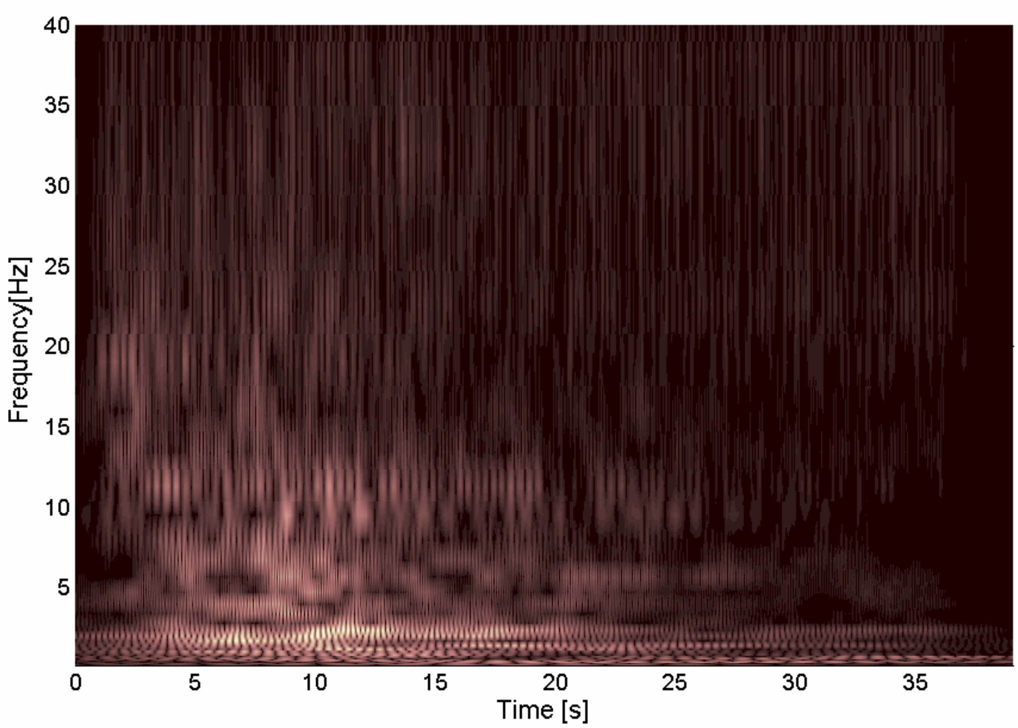

Figure A.10. Wavelet Map of the modified record of the Loma Prieta earthquake

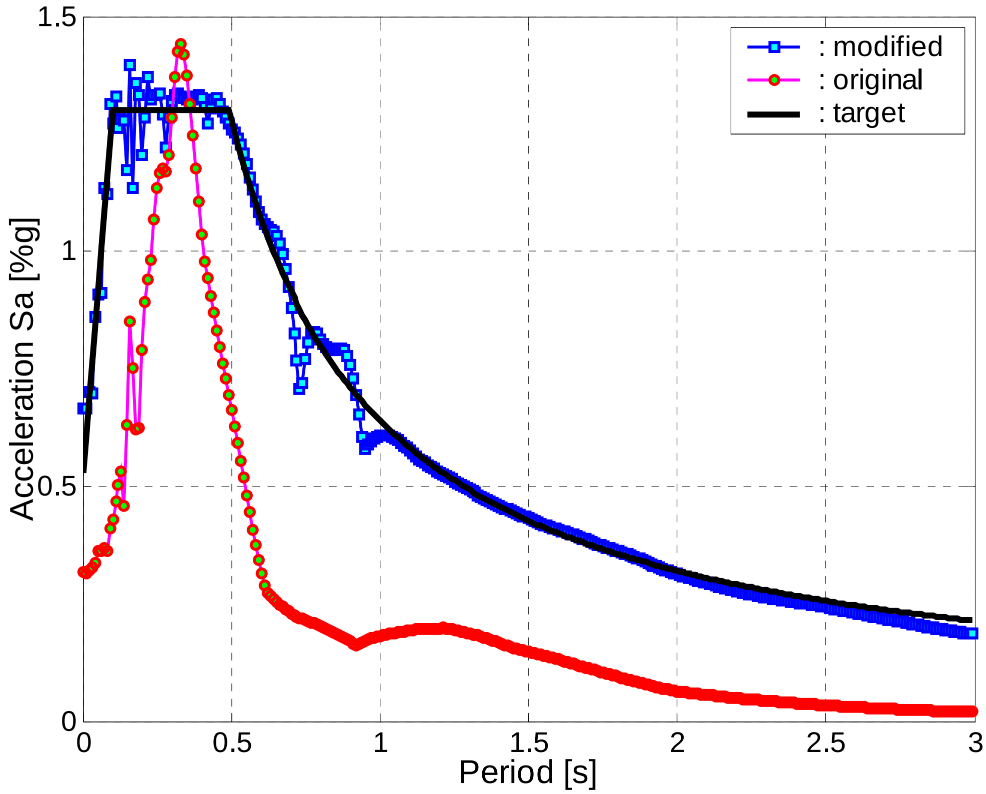

Figure A.11. The target spectrum and the spectra of the original and modified record of the Coyote Lake earthquake

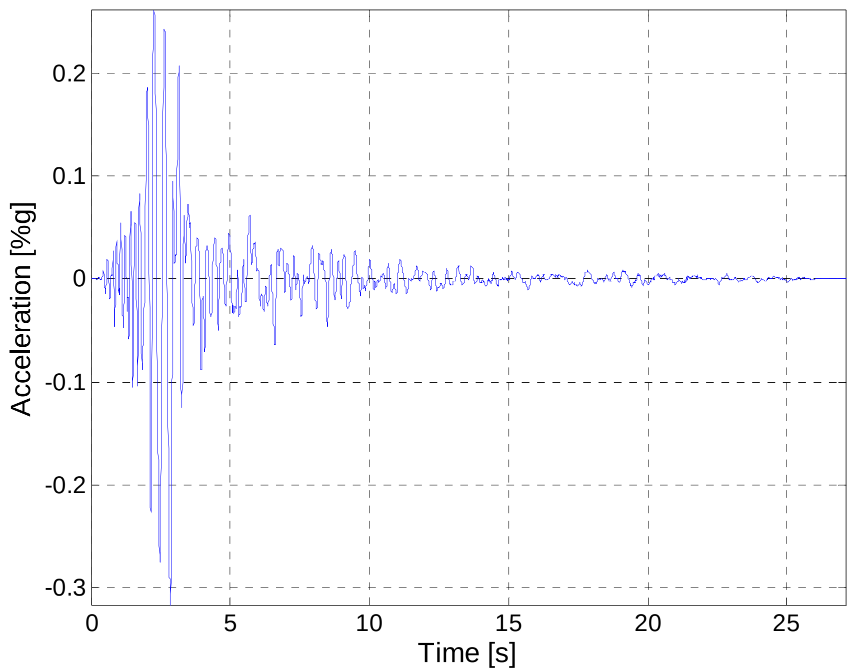

Figure A.12. Original record of the Coyote Lake earthquake

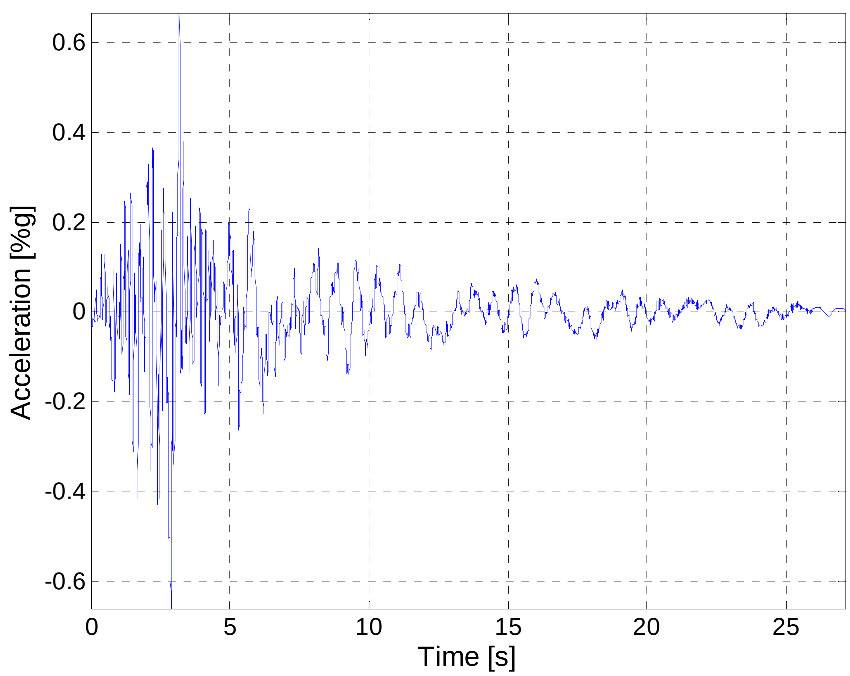

Figure A.13. Modified record of the Coyote Lake earthquake

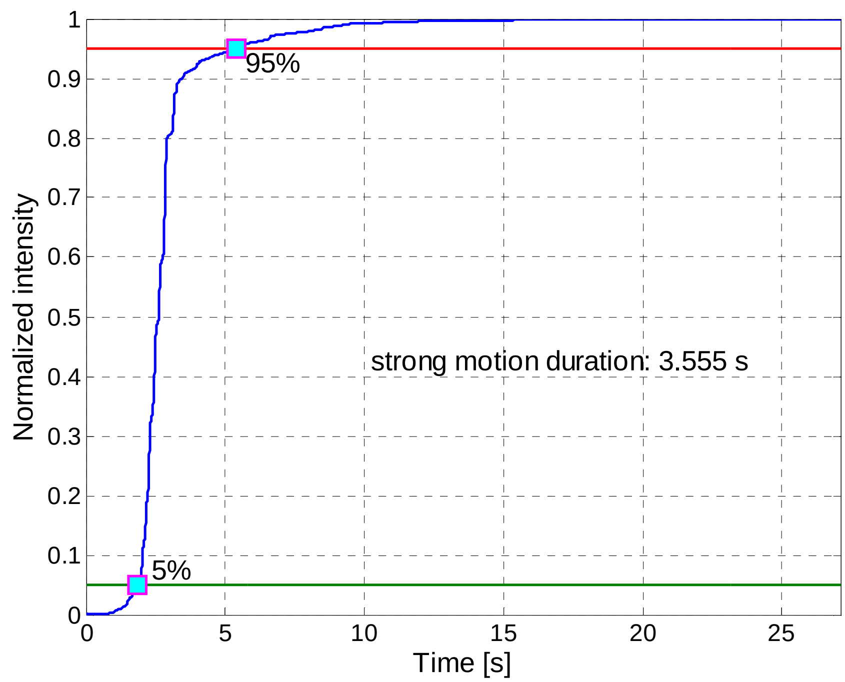

Figure A.14. Significant duration of the original record of the Coyote Lake earthquake

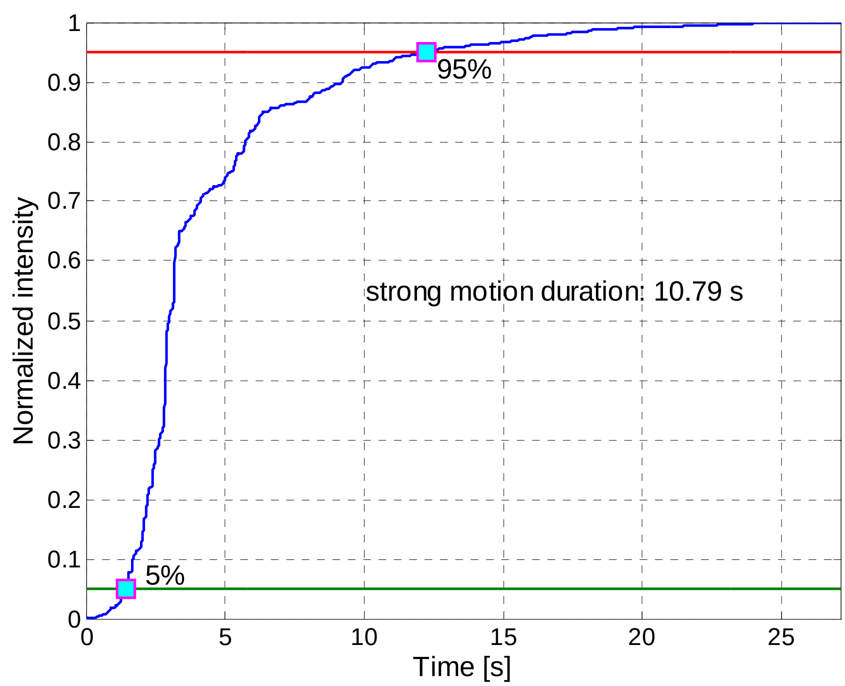

Figure A.15. Significant duration of the modified record of the Coyote Lake earthquake

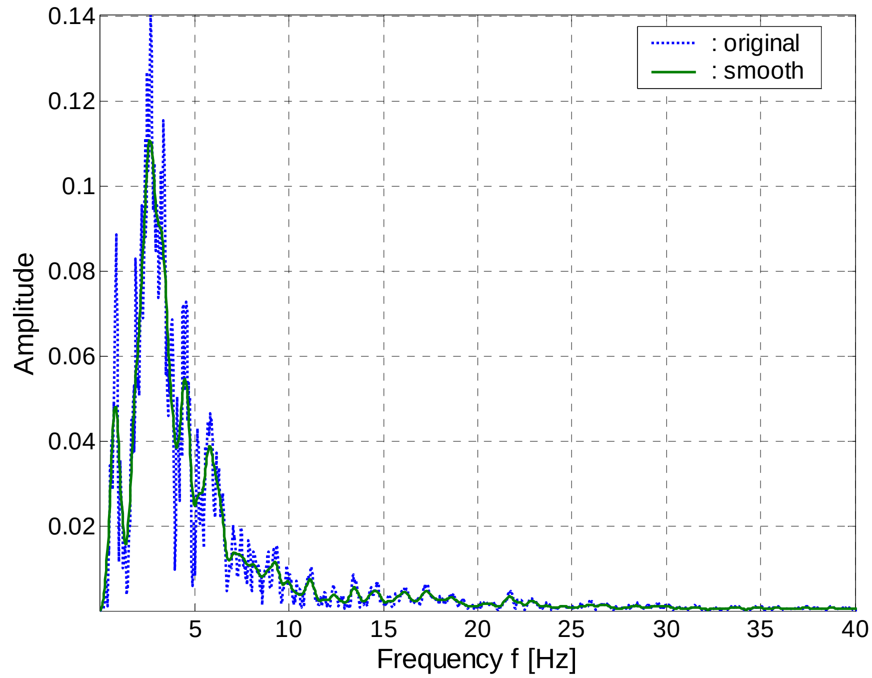

Figure A.16. Fourier spectrum of the original record of the Coyote Lake earthquake

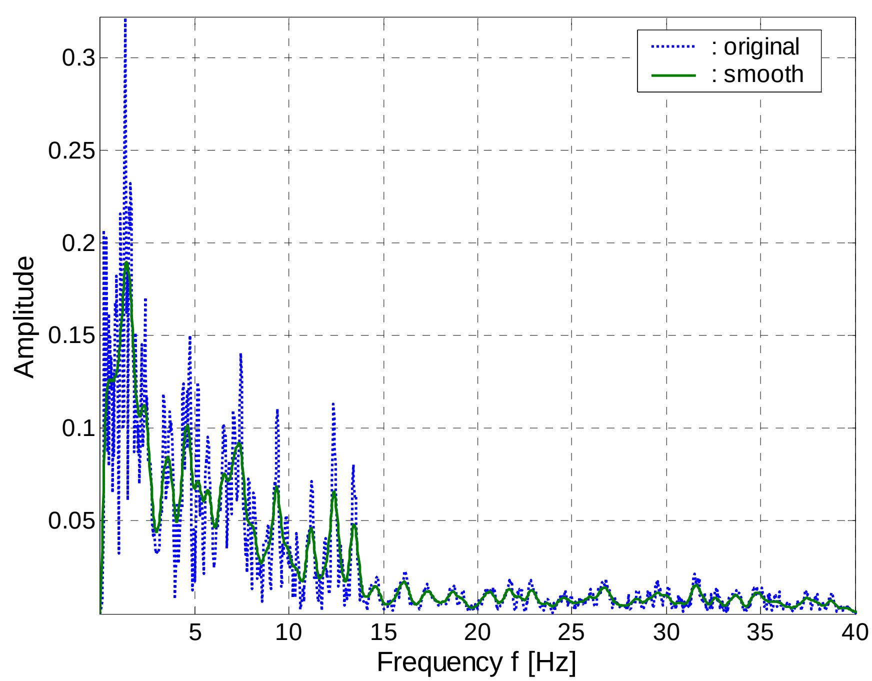

Figure A.17. Fourier spectrum of the original record of the Coyote Lake earthquake

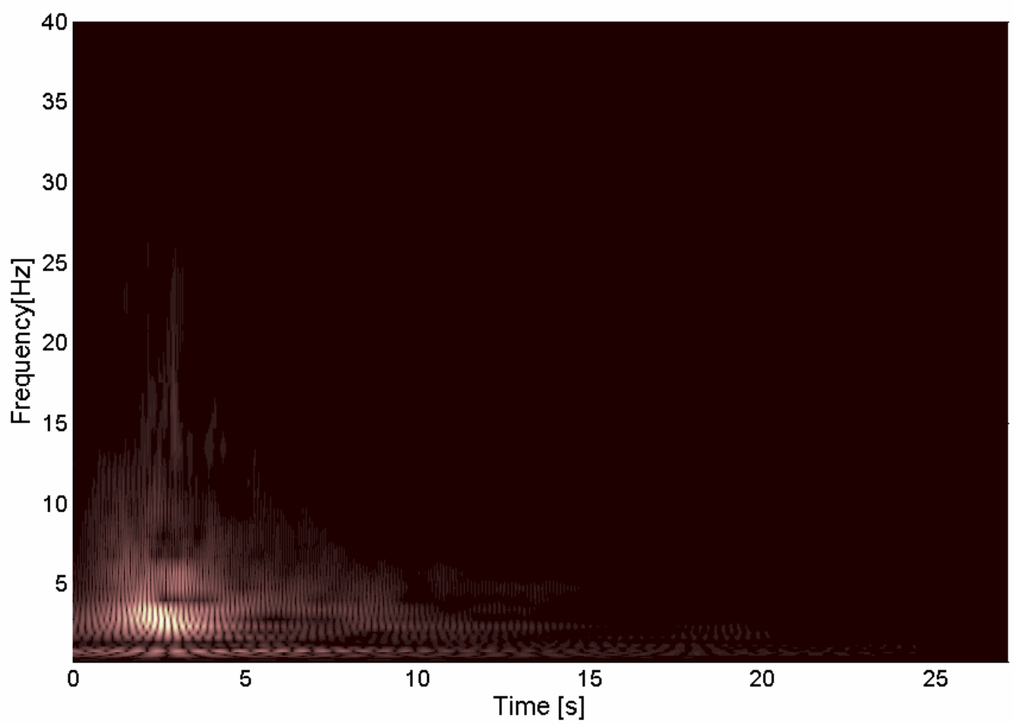

Figure A.18. Wavelet Map of the original record of the Coyote Lake earthquake

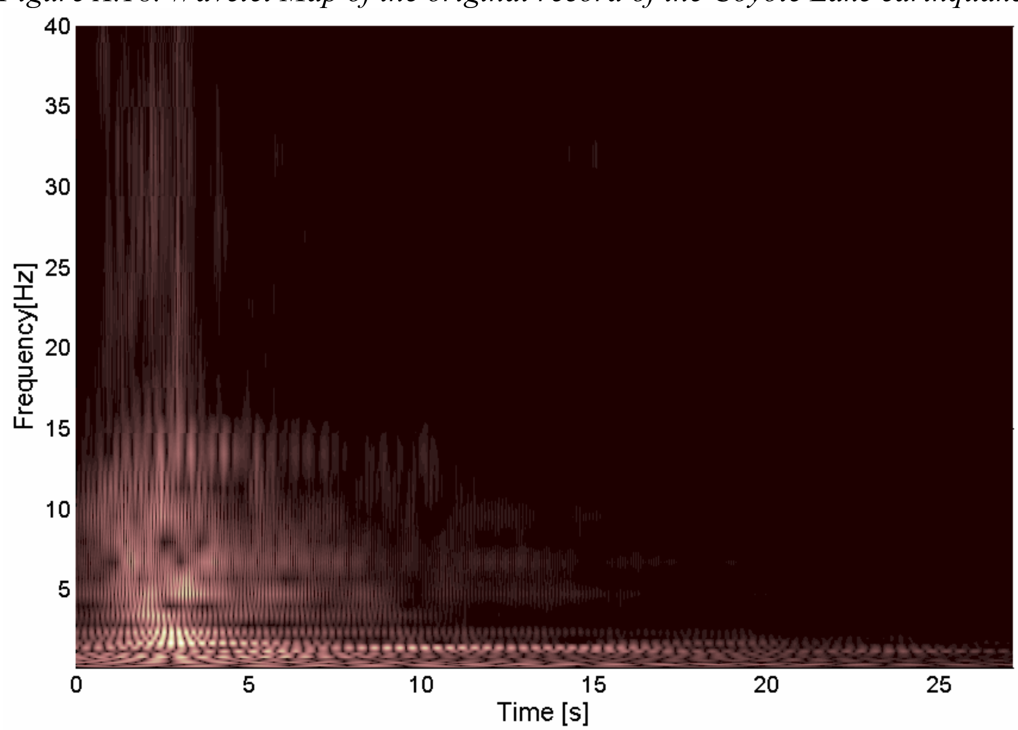

Figure A.19. Wavelet Map of the modified record of the Coyote Lake earthquake

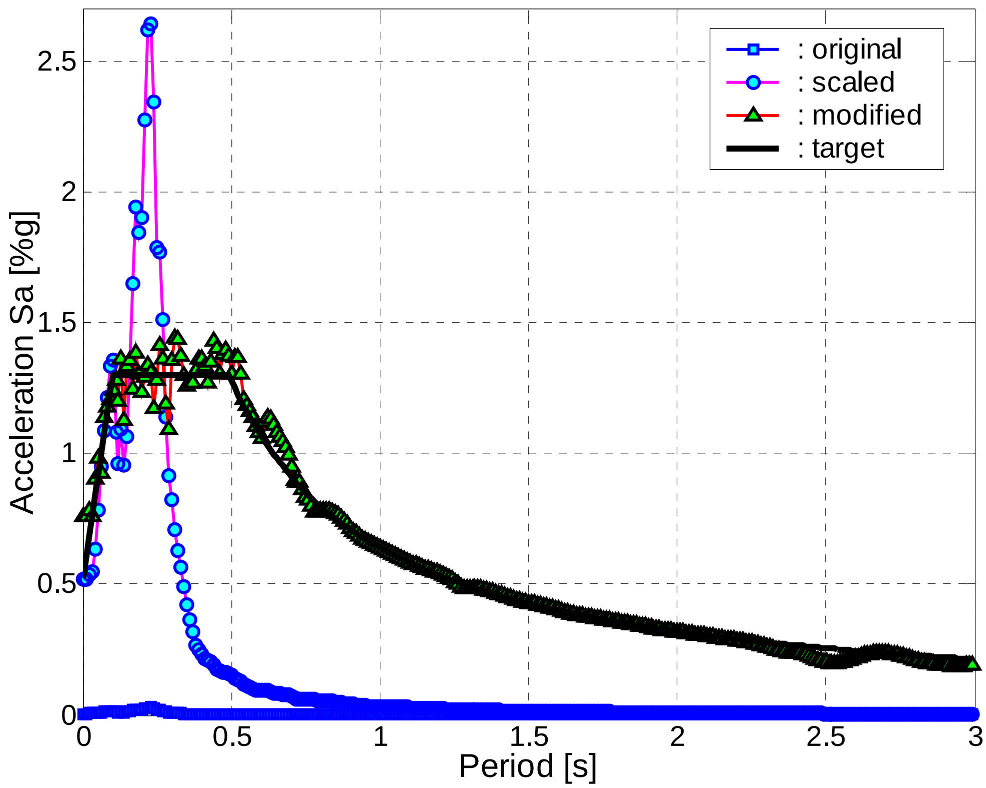

Figure A.20. The target spectrum and the spectra of the original and modified record of the Puerto Real earthquake at Maricao

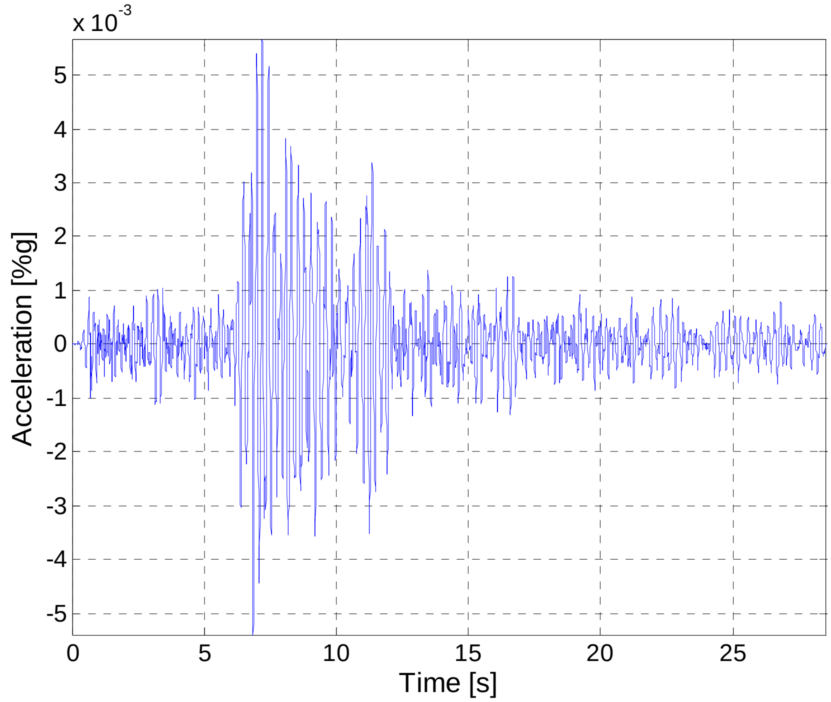

Figure A.21. Original record of the Puerto Real earthquake at Maricao

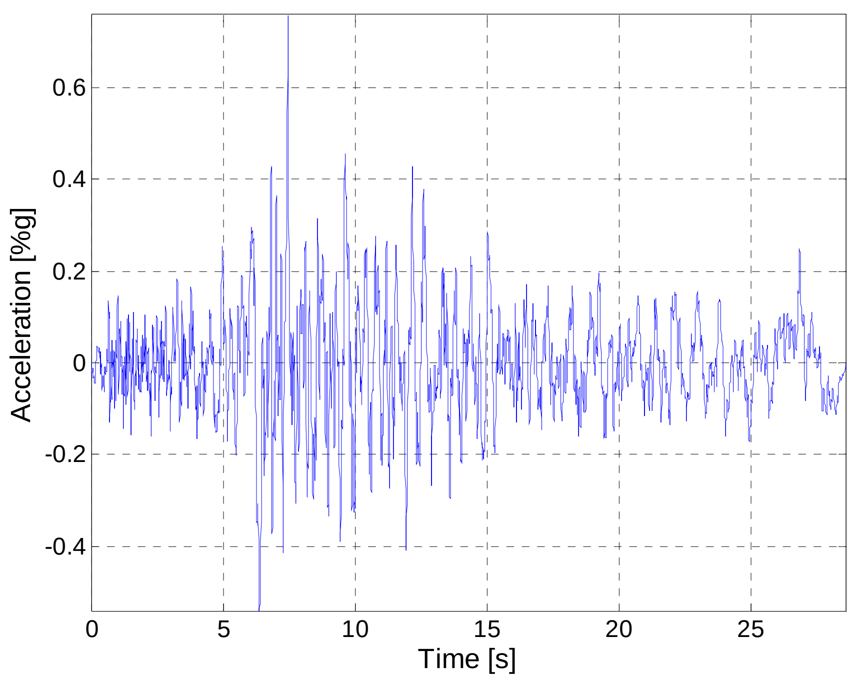

Figure A.22. Modified record of the Puerto Real earthquake at Maricao

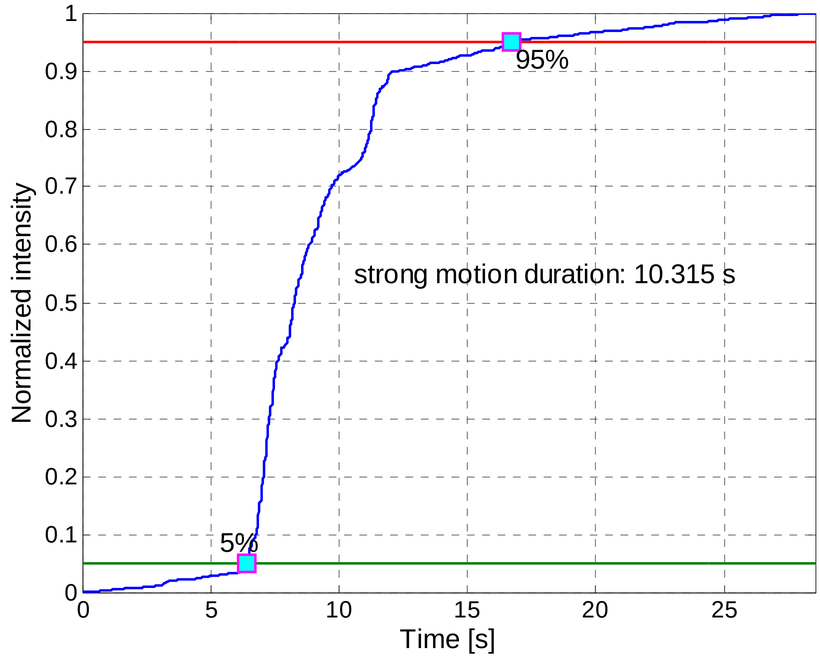

Figure A.23. Significant duration of the original record of the Puerto Real earthquake at Maricao

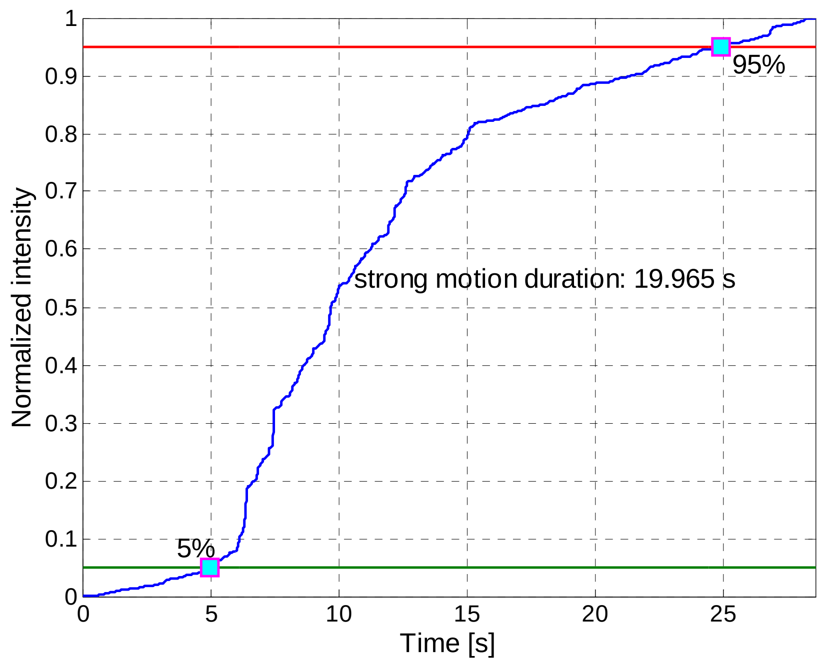

Figure A.24. Significant duration of the modified record of Puerto Real earthquake at Maricao

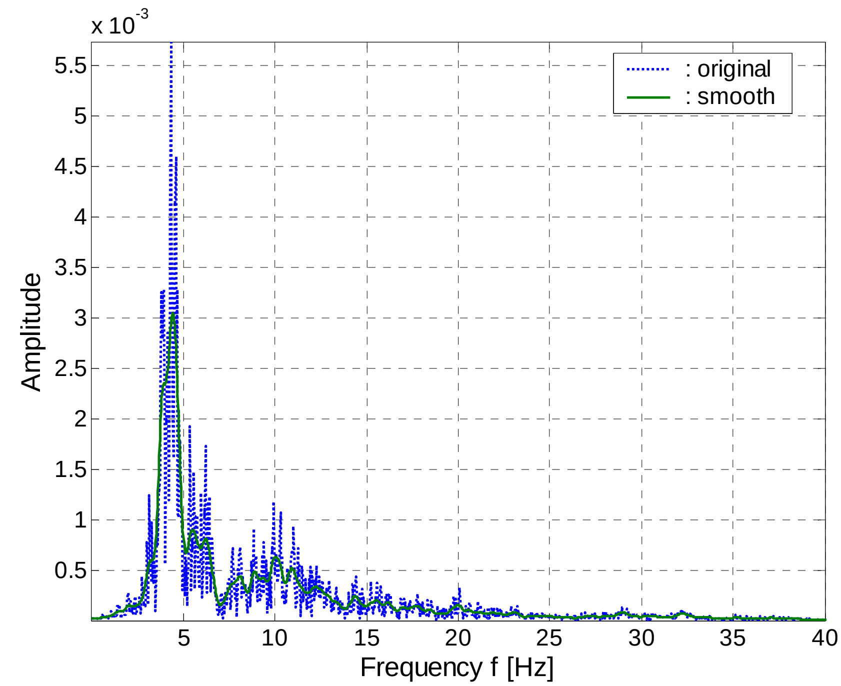

Figure A.25. Fourier spectrum of the original record of the Puerto Real earthquake at Maricao

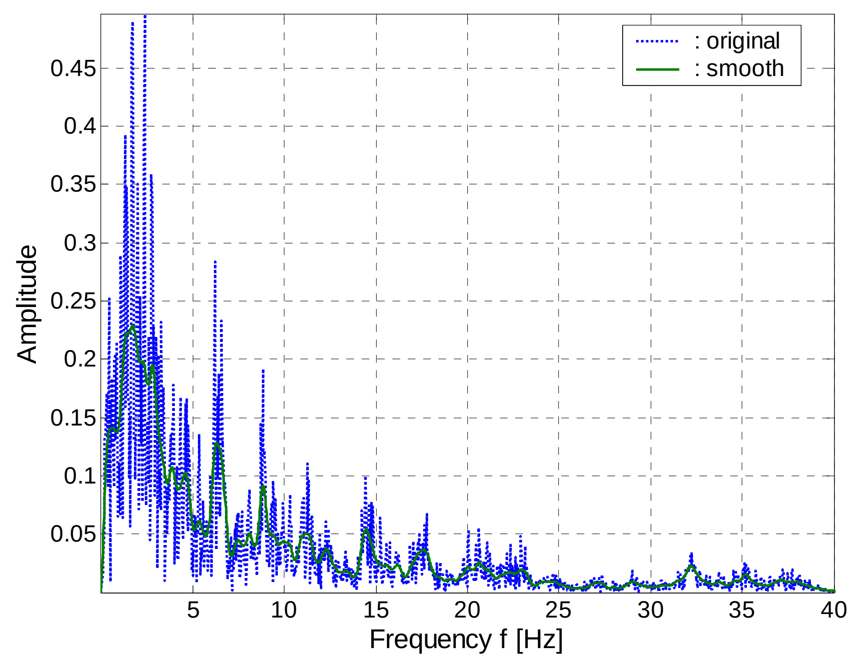

Figure A.26. Fourier spectrum of the original record of Puerto Real earthquake at Maricao

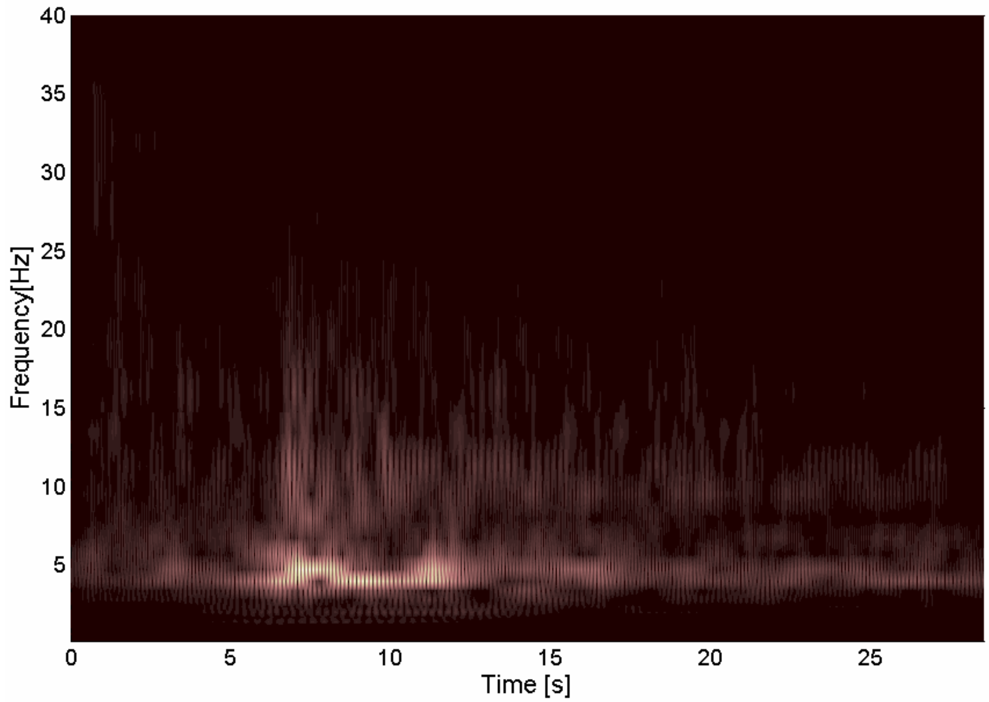

Figure A.27. Wavelet Map of the original record of the Puerto Real earthquake at Maricao

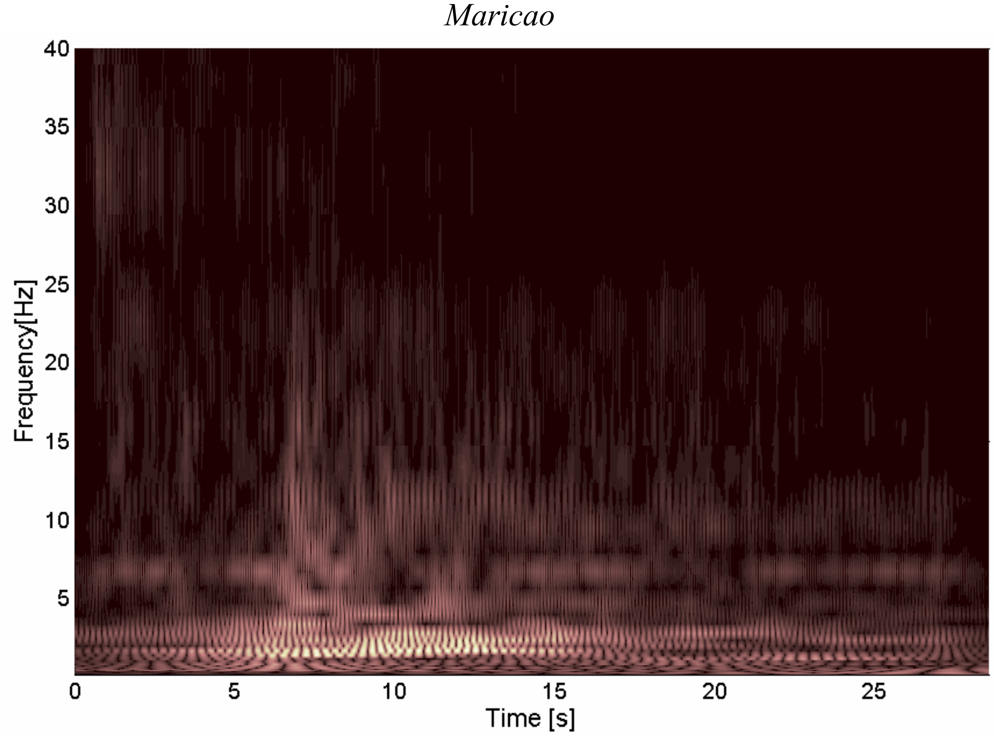

Figure A.28. Wavelet Map of the modified record of the Puerto Real earthquake at Maricao

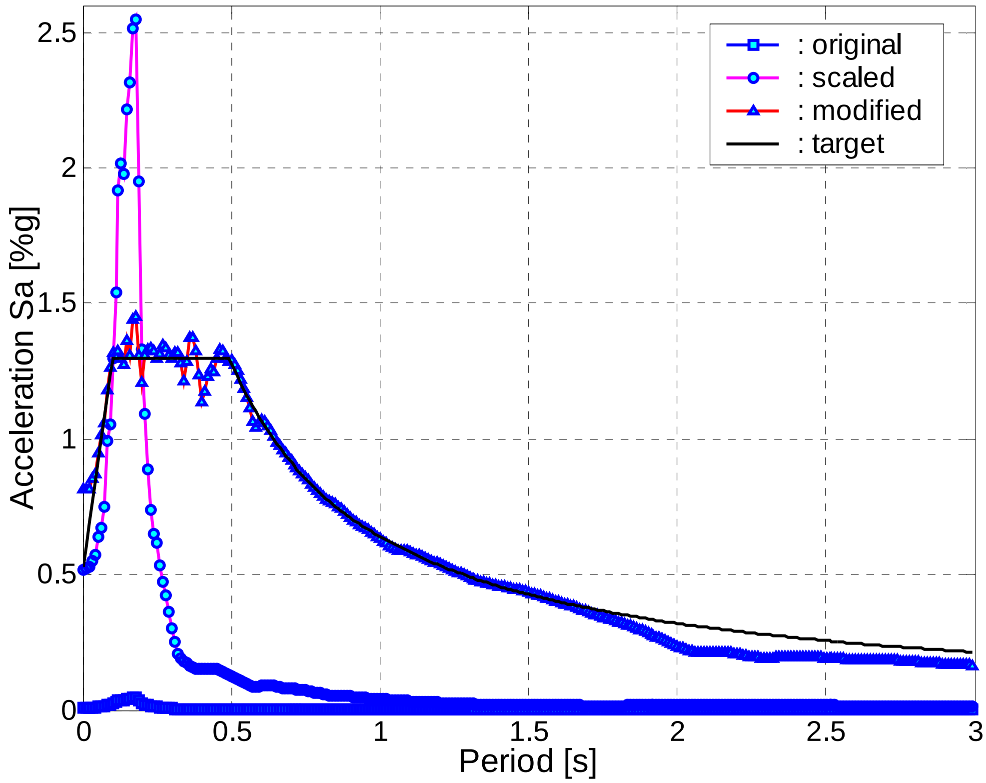

Figure A.29. The target spectrum and the spectra of the original and modified record of the Puerto Real earthquake at San Germán

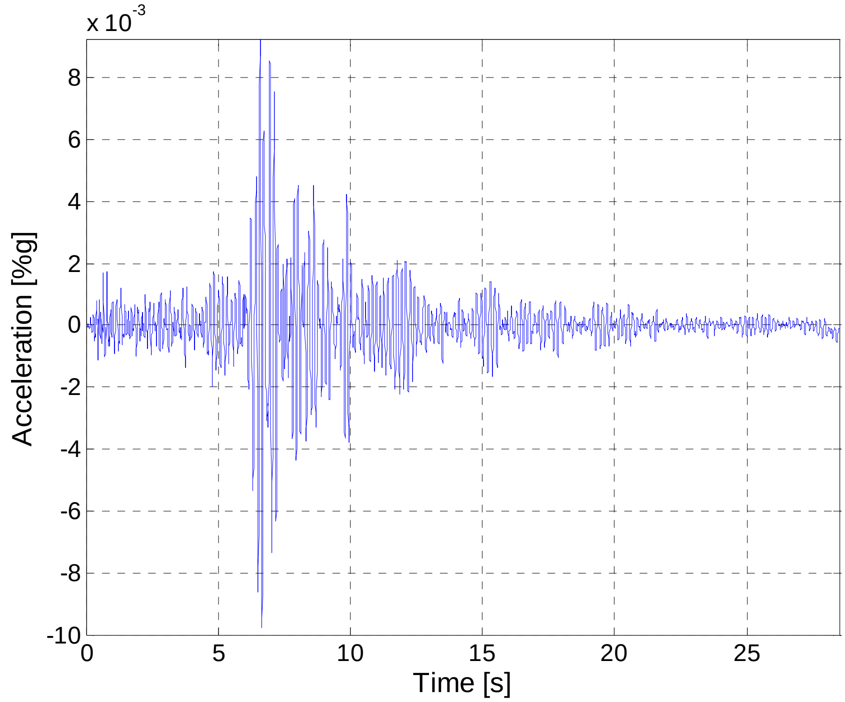

Figure A.30. Original record of the Puerto Real earthquake at San Germán

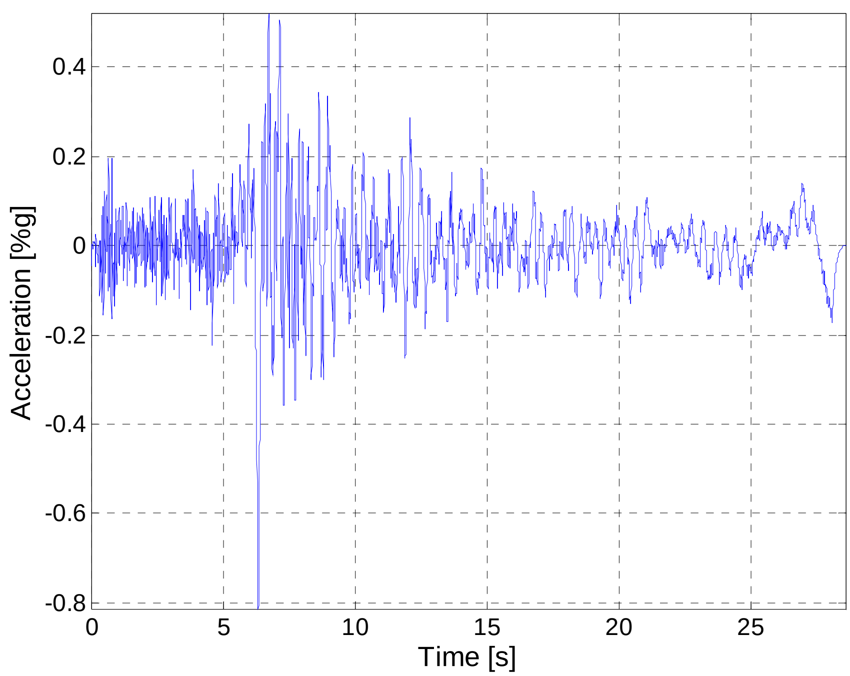

Figure A.31. Modified record of the Puerto Real earthquake at San Germán

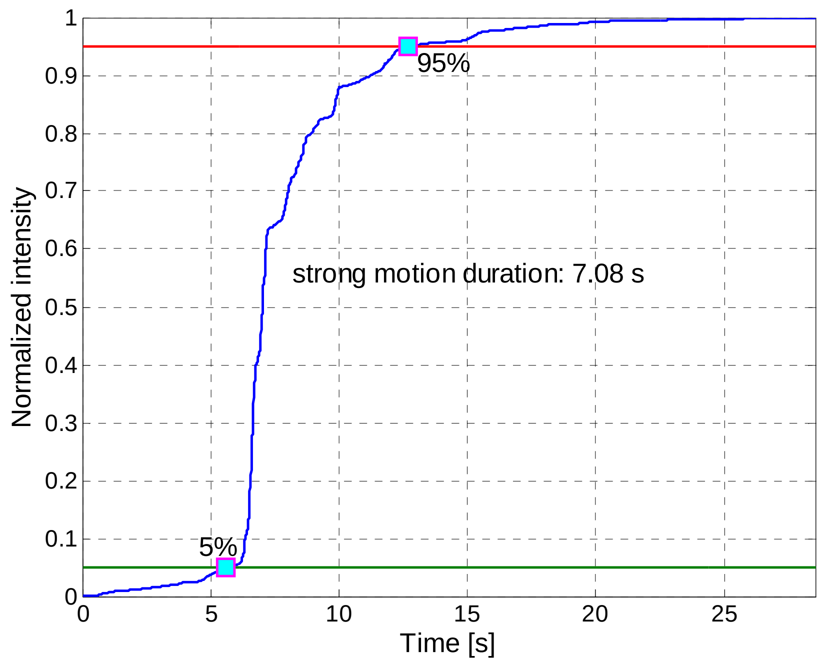

Figure A.32. Significant duration of the original record of the Puerto Real earthquake at San Germán

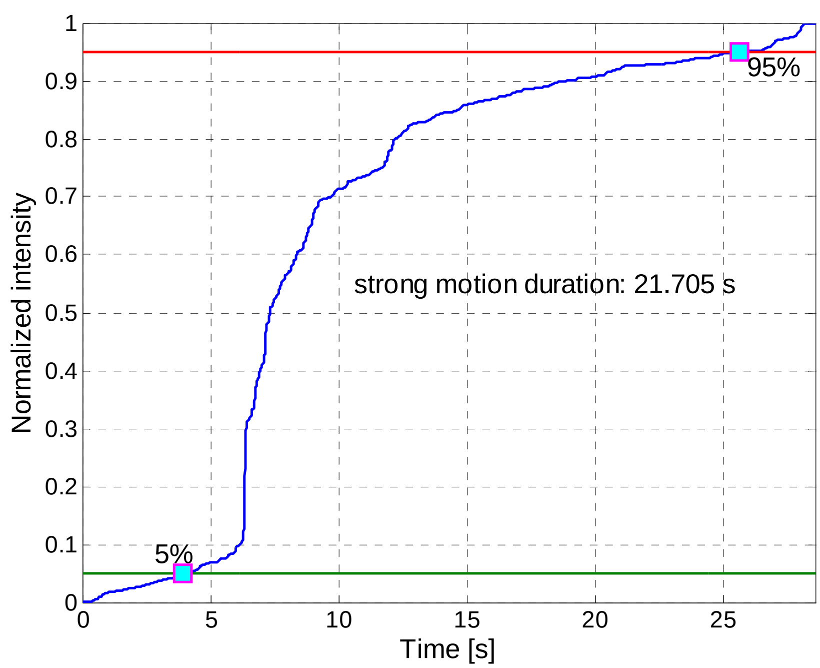

Figure A.33. Significant duration of the modified record of Puerto Real earthquake at San Germán

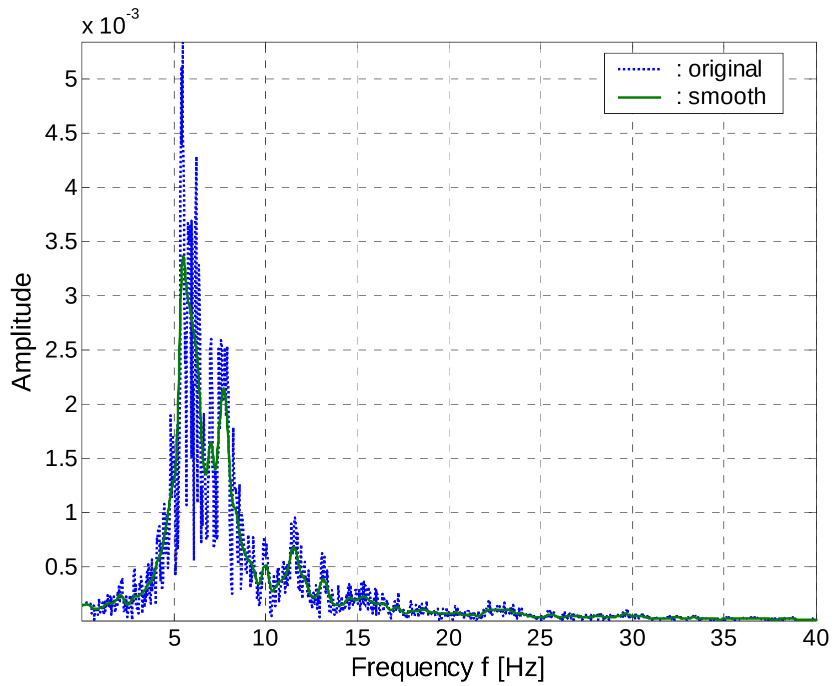

Figure A.34. Fourier spectrum of the original record of the Puerto Real earthquake at San Germán

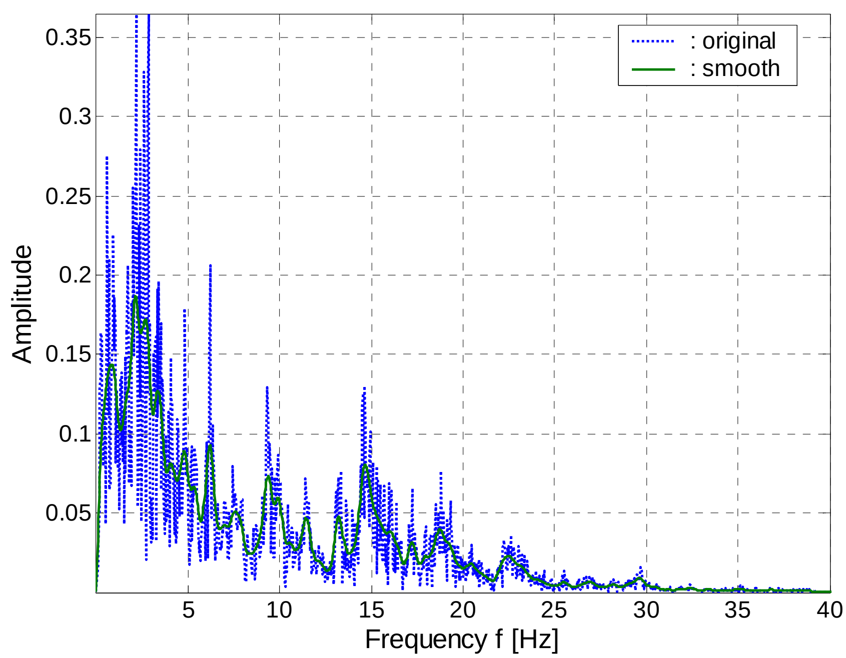

Figure A.35. Fourier spectrum of the original record of Puerto Real earthquake at San Germán

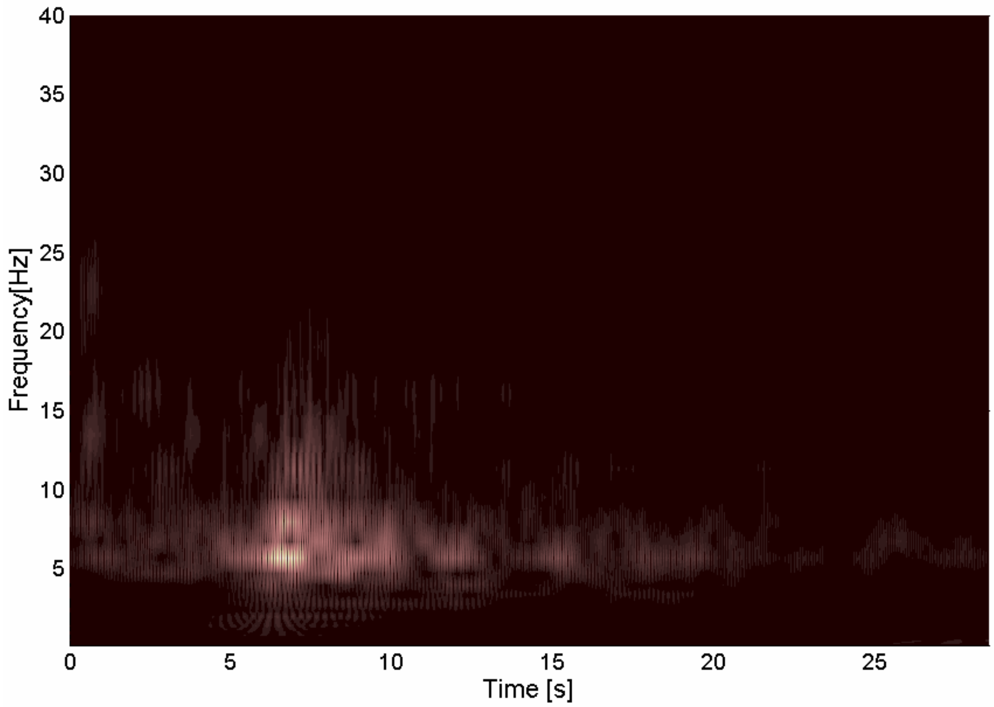

Figure A.36. Wavelet Map of the original record of the Puerto Real earthquake at San Germán

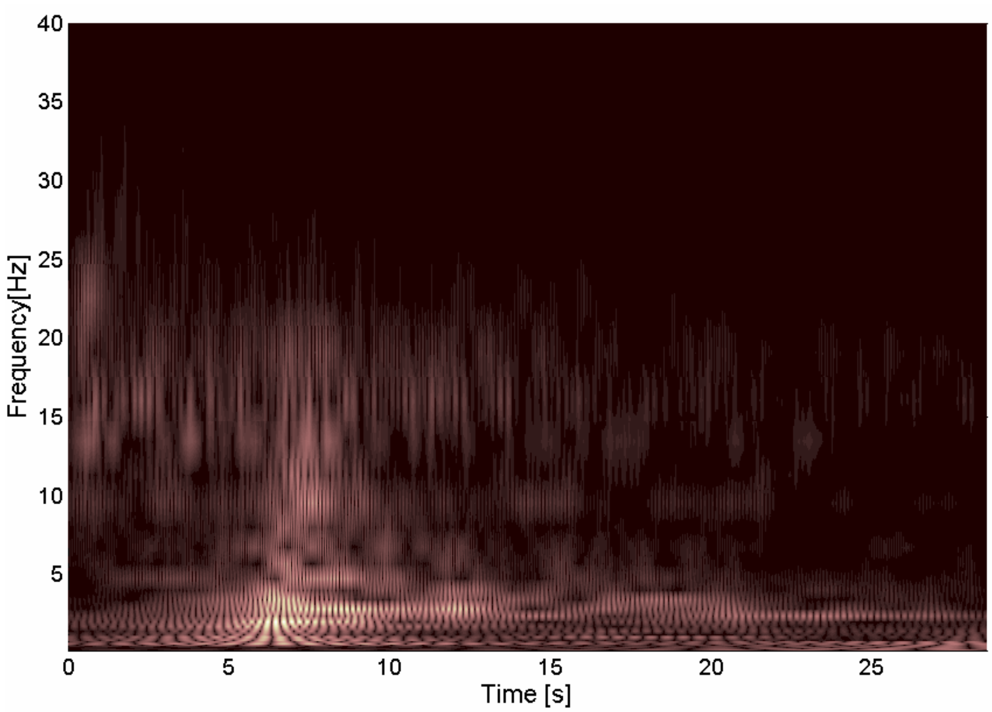

Figure A.37. Wavelet Map of the modified record of the Puerto Real earthquake at San Germán

APPENDIX B

MATLAB PROGRAMS

B.1 Program to generate the artificial earthquakes

```
%---------------       Program ArtifEarthquake.m        --------------%

% Program to decompose a recorded accelerogram into a desired
% number of time histories, and then each of the
% time histories is suitably scaled to match the response
% spectrum of the revised accelerogram with a specified design spectrum
% using the impulse response wavelet function

%--------------------------- Luis A. Montejo ----------------------------%
%------------------------ montrex79@hotmail.com --------------------%
%---------------------- Last updated: March-2004 --------------------%


clc; clear all; close all;
addpath('C:\eqks')                 % directory with the accelerograms


B  = 0.05;
w  = pi;                           % constants of the wavelet

expo = 4;
ji  = -26;
jf  =  6;
vj  = ji : jf;
a   = 2.^(vj/expo);                % vector with the coefficients
na  = length(a);

zi  = 0.05;                        % damping ratio for response spectra
dt   = 0.005;                      % time step of accelerogram [sec]
nom  = 'roundvaley';               % name of earthquake file
nit = 11;                          % number of iterations



terr = load ([nom,'.txt']);        % read earthquake data file
[nr,nc]  = size(terr);             % columns and rows of data file
nt      = nr*nc;                   % original number of data points
ag(1:nt) = terr';                  % copy accelerogram in a vector
xg       =  [zeros(1,1) ag zeros(1,1)];
nt      = length(xg);
b  = 0 : dt : (nt-1)*dt;
nb = length(b);

figure; plot( b,xg ,'LineWidth',1); grid on; axis tight;
```

```
title('Original time signal');
xlabel('Time [sec]'); ylabel('Acceleration [%g]');



%==============   continuous wavelet decomposition ======================

C  = zeros(na,nb);                    % matrix with the coefficients
for i = 1 : na
   a0 = a(i);
   for j = 1 : nb
       x  = ( b - b(j) )/a0;
       wv = exp( -B*w*abs(x) ) .* sin( w*x );
       CC = 1/sqrt(a0) * wv .* xg;
       C(i,j) = dt * trapz(CC);
   end
end

figure; surfl(b,a,(C)); shading interp; colormap gray ; grid on;
xlabel('P'); ylabel('S'); zlabel('Csp')

figure; surf(b,a,abs(C),'FaceColor','interp',...
  'EdgeColor','none',...
  'FaceLighting','phong'); colormap pink;
axis tight; view(0,90); grid on;
title('Absolute Values of Coefficients Cab');
xlabel('Time [s] or P'); ylabel('Scale [1/Hz]');zlabel('Csp')

%================== new time histories - detail functions ===================

D    = zeros(na,nb);
Inte = zeros(1,nb);
s    = zeros(1,nb);
for i = 1 : na
   a0 = a(i);
   for k = 1 : nb
      b0 = b(k);
      for j = 1 : nb
         x      = ( b0-b(j) ) / a0;
         wv     = 1/sqrt(a0) * exp( -B*w*abs(x) ) * sin( w*x );
         Inte(j) =  C(i,j) * wv /  a0^2 ;
      end
      D(i,k) = dt * trapz(Inte);
   end
end

s = sum(D);

ff = max(abs(xg)) /  max(abs(s));
s  = ff * s;
D  = ff * D;

figure; plot( b,s, b,xg); grid on;
legend(': reconstructed',': original');
xlabel('Time'); ylabel('Acceleration [%g]')

%================= spectrum from the reconstructed signal =================

T     = 2*pi * a/w;
SDbc  = zeros(na,1);
```

```
PSAbc = zeros(na,1);

for j = 1 : na
   om      = 2*pi/T(j);
   ub      = duhamel(om,zi,1,dt,nb,0,0,-s);
   SDbc(j) = max( abs(ub) );
end
PSAbc = (2*pi./T').^2 .* SDbc;              % pseudo-accel. spectrum: base


%================  design spectrum (UBC 97) =======================

Ca  = [0.24 0.30 0.33 0.36 0.36];
Cv  = [0.24 0.30 0.45 0.54 0.84];
St  = ['Sa', 'Sb', 'Sc', 'Sd', 'Se'];
js  = 2;
Ts = Cv(js) / (2.5*Ca(js));
To = 0.2 * Ts;

for i = 1 : na
  if T(i) < To
    ds(i) = (1 + 1.5/To*T(i)) * Ca(js);
  end
  if (T(i) >= To) & (T(i) <= Ts)
    ds(i) = 2.5*Ca(js);
  end
  if (T(i) > Ts)
    ds(i) = Cv(js) / T(i);
  end
end

meane  = zeros (1,nit);
rmse   = zeros (1,nit);
hPSAbc = zeros(na,nit+1);
hPSAbc(:,1) = PSAbc;

for m = 1 : nit
   for n = 1 : na
      factor(n) =  ds(n) / PSAbc(n) ;
      D(n,:)    = factor(n) * D(n,:);
   end
   s = sum(D);
   SDbc  = zeros(na,1);
   PSAbc = zeros(na,1);
   SDbc  = zeros(na,1);

   for j = 1 : na
      om      = 2*pi/T(j);
      ub      = duhamel(om,zi,1,dt,nb,0,0,-s);
      SDbc(j) = max( abs(ub) );
   end

   PSAbc  = (2*pi./T').^2 .* SDbc;
   hPSAbc(:,m+1) = PSAbc;
   dif = abs( PSAbc' - ds ) ./ ds;
   meane(m) = mean(dif) * 100;
   rmse(m)  = norm(dif) / sqrt(length(dif)) * 100;
end

figure ; plot( T,hPSAbc(:,1), T,hPSAbc(:,nit+1),'-o', T,ds,'MarkerSize',2 );
```

```
axis([0 4 0 1.1]); legend(': original record',': last iteration',': target spectrum');grid on
xlabel('Period [s]'); ylabel('Spectral acceleration [%g]')



figure; plot( b,s,'LineWidth',1); grid on; axis tight;
title('Compatible Accelerogram');
xlabel('Time [s]'); ylabel('Acceleration [%g]');


figure; plot(rmse,'-rs','LineWidth',2,...
            'MarkerEdgeColor','k',...
            'MarkerFaceColor','g',...
            'MarkerSize',10); grid on; xlabel('Iteration No.'); ylabel('Error in percent')

ns = s;

save C:\ns.txt ns -ASCII
```

B.2 Program to perform baseline correction

```
%------------------    Program AccelCorrect     -----------------------%

%  Program to perform baseline correction

%--------------------------- Luis A. Montejo ----------------------------%
%------------------------ montrex79@hotmail.com --------------------%
%----------------------  Last updated: March-2004  --------------------%

clc; clear all; close all

imax = 80 ;                          % maximum number of iterations
tol  = 0.0001;                       % tolerance percent of the max

g    = 980;                          % acceleration of gravity [cm/s^2]
dt   = 0.01;                         % time step of accelerogram [sec]
nom  = 'parkfieldTMB295mod';         % name of earthquake file
addpath('C:\eqks')                   % directory with the accelerograms

terr    = load ([nom,'.txt']);       % read earthquake data file
[nr,nc] = size(terr);                % columns and rows of data file
xg(1:nr*nc)= terr';                  % copy accelerogram in a vector
xg = g*[0 ,xg, 0];                   % add trailing zeros to accelerogram
np = length(xg);                     % new number of data points
cxg = zeros(1,np);
tf = (np-1)*dt;                      % final time of accelerogram
t  = 0: dt: tf;                      % row vector with time steps

vel   = dt*cumtrapz(xg);
despl = dt*cumtrapz(vel);



figure;subplot(3,1,1); plot( t,xg/g, 'b',t,zeros,'r','LineWidth',1); grid on;
axis tight; title(['acceleration, velocity and displacement time histories for ',nom]);
ylabel('accel. [%g]');

subplot(3,1,2); plot( t,vel,'b', t,zeros,'r' ,'LineWidth',1); grid on;
```

```
axis tight; ylabel('vel. [cm/s]');

subplot(3,1,3); plot( t,despl,'b', t,zeros,'r' ,'LineWidth',1); grid on;
axis tight; xlabel('time [s]'); ylabel('displ. [cm]');


L  = round(1/(dt))-1;
M  = np-L;

for q = 1:imax

  dU = 0;
  ap = 0;
  an = 0;

  dV = 0;
  vp = 0;
  vn = 0;
  for i = 1:(np-1)
     dU = dU + (t(np)-t(i+1)) * xg(i+1) * dt;
  end

  for i = 1:L+1
     aux = ((L-(i-1))/L)*(t(np)-t(i))*xg(i)*dt;
     if aux >= 0
        ap = ap + aux;
     else
        an = an + aux;
     end
  end

  alfap = -dU/(2*ap);
  alfan = -dU/(2*an);

  for i =2:np
     if i<=L+1
        if xg(i)>0
           cxg(i) = (1 + alfap*(L-(i-1))/L) * xg(i);
        else
           cxg(i) = (1 + alfan*(L-(i-1))/L) * xg(i);
        end
     end
     if i>L+1
        cxg(i) = xg(i);
     end
  end

  xg = cxg;

  %==========================================================

  for i = 1:(np-1)
     dV = dV + xg(i+1) * dt;
  end


  for i = M:np
     auxv = ((i - M)/(np-M))*xg(i)*dt;
     if auxv >= 0
        vp = vp + auxv;
```

```
    else
        vn = vn + auxv;
    end
  end

  valfap = -dV/(2*vp);
  valfan = -dV/(2*vn);

  for i =2:np
    if i>=M
        if xg(i)>0
           cxg(i) = (1 + valfap*((i - M)/(np-M))) * xg(i);
        else
           cxg(i) = (1 + valfan*((i - M)/(np-M))) * xg(i);
        end
    end
    if i<M
        cxg(i) = xg(i);
    end
  end

  xg     = cxg;
  cvel   = dt*cumtrapz(xg);
  cdespl = dt*cumtrapz(cvel);
  errv(q) = abs(cvel(length(cvel))/ max(abs(cvel)))
  errd(q) = abs(cdespl(length(cdespl)) / max(abs(cdespl)))

  if errv(q) <= tol & errd(q) <= tol, break,
  else
    xg = cxg;
  end


end

ns = (xg./g);

save C:\nsc.txt ns -ASCII -tabs

figure;subplot(3,1,1); plot( t,cxg/g, 'b',t,zeros,'r' ,'LineWidth',1); grid on;
axis tight; title(['acceleration, velocity and displacement time histories for ',nom]);
ylabel('accel. [%g]');

subplot(3,1,2); plot( t,cvel,'b', t,zeros,'r' ,'LineWidth',1); grid on;
axis tight; ylabel('vel. [cm/s]');

subplot(3,1,3); plot( t,cdespl,'b', t,zeros,'r','LineWidth',1); grid on;
axis tight; xlabel('time [s]'); ylabel('displ. [cm]');

xx = [1:q];
figure; plot(xx,errv,xx,errd)
plot(xx,errv,'--rs',xx,errd,'--bo','LineWidth',2,...
                'MarkerEdgeColor','k',...
                'MarkerFaceColor','g',...
                'MarkerSize',7); grid on
xlabel('iteration #'); ylabel ('final value/ max value');
legend(' : velocity ',' : displacement')
```

B.3 Program to analyze earthquake records in the time-frequency domain

```
%------------------ Program AnalisisEarthq.m ----------------------------%

% Program to analyse groun motions by performing: Arias, Fourier and
% and wavemap
%-----------------------      Luis E. Suarez   -----------------------------%
%--------------------------- Luis A. Montejo ----------------------------%
%------------------------ montrex79@hotmail.com ---------------------%
%----------------------  Last updated: March-2004  ---------------------%
close all;clc; clear all;


g    = 980;                        % acceleration of gravity [cm/s^2]
nit  = 10                     % iterartions for smooth fourier
B  = 0.05;                    % wavelet parameter
ww  = pi;                     % wavelet parameter
expo = 4;                     % wavelet parameter
ji  = -26;                    % wavelet parameter
jf  =  6;                     % wavelet parameter
vj  = ji : jf;
a   = 2.^(vj/expo);           % vector with the coefficients
na  = length(a);
nom  = 'parkfield';           % name of earthquake file
dt   = 0.01;                        % time step of accelerogram [sec]
addpath('C:\eqks')

terr    = load ([nom,'.txt']);        % read earthquake data file
[nr,nc] = size(terr);               % columns and rows of data file
xg(1:nr*nc)= terr';                   % copy accelerogram in a vector

np = length(xg);                     % number of data points

if np ~= 2*fix(np/2)                  % verify that N is an even number
   np     = np + 1                  % add one point if N is an odd number
   xg(np) = 0;                      % add one zero to the accelerogram
end

N  = round(1*np);                     % no. of points for plotting: % of total

tf = (np-1)*dt;                     % final time of accelerogram
t  = 0: dt: tf;                                % row vector with time steps
b  = t;                       % wavelet aux
nb = length(b);

figure; plot( t,xg, t,zeros(1,length(xg)) ); grid on;
axis tight; title(['Acceleration time historie of ',nom]);
xlabel('Time [s]'); ylabel('Acceleration [%g]');

%-------------- Calculate Arias strong motion duration ---------------------

Ia = zeros(1,np);
for n = 1 : np
    Ia(n) = pi/(2*g)*dt*trapz( xg(1:n).^2 );
end
Ia = Ia/Ia(np);
x1 = 0.05*ones(1,np);
x2 = 0.95*ones(1,np);
[xmin,imin] = min( abs(Ia-0.05) )
```

```
[xmax,imax] = min( abs(Ia-0.95) );
dur = t(imax) - t(imin);

figure;  plot( t,Ia, t,x1, t,x2, t(imin),Ia(imin),'s', t(imax),Ia(imax),'s','LineWidth',2,...
              'MarkerEdgeColor','m',...
              'MarkerFaceColor','c',...
              'MarkerSize',12);
grid on; axis tight; title(['Arias intesity of ',nom]);
xlabel('Time [s]','FontSize',16); ylabel('Normalized intensity','FontSize',16);
text(7,0.07,'5%','FontSize',16); text(7,0.97,'95%','FontSize',16);
text(tf/2.7,0.55,['strong motion duration: ',num2str(dur),' s'],'FontSize',16)


disp('Tiempos para 5% y 95% de la intensidad:'); disp(' '); disp([t(imin),t(imax)])
disp('Duración del movimiento fuerte:'); disp(' '); disp(dur)

%------------- Calculate the discrete FT of the ground motion ----------------------


wny = pi/dt                       % Nyquist frequency: rad/sec
dw  = 2*pi / tf                   % frequency interval: rad/sec
Np  = round(1*wny/dw);            % number of frequencies for plotting
w   = 0.00001: dw: N/2*dw;        % vector with frequencies in rad/sec
f   = w/(2*pi);                   % vector with frequencies in cycles/sec
Amp = dt * abs( fft(xg) );        % calculate the FT of the earthquake

%------ Smooth out and plot the amplitude of the FT of the ground motion -------------

Xg   = Amp;
for k = 1 : nit

   Sw(1)      = Xg(1);
   Sw(2)      = ( Xg(1)+Xg(2)+Xg(3) )/3;
   Sw(Np-1)   = ( Xg(Np-2)+Xg(Np-1)+Xg(Np) )/3;
   Sw(Np)     = Xg(Np);
   Sw(3:Np-2) = ( Xg(1:Np-4)+Xg(2:Np-3)+ Xg(3:Np-2)+Xg(4:Np-1)+Xg(5:Np) )/5;
   Xg         = Sw;

end


figure; plot( f(1:Np),Amp(1:Np),':', f(1:Np),Sw(1:Np),'LineWidth',2); grid on;
axis tight; title(['Fourier spectrum of ',nom])
xlabel('Frequency f [Hz]','FontSize',16); ylabel('Amplitude','FontSize',16);
legend(': original',': smooth');

%-------------   continuous wavelet decomposition ----------------------

frhz  =  (ww./a)/(2*pi);

C  = zeros(na,nb);                  % matrix with the coefficients
for i = 1 : na
    a0 = a(i);
    for j = 1 : nb
        x  = ( b - b(j) )/a0;
        wv = exp( -B*ww*abs(x) ) .* sin( ww*x );
        CC = 1/sqrt(a0) * wv .* xg;
        C(i,j) = dt * trapz(CC);
    end
end
```

```
figure; surf(b,frhz,abs(C),'FaceColor','interp',...
    'EdgeColor','none',...
    'FaceLighting','phong'); colormap pink;
axis tight; view(0,90); grid on;
title('Absolute Values of Coefficients Cab');
xlabel('Time [s]','FontSize',16); ylabel('Frequency[Hz]','FontSize',16); zlabel('coefs','FontSize',16);
```